TECHNISCHE UNIVERSITÄT MÜNCHEN

WACKER-Lehrstuhl für Makromolekulare Chemie

Differences of Zirconocenes and Hafnocenes

From Low Isotactic, Elastic - to High Isotacticity, High Melting Polypropylene

Alexander Schöbel

Vollständiger Abdruck der von der Fakultät für Chemie der Technischen Universität München zur Erlangung des akademischen Grades eines

Doktors der Naturwissenschaften

genehmigten Dissertation.

Vorsitzender: Univ.-Prof. Dr. K.-O. Hinrichsen

Prüfer der Dissertation:

1. Univ.-Prof. Dr. Dr. h.c. B. Rieger
2. Univ.-Prof. Dr. F. E. Kühn

Die Dissertation wurde am 13.06.2012 bei der Technischen Universität München eingereicht und durch die Fakultät für Chemie am 19.10.2012 angenommen.

Die vorliegende Arbeit entstand in der Zeit von Juni 2008 bis Januar 2012 unter Leitung von *Prof. Dr. Dr. h.c. Bernhard Rieger* am Wacker-Lehrstuhl für Makromolekulare Chemie der Technischen Universität München.

Mein besonderer Dank gilt *Prof. Dr. Dr. h.c. Bernhard Rieger*. Nicht nur dafür, dass er es mir ermöglicht hat in seinem Arbeitskreis diese Promotionsarbeit anzufertigen, sondern auch für viele fachliche und allgemeine Diskussionen und für das in mich gesetzte Vertrauen und die Freiheiten, welche ich während meiner Zeit in seinem Arbeitskreis genießen durfte.

Für all die organisatorischen Angelegenheiten die in einem Arbeitskreis so anfallen um einen reibungslosen Ablauf zu gewährleisten hat sich *Dr. Carsten Troll* gekümmert. Hierfür und für die Unterstützung bei Fragen rund um die technischen Belange bei den Autoklaven bin ich ihm sehr dankbar.
Frau *Baur*, Frau *Saul-Hubrich* und Frau *Uruk* möchte ich für die Unterstützung bei den formalen Angelegenheiten die während meiner Promotion zu erledigen waren danken.
Natürlich möchte ich auch unseren technischen Angestellten *Aleksandra Jonovic*, *Sabine Martinetz-Große* und *Katja Rodewald* für die durchgeführte Analytik danken.

Dr. Sergei Vagin danke ich für seine allzeit vorhandene Diskussions- und Hilfsbereitschaft sowohl bei chemischen Fragen, als auch für seinen unermüdlich geleisteten Einsatz bei einigen analytischen Geräten.
Einen wesentlichen Teil meiner Zeit habe ich natürlich im Labor verbracht, wo ich stets eine sehr angenehme Atmosphäre erleben durfte. Hierfür möchte ich mich bei meinen Laborkollegen *Andreas Feigl*, *Ulrike Will*, *Udo Schmidt*, *Marin Steenackers*, *Frank Deubel* und *Victor Bretzler* herzlichst bedanken. Beiden Letzteren bin ich natürlich auch für die Durchsicht meines Manuskripts sehr dankbar. *Stephan Salzinger* gebührt ebenfalls mein Dank für die Durchsicht meines Manuskripts und für die netten kulinarischen Abende in Denver.

Des Weiteren möchte ich mich bei *Manuel Winkenstette* und *Timo Anselment* für die gute Zusammenarbeit bei der Erstellung unseres Buchkapitels bedanken sowie bei *Dr. Carly Anderson* für die Korrekturen hierzu. (Thank you *Dr. Anderson* for reading our manuscript).

Ein großer Dank für eine durchweg schöne Zeit im Arbeitskreis geht natürlich auch an alle anderen Kollegen des Wacker-Lehrstuhls und des Silicium-Instituts.
Gesondert möchte ich mich noch bei *Pierre Göppert*, *Timo Korfmann*, *S(us)anna Zimmer*, *Franziska Graf*, *Philip (Pippo) Zehetmaier*, *Maximilian Lehenmeier*, *Naïma Hutter*, *Paul Heinz* und *Monika Kellner* bedanken mit denen ich neben der Arbeit auch immer bei privaten Unternehmungen viel Spaß hatte.
Neben allen Studenten die ihren Teil zu dieser Arbeit beigetragen haben gebührt mein Dank besonders den beiden Auszubildenden, *Nadine Härtl* und *Heike Wolf*, sowie den beiden Masteranden *Dominik Lanzinger* und *Andreas Eisele* die für mich wertvolle Arbeit geleistet haben.

Nicht zuletzt gilt mein Dank auch der *Borealis GmbH* für die finanzielle Unterstützung dieser Arbeit und deren Mitarbeitern, *Luigi Resconi*, *Norbert Reichelt*, *Christian Paulik* und *Sebastian Babik* die mich während unserer Zusammenarbeit begleitet haben. Besonders möchte ich mich bei *Matthew Parkinson* und seinem Team für die durchgeführten NMR Messungen bedanken.

Ein ganz besonderer Dank geht an meine Eltern, meine Oma, meine Schwester sowie meinen besten Freund *Timo Dumberger* für all den Rückhalt und die Unterstützung die Sie mir bis zum heutigen Tage entgegengebracht haben.
Zuletzt möchte ich der für mich wichtigsten Person, meiner Freundin *Anja Eberlein*, dafür dass Sie mich stets tatkräftig und liebevoll bei all meinen Vorhaben unterstützt hat meinen Dank aussprechen.

“There is no sadder sight in the world than to see a beautiful theory killed by a brutal fact.“

Thomas Henry Huxley (1825-95)

AFM	atomic force microscopy
Å	Ångström, $1 \cdot 10^{-10}$ m
aPP	atactic polypropylene
Ar	aryl
CEP	chain end epimerization process
cfrp	carbon fiber reinforced plastic
cga	coordination gap aperture
Cp	cyclopentadienyl
Cy	cyclohexane
d	dublet (NMR)
DCM	dichloromethane
DIBAL-H	diisobutylaluminum hydride
DMTA	dynamic mechanical thermal analysis
DSC	differential scanning calorimetry
EA	elemental analysis
ESI	electronspray-ionization
ePP	elastic polypropylene
e	erythro
eV	electron-volt
Flu	fluorenyl
GPC	gel permeation chromatography
HOMO	highest occupied molecular orbital
Ind	indenyl
iPP	isotactic polypropylene
LCB	long-chain-branched
LMCT	ligand to metal charge transfer
LUMO	lowest unoccupied molecular orbital
m	meso dyad
M	molar mass
MM	macromonomer
MS	mass spectrometry
MAO	methylaluminoxane
n-BuLi	*n*-Butyllithium
NMR	nuclear magnetic resonance

PDI	polydispersity index
Ph	phenyl
PE	polyethylene
PP	polypropylene
PS	polystyrene
PVC	polyvinylchloride
P_n	degree of polymerization
q	quartet (NMR)
r	racemic dyad
rac	racemic
RI	refractive Index
RSA	ring slippage angle
rt	room temperature
s	singlet (NMR)
sPP	syndiotactic polypropylene
t	threo
t	triplet (NMR)
TEA	triethylaluminum
THF	tetrahydrofurane
TIBA	triisobutylaluminum
TLC	thin layer chromatography
TMA	trimethylaluminum
T_m	melting transition
TPE	thermoplastic elastomer
UV	ultraviolet
vdW	*van der Waals*
viPP	variable isotactic polypropylene
wt-%	weight percent
ZN	*Ziegler-Natta*

1 Introduction

Today, polymers can be found in nearly all types of application. They are known to be the construction material of the 21th century. Since 1950s the produced amount has constantly increased from 1.7 to 265 mio t in 2010 (Figure 1).[1] A major reason for this significant increase is the high cost efficiency and the broad range of applications of these materials.

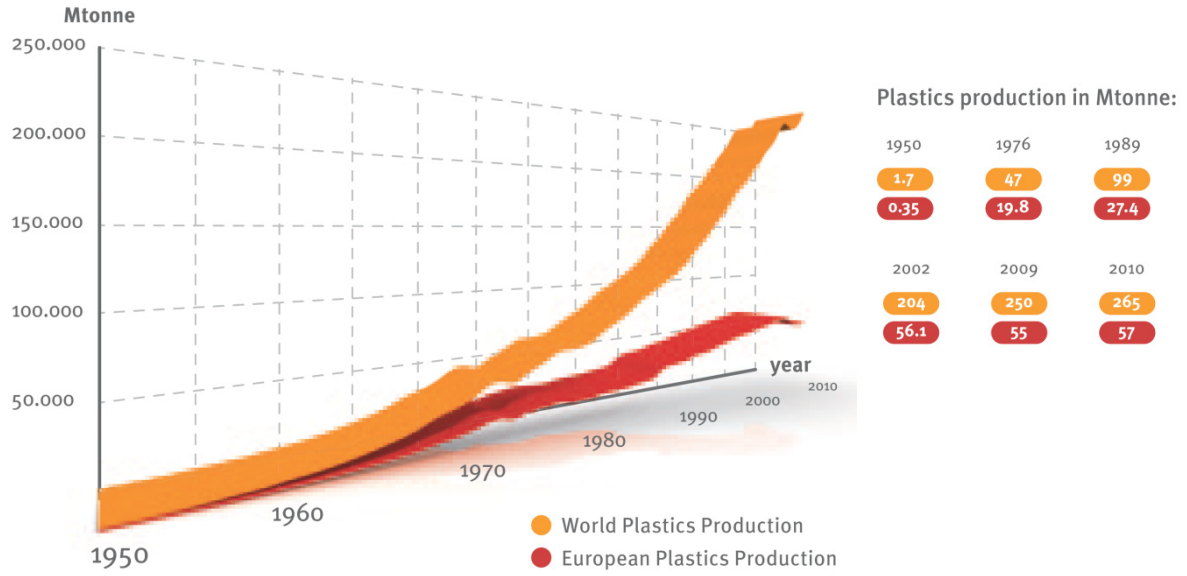

Figure 1: World and European plastic production from 1950 to 2010.

A more detailed look at the field of applications of polymers reveals a significant development. In the beginning, polymers were only used for simple articles, e.g. as packaging material or for housings of smaller electronic devices. Nowadays, polymers are also applied in high tech applications. For example, low weight of polymers helped to afford the successful construction of huge airplanes. More than half of the total weight of these airplanes can consist of carbon fiber reinforced polymers (cfrp).[2] Even if there is a huge multitude of different polymer materials, there are only five big families of polymers, namely polypropylene (PP), polyethylene (PE), polystyrene (PS), polyvinylchloride (PVC), and polyethyleneterephtalate (PET) accounting in Europe for about 75 % of the total volume of produced polymers. From those, especially the polyolefins PE and PP are the most important polymers with a market share of still 48 % (Figure 2).[1]

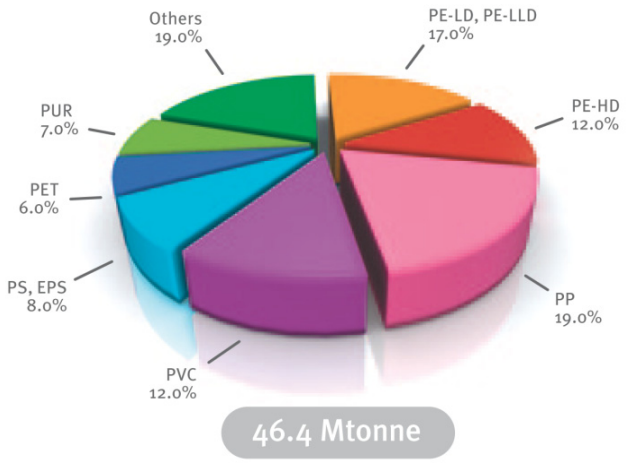

Figure 2: European plastic demand by resin type.

PE and PP underwent a significant development since the discovery of the catalytic polymerization by *Ziegler* in 1953.[3] This was the first time PE was produced by a low pressure and low temperature process affording high density PE (HDPE). Before, only low density polyethylene (LDPE) was accessible via a high temperature and high pressure process. Shortly afterwards, *Natta* applied the catalysts of *Ziegler* for polymerization of propene.[4] Today, variations of *Ziegler´s* heterogeneous catalysts are industrially used for the production of the main part of isotactic polypropylene (iPP). However, besides these heterogeneous systems also homogeneous complexes, the metallocenes, were developed for the polymerization of propene. A major difference compared to the heterogeneous *ZN* catalysts is the possibility to form PP with microstructures different than isotactic.[5] With these complexes, e.g. syndiotactic polypropylene (sPP), variable isotactic polypropylene (viPP) and copolymers with homogeneously distributed comonomers are accessible. The control over the microstructure gives the control over the mechanical behavior of these polymers and thereby the field of application of PP was broadened by metallocene produced PP. PP ranging from atactic waxes over polymers with elastic behavior up to thermoplastic polypropylene can be obtained.

In the last two decades, also the amount of metallocene produced polyolefins such as LLDPE, iPP or sPP in industry was increased. For the industrial polymerization of propene, temperatures of 50 °C and higher are usually applied. At these temperatures, the performance of metallocene catalysts is often reduced, resulting in less controlled microstructures or lower molecular weights of the polymers formed, compared to those produced at moderate polymerization temperatures. Hence, one major aspect of this thesis will be the investigation of the polymerization behavior of metallocene catalysts at high temperatures and the development of new temperature stable metallocenes.

2 Theoretical Background

2.1 Definition of Metallocenes

A metallocene is typically defined as a complex with a metal in the oxidation state II coordinated by two coplanar cyclopentadienyl anions. For the polymerization of olefins common metallocene derivatives are pseudo-tetrahedral d^0 complexes of group 4 metals (Ti, Zr and Hf). In addition to the two anionic cyclopentadienyl, also σ-bonded ligands are present in these complexes. Today the cationic form is accepted to be the polymerization active species.[6] Therefore one of the two σ-bonded ligands has to be abstracted. In the following the term metallocene is used for the complexes of group 4 metals that are applied in the olefin polymerization.

2.2 A Brief History of Homogeneous Olefin Polymerization Catalysts

First homogeneous systems, Cp_2TiCl_2 **I** together with Et_3Al or Et_2AlCl (Figure 3), which are able to catalytically oligomerize propene at low temperatures and low propene concentrations were reported by *Natta* and *Breslow* in 1957.[7, 8] These bent complexes, compared to the known heterogeneous *Ziegler-Natta* systems, have the advantage that their analysis is much easier. Hence, first mechanistic and kinetic investigations were performed short after these first polymerization experiments.[9, 10] The deeper understanding of these homogeneous catalysts created different mechanistic models describing the polymerization mechanism taking place in both the homogeneous and heterogeneous case (2.5). Further important developments concerning ligand design are depicted in Figure 3. Changing symmetry from C_{2v} **I** to C_2 **II**, affords an influence on the polymer microstructure when prochiral monomers (e.g. propene) are used. With *Brintzinger´s* complex **II**, *Ewen* showed the correlation between the C_2-symmetry of the complex and its stereoselectivity in the polymerization of propene to *i*PP.[11, 12] Besides the microstructure of the polymers especially activation (2.4) of the complexes is important. Higher activities and higher molecular weights were achieved by adding small amounts of water to the actually used catalysts of *Breslow* and *Natta* **I**.[13] Further investigations by *Kaminsky* and *Sinn* in 1980 resulted in the controlled formation of methylaluminoxane (MAO) which afforded increased activities of the catalysts.[14, 15] Changing

the metal center from Ti to Zr (**III** and **IV**) gave even higher activities.[16, 17] In the following 15 years, developments of the ligand structure - polymer microstructure dependancy caused several different metallocene structures (2.8) e.g. the C_1-symmetric complexes of *Rieger et al.*, which are able to form elastic PP (2.9).[18]

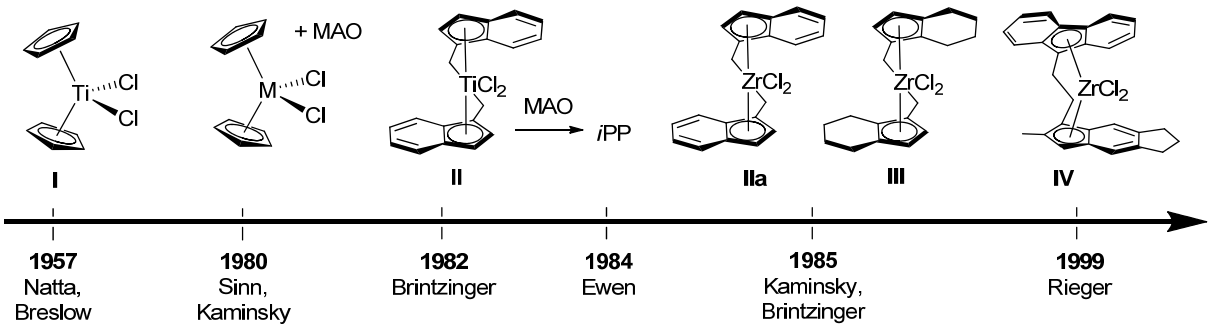

Figure 3: Timeline of important developments for the homogeneous polymerization of olefins by metallocenes.

2.3 Important Structural Parameters of *ansa*-Metallocene Complexes

Ansa-metallocenes are complexes with two cyclopentadienyl based ligands that are connected via a bridge (e.g. ethylene, SiR_2, CR_2). Besides the most frequently used and thus here discussed bridges a huge number of different *ansa*-metallocenes has been developed (e.g. double bridged metallocenes). In most of the cases a second bridge affords a detrimental effect on the polymerization behavior.[19] The ligand of a single bridged C_2-symmetric *ansa*-metallocene has two chiral centers giving 3 different stereoisomers. Two of them are enantiomers (R, R and S, S) and the third one is a diastereomer (R, S) (Figure 4).

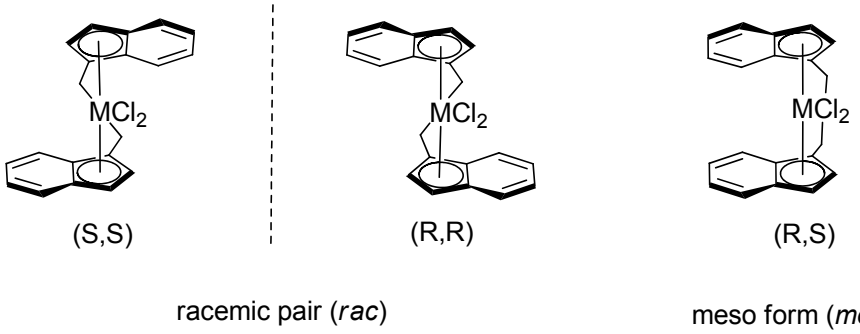

Figure 4: Stereoisomers of a C_2-symmetric *ansa*-metallocene.

For the formation of iPP only the *racemic*-form (*rac*) can be used as the *meso*-form produces atactic PP (aPP). In the following for discussions concerning C_2-symmetric metallocenes, if not otherwise specified, always the *rac*-form is supposed.

The most important parameters for the description and comparison of different *ansa*-metallocenes and their influence on the polymerization behavior, will be briefly described. Figure 5 shows the side view of an *ansa*-metallocene with these important parameters. During the whole catalytic polymerization reaction the two Cp-ligands remain bonded to the metal and are therefore also called spectator or ancillary ligands. The longer the centroid-M (cen-M) distance the more facile is the cleavage of the Cp-ligands. Hence, the cen-M distance has a direct influence on the stability of the complex.

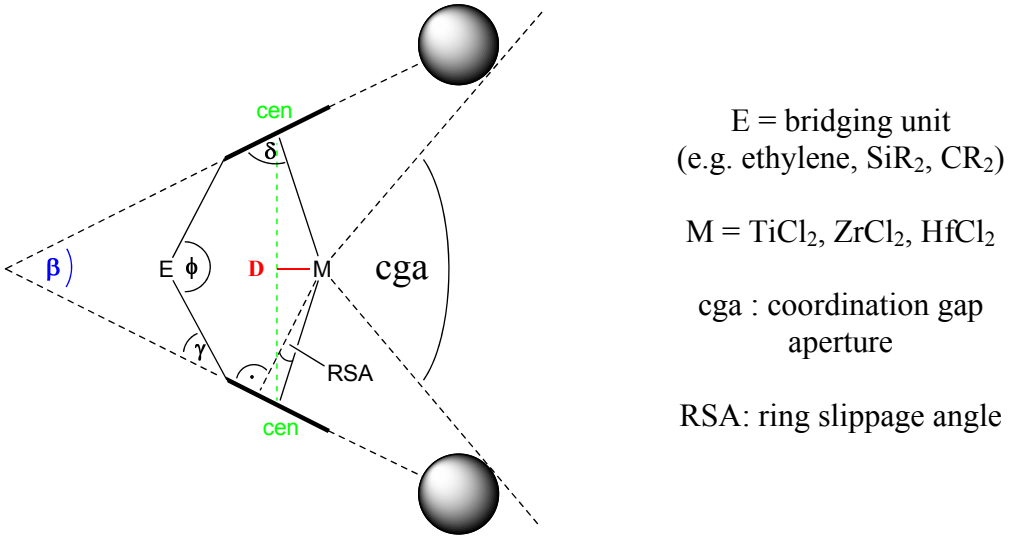

Figure 5: Most frequently used geometry parameters for *ansa*-metallocenes.

The activity of a metallocene catalyst is amongst others, influenced by the accessible spatial room at the metal center and can be described by the parameters cga and β. The coordination gap aperture (cga), originally defined for substituted and bridged Cp_2MCl_2 metallocenes, is the largest possible angle between the two planes which contain the metal center and touch the inner *van der Waals* (vdW) surfaces of the β-substituents of the Cp fragment. [20-22] The bite angle β can be used as a dimension for the accessibility of the metal center and is defined as the dihedral angle between the two planes, each containing the five carbon atoms of one Cp ring. Additional substituents on the Cp moiety can influence the bite angle, but β does not directly represent the spatial room available on the metal center for the catalytic reaction. The relative position of the metal towards the Cp rings is also very important for the polymerization behavior of a metallocene catalyst. For an evaluation of this relative position the parameter D was introduced. D is the distance of the metal to the imaginary line connecting the two centroids of the Cp rings (cen-cen). The parameter D gives information about the accessibility of the metal and the overlap of the Cp-ligand molecular orbitals with

the metal atom orbitals.[23] Especially latter has a big influence on the electronic properties of the metal center itself and therefore on the activity and stability of the metallocene catalyst. A second geometric parameter describing the position of the metal, relative to the Cp-ligands, is the ring slippage angle (RSA).[24, 25] This is the angle between the line connecting M and cen, and the normal of the Cp plane through the metal. Comparing different metallocenes one has to take into account the different influences of all afore mentioned parameters.

To give an example, the influence of the bridging unit on these structural parameters and thus on the polymerization behavior will be briefly discussed. In general, by going from more atoms to one atom bridges flexibility and conformational variety especially at elevated temperatures is reduced.[26-28] This higher rigidity is known to increase regio- and stereoselectivity (2.6).[29] A straightforward influence of the bridge on the bite angle is shown in Table 1. With decreasing length of the bridge for the Cp_2ZrCl_2 metallocenes the bite angle increases. For $(Ind)_2ZrCl_2$ the bite angle is quite similar for the ethylene and the $SiMe_2$ bridging unit. The largest bite angle is obtained in all cases with the short and small CMe_2 unit.

Table 1: Comparison of the bite angles of different metallocenes with different bridging units.[23, 30, 31]

	bridging unit		
	$-C_2H_4-$	$-SiMe_2-$	$-CMe_2-$
metallocene	**bite angle β [°]**		
Cp_2ZrCl_2	56,4	60,1	71,4
$(CpMe_4)_2ZrCl_2$	57,7	60,8	-
$(Ind)_2ZrCl_2$	62,1	61,8	70,9

Despite the clear correlation of bridge length and β the corresponding activities do not show the same trend. Apparently it is important to understand the contribution of all afore mentioned parameters. As an example the $SiMe_2$- and CMe_2-bridged Cp_2ZrCl_2/ MAO catalysts will be compared. The coordination and insertion of the monomer should be more facile for the CMe_2-bridged catalyst due to the larger bite angle and thus also higher propagation rates could be assumed. However, experimentally determined activities show a higher acticity for the $SiMe_2$-bridged catalyst. As a reason the parameter D can be mentioned as the position of the metal is changed towards a more outward position with an increased value of D for the CMe_2-bridged metallocene. As mentioned before, this situation decreases the stability of the complex due to a reduced overlap of the molecular orbitals, and finally lower productivities are observed for the Cp_2ZrCl_2/ MAO catalyst with a CMe_2 bridge.[25, 32]

2.4 Activation of Metallocenes

2.4.1 *General Aspects*

Today the monocationic form of a metallocene of group 4 metals is accepted to be the active species for the polymerization of α-olefins.[6] Using a precursor complex with the general formula L_2MX_2 (M = Ti, Zr, Hf; X = Cl, alkyl), the addition of a *Lewis* acidic co-catalyst which is able to generate the cationic active species is necessary. Therefore various different activation agents are available. Big differences in activity, e.g. due to an incomplete activation or due to side reactions and the formation of polymerization inactive species, are present depending on the nature of the used co-catalyst.

2.4.2 *MAO Activation*

The already mentioned and most common activation reagent is MAO. MAO can be obtained by the controlled reaction of trimethylaluminum (TMA) with water. Due to simplification, MAO is often presented with a trivalent aluminum and a $[\text{-Al(Me)-O-}]_n$ building block. Some studies, also including DFT calculations, propose a more cage like structure with a tetravalent aluminum.[33-35] However, recently a publication also deals with a linear to slightly branched structure having a degree of polymerization (P_n) of about 300.[36] Next to the aluminoxane unit itself, MAO also contains free and associated TMA. Latter cannot be easily removed by evaporation but in a chemical reaction.[37] The different structures in MAO are in an equilibrium, influenced by different factors like reaction conditions during the formation of MAO and the amount of TMA.[38] These structural differences make it difficult to elucidate the role of each of the different components in the activation process of the metallocene dichloride. A good analytic method has been found to be UV-Vis spectroscopy. Typically used concentrations for this method are similar to the concentrations of the different compounds used during the polymerization reaction. Hence this method is suitable to obtain further information on the reaction products and the kinetics of their formation.[39-46] A simplified reaction scheme for the activation of a metallocene dichloride includes the mono or dialkylation reaction, followed by the abstraction of a methyl or a chloride anion, resulting in the formation of the polymerization active cationic species (Scheme 1).

Scheme 1: MAO activation of a metallocene dichloride.

The generated anion significantly influences the activity. The stronger the anion is coordinated to the metal the lower is the activity in olefin polymerization. The very complex structure of MAO makes it often difficult to determine the real active species in the catalytic polymerization of olefins. Additionally varying activities can be observed using slightly different MAO compounds.[46] Also, the so far presented straightforward generation of the polymerization active species can be affected by side reactions leading to polymerization inactive species. Different activities, as a result of an incomplete activation process, are due to side reactions, which can depend on the structure of MAO and on the structure of the metallocene complex. Thus a direct comparison between activities for these catalysts is often difficult.[45, 46] For a high activity often large amounts of the MAO co-catalyst have to be applied (Al:M ≥ 2000; M = Ti, Zr and Hf).

2.4.3 *Boron-based Activation*

One of the major advantages of boron-based co-catalysts is their well known structure, affording a clear structure reactivity correlation. For some of these catalysts even the crystal structures of the activated complex could be obtained.[47, 48] Further difference compared to MAO is the low amount of co-catalyst, required for a quantitative activation. Typically the ratio of boron to M (M = Ti, Zr, and Hf) is 1:1 up to 5:1. Using the boron based activation agents a dialkylated precursor of the metallocene has to be used. The boron derivative acts as a *Lewis* acid and abstracts one of the alkyl groups of the metallocene resulting in the formation of the active cationic form of the complex (Scheme 2).

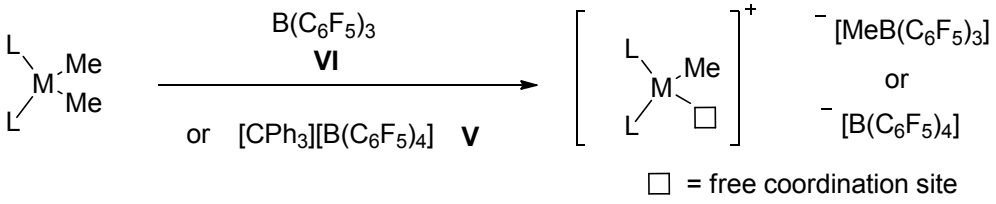

Scheme 2: Activation of dimethylmetallocenes with boron-based co-catalysts.

The activity of these catalysts depends on the coordination ability of the counteranion and on possible, reversible or irreversible, side reactions leading to polymerization inactive species. Trityl tetrakispentafluorophenylborate $[CPh_3][B(C_6F_5)_4]$ **V** is known to be an activation agent for dialkylmetallocene complexes with a weakly coordinating anion, thus affording high activities. Lower activities are obtained, if trispentafluorophenylborane $B(C_6F_5)_3$ **VI** is applied as co-catalyst. During activation **VI** is converted to $[RB(C_6F_5)_3]^-$ (R = alkyl), a stronger coordinating anion. The stronger bonded contact ion pair formed, is the reason for the lower activity. In contrast the borate generated catalyst consists of a weaker bonded contact ion pair, and is thus more active.[49]

Depending on the structure of the metallocene complex, the nature of the counteranion and their ratio in the reaction mixture not only the depicted reaction to the mononuclear cationic form of the complex depicted in Scheme 2, but also a varying amount of a binuclear cationic complex can be formed (Scheme 3).[50] The binuclear cationic complex is a resting state which is, due to the lack of a free coordination site, not catalytically active in the coordination-insertion polymerization of olefins.[51]

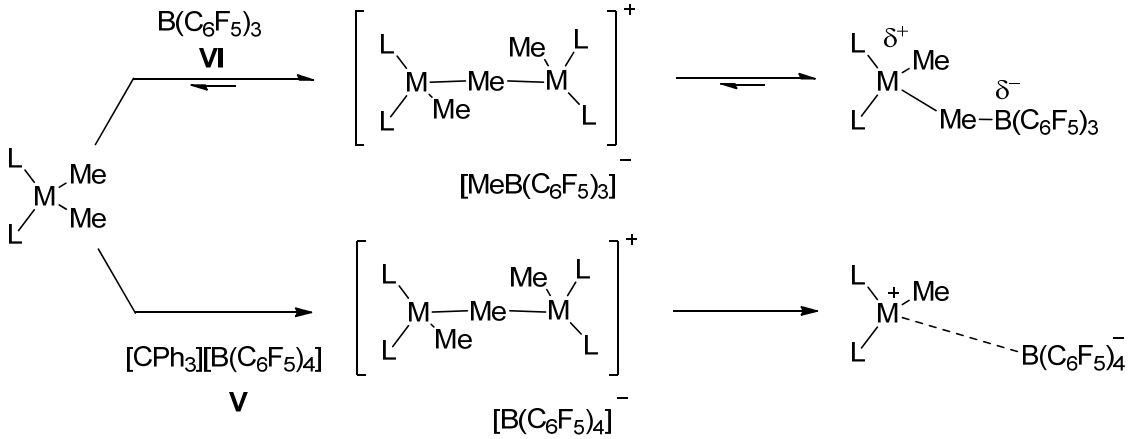

Scheme 3: Formation of mononuclear- and dinuclear metallocene complexes in the activation reaction with boranes and borates.

Using the dimethylmetallocene together with the borane/ borate co-catalyst often results in decreased activities due to the high sensitivity of the dimethyl precursor towards moisture. A convenient route giving higher activities was reported by *Chien et al.* with the ternary system $Et(Ind)_2ZrCl_2$/ $AlEt_3$/ borane **VI** or borate **V**.[52, 53] In addition to the straightforward alkylation by the alkylaluminum reagent followed by the generation of the active species with the boron-based co-catalyst, also a side reaction between the boron-based co-catalyst and the alkylaluminum compound takes place. In this side reaction a transfer of the perfluorenated phenyl rings from boron to aluminum and the transfer of the alkyl group vice versa occurs.[54]

Hence, for aluminum derivatives such as TMA together with borane **VI** (Al:B > 1) this side reaction results in a close contact ion pair of the metallocene cation and the aluminum anion, which is inactive in the polymerization of ethylene.[55] TEA together with a borate as co-catalyst was also reported to form an inactive complex.[56] However, TIBA can be used together with borane **VI** and borate **V** to form active metallocene catalyst for the coordination-insertion polymerization of α-olefins.[55, 56] This behavior is most presumably due to the weaker coordination of the aluminum derivative, which is formed in the reaction with borane **VI** or borate **V**, to the metallocene cation.

2.4.4 *Activation Investigations via UV-Vis Spectroscopy*

For a deeper understanding of the activation process several analytic methods have been used. Among these methods, especially NMR and UV-Vis spectroscopy were proven to afford good results. One advantage of UV-Vis measurements is that for the data collection only short times are necessary, thus fast kinetic measurements can be performed. In addition, compared to NMR spectroscopy lower concentrations, which are in the range of those used in the activation and polymerization process, are accessible. Therefore the observed kinetic data are in good accordance with the real reaction rates of the activation and polymerization reaction. The observed absorption band for the metallocenes is a ligand to metal charge transfer (LMCT) band.[39, 57, 58] Aluminum derivatives (e.g. MAO, TIBA, TMA) do not give an absorption band in the region of the LMCT band of the metallocenes. Hence, also high amounts of aluminum derivatives, which are necessary for high activities during the polymerization procedure, can be applied. The lowest energy absorption band in the UV-Vis spectrum of bent metallocenes arises from a charge transfer of the highest occupied molecular orbital (HOMO) to the lowest unoccupied molecular orbital (LUMO). The former, in case of d^0 metallocenes, has predominantly the character of the Cp-based ligand and the LUMO has mainly the character of the metal.[59, 60] Substitution or abstraction of a σ-bonded ligand changes the electron density on the metal, thus leading to a different HOMO-LUMO gap and to a shift of the LMCT band. Several investigations on the activation of metallocene dichlorides with MAO have been performed.[39-46, 57, 58, 61, 62] Low amounts of MAO lead to a hypsochromic shift of the LMCT band. This shift is a result of a monoalkylation process. The chloride- is substituted by a stronger electron donating methyl-ligand resulting in an increased HOMO-LUMO gap due to a higher electron density on the metal. With higher amounts of MAO a consecutive reaction forms the cationic active species affording a bathochromic shift due to decreased electron density on the metal (Scheme 4).

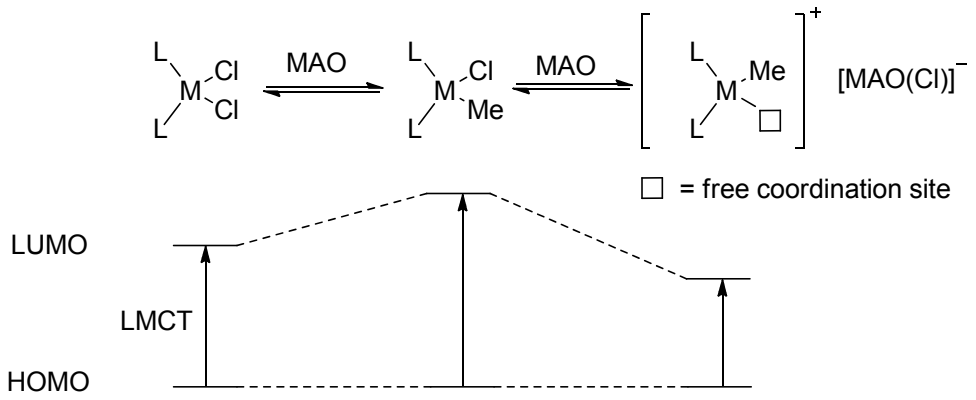

Scheme 4: Qualitative presentation of the change of the HOMO-LUMO gap during the MAO activation process.

Also, the formation of the catalytic active species of the metallocene with boranes or borates was studied by UV-Vis measurements.[39] A bathochromic shift of the LMCT band can be observed during the reaction of the dimethyl precursor of the metallocene with borates. This shift is analog to that, observed during the cationization reaction if higher amounts of MAO are applied. The LMCT band of the resulting ion pair in case of the borate activated catalyst is always shifted to slightly higher wavelengths. This can be explained by lower electron density on the metal due to a less strong coordination of the anion to the metal. For some of the used borates (e.g. borate **V**) the cationization reaction itself cannot be monitored by UV-Vis spectroscopy as the borates show absorption bands in the significant region themselves. For ternary systems with aluminum reagents and borates, besides the cationization reaction, the *in situ* preactivation reaction can be followed by UV-Vis spectroscopy. In general the use of TMA, TEA or TIBA is known to result in a mono or dialkylation of the metallocene dichloride precursor, depending on the amount of the aluminum compound, the metal and the structure of the metallocene.[42, 44, 46, 61, 63, 64]

2.4.5 *Hf and Zr: The Difference in Activation/Activity*

Hafnium and zirconium have rather similar atom (1.564 and 1.590 Å, respectively) and ionic radii (0.72 and 0.73 Å, respectively).[65] The main reason for the smaller expansion of hafnium compared to zirconium is the additional 4-f shell which is introduced between zirconium and hafnium. The f-shell is known to have influence on the valence electrons due to its diffuse character. This effect is called the lanthanide-contraction, as the diffuse character of the f-shells leads to a worse shielding of the positive charge, thus resulting in a stronger attraction of the 6s and 5d valence electrons in case of Hf (0) or of the 5s and 5p valence electrons in case of Hf (IV). Other factors influencing the radii of the atoms are relativistic effects. The

electrons near the core are moving very fast. This leads to an increasing mass and finally affords a stronger attraction between the core and the electrons caused by gravity. The probability of the electrons being near the core is high for s- and p-orbitals but low for f- and d-orbitals. Hence the contraction of the f- and d-orbitals is lower leading to an overall expansion of the f- and d-orbitals due to better shielding of the core by electrons in the contracted orbitals (s- and p-).

The chemical behavior of Hf and Zr compounds is often described to be analog due to their similar structures. In first reports on hafnocene complexes, polymerizing α-olefins, the activity of MAO-activated hafnocenes is reported to be lower compared to MAO-activated zirconocenes.[66, 67] This effect was assumed to be due to the more stable M-C σ-bond in case of the hafnocenes, thus having lower chain propagation rates.[66] Using borates as co-catalyst showed increased activities of the hafnocene complexes similar to the values obtained with the corresponding zirconocenes. Therefore the lower observed activity for the hafnocene is mainly not an intrinsic property of the metal itself but a problem of activation.[68] The actual problem of MAO activation for hafnocenes was calculated to be TMA contamination present in MAO. TMA can form quite stable dinuclear methyl-bridged complexes (Scheme 5).[69] They were calculated to be more stable by 3 kcal·mol^{-1} for the hafnocene compared to the corresponding zirconocene. Hence, for the hafnocene this complex can be regarded as a resting state not active in olefin polymerization any more.[70]

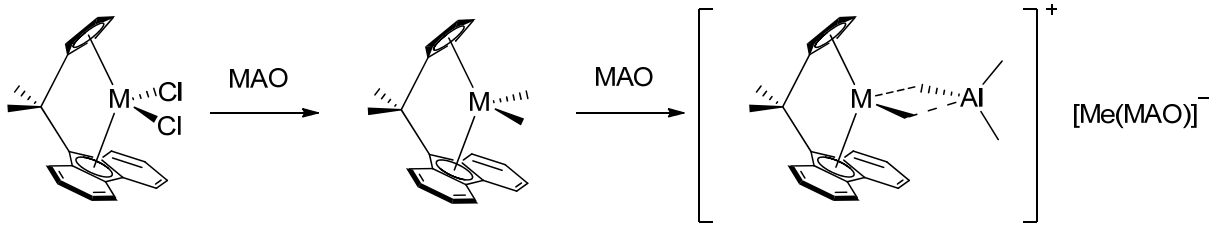

Scheme 5: Formation of a dinuclear methyl-bridged resting state during MAO activation of a metallocene.

More stable and therefore shorter M-Cp bonds in case of hafnocenes lead to a smaller bite angle, which was assumed to contribute to the lower observed activities for hafnocenes, probably due to a more hindered structure resulting in a worse accessibility of the metal cation.[24]

2.5 Chain Propagation Mechanism in the Coordination-Insertion Polymerization of α-Olefins with Metallocenes

For the mechanism of chain propagation several different mechanisms have been proposed. One of the first was the *Cossée* mechanism (Scheme 6).[71-74] The catalytic active species is a metallocene cation with a free coordination site and a weakly coordinating anion. The olefin can coordinate to the free site forming a π-complex. Via a four-membered cyclic transition state the olefin is opened in a *cis* selective way and the growing polymer chain migrates to the closest carbon atom of the former olefin. The site where the growing polymer chain was located is now free for the coordination of the next olefin.

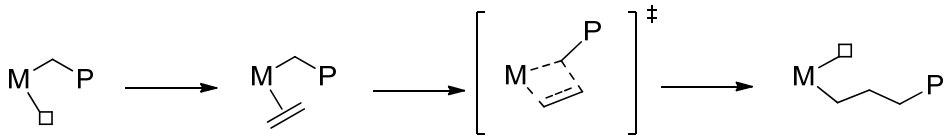

Scheme 6: Cossée mechanism (positive charge of the active species and counteranion are omitted).

Some further modifications of the *Cossée* mechanism including α-, β-, and γ-agostic interactions, stabilizing the cationic species were proposed. Finally the *Modified Green-Rooney* mechanism which is today the accepted one was reported (Scheme 7).[75-81]

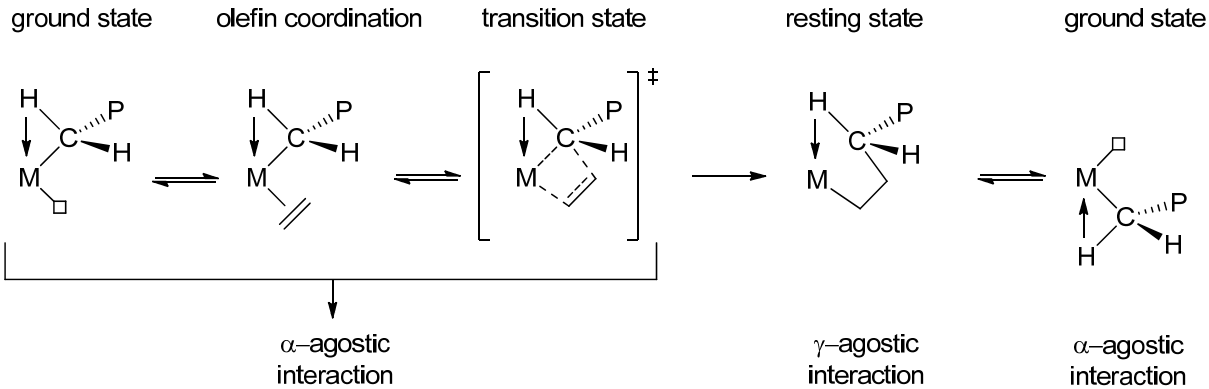

Scheme 7: *Modified Green-Rooney* mechanism (positive charge of the active species and counteranion are omitted).

In addition to the already mentioned steps for the *Cossée* mechanism, in the *Modified Green-Rooney* mechanism α-agostic interactions are proposed in the ground and transition state. After the migratory insertion a γ-agostic stabilization which can be again transformed to the ground state with the α-agostic interaction is present.

2.6 Stereo- and Regiochemistry in Metallocene-based α-Olefin Polymerization

2.6.1 *Stereo- and Regiocontrol in the Homogeneous Polymerization of Propene to iPP*

In case of the coordination polymerization of prochiral olefins (e.g. propene and the higher homologue α-olefins) each insertion step generates a stereogenic center. The enantiofacial selectivity of the olefins is controlled in two ways. One of them is called chain-end control. The last inserted monomer generates the stereogenic center, triggering a specific orientation of the polymer chain.[82] The next olefin is coordinated with its methyl group in an *anti* selective way to the growing polymer chain. Hence the last stereogenic centre induces a preferred selection of one enantioface. To be more precise, a *si* polymer chain (last inserted monomer was *si*-coordinated) prefers a *si*-coordination of the next monomer. The chain-end control only leads to a low enantiofacial selectivity ($\Delta\Delta E^{\ddagger} \approx 2$ kcal·mol^{-1}).[83] For example Cp_2MCl_2 (M = Ti, Zr and Hf) can produce PP via this chain-end control mechanism with increased stereoselectivity only at temperatures far below 0 °C.[12, 84] Even at low temperatures the stereoselectivity is not high enough to get isotactic sequences longer than 12 monomer units.[5] This affords PP with low crystallinity and low melting transitions.

The other mechanism controlling stereoselectivity is enantiomorphic site control. The direct control of the ligand itself on the enantiofacial selectivity was determined by several groups. To exclude the influence of the growing polymer chain the first insertion of a propene monomer into a Ti-CH_3 or a Zr-CH_3 bond of several C_2-symmetric ligands (e.g. $Et(Ind)_2$) was calculated.[85, 86] Indeed the energy difference between the *re*- and the *si*-coordination of the propene monomer is usually smaller than 1 kcal·mol^{-1}, due to only minor steric interaction of the methyl group of the coordinated propene with the ligand skeleton for both enantiofaces. Experimental results for insertion of the first propene monomer into the metal alkyl bond also support the nonstereoselective insertion of the first propene molecule.[87, 88] An increased energy difference in the enantiofacial selectivity was calculated for longer alkyl chains.[85] The chirality of the complex affords a favored orientation of the chain into the less crowded region (Figure 6). The polymer chain itself influences the coordination of the propene monomer. The most favored coordination is analogue to the chain-end control mechanism in an *anti* selective way, with the methyl group of the propene being away as far as possible from the β-carbon and the subsequent atoms of the polymer chain.

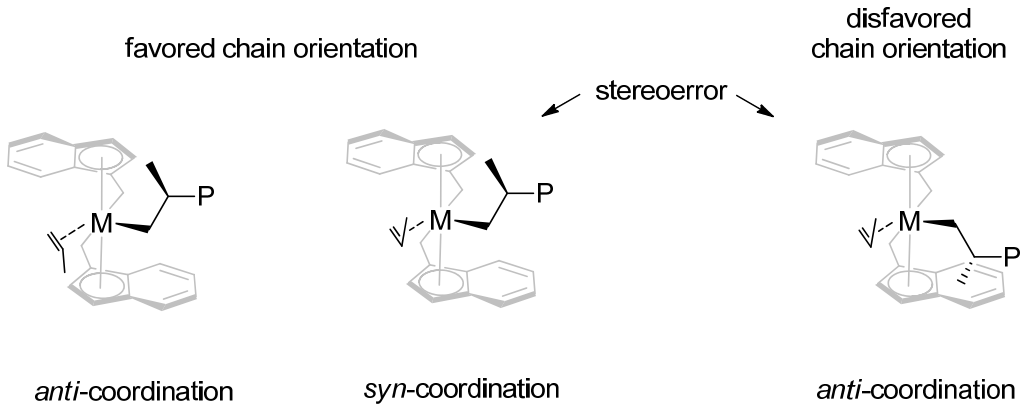

Figure 6: Enantiomorphic site control in C_2-symmetric *ansa* metallocenes.

In principal there are two ways of a direct stereoerror formation (Figure 6). One proceeds via the *syn*-coordination of the propene monomer while the polymer chain is oriented into the less crowded region.[85, 89, 90] However, also the unfavored orientation of the chain together with the *anti*-coordination of the propene monomer can generate a stereoerror.[91, 92] The π-complex of latter intermediate has the highest energy, but compared to the stereoerror producing intermediate, with the *syn*-coordinated monomer and favored chain orientation, the four centered transition state is significantly less sterically hindered. Therefore the formation of a stereoerror via the *syn*-coordinated monomer and the favored chain orientation was assumed to be unsuitable for the successive monomer insertion.[93]

Activated C_2-symmetric metallocenes can also show a decrease of stereoselectivity with decreasing propene concentration.[94] As the direct enantiofacial selectivity with afore mentioned mechanism cannot explain this behavior, investigations revealed a further reaction, the chain end epimerization to be the reason therefore. Equilibrium of two states, catalyst with and without coordinated propene molecule, is always present during the polymerization reaction. In addition metallocene cations with a σ-bonded polymer chain are known to undergo an epimerization reaction.[95] Decreasing propene concentration increases the amount of catalyst species without a coordinated olefin (epimerization catalyst), resulting in a higher amount of stereoerrors. For this epimerization reaction several mechanisms were proposed. *Busico et al.* proposed a mechanism starting with a β-hydrid transfer to the metal (2.7.1), forming a metallocene olefin complex (Scheme 8).[96] In plane rotation of the propene monomer (for the required *cis* orientation of the olefinic CH_2-group and the hydrogen atom bonded to the metal), secondary insertion, rotation around the M-C_α bond, and again β-hydrid transfer to the metal leads to the olefin complex with a propene, coordinated with the opposite

enantioface (enantiofacial switching). After an in plane rotation of the propene monomer and the primary insertion the configuration of the last inserted monomer unit is inverted.

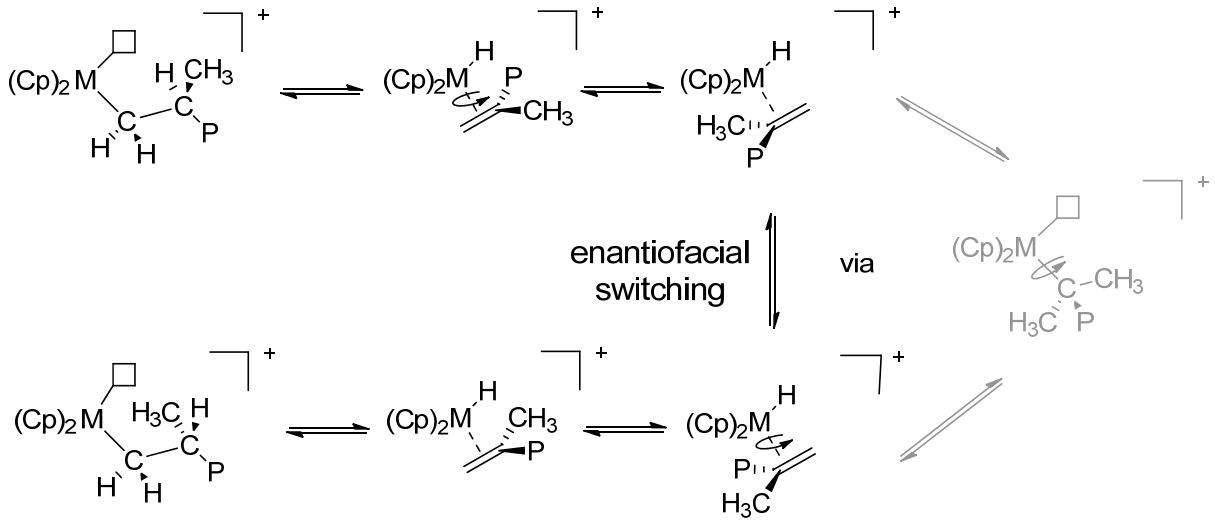

Scheme 8: Busico´s proposed mechanism for the chain end epimerization.

A different mechanism proposed by *Resconi et al.* proceeds via the formation of a dihydrogen/ η^3-allyl complex.[97] In this case the enantiofacial switching is obtained by the allyl rotation. Further labeling studies using CH_2=$CD^{13}CH_3$ for polymerization with C_2-symmetric metallocenes by *Bercaw et al.* revealed *Busico´s* mechanism to be more likely.[98]

Besides stereo- also regioselectivity has a big influence on the microstructure of the polymer chain, thus affecting the physical and chemical properties of the polymer. A propene monomer can be incorporated either in a 1,2- (primary) or in a 2,1-selective (secondary) way (Scheme 9).[5] Both, electronic and steric reasons are responsible for higher selectivity of the 1,2 propene insertion.[99] In propene polymerization reactions the formation of the 2,1-regioselective π-complex is calculated to be energetically favored due to the inductive effect (+I) of the methyl group.[89] However, the transition state of the 1,2-regioslective insertion reaction is calculated to be preferred. The reason therefore is the arising positive partial charge at the C-2 carbon atom which can be stabilized by the inductive effect of the methyl group. Additional steric hindrance on the Cp-fragment can destabilize the π-complex and the transition state in case of a 2,1-regioselctive coordination. Hence both, electronic and steric reasons afford an overall lower activation barrier for the 1,2-regioselective insertion. The amount of regioerrors is dependent on the polymerization conditions (e.g. temperature and propene concentration) and the ligand structure. The enantiofacial selectivity of a regioirregular insertion is generally opposite to that obtained in the regioregular insertion.[92] This behavior was calculated for the well-studied zirconocenes with a $Et(Ind)_2$ ligand to be a

result of a direct steric interaction of the methyl group of the coordinated propene monomer with the ligand skeleton.[91] This means in case of the (R, R) enantiomer of the complex for the primary insertion a preference of the *re*-coordinated monomer, whereas in case of the secondary insertion a higher selectivity for the *si*-coordinated propene monomer is obtained.

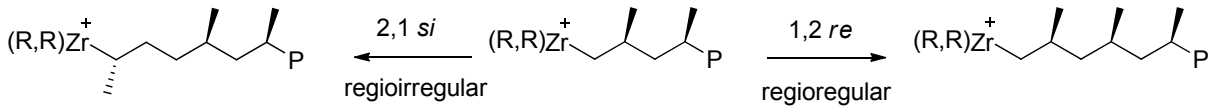

Scheme 9: 1, 2- and 2, 1-regioselective insertion reactions of a C_2-symmetric metallocene during propene polymerization (S, S enantiomer and counteranion are omitted).

Compared to the rate of insertion following a primary insertion, that following a secondary insertion is decreased and often results in chain transfer reactions (2.7).[100] Metallocenes with decreased regioselectivities produce in general PP with low molecular weight at low activities. Consecutive insertions after a regiomisinsertion are regioselective and can result in two different structural motives regarding stereoselectivity, which can be distinguished via ^{13}C NMR spectroscopy.[101-103] Those are the erythro (e) and the threo (t) units (Scheme 10). Besides these, a third one, the 3,1-unit can be obtained.[102, 104] Formation of the 3,1-unit was proposed by different authors via different mechanisms, but most likely is the one shown in Scheme 10, because of the lowest energy barriers in the two activation steps.[105, 106] It proceeds via a unimolecular isomerization process and is thus preferred over the bimolecular propagation with decreasing propene concentration. The lower the propene concentration, the higher is the amount of the conversions from a 2,1- to a 3,1-unit.

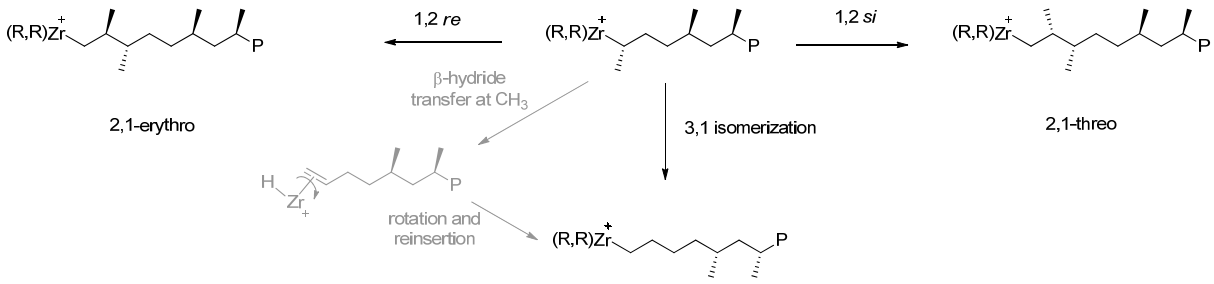

Scheme 10: Formation of 2,1-erythro, 2,1-threo and 3,1-units during the polymerization of propene with a C_2-symmetric metallocene (S, S enantiomer and counteranion are omitted).

Besides lower propene concentration, also higher polymerization temperature increases the amount of 2,1 → 3,1 isomerization reactions. The different steps during the isomerization are a β-hydride transfer reaction forming a π-complex, rotation of the polymer chain and reinsertion of the allylic chain end.

2.6.2 *Hf and Zr: The Difference in Regio- and Stereocontrol*

The available data for a comparison between zirconocenes and hafnocenes concerning regio- and stereoselectivity is limited. Especially for the hafnocenes only few reports are available, probably due to the lower activity observed in MAO activation. Another problem is the lack of precise analytic data in earlier publications. Particularly the determination of the regioerrors was often not performed as high resolution NMR spectroscopy was not available. Nevertheless, there are some examples showing a specific trend. Earlier publications often report on slightly higher melting transitions for polymers produced with the C_2-symmetric hafnocenes compared to these produced with the corresponding zirconocenes.[66] The explanation therefore was a higher stereoselectivity. But evaluating these reports one should consider higher regioselectivities leading to the higher observed melting transitions. However, also directly determined higher stereoslectivities and regioselectivities are reported for some C_2-symmetric hafnocenes which are similar to the values of the corresponding titanocenes.[107] Very recently, the differences in stereo- and regioselectivity for Cp_2MCl_2 (M = Zr, Hf) were theoretically examined. The calculated trends are in accordance with former experiments concerning regioselectivities, and differ slightly with respect to stereoselectivity.[108]

2.7 **Chain Release Reactions**

The polymerization of propene with *ansa*-metallocenes is a catalytic reaction, including chain propagation and chain release reactions. The equilibrium constants of these reactions strongly influence the molecular weights of polymers obtainable with metallocene catalysts. As already mentioned in chapter 2.6.1 for the propene polymerization there are two possible regioselectivity insertion products. These intermediates can afford, as a result of different chain release reactions, polymer chains with several end- and starting groups. The miscellaneous chain release reactions are therefore discussed in the following chapters.[100]

2.7.1 *β-Hydride Transfer*

One of the most common chain transfer reactions leading to the chain release is the β-hydride transfer of the σ-bonded polymer chain, followed by a dissociation of the resulting π-complex. This transfer reaction is known to occur in two ways. One is the transfer of the β-hydride directly to the metal (unimolecular), the other the transfer of the β-hydride to the next

coordinated monomer (bimolecular). In both cases, the new polymer chain has an *n*-propyl starting group.

2.7.1.1 β-Hydride Transfer to the Metal

A direct transfer of the β-hydride to the metal generates a hydride metallocene complex with the coordinated olefinic chain end of the polymer. In principle, this π-complex can undergo an associative or a dissociative release of the polymer chain (Scheme 11).

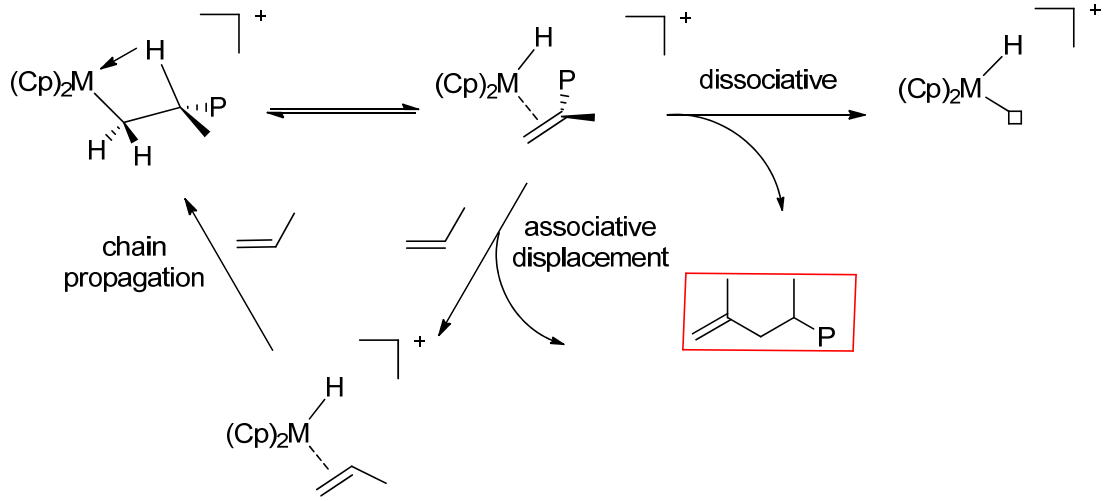

Scheme 11: β-Hydride transfer to the metal after a 1,2-insertion (counteranion is omitted).

The dissociative replacement of the chain was calculated to be unlikely having a high energy barrier and affording an even more unstable product as the already unstable hydride metallocene olefin complex.[109, 110] Associative replacement by propene or the reinsertion of the olefin polymer chain, which can also result in the already discussed epimerization reactions, is much more preferred. If the insertion of the last monomer proceeded in a 1,2-regioslective way the chain end will be for both discussed routes a vinylidene. After a 2,1-insertion there are two carbon atoms in β-position to the metal, the methylene and the methyl group, leading after the hydride transfer to a 2-butenyl or a 3-butenyl polymer chain end respectively. However, experimental investigations of *rac*-C_2H_4(4,7-Me_2-Ind)$_2$$ZrCl_2$/MAO showed these transfer reactions to occur via transfer of the β-hydride to the monomer and will be therefore discussed in the following section.[5, 100, 111]

2.7.1.2 β-Hydride Transfer to the Monomer

β-Hydride transfer to the monomer was calculated for sterically relatively undemanding C_2-symmetric complexes to have a lower activation energy barrier compared to the

unimolecular pathway.[112] As the rate of the transfer reaction (r_t) is dependent on monomer concentration, following $r_t = k_{\beta\text{-h}} \cdot [M^+] \cdot [\alpha\text{-olefin}]$, the rate is increased with increasing monomer concentration. Chain propagation rate, following $r_p = k_p \cdot [M^+] \cdot [\alpha\text{-olefin}]$, behaves analog. Hence, an increase of propene concentration does not give polymers with significantly higher molecular weights. This behavior can be observed for different sterically undemanding C_2-symmetric metallocenes (e.g. $SiMe_2$(Benzindenyl)$ZrCl_2$).[113] Depending on the substitution pattern of the metallocene the bimolecular transfer reaction can be suppressed. Thus, the chain release is than predominantly unimolecular and an increase of molecular weight of polymers produced at higher propene concentrations can be observed (2.10.2.1). Compared to the four-membered transition state of chain propagation the bimolecular β-hydride transfer transition state is six-membered, increasing the distance of the polymer chain and the propene monomer. After a 1,2-insertion analog to the unimolecular transfer reaction a vinylidene chain end is obtained (Scheme 12).

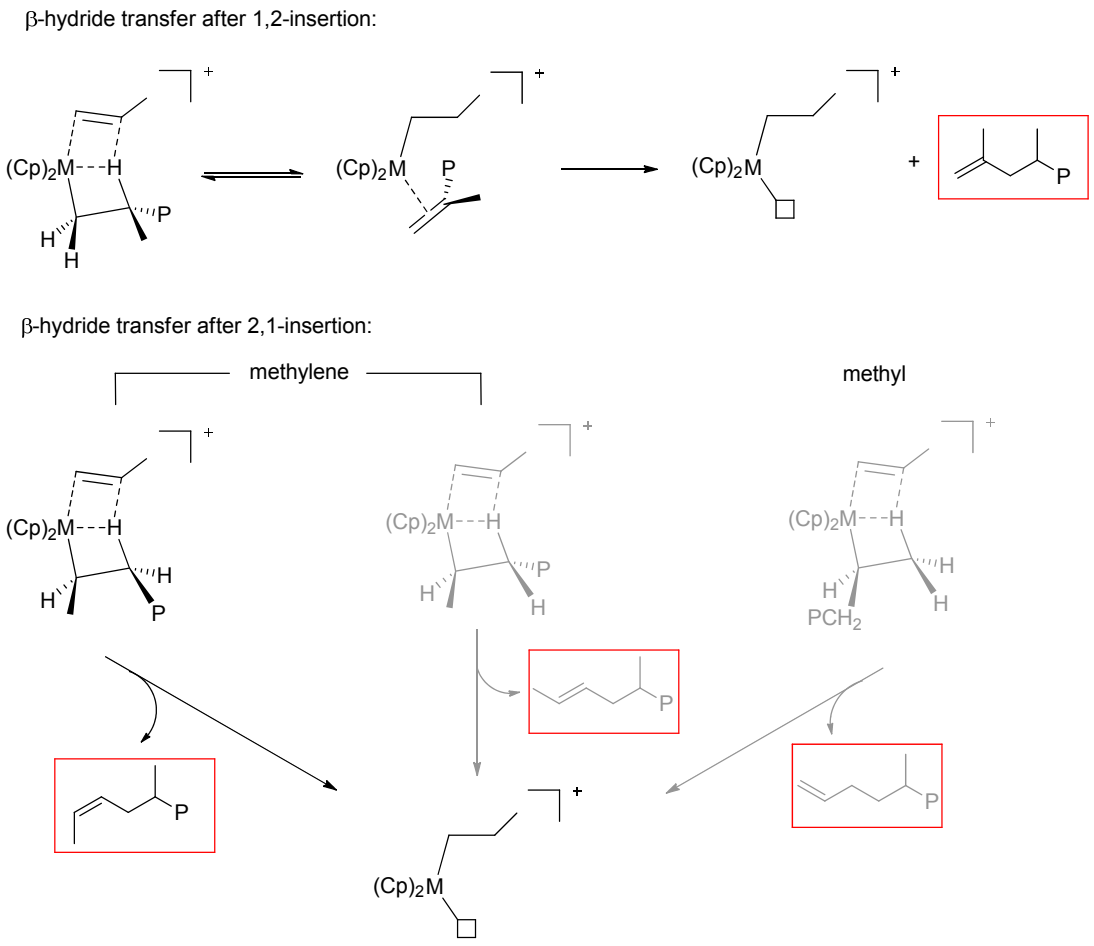

Scheme 12: β-Hydride transfer reactions after 1,2- and 2,1-insertions and formed polymer chain ends (counteranion is omitted).

If the last monomer insertion was 2,1-regioselective theoretically three different chain ends can be formed. These are *cis*- and *trans*-2-butenyl, if the β-hydride originates from the methylene, and 3-butenyl, if it is transferred from the methyl group. Experimental results of C_2-symmetric metallocene catalysts at higher propene concentration show exclusively formation of vinylidene and *cis*-2-butenyl end groups.[111] With decreasing propene concentration also the formation of allylic chain ends arising from the unimolecular β-methyl transfer (2.7.2), was observed. Neither the *trans*-2-butenyl nor the 3-butenyl chain end was detected for the studied C_2-symmetric metallocenes.

Very recently, theoretical investigations revealed that a direct interaction of the chain with the ligand skeleton in the transition states affording the *trans*-2-butenyl or the 3-butenyl chain end occurs.[109] Besides these pathways, *Talarico et al.* reported an analog pathway, with a transition state of β-hydride transfer to the monomer, having a less close contact of the β-hydride to the metal.[114] Especially for metallocenes with a more sterically demanding ligand structure this pathway is reported to be preferred as the angle on the metal ($C_{\alpha\text{-chain}}$-M-C_{olefin}) is smaller and therefore also the steric interaction of the polymer chain and the coordinated olefin with the ligand skeleton is reduced.

2.7.2 *β-Methyl Transfer*

Besides the β-hydride, also the transfer of a methyl group in β-position was revealed as an important chain release mechanism for early transition metallocenes. This was first proven with $Cp^*_2MCl_2$ (M = Zr, Hf).[115-117] This chain transfer pathway produces polymer chains with isobutyl starting groups and allyl end groups (Scheme 13). Experimental evidence and theoretical calculations suggest this transfer reaction to be unimolecular, competing with the bimolecular β-hydrogen transfer.[5, 118, 119] Especially at lower propene concentrations, the unimolecular pathway is more likely and allylic polymer chain ends are predominantly produced by sterically hindered metallocenes.

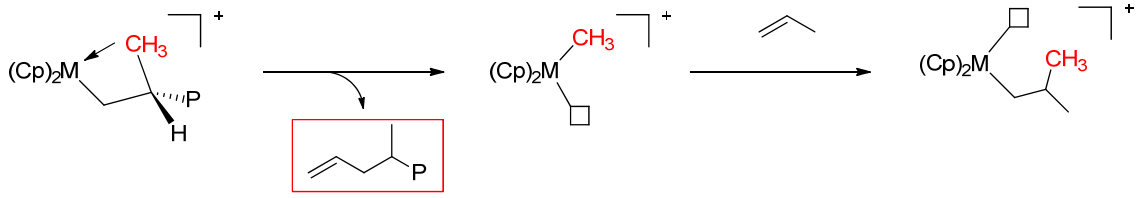

Scheme 13: β-methyl transfer to the metal after a 1,2-insertion (counteranion is omitted).

The preference for the unimolecular β-methyl transfer compared to the unimolecular β-hydrogen transfer occurs especially for sterically crowded metallocenes.[100, 120, 121]

Compared to the β-hydride transfer, in case of the β-methyl transfer the polymer chain has another conformation with a good overlap of the molecular orbitals of the methyl group and the metal. Recently an additional γ-agostic interaction was assumed to be present in this kind of chain orientation.[122] For highly substituted metallocenes the steric interaction of the chain with the substituents on the Cp moiety is lower in case of the orientation necessary for the β-methyl transfer compared to the conformation for the unimolecular β-hydride transfer (Figure 7).[117] Besides the unimolecular transfer of the methyl group some reports also suggest a bimolecular pathway.[123-125] In these studies, a dependency of the propene concentration on the β-methyl transfer was observed either via NMR spectroscopy or in kinetic investigations. However, in both investigations an unambiguous proof for the bimolecular pathway could not be given.

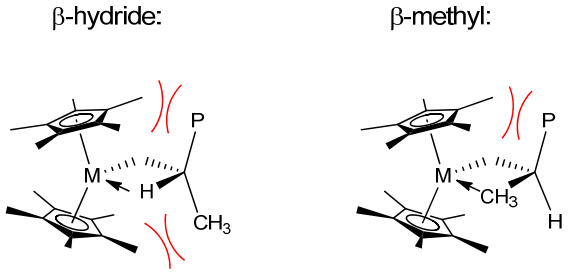

Figure 7: Chain orientation and the steric interaction occurring for β-methyl and β-hydride transfer reactions in case of sterically crowded metallocenes.

2.7.3 *Chain Transfer to Aluminum and Other Transfer Agents*

Transmetalation of the growing polymer chain to an aluminum co-catalyst can occur during the polymerization, resulting after hydrolysis in a saturated chain end. Especially by using unmodified MAO as a co-catalyst which always contains TMA the transmetalation reaction becomes very likely.[126-128] After hydrolysis, both polymer chain ends have isobutyl groups. (Scheme 14).

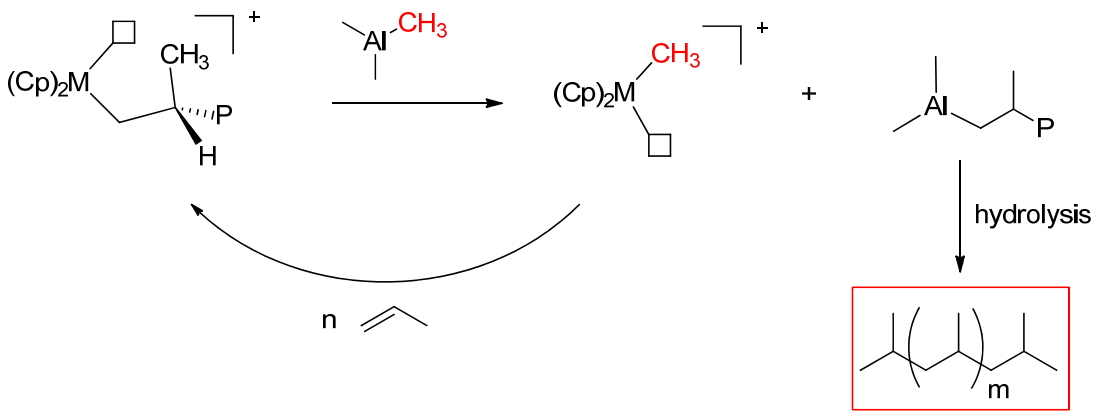

Scheme 14: Transalkylation to aluminum.

This kind of transmetalation is predominantly present in polymerization reactions for which high amounts of insufficiently shielded aluminum species are used. In case of borane or borate activation, which requires only low amounts of aluminum-based scavenger (e.g. TIBA) the transmetalation plays only a minor role. Furthermore, sterically crowded aluminum derivatives such as TIBA are better shielded against transmetalation reactions, thus lowering the probability for this kind of chain release.

Another transfer agent is molecular hydrogen. Its addition is a standard procedure to control the molecular weight of polymers produced in the polymerization process with metallocene catalysts.[129, 130] Besides the control of the chain length, hydrogen can also increase the productivity especially in case of existent resting states of the catalyst which normally reduce the observed overall propagation rate. A typical example is the 2,1-insertion slowing down the coordination and insertion of the next monomer. By adding molecular hydrogen chain transfer of these dormant states occurs. This reaction was also used to analyze the 2,1-insertion in more detail. A third possibility is the addition of transfer agents to transport the chain from one catalytic center to another.[131, 132] This process is also called chain shuttling and can be used to produce block copolymers by applying different catalysts in which at least one of them has a high selectivity for one of the added monomers. An example therefore is a copolymer of 1-octene and ethene produced with two different catalysts. One polymerizes only ethene the other affords an increased incorporation of 1-octene, and diethyl zinc as shuttling agent.[131, 132]

2.7.4 *Hf and Zr: The Difference in Transfer Reactions*

Some reports can be found concerning differences between hafnocenes and zirconocenes in their chain transfer reactions. One aspect is the higher molecular weight of polymers obtainable with hafnocenes compared to these of the corresponding zirconocenes.[66, 68, 133, 134] This behavior was ascribed to relativistic effects (2.4.5), stabilizing the 6s orbital and affording a stronger Hf-C-σ bond.[135] The relativistic expansion of the frontier orbitals mainly formed by the 5d atom orbitals is assumed to favor an overlap towards α- instead of β-agostic interactions. Both explanations disfavor β-hydride transfer in case of hafnocenes compared to zirconocenes. Recently theoretical calculations with the most simple metallocenes (Cp_2MCl_2 M = Zr, Hf) confirm the higher molecular weights of polymers produced with hafnocenes and also address the reason to a more facile β-hydride transfer in case of zirconocenes.[108] Especially after a 2,1-insertion, the activation barrier for a β-hydride transfer to the metal is distinctly higher for the hafnocene. This behavior is again assumed to be due to the more

stable Hf-C bond and the weaker β-agostic interaction for the hafnocene. Comparing the amount of β-methyl and β-hydride transfer reactions, sterically demanding hafnocenes are reported to undergo more β-methyl transfer reactions than zirconocenes.[117] The already mentioned additional transition state for the β-hydride transfer to the coordinated monomer with a less close contact of the β-hydride to the metal is assumed to become more important going from the zirconocenes to the hafnocenes. [114]

2.8 Complex- and Polymer Structure Correlation

As already mentioned for iPP, there is a connection between ligand structure of the complex and obtained polymer microstructure (2.6). A correlation between symmetry and resulting polymer microstructure was reported by *Ewen et al.* and *Kaminsky et al.* Today this is known as *Ewen´s* symmetry rules. Besides the iPP with all methyl groups located on the same side of the polymer backbone, syndiotactic, hemiisotactic and atactic polypropylene can be synthesized via metallocene catalysts of different symmetries (Table 2).[12, 17, 133, 136]

Table 2: Different complex symmetries and their polymer structure correlation.

polymer microstructure	complex symmetry	example
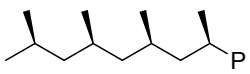 isotactic	C_2 (chiral)	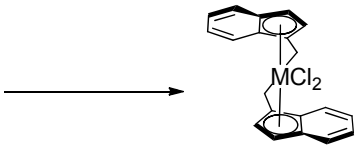
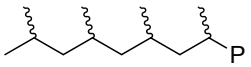 atactic	C_{2v} (achiral)	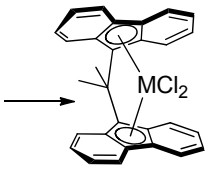
	C_s (achiral)	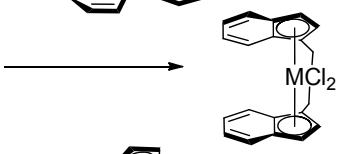
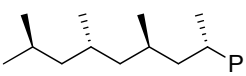 syndiotactic	C_s (prochiral)	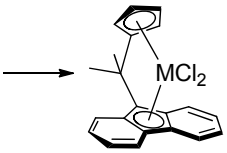
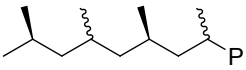 hemiisotactic	C_1 (chiral)	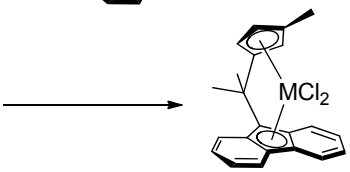

For C_2-symmetric metallocenes the two sites of the complex are homotop, in case of the C_s-symmetric metallocenes producing the syndiotactic PP thus the two coordination sites are enantiotop. Introduction of a small additional group on one side of the Cp fragment reduces symmetry of the C_s-symmetric complex. The obtained C_1-symmetric complex has diastereotopic sites affording the hemiisotactic PP. Studying these complexes with their different structures gave additional proof on the site-switching mechanism taking place during the chain migratory insertion polymerization as the formation of hemiisotactic polypropylenes cannot be explained without chain-switching. More specific microstructures can be produced with certain complexes. For example, *Rieger´s* C_1-symmetric complexes afford variable isotactic polypropylene (viPP) with elastic behavior (2.9.1). But also blocklike structures of an atactic combined with an isotactic block can be achieved using e.g. oscillating non-bridged metallocenes switching between a C_2- and a C_s-symmetry.[137]

The microstructures of polypropylene can be analyzed by ^{13}C NMR spectroscopy via the signals of the methyl carbon atoms.[138] The chemical shift of every methyl group is influenced by the orientation of the neighboring methyl groups. Two following methyl groups having the same configuration are called a meso dyad (m), if they have different configuration it is called a racemic dyad (r). Today standard ^{13}C NMR measurements can resolve the microstructure of polypropylenes up to the pentad level. Ten of these pentad units are principally obtainable (Figure 8).

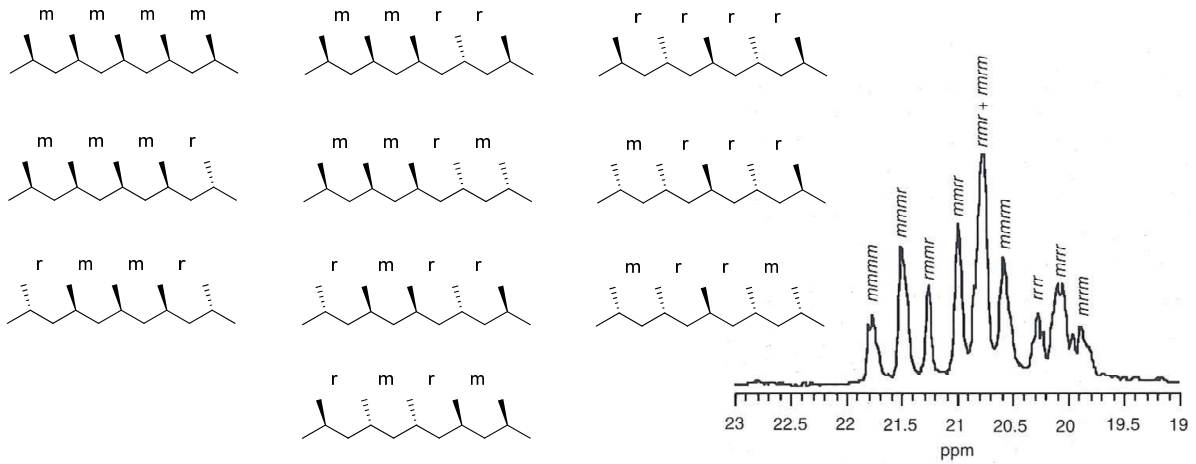

Figure 8: The ten available pentad units of PP with ^{13}C NMR spectroscopy.[139]

The methyl groups of an iPP produced with a C_2-symmetric metallocene shows predominantly the signal of the mmmm-pentad. Furthermore some minor signals from methyl groups of stereo- and regioerrors can be present. Chain end control and enantiomorphic site

control in iPP can be distinguished by the kind of produced stereoerrors and their corresponding mmmm-pentads.[12, 83] In case of chain end control the typical produced stereoerror is the mmrm and mmmr having a ratio of 1:1. The misinserted monomer directs the coordination of the next monomer. Hence the next monomer is incorporated into the chain by choice of the same enantioface compared to the monomer which produced the stereoerror. This behavior affords the mentioned pentad units. In contrast, a complex that polymerizes via the enantiomorphic site control coordinates the next monomer after a misinsertion again with the enantioface preferred by the indirect control of the ligand structure. The produced stereoerrors generates mmrr and mrrm pentad units with a ratio of 2:1.[5]

2.9 **Elastic Polypropylene**

Elastic PP (ePP) is a thermoplastic material that can be processed in the molten state. Conventional rubbers which are chemically crosslinked show high elasticity and a good elastic recovery but they cannot be molten due to the chemical crosslink between the different chains.[140] ePP having both, the advantage of the processability of a thermoplastic material and the behavior of an elastic material, thus counts to the group of thermoplastic elastomers (TPE). Different ways have been developed to obtain polypropylene with elastic behavior (2.9.1). All of them have in common a reduction of the crystallinity in order to obtain small crystallites acting as physical crosslinkers in an otherwise amorphous polymer matrix. There are two different possibilities to disturb the crystallization of the polypropylene. One is to introduce other co-monomers (e.g. ethene), the other to use complexes polymerizing propene with a higher amount of stereoerrors. Detailed information about the correlation between mechanical behavior and microstructure can be achieved by combining stress-strain measurements with ^{13}C NMR spectroscopy and atom force microscopy (AFM) (Figure 9).[141, 142] Stress-strain measurements can show the elasticity of the polymer, the amount of the mmmm-pentad can be determined via ^{13}C NMR spectroscopy and finally, AFM affords the information of the amount and size of the crystalline phase. From these results, a model explaining the elastic behavior induced by decreased crystallinity can be received. As shown, a lower amount of the mmmm-pentad results in reduced crystallinity. With a low level of the mmmm-pentad (below 40 %) only small crystalline regions are visible. In model, the situation changes from folding crystals, which are formed by the intramolecular backfolding of the polymer chain to the so called fringed micelles. For backfolding the length of the isotactic segments has to be long enough. With increasing amounts of stereoerrors the length of the

isotactic segments is reduced disturbing the backfolding in the polymer chain. Small crystals, so called fringed micelles, are formed at a low level of isotacticity due to an intermolecular interaction of the short isotactic segments of the polymer chains.

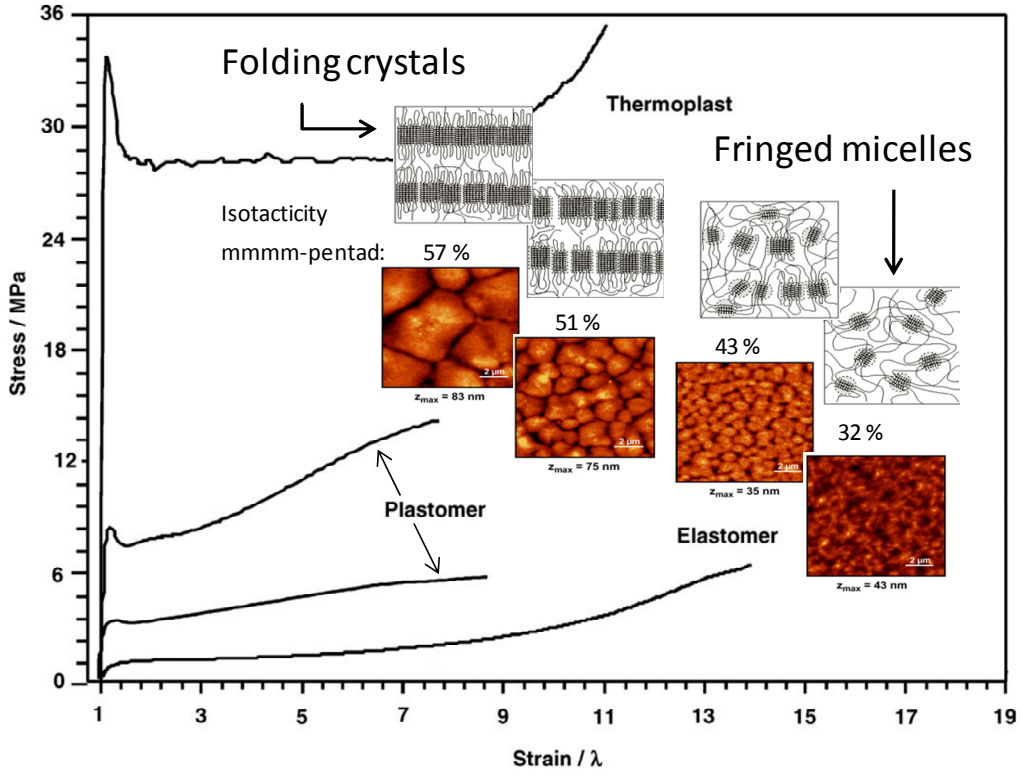

Figure 9: Correlation of the polymer microstructure and the mechanical behavior and the model behind.

2.9.1 *Different Ways for the Production of Elastic PP*

First ePP was already discovered by *Natta* in the very beginning of the *Ziegler-Natta* polymerization catalyst development in the 1950s as a heptane soluble fraction.[143] He assumed this fraction to be a stereoblock polymer consisting of isotactic and atactic sequences due to its intermediate behavior in solubility and mechanical tests ranging between that of atactic and isotactic polypropylene. The development of homogeneous metallocenes allowed the possibility to produce microstructures different than isotactic. Reducing symmetry of metallocene complexes, *Chien et al.* obtained an unsymmetric complex (Scheme 15).[144-146] This C_1-symmetric complex can produce ePP. As the underlying mechanism, two different states of the catalyst, one producing atactic the other isotactic sequences was proposed. Additionally these are converted into each other with a lower rate than each of the propagations, leading to either an isotactic or atactic sequence. This polymerization

mechanism finally gives blockstructures with isotactic and atactic sequences resulting in the observed elastic behavior of the polymer.

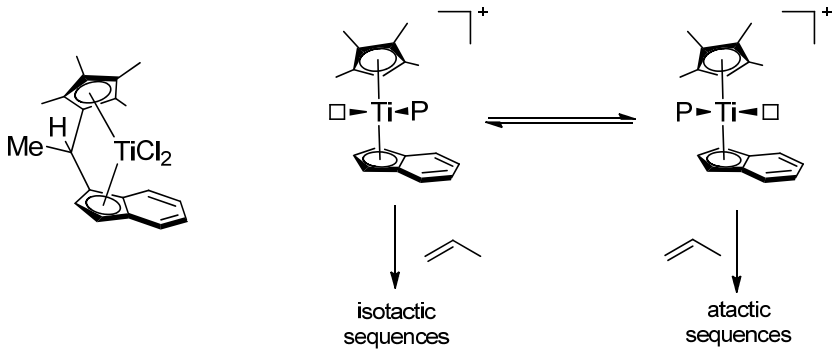

Scheme 15: C_1-symmetric titanocene from *Chien et al.* and its proposed polymerization mechanism affording ePP (mechanism: bridge is omitted for clarity).

Using CMe_2 and $SiMe_2$ bridging units instead of a CMeH bridge and a Cp ancillary ligand instead of a Cp* *Collins et al.* studied the different metallocenes (Ti, Zr and Hf) thereof and possible propagation models for the production of ePP. [134, 147] Probability calculations for the different models were conducted and compared with the experimentally determined pentad distribution (by ^{13}C NMR spectroscopy) of polymers produced by these complexes. As a result for these metallocene catalysts the previously assumed blocklike structure was shown to be more random.

As already described, a change in the substitution pattern of the C_s-symmetric metallocene [2-(9-η^5-fluorenyl)-2-(η^5-cyclopentadienyl)propane] zirconium dichloride by introduction of a methyl group on the cyclopentadienyl ligand results in complexes polymerizing propene to hemiisotactic poylypropylene.[136] A *tert*-butyl group instead of the methyl group blocks one coordination site of the complex for chain migratory insertion affording iPP for these C_1-symmetric complexes (Scheme 16).[148]

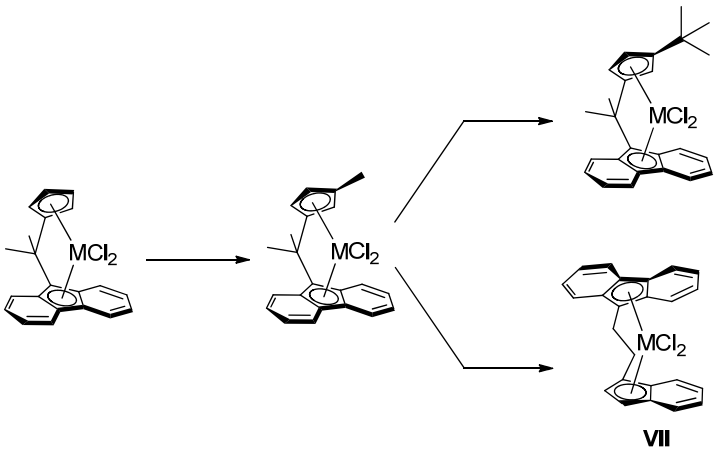

Scheme 16: From the C_s-symmetric complex to C_1-symmetric complexes producing either iPP or ePP (**VII**).

Changing the bridge from CMe_2 to ethylene and the cyclopentadienyl ligand to indenyl gave the C_1-symmetric complex **VII** which afforded polymers with microstructures in between these of 3-methyl and 3-*tert*-butyl substituted complexes.[149] Interestingly the amount of stereoerrors and thus the microstructure is strongly dependent on the propene concentration. *Rieger* proposed a polymerization mechanism for these complexes forming PP with different stereoregularities with varying propene concentration. The main reason for this behavior is assumed to be caused by the two different sites of the complex having different stereoselectivity combined with a chain migration, possible after each insertion and influenced by propene concentration and polymerization temperature. With these complexes, the amount of stereoerrors and thus the microstructure and the mechanical behavior of the PP can be controlled by propene concentration and T_p. Unfortunately polymers with only low molecular weights are obtainable limiting their application as an elastic material.

Higher molecular weights are accessible with C_1-symmetric metallocenes based on C_2-symmetric bisindenyl complexes by reducing symmetry through the introduction of a substituent on one of the indenyl ligands.[150] These complexes also show a small dependency of propene concentration. A drawback is the required separation of the *rac*- and *meso*-like isomers analog to the C_2-symmetric complexes which was for these unsymmetric complexes reported not to be quantitative. The *meso*-like isomer produces only low molecular weight PP. In addition the microstructure of the obtained polymers is also ascribed to more randomly blocklike structures (atactic-isotactic) and, molecular weights of most of the produced polymers are still too low.

Further improvement of molecular weight and propene concentration influence was achieved by *Rieger et al.* by new C_1-symmetric complexes on the basis of metallocene **VII** (Scheme 17).[18] A detailed study concerning the pentad distribution and the propene concentration dependency was performed in order to reveal the polymerization mechanism underlying these complexes. With increasing propene concentration, ^{13}C NMR spectroscopy shows a deacrease of the mmmm pentad combined with an increase of the pentads typical for isolated stereoerrors (mmrr, mmmr and mrrm). With a mmmm pentad over 40 %, the ratio of mmrr:mmmr:mrrm is 2:2:1 which is expected for isolated stereoerrors. Further increase of the propene concentration results in lower amounts of the mmmm pentad (< 40 %) and longer stereoerror sequences arise. An additional indication for isolated stereoerrors is the very low amount or absence of the mrmr pentad, which is typically detected in case of atactic polymers.[151] The amount of the mmmm pentad can be varied in a broad range (20 – 70 %), depending on the polymerization conditions. This high concentration dependency and the

^{13}C NMR results underline the shown mechanism and the formed microstructure of ePP. The catalyst is a "dual site" catalyst as it has two different sites being different in stereoselectivity; while one site is stereoselective the other is majorly not. After the coordination of a monomer on the stereoselective site (right site of the depicted complex, Scheme 17) and its insertion a further isotactic unit is formed. Afterwards the polymer chain rests on the sterical more hindered site and can undergo a so called chain back skip. The stereoselective site is free again and a coordination and insertion produces a further isotactic unit. A stereoerror is only produced if the chain back skip is slower than the coordination and insertion of the next propene monomer (blue cycle). In case of high propene concentration and lower temperatures, the rate of formation of the isolated stereoerrors, relative to the rate of formation of the isotactic sequences, becomes faster and therefore longer stereoerror sequences arise. The amount of stereoerrors and thus the length of the isotactic sequences, which is important for the elastic behavior of the polymer, can be controlled by propene concentration and temperature. Besides the shown studies also theoretical investigations with similar complexes and the determination of the chain back skip rate give further proof for the depicted mechanism.[69, 152]

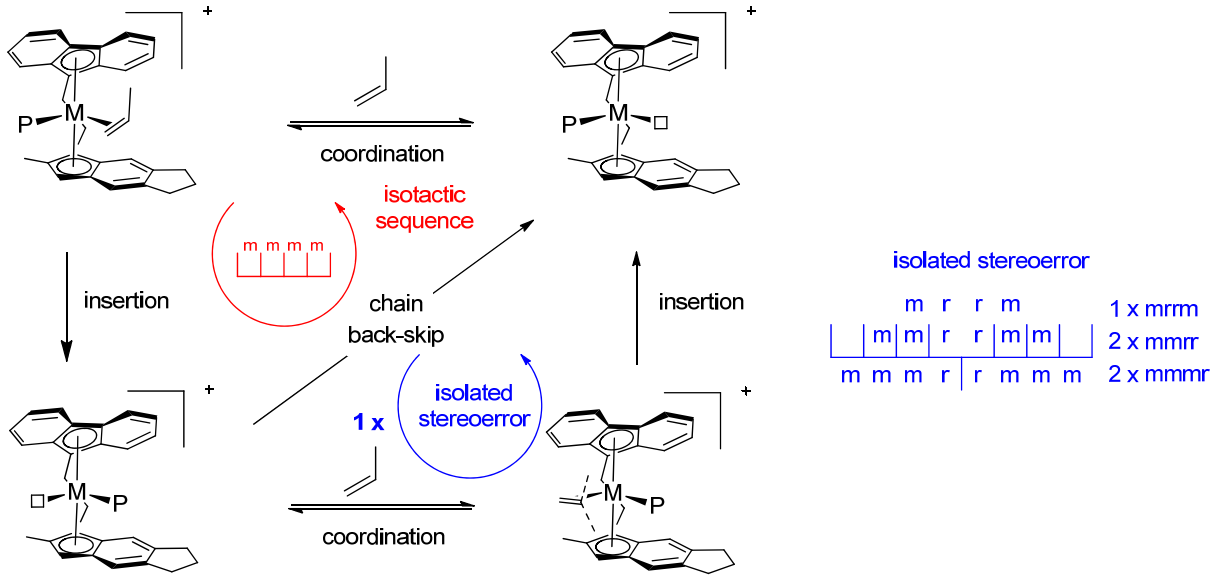

Scheme 17: Polymerization mechanism of *Rieger's* C_1-symmetric metallocenes.

Waymouth et al. obtained ePP with an isotactic-atactic blockstructure employing unbridged metallocenes of the type (2-Ph-Ind)$_2$ZrCl$_2$.[137, 153-155] Absence of the bridging unit allows an isomerization between the *meso*-form, being the atactic state, and the *rac*-form producing the isotactic sequence. Important for such complexes is the rate of isomerization. The 2-phenyl substituent slows down the isomerization rate compared to the unsubstituted complex in order

to allow several monomer insertions on the respective site of the complex. Concentration and temperature dependency for these systems is contrary to above discussed C_1-symmetric metallocenes. Higher temperature increases the isomerization rate affording shorter isotactic sequences and a lower amount of the mmmm-pentad. Increasing propene concentration results in a faster propagation affording longer isotactic sequences and a higher amount of the mmmm-pentad.

Another possibility for the production of ePP not based on a small degree of crystallinity is the use of high molecular weight atactic PP (aPP). The elastic behavior of these polymers arises from the entanglement of the long polymer chains which must have at least a M_n over 100 000 g/mol to behave as a nonsticky elastic material. Complexes forming these kind of polypropylenes are the C_{2v}-symmetric $SiMe_2(Flu)_2MCl_2$ (M = Zr, Hf) metallocenes or $Cp^*Ti(OCH_2\text{-}CH{=}CH_2)_3$.[156, 157] Main reason for the high molecular weights of the polymers formed with these C_{2v}-symmetric complexes is the reduced rate of the β-hydride transfer reaction due to their high steric hindrance, while having at the same time a relatively fast propagation rate. However, the mechanical properties of these polypropylenes are different from the slightly crystalline ePP. A polymer produced with the C_{2v}-symmetric metallocene shows good elastic recovery up to the yield point (e.g. 300% strain) afterwards disentanglement occurs and a viscous flow of the polymer starts which decreases the elastic recovery.[158] In case of the slightly isotactic polymers, depending on the isotacticity, the stress at the yield point is higher and reached more readily. Afterwards, depending on crystallinity and molecular weight stretch induced crystallization processes take place (being more pronounced with higher crystallinity) increasing again stress with increasing strain.

2.9.2 *Rieger´s C_1-symmetric Metallocenes and the Influence of the Co-catalyst on the Microstructure*

Using C_1-symmetric complexes similar to that depicted in Scheme 17 and comparing the different influence of the co-catalyst, a strong influence of the aluminum reagent in case of MAO activation can be seen. An increased amount of MAO reduces activity and molecular weight whereupon isotacticity is not changed.[159, 160] Activation of the corresponding dimethylated catalyst precursor with $[CPh_3][B(C_6F_5)_4]$ **V** gives higher molecular weights, higher activities and also higher isotacticities. The difference was ascribed to an additional stereoerror generating mechanism. Besides the mentioned back skip mechanism there are principally two processes which can form the stereoerrors with this kind of complexes. One of them is chain-end epimerization which could be ruled out with deuterium labeled propylene

polymerization studies. The other mechanism which was proposed to occur for these complexes in case of MAO activation is a transfer of the growing polymer chain to an aluminum derivative being most presumably TMA, acting as a shuttling agent.[141] There are always two enantiomers of the metallocene catalyst present (R and S), having different enantiofacial selectivity on the stereoselective site of the complex. A shuttling of the polymer chain by TMA from one enantiomer to the other generates a switch of the enantiofacial selectivity and thus a single stereoerror is generated. This mechanism is especially preferred for higher amounts of aluminum reagent and such transfer processes can also explain lower molecular weights and lower activities.

Besides the polymerization behavior also the microstructure of the polymer was shown to be influenced by the choice of the co-catalyst.[142] Borate activation forms more homogeneous distributed isotactic blocks compared to co-catalysts such as MAO. These differences in microstructure also result in the formation of different crystalline modifications. In general for PP α-, β-, γ- and the smectic-form are reported (2.10) whereas metallocene produced PP usually consists of the α- and γ-form. ePP produced with these C_1-symmetric metallocenes by MAO activation crystallizes in a mixture of α- and γ-modicication with slight preference for the α-modification. In case of borate activation the γ-modification is preferred and intensively increased with higher amount of the mmmm-pentad. As a result also the mechanical behavior of the polymers was shown to be influenced.[142]

2.9.3 *Hf and Zr: The Difference in the Formation of ePP*

Besides the microstructure, the elastic behavior is controlled by the molecular weight which also ensures a good elastic recovery of the polymer. For the C_1-symmetric metallocenes (Scheme 17) two facts are obvious. Use of $[CPh_3][B(C_6F_5)_4]$ **V** as co-catalyst results in similar or even higher productivities for the hafnocene compared to the corresponding zirconocene. In addition stress-strain measurements clearly show significantly improved elastic recovery for PP with higher molecular weight, reaching values comparable to commercially available TPEs like Kraton® (Figure 10).[68] These ultrahigh molecular weight polypropylenes above 1 000 000 g/mol are only accessible with the C_1-symmetric hafnocene, not with the corresponding zirconocene.

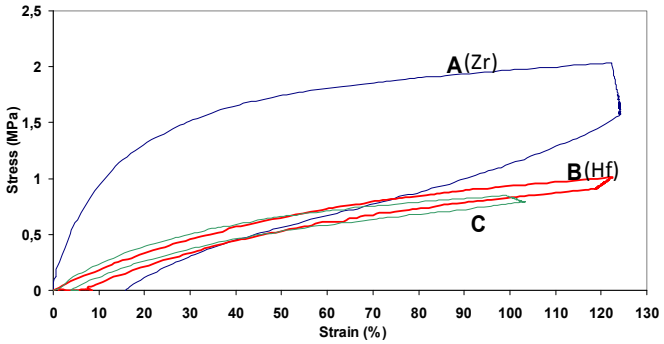

A: ePP (M_w 250,000 g·mol^{-1})

B: ePP (M_w 1,600,000 g·mol^{-1})

C: Kraton® (SBS)

Figure 10: Stress-strain hysteresis curves for ePP with different M_w compared to Kraton®.

2.10 **High Melting Isotactic Polypropylene**

iPP is known for a long time and today predominantly produced by ZN-catalysts. Beside these catalysts, it can also be made by metallocene catalysis. Latter can produce iPP with an even higher isotacticity but a generally lower melting transition. One of the reasons therefore is the difference in the distribution of the stereoerrors. iPP produced with ZN-catalysts has more a block-like structure with longer isotactic sequences linked to sequences with more stereoerrors. In contrast the metallocene-produced PP has a statistical distribution of the stereoerrors. Hence, the isotactic sequences for the metallocene PP are shorter affording the lower melting transition at similar mmmm-pentad levels.

iPP is a semicrystalline material and the crystalline part is composed of chains with a 3_1 helical conformation. Depending on the polymer properties such as microstructure, M_w and PDI, and on the processing conditions different forms of the crystalline part are generated during the crystallization, being α-, β-, γ- and the smectic-form.[161-164] In highly iPP predominantly the α-form is generated. The α-form is the thermodynamically stable form with a cross-hatched structure and a good mechanical strength, but suffering of toughness especially at lower temperatures. The β-form is a thermodynamically metastable form and in ZN-catalyst produced PP present, in an extent depending additionally on the processing conditions. Compared to the α-, the β-form shows improved elongation at break and impact strength.[165] The amount of the β-form can be increased by adding β-nucleating agents or via applied shear forces during the crystallization process.[166-169] Shear forces induce the formation of oriented α-nucleis affording the growth of the β-crystals on their surface.[169] The formation of the β-form in polymers produced with ZN-catalysts is assumed to proceed via an interaction of long isotactic with more atactic chains.[170]

For iPP produced with metallocenes, depending on the amount of stereoerrors, the α-form coexists with a variable amount of γ-form.[171] Compared to α-, the γ-form exhibits a more

densely packed unit cell, which may also contain some stereodefects.[172-174] The more stereoerrors, the shorter the isotactic sequences and the less α-form is formed during the crystallization. γ-form or a disordered α-form is generated instead.[175] The amount of the γ-form is also dependent on the amount of 2,1-regioerrors.[176, 177] Additionally it is influenced by the crystallization temperature and in some extent by the molecular weight. Low molecular weight metallocene-generated iPP was shown to form less γ- and instead more α-form due to an accelerated growth rate of the α-form.[175]

Beside the two commonly used catalysts, activated metallocenes and ZN-catalysts, which will be discussed in the following sections, very recently, salalen titanium complexes were reported to produce highly isotactic PP with a melting transition of up to 170 °C.[178] This is the so far highest reported melting transition for unextracted or not annealed iPP. This polymer was generated with the mentioned complex at room temperature at a propene pressure of 33.5 psig and short reaction times (30 s). Beside the high melting transition activity is reported to exceed 10 000 kg PP/(mol(Ti)·h). In contrast, the polymerization reaction with the same catalyst in liquid propene afforded during 13 to 14 h a polymer with M_w of 291 000 g/mol and decreased T_m of 168 °C. Unfortunately productivities have not been reported. In addition M_w of the polymer with the highest melting transition (171 °C) is not reported but according to the conditions and the results moderate or low molecular weights (below 200 kg/mol) can be assumed.

2.10.1 *State of the Art Ziegler-Natta Catalysts*

Since their discovery the heterogeneous *Ziegler-Natta* catalysts have undergone a vast development. In principle, today a ZN-precatalyst consists of a support (e.g. activated magnesium chloride), titanium tetrachloride and an internal donor.[179, 180] For the polymerization reaction, the co-catalyst comprising an aluminum alkyl (e.g. $AlEt_3$) and an external donor are added. Latter is unnecessary for some internal donors. The internal and the external donor are known to influence the stereoselectivity, the molecular weight distribution and the hydrogen response. Latter is important to control the molecular weight of the resulting polymer. Besides the components itself, also the architecture of the catalyst particle influences the polymerization behavior (e.g. activity or polymer particle size distribution). The architecture of the catalyst is controlled by the components itself and additionally by the technique of its formation. Hence there is a broad variety of different catalysts available, each producing iPP with more or less specified properties. Typically used donors and their

influence on the polymerization behavior and on the polymer properties are depicted below (Figure 11, Table 3).[179]

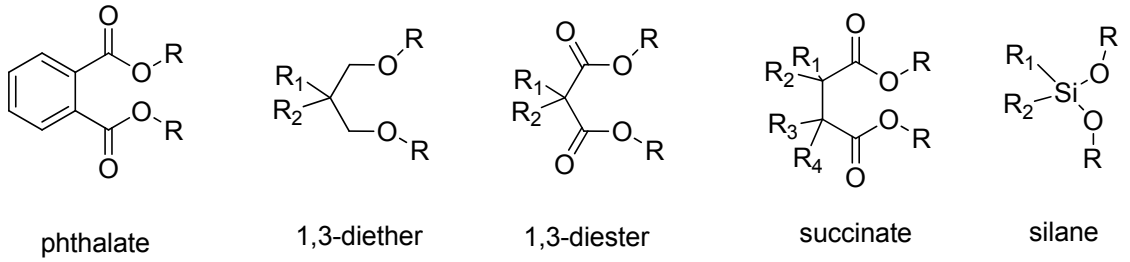

Figure 11: General structures of internal and external donors for *Ziegler-Natta* catalysts.

Besides above shown silanes which today are mainly used as external donors, much attention has also been attracted by aminosilanes. These are for example reported to broaden the molecular weight distribution without reducing the isotacticity in contrast to the corresponding ZN-catalyst with an alkylsiloxane as external donor.[181, 182]

Table 3: Influence of internal and external donors on the polymerization behavior of ZN-catalysts and the properties of the resulting PPs.

I.D.[a]	E.D.[b]	productivity/ kg PP/g Cat	mmmm/ %	PDI	H_2 response
phthalate	silane	40 - 70	94 - 99	6.5 - 8	medium/low
diether	-	100 - 130	95 - 97	5 - 5.5	excellent
diether	silane	70 - 100	97 - 99	4.5 - 5	excellent/high
succinate	silane	40 - 70	95 - 99	10 - 15	medium/low

[a] I.D. = internal donor.
[b] E.D. = external donor.

Above it is shown that ZN-catalysts can achieve a mmmm-pentad level of up to 99 %. A deeper look into the literature concerning the highest melting transitions for ZN-catalysts show values of up to 168 °C.[183] For this high melting transition a ZN-catalyst with di-*n*-butyl phthalate as internal donor and dimethoxydicyclopentylsilane as external donor is used. This combination can produce very high tacticities but is known to have a worse hydrogen response. In addition activities are in the lower range of these typically known for ZN-catalysts.[180]

2.10.2 *State of the Art Homogeneous Metallocenes*

For the production of highly iPP C_2-symmertric homogeneous metallocenes were proven to be good candidates. Since first reports on these metallocenes from *Brintzinger*, *Kaminsky* and *Ewen* (2.2), the ligand structure of these bisindenyl-based metallocenes has been widely varied to obtain certain effects on their polymerization behavior. The different substitution pattern in 2-, 4- and 7-position of the indenyl fragment can lead to different improvements such as higher molecular weights, higher activity or stereoselectivity or improved comonomer incorporation. Following sections will discuss these substitution patterns, their synthetic availability and especially their performance for the production of high molecular weight and high stereo- and regioregular PP. In addition, effects of the bridge are included in these sections. In general a better performance of the Me_2Si-bridged compared to the ethylene-bridged metallocenes, with respect to higher stereo-, regioselectivity and higher M_w is reported, as it was already briefly mentioned (2.3).

2.10.2.1 Indenyl-based Metallocenes with 2-Substitution Pattern

An important effect of the 2-substitution in case of indenyl-based metallocenes is its influence on the molecular weight of the formed PP. A methyl group in this position was proven to increase the molecular weight of the polymer compared to PP produced with the corresponding unsubstituted metallocene.[184] This effect was observed with standard complexes such as Et(2-Me-Ind)$_2$ZrCl_2 or its Me_2Si-bridged analog, which has additionally also a higher stereoselectivity due to the higher rigidity of the bridge.[185] The reason for the higher molecular weights is reported to be a suppression of the hydrogen transfer reaction to the monomer which is faster as the unimolecular β-hydride transfer reaction. This behavior can also be observed for bisindenyl metallocenes possessing further substituents beside the 2-methyl group.[113] Copolymerization reactions of propene and ethene revealed the effective suppression of the β-hydride transfer reaction to propene for 2-Me substituted bisindenyl metallocenes.[186] However, for a inhibition of the β-hydride transfer reaction to ethene the 2-Me group is insufficient. In addition to these experimental results also theoretical calculations confirm for 2-Me-substituted bisindenyl metallocenes increased molecular weight PP with increasing propene concentration due to the suppression of the bimolecular β-hydride transfer reaction.[112] The enlarged angle in the transition state for the β-hydride transfer reaction to the monomer affords a significant interaction of the 2-methyl substituents

with the C_α of both, the monomer and the growing chain. Hence, the activation barrier for this reaction is increased.

In case of some Me_2Si-bridged bisindenyl complexes, also the stereo- and regioselectivity is reported to be improved by a 2-Me substitution pattern.[113] The higher regioselectivity further increases the molecular weight of the resulting polymers as a transfer reaction is much more likely after such a regiomistake (2.6.1). Some general syntheses for the bisindenyl metallocenes with a 2-alkyl-substituent will be discussed in the next section together with the 4-substitution pattern.

2.10.2.2 Indenyl-based Metallocenes with 2,4-Substitution Pattern

The 2,4-substitution pattern of bisindenyl-based metallocenes has several influences on the propene polymerization behavior. Among these the influence on the stereoselectivity is important and will be briefly discussed. As already mentioned in section 2.6.1, the enantiofacial selectivity is predominantly controlled by the indirect control of the ligand skeleton. Besides the indirect control the 4-substituent reduces enantiofacial selectivity due to a direct influence. This effect is a result of steric interaction of the substituent in 4-positon of the indenyl moiety with the methyl group of propene during its coordination with the favored enantioface (Figure 12).[187]

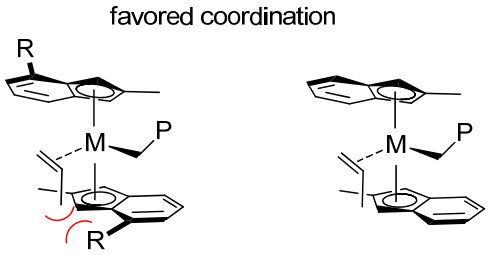

Figure 12: Steric interaction of the 4-substituent with a propene monomer coordinated with its favored enantioface (re-coordinated propene on the R, R enantiomer of the complex, bridging unit is omitted for clarity).

However, depending on the steric hindrance of the substituent the benefit of the indirect control can outperform the direct, affording an overall increased stereoselectivity. For example, a methyl- or isopropyl-substituent is calculated to result in higher stereoselectivity whereas a 4-*tert*-butyl-substituent would lead to a decrease.[90, 188] Compared to a methyl or an isopropyl group, the indirect control was calculated to be similar or even bigger for aryl substituents such as naphthyl or phenyl groups. A combination of 2-, and 4-substitution on the indenyl moiety affords a synergistic effect increasing the stereoselectivity more significantly as expected just from results of only 2-methyl-, or 4-phenyl-substituted bisindenyl zirconocenes.[189] Thus, 2,4-substituted bisindenyl based metallocenes especially with a 2-alkyl

and 4-aryl substituent are reported to be among the most promising metallocenes for the formation of highly iPP (Figure 13, Table 4).

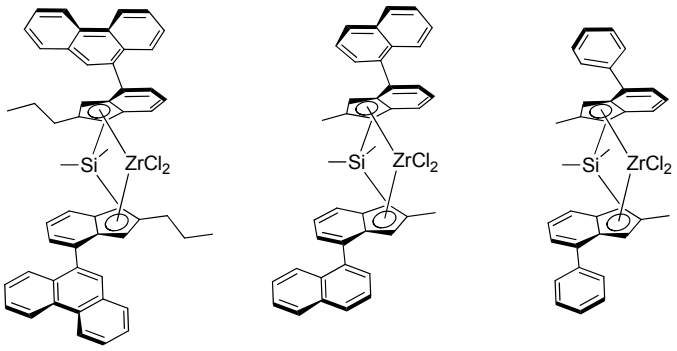

VIII IX X

Figure 13: Highly stereo- and regioselective C_2-symmetric metallocenes with 2,4-substitution pattern.

Besides higher stereoselectivities also the activity is significantly increased, especially for ligands with an aryl substituent in 4-position. Comparing the 2-methyl-4-phenyl-substituted bisindenyl-based metallocene with the corresponding 2-methyl-substituted complex shows for former increased molecular weights of the PP and an increase of the catalysts productivity (from 99 kg PP/(mmol(Zr)·h) with a M_w of 200 kg/mol to 755 kg PP/(mmol(Zr)·h) with a M_w of 730 kg/mol respectively). The given explanation is a less tight contact of the anion to the cation due to increased steric hindrance.[190, 191] Additionally the 4-phenyl substituent affords an increased electron density. This can stabilize the cationic species and therefore facilitate its formation, leading to a higher amount of catalytically active centers.

Table 4: Values for some of the most stereo- and regioselective C_2-symmetric metallocene complexes.[192, 193]

complex	T_p/ °C	productivity kg PP/(mmol(Zr)·h)	M_w/ g/mol	mmmm/ %	2,1/ %	3,1/ %	T_m/ °C
VIII	50	46.8[a]	400 000	99.2	0.15	0.07	160
IX	50	22.5[a]	380 000	98.6	0.29	0.05	156
X	70	1300[b]	730 000[c]	99.6	0.46	na	na

[a] in toluene, propene pressure 1 bar.
[b] in liquid propene.
[c] M_v instead of M_w.

It is difficult to find a relationship between the influence of the 4-substitution pattern and the regioselectivity as there is only few (M = Zr) or no (M = Hf) data available. However, in general, all of the highly substituted metallocenes which can be found in the literature and afford highly iPP are not totally regioselective. Together with the metallocene typical

distribution of the stereoerrors (2.10.1), during formation of iPP this is the reason for lower melting transitions compared to iPP produced with ZN-catalysts.

A standard procedure for the synthesis of 2,4-substituted indenes for the formation of above shown bisindenyl metallocenes was developed by *Spaleck et al.*(Scheme 18).[191]

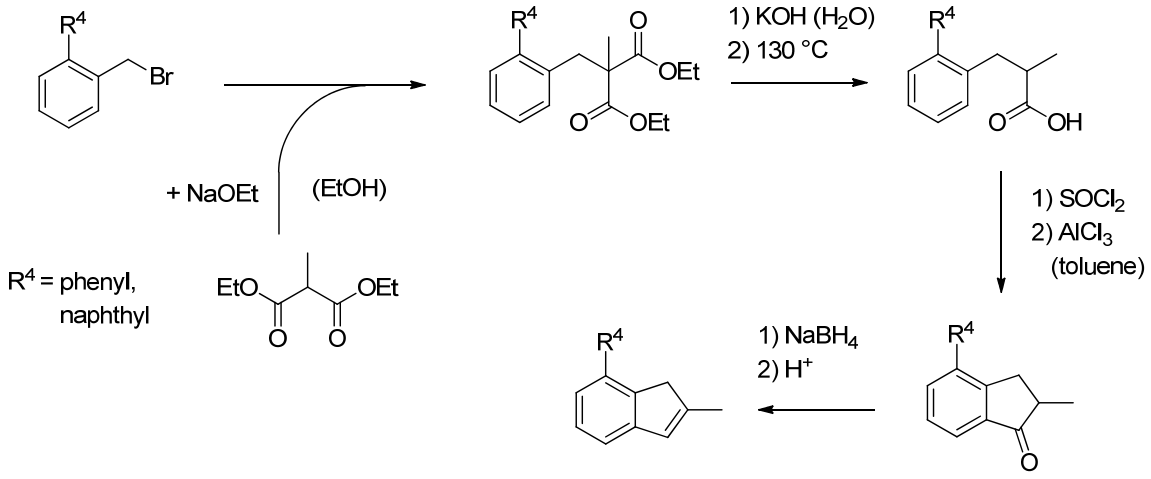

Scheme 18: Spaleck´s synthesis route for 2, 4-substituted indenes.

The starting materials are either very expensive (R^4 = Ph), or commercially not available and have to be synthesized in additional steps (R^4 = naphthyl). *Izmer et al.* modified *Spaleck´s* synthesis route in order to obtain a more versatile procedure (Route **B** in Scheme 19).[194] Instead of 2-R^4-benzyl bromide, 2-bromobenzyl bromide was used and the corresponding indene was synthesized in an analog procedure. In a C-C coupling reaction, which can be conducted either before or after the complexation reaction with MCl_4 (M = Zr, Hf), different aryl substituents can be introduced.[195] Additionally two more synthesis procedures towards the versatile building block, 7-bromo-2-methylindene were reported (**A** and **C** in Scheme 19).[194] The additional route **A** is analog to the modified Spaleck route a 6 to 7 step procedure up to the desired indene. The starting material, 2-bromo-benzaldehyde is converted in a *Horner-Wadsworth-Emmons* reaction, followed by a reduction with HI and red phosphorus to 3-(2-bromophenyl)-2-methylpropanoic acid an intermediate also obtained in the modified Spaleck route **B**.[196] Route **C** is much shorter starting with the 1-indanole, which is converted in an ortho-lithiation reaction followed by the bromination using $BrCF_2CF_2Br$.[197, 198] Although the indanole is commercially available it is rather expensive.

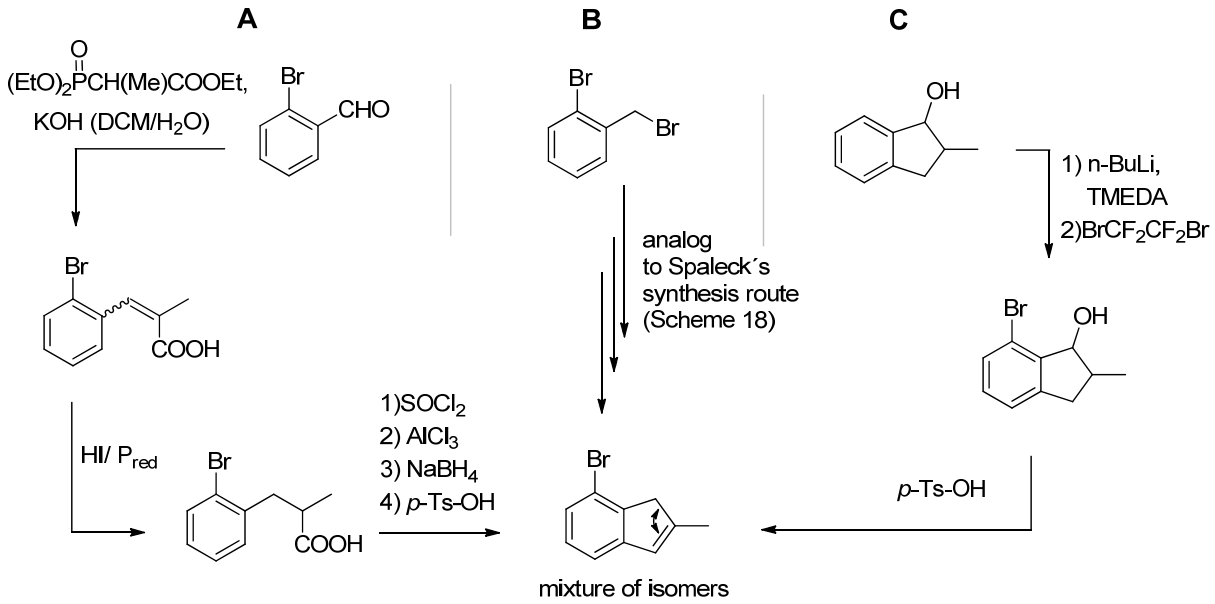

Scheme 19: Synthesis routes to 7-bromo-2-methylindene (and 4-bromo-2-methylindene).

2.10.2.3 Indenyl-based Metallocenes with 2,4,7-Substitution Pattern

Rac-ethylene-bis(2,4,7-trimethyl-1-η^5-indenyl)titanium dichloride and its zirconium analog **XI** are reported to afford regioregular and highly isotactic PP also with high molecular weights in case of the zirconocene (Table 5).[199, 200]

Unfortunately, the resolution of performed NMR spectroscopy is rather low and thus the determination of both the mmmm-pentad level and the amount of regioerrors might be imprecise. However, very high stereo- and regioselectivities can be assumed due to the high melting transitions of the produced iPP of up to 168.9 °C, which is actually the highest reported melting transition for unextracted and not annealed metallocene-produced iPP. These high melting transitions are only accessible at very low polymerization temperatures. At moderate polymerization temperatures PPs with low molecular weights and moderate isotacticities and thus significantly reduced melting transitions are generated.

The polymerization behavior at higher temperatures is also in accordance with theoretical calculations, performed for these temperatures, which assume a negligible- or even a negative effect of the 7-substituent concerning stereoselectivity compared to the corresponding complexes without a 7-substituent.[188] Experimental results also show an influence of the co-catalyst on the isotacticity and the molecular weights. Both parameters are improved by using $[CPh_3][B(C_6F_5)_4]$ instead of MAO.

Table 5: Polymerization of propene with r*ac*-ethylene-bis(2,4,7-trimethyl-1-η^5-indenyl)zirconium dichloride **XI** at various conditions.[a]

complex	co-catalyst	T_p/ °C	M_w/ g/mol	T_m/ °C	mmmm/ %
XI	$[CPh_3][B(C_6F_5)_4]$[b]	-78	1 400 000	168.9	-
XI	$[CPh_3][B(C_6F_5)_4]$[b]	-30	1 000 000	168.0	98.2
XI	$[CPh_3][B(C_6F_5)_4]$[b]	30	19 000	158.1	90.6
XI	MAO[c]	-30	580 000	166.2	96.7

[a] polymerization reactions were carried out in 30 mL of toluene with $[propene]_0$ = 10.4 M.
[b] [TIBA] = 33 mM.
[c] Al/ Zr = 2000.

Besides some heteroatom substituted metallocenes which will be discussed in the following section (2.10.2.4), there are only few reports on bisindenyl metallocenes with a 2,4,7-substitution pattern which are in all cases patent applications. *Schulte et al.* described the formation of 4-aryl-2,7-dimethyl-substituted indenes (Scheme 20) and the corresponding ethylene-bridged metallocenes.[201]

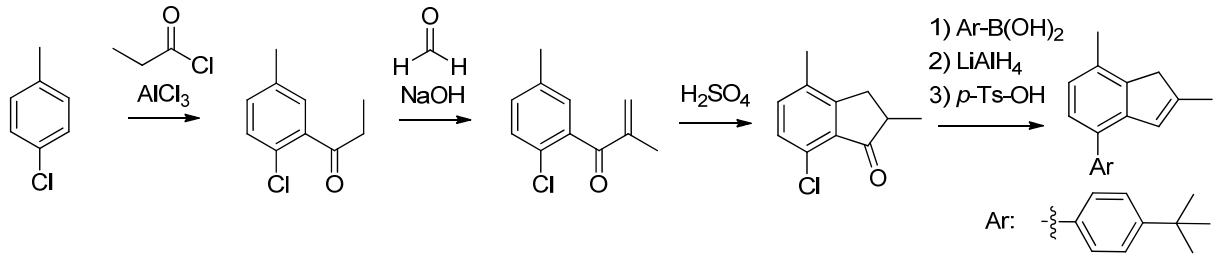

Scheme 20: Synthesis of 2,7-dimethyl-4-(*p-tert*-butylphenyl)indene.

In another patent application synthesis of 2-methyl-4,7-diaryl-substituted bisindenyl metallocenes is reported (Scheme 21).[202] The first step proceeds via a *Friedel Crafts* acylation followed by a *Nazarov* cyclization reaction. The starting material, dibromobenzene is a double deactivated aromatic compound and therefore only low yields (16 %) are obtained in the first step of the synthetic route.

Bis[2,7-dimethyl-4-(*p-tert*-butylphenyl)indenyl]zirconium dichloride is reported to polymerize propene, after activation with MAO to highly isotactic PP. The melting transitions and therefore the stereo- and regioselectivity is higher for metallocenes with an additional methyl group in 7-position of the indenyl moiety compared to the corresponding complex without a 7-alkyl substituent (156.4 and 154.7 °C respectively). For the diaryl substituted complexes iPP with only moderate stereo- and regioregularity are obtained (melting transitions of these PPs are in the range of 145 to 150 °C). However, an advantage of these

complexes is the selective *rac*-form synthesis of the C_2-symmetric metallocenes, occurring most presumably due to the increased steric interaction of the 7-substituents in the *meso*-form of the complex.

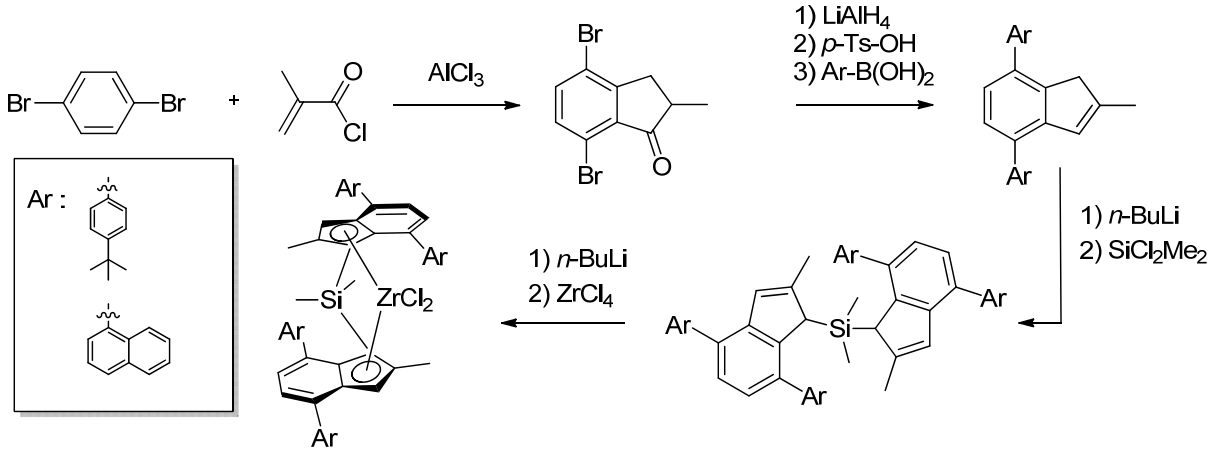

Scheme 21: Synthesis of $SiMe_2(4,7\text{-}Ar_2\text{-}2\text{-}Me\text{-}Ind)_2ZrCl_2$.

The individual influence of the 7-substituent in 2,4,7-substituted bisindenyl metallocenes on the stereo- and regisoelectivity is difficult to determine, as there is either no data available for the stereo- and regioselectivity (in most of the patent applications only the melting transitions are presented) or one of the necessary complexes is completely missing. For example, comparison of the unsubstituted bisindenyl with the 4,7-substituted bisindenyl metallocene shows a decrease of the regioselectivity and is thus often reported as a result of the 4,7-substitution pattern.[111, 203] Compared to their unsubstituted analogs, also 4-substituted bisindenyl metallocenes already lead to lower regioselectivities.[189] Hence, the specific influence of the 7-substituent cannot be determined from results of the unsubstituted and the 4,7-substituted bisindenyl metallocenes.

One patent application of 4,7-substituted bisindenyl metallocenes is available reporting both, stereo- and regioselectivities together with polymer melting transitions.[204] The compared complexes are *rac*-dimethylsilyl-bis[1-(4-^{i}Pr-2,7-dimethylindenyl)zirconium dichloride and its analog without the 7-Me substituent. The results show slightly lower stereo- and regioregularity together with a lower melting transition for polymers produced with the 2,7-dimethyl substituted complex.

These results are in contrast to the 2,7-dimethyl-4-aryl-substituted bisindenyl metallocenes shown above, where higher melting transitions are reported for the complexes with a 7-Me-substituent. Thus, there seems to be an important mutual influence of the 4-, and 7-substituent and their steric and electronic properties.

2.10.2.4 Heteroatom-substituted Indenyl-based Metallocenes

Besides the alkyl-, or aryl-substitution on the indenyl moiety, also heteroatom-substituted ligands are known.[205] Heteroatoms predominantly used are oxygen and nitrogen. These differ especially in their electronic properties from the alkyl- or aryl-substituents and therefore a specific influence on the complex and its polymerization behavior can be expected. These heteroatoms are *Lewis* basic in nature and could in principle coordinate via σ-coordination to the metal cation during the polymerization reaction, which results either in reduced activities or most likely in a complete deactivation. In order to preclude direct interaction, sufficient protection must be applied. The protection of the heteratom functionality can be either achieved by separately introducing a protecting group with high steric demand, or *in situ* by reaction of the co-catalyst (e.g. TMA, TIBA, MAO) with the polar group. However, the influence of these two protecting techniques on the catalyst is very different. Theoretically expected effects will be discussed and afterwards few specific examples will be given.

Separate introduction of a sterically demanding protecting group affords a complex with donor functionality increasing the electron density on the cyclopentadienyl fragment. Hence, a stronger M-Cp bond compared to a similar alkyl or unsubstituted metallocene is obtained. The *Lewis* acidity of the complex is reduced and, due to the shorter M-Cp bond, also the spatial room for the catalytic reaction. These two effects lead to a slower coordination and insertion of the olefin and thus lower the activity of the catalyst. However, the influence of the counteranion must also be considered. Lower *Lewis* acidity and less spatial room afford a weaker coordination of the counteranion leading to higher activities. Hence, the effect created by the heteroatom substituents depends on the entire catalyst system and therefore a general and simple trend cannot be expected.

In contrast, aforementioned effects are changed by using the co-catalyst as protecting agent. The high *Lewis* acidity of the co-catalyst results in decreased electron density of the ligand, affording a longer M-Cp bond and higher *Lewis* acidity of the complex. On the one hand coordination and insertion rates of α-olefins should be directly enhanced. On the other hand the complex is destabilized (reduced temperature stability) and due to electronic and steric reasons the counteranion can coordinate stronger to the active center leading to lower activities.

In order to specify the effects discussed, few examples will be briefly mentioned. Examples of 2-heteroatom-substituted bisindenyl metallocenes are bis(2-N,N-dimethylaminoindenyl) zirconium dichloride complexes known with a Me_2Si or an ethylene bridge.[206, 207] For the

Me_2Si-bridged metallocene activated with MAO, an induction period and slightly lower activities compared to the analog alkyl-substituted complexes are reported. The induction period is prolonged with increasing amount of TMA, the molecular weights of the PP are reported to be lower, and an increased amount of isopropyl end groups is observed compared to the alkyl substituted metallocenes. Lower molecular weights and more isopropyl end groups are a result of an increased amount of transfer reactions to TMA or similar aluminum derivatives. In this case the insufficiently shielded heteroatom facilitates the coordination of the aluminum compound and thus the probability of a chain transfer reaction is enhanced.

Examples for metallocenes with a heteroatom that is spatially more separated from the active center are the 4,7- and 5,6-dimethoxy substituted bisindenyl metallocenes.[190, 208] After MAO activation, decreased activities compared to the alkyl-substituted analogs are reported for these catalysts. The reason therefore was considered to be the reaction of the co-catalyst (TMA, MAO) with the methoxy group forming a net electron withdrawal group, destabilizing the catalyst.

Complexes with more efficiently protected heteroatoms such as siloxy-, or 5,6-ethylenedioxy-substituted metallocenes show increased activities at low Zr/MAO ratios.[160, 205] The protecting group prevents the polar group from a reaction with MAO. However, rac-{1-[5,6-(ethylenedioxy)-2-methyl-1-η^5-indenyl]-2-(9-η^5-fluorenyl)ethane}zirconium dichloride shows decreased activity and lower molecular weights for polymers produced at higher MAO concentration (transfer reaction to Al) due to the enhanced proximity of the co-catalyst to the metal induced by the oxygen atoms.

These examples show that the processes involved in activation with MAO are complex. This is owed to an interaction of the above mentioned effects that are present within these heteroatom-substituted metallocenes compared to their alkyl- or non-substituted analogs.

3 Concept of this Work

The aim of this work can be divided in two main parts. In the first part formation of ePP at elevated temperatures using different metallocenes, i.e. C_1- and C_2-symmetric, is discussed. The second part examines a versatile and convenient synthesis route towards C_2-symmetric metallocenes that are able to produce highly isotactic polypropylenes. Besides the synthesis of the complexes necessary for the different polymerization reactions, the autoclave setup for the polymerization reactions has to be modified in order to obtain reproducible results. Additionally to the synthetic and technical part, the polymers will be analyzed in detail using common analytic methods such as GPC, DSC and, if possible, also NMR spectroscopy.

Rieger´s C_1-symmetric complexes **1** and **2** (Figure 14, 2.9.1) proved to efficient catalysts for the preparation of ePP with good elastic behavior, as long as moderate polymerization temperatures are used. However, for an industrial approach higher polymerization temperatures around 100 °C and above, are necessary.

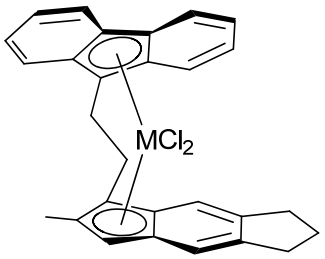

M = Zr **(1)**,
Hf **(2)**

Figure 14: Investigated C_1-symmetric complexes for the formation of ePP in a high temperature solution polymerization process.

Therefore the polymerization behavior of these C_1-symmetric complexes will be examined concerning their temperature stability together with the microstructure of the resulting polymers. Especially the effect of high polymerization temperature on the special polymerization mechanism (2.9.1) that influences the microstructure and thus the mechanical behavior of the produced polymers will be analyzed.

As a second approach towards ePP, C_2-symmetric complexes will be investigated. These are generally known to produce iPP at moderate temperatures. However, the amount of stereoerrors which controls the mechanical behavior of the produced polymers is known to increase for increasing polymerization temperature. Hence, at higher polymerization temperature formation of ePP with an mmmm-pentad level in the range of 20-30 % could be possible. Besides the trend of stereoerrors with increasing polymerization temperature, the

molecular weights of the produced polymers will be reduced due to faster chain transfer reactions. In order to produce ePP with a good elastic recovery, polymers with high molecular weight are necessary. As hafnocenes are known to produce polymers with higher molecular weights compared to the corresponding zirconocenes especially these complexes will be examined in more detail concerning their polymerization behavior at elevated and high temperatures. The often reported low activity of hafnocenes is shown to be rather a result of an inefficient activation method than of lower intrinsic activity of the metal. In order to prevent lower activities of hafnocene catalysts, borate activation, which typically affords high activities in case of hafnocenes, will be used.

The second part, the development of a versatile synthesis route towards metallocenes producing highly iPP is based on *Rieger's* patent application for the formation of 4-aryl-7-hydroxy-substituted indanones (Scheme 22).

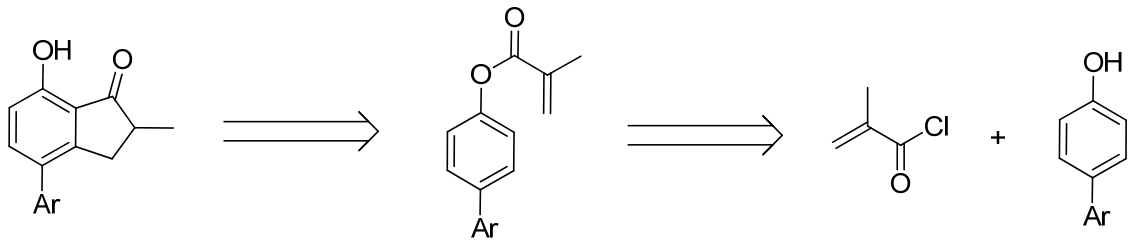

Scheme 22: Synthesis route towards new indanones developed and patented by *Rieger et al.* in 1999.

In the literature, especially bisindenyl based metallocenes with a 2,4,7-substitution pattern are known for the formation of iPP with high melting transitions. This is a result of the positive influence of these substituents on the stereo- and regioselectivity during propene polymerization. In addition also improved activities can be obtained. So far, there is no versatile and convenient synthesis route towards these 2,4,7-substituted indenes (Figure 15) with varying substituents on these positions. Particularly, convenient synthesis route affording a substitution pattern on the indenyl moiety is important for which the substituents on the 4- and 7-position can be changed independently. This opportunity allows ultimate control over the steric and electronic factors controlling the polymerization behavior of these catalysts.

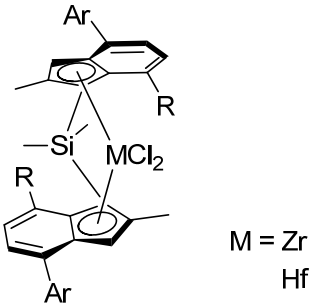

Figure 15: General structure of the 2,4,7-substituted bisindenyl metallocenes considered for the formation of iPP with high melting transitions.

Additionally to the effect of the substituents during the polymerization reaction, the 7-substituent can have an influence on the formation of the *rac:meso* ratio which is usually around 1:1 during the synthesis of *rac*-bisindenyl metallocenes. In order to obtain the pure *rac*-form generally the *meso*-form has to be separated from former. During complex formation of the presented indenes with additional 7-substituent, the steric interaction of these in case of the *meso*-form can help to improve the *rac*:*meso* ratio towards a higher amount of *rac*-form of the complex. Hence, the yield of the desired complex can be theoretically higher than 50 %, which is normally the maximum for the synthesis of these *rac*-bisindenyl metallocenes by standard synthesis procedures.

4 Results and Discussion

4.1 C_1-symmetric Metallocenes for the Formation of ePP

The C_1-symmetric metallocenes (**1** and **2**, Figure 14) developed by *Rieger* and co-workers are known to form ePP via a chain back skip mechanism (2.9.1). ePP produced by these complexes at low to moderate polymerization temperatures and high propene concentrations show an elastic behavior similar to commercially available TPE (e.g. Kraton). For an industrial solution polymerization process, it is necessary to apply higher polymerization temperatures (80 °C and above). To get more information about temperature stability, especially considering deactivation reactions leading to decreased productivities, these complexes are studied in more detail at higher polymerization temperatures. Besides temperature stability of these complexes, also the polymers produced at elevated and high temperatures are analyzed in more detail concerning their molecular weight and microstructure, which are the two most important parameters influencing the elastic behavior.

4.1.1 *Temperature Stability of the Catalyst*

First of all, a brief theoretical examination of the bond situation for investigated C_1-symmetric complexes **1**, **2** and their stability is made. The studied complexes possess a fluorenyl and an indenyl ligand. In order to evaluate the strength of the M-Cp bond, its length can be used. This length is increased from a Cp over an indenyl up to a fluorenyl ligand (Table 6). Hence, fluorenyl ligands are generally less strongly coordinated to the metal center. This trend can be explained by the different electron density distribution. Electron density in case of a fluorenyl ligand is more located resulting in a hapticity decrease going from Cp to Flu.[209] Cp ligands are known to have a η^5-coordination while for the unbridged $(Flu)_2ZrCl_2$ the two fluorenyl ligands are reported to coordinate with different hapticity, one in a η^3- the other in a η^5-manner.[210] In addition, the M-Cp distance is influenced by the bridge, resulting in longer M-Cp distances for $SiMe_2$-bridged compared to ethylene bridged complexes (entries 2, 4). This is also in accordance with reports on the $SiMe_2$-bridged analog of metallocene **1** showing a deactivation of the catalyst during the polymerization process.[159] Hence, compared to their $SiMe_2$-bridged analogs, investigated complexes **1** and **2** are more stable due to the ethylene bridge. Comparison of metallocenes **1** and **2** reveals slightly shorter M-Cp distances for the hafnocene **2,** indicating a more stable complex. Both complexes have two different M-Cp

distances (Flu, Ind). In particular, the longer M-Cp distance and the increased difference of the M-C distances for the fluorenyl ligand compared to an indenyl or cp ligand (entries 1, 3, 5) indicates a weaker coordinated fluorenyl ligand. This can finally result in a limitation of the temperature stability during the polymerization reaction.

Table 6: Examples for metal-ligand bond distances in some Cp-, indenyl-, and fluorenyl-based metallocenes.

entry	complex	M-Cp/ Å	M-C distance/ Å
1	$Me_2Si(Cp)_2ZrCl_2$[211]	2.197	2.47 – 2.55
2	$Et(Flu)_2ZrCl_2$[212]	2.269	2.42 – 2.66 (Flu 1) 2.44 – 2.70 (Flu 2)
3	Et(Flu)(5,6-cyclopenta-2-Me-Ind)$ZrCl_2$[18] **(1)**	2.267 (Flu) 2.226 (Ind)	2.42 – 2.67 (Flu) 2.43 – 2.60 (Ind)
4	$Me_2Si(Flu)_2ZrCl_2$[156]	2.298	2.44 – 2.72
5	Et(Flu)(5,6-cyclopenta-2-Me-Ind)$HfCl_2$[213] **(2)**	2.252 (Flu) 2.203 (Ind)	2.41 – 2.66 (Flu) 2.47 – 2.59 (Ind)

In order to examine the temperature stability of complexes **1** and **2**, polymerization experiments were performed at slightly elevated (50 °C) and high temperatures (80 °C). For the activation of the metallocene dichlorides **1**, **2**, a standard procedure including a preactivation step with TIBA (1 h at 60 °C) and the formation of the cationic species by adding $[CPh_3][B(C_6F_5)_4]$, was applied. An important proof for the temperature stability of the catalyst is the propene uptake during the polymerization process which was measured and recorded online (Figure 16).

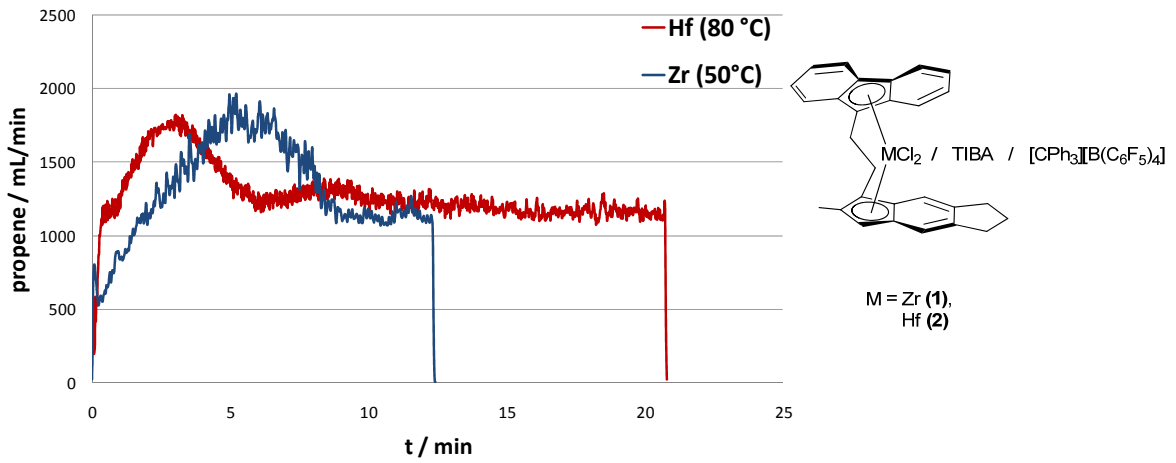

Figure 16: Propene uptake during the polymerization of propene with metallocenes **1** and **2.**

After activation with $[CPh_3][B(C_6F_5)_4]$ the curves show an increased propene uptake within the first minutes. This behavior is a combination of an overmodulation by the pressure controller and the process thermostat trying to cool the exothermic reaction. Lower temperatures reached in the beginning result in an increased solubility of propene. After this initial period, both complexes studied show a constant propene uptake at slightly elevated (50 °C) and higher (80 °C) temperatures during the whole polymerization reaction until it was stopped by adding a small amount of methanol via a pressure burette. Hence, no significant deactivation reactions of the active species during the polymerization process are observed.

Besides the propene uptake, the dependency of productivity upon polymerization temperature is an indication for the stability of the complexes (Table 7). Increased polymerization temperatures together with slightly increased propene pressures led to similar (entries 1, 2) or even higher productivities (entries 3, 4). The activity of a metallocene catalyst is increased for increasing propene concentration and temperature. Hence, in consideration of the lower solubility of propene at higher temperatures, similar or higher productivities can be ascribed to increased propagation rates (entries 1, 3). This observation underlines the absence of a significant degradation reaction at elevated and higher polymerization temperatures.

Table 7: Polymerization of propene with metallocenes **1**, **2** at elevated and high temperatures.[a]

entry	complex	t_p[b]	T_p[c]	p[d]	productivity[e]	M_w[f]	PDI
1	1	12	80	7.6	69000	17000	2.0
2	1	13	60	7	70000	60000	1.9
3	2	11	100	7.6	34000	4000	2.2
4	2	16	60	7	22000	36000	1.9

[a] Polymerization conditions: $n_{complex}$ = 5 µmol activated with TIBA (200 eq; at 60 °C)/$[CPh_3][B(C_6F_5)_4]$ (5 eq). [b] In min. [c] In °C. [d] $p = p_{Ar} + p_{propene}$ in bar, with $p_{Ar} = 1.9 \pm 0.2$ bar. [e] In kg (PP)/ (mol(M) h). [f] In g/mol.

Productivities are stronger affected by polymerization temperature in case of the hafnocene **2** compared to zirconocene **1**. A reasonable explanation is a stronger coordination of the counteranion for the hafnocene, but in order to prove this assumption further polymerization experiments are necessary. The stability of the described complexes up to high temperatures (100 °C) is obvious. However, a comparison of the two complexes reveals lower productivities and lower molecular weights for the hafnocene **2** relative to the zirconocene **1**. Especially lower molecular weights observed at elevated temperatures for PP produced with

hafnocene **2** were not expected. Further investigations concerning the molecular weight dependency of metallocenes **1**, and **2** as a result of the occurring chain transfer reactions will be discussed separately in more detail (4.1.3, 4.1.4).

Lower observed activities for hafnocenes are often explained by a more stable Hf-C σ-bond. However, using the dimethylated catalyst precursors of metallocenes **1** and **2** resulted in similar productivities for both Hf and Zr after activation with $[CPh_3][B(C_6F_5)_4]$.[68] In order to find the reason for the observed lower productivities in case of hafnocene **2,** when activated with TIBA and $[CPh_3][B(C_6F_5)_4]$, a more detailed investigation of the preactivation reaction with TIBA was performed by UV-Vis spectroscopy and will be discussed in the next section.

4.1.2 *Preactivation with TIBA: UV-Vis and NMR Measurements*

For metallocene dichloride precursors the reaction with alkylaluminum reagents is reported to afford several different reaction products, strongly depending on the complex structure, the metal, and the amount and structure of the used alkylaluminum compounds.[63, 69, 214] Thus, a more precise investigation of the preactivation reaction with TIBA was performed for the metallocenes **1** and **2**. UV-Vis analysis can be used as a versatile instrument for an *in situ* measurement of this reaction at concentrations comparable to those commonly used for the preactivation reaction of metallocene dichlorides with TIBA (2.4.4). The shift of the lowest energy absorption band, in case of bent metallocenes the LMCT-band of the complex, can be detected during the reaction at different temperatures and at low to high concentrations of TIBA. The UV-Vis spectra of complex **1**, recorded within one hour, shows a hypsochromic shift of the LMCT-band after addition of TIBA from 482 to 465 nm (with t = 0, before TIBA addition, blue line, λ_{LMCT} = 482 nm, Figure 17). This shift is in accordance with a larger HOMO-LUMO gap as a result of an exchange reaction of the chloro ligand with a more electron donating group. In addition, one point of intersection for all curves (474 nm) is present that is a so called isosbestic point. In kinetic UV-Vis investigations of chemical reactions this point occurs if side reactions or consecutive reactions are absent.[215] Hence, the dichloro precursor is converted into only one other derivative without any consecutive reaction. In this case it is most presumably the monoalkylated compound of the dichloro precursor. The observed monoalkylation is also in accordance with the reaction mechanism proposed by *Bochmann* and co-workers with the analog ternary catalyst *rac*-$Me_2Si(Ind_2)ZrCl_2$/ TIBA/ $[CPh_3][B(C_6F_5)_4]$.[63] In case of the analog reaction with hafnocene **2**, the LMCT-band is only slightly shifted to lower wavelengths with low amounts of TIBA at 25 °C (Figure 18).

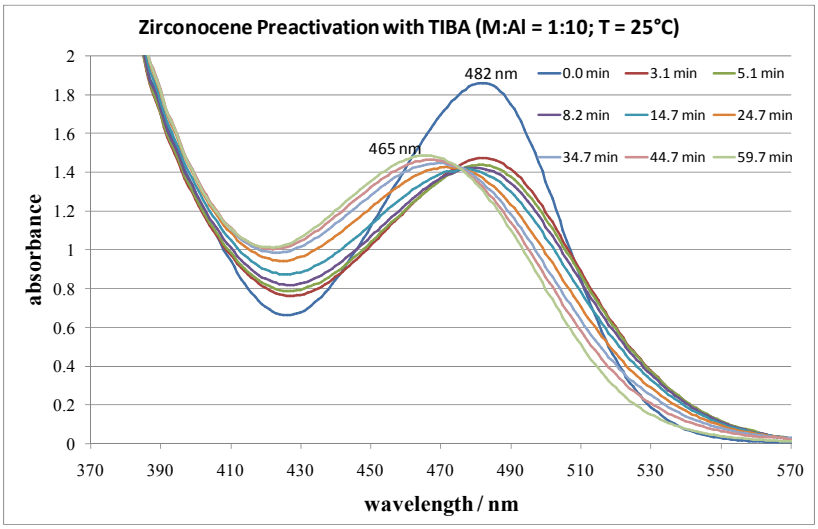

Figure 17: Preactivation of zirconocene **1** with TIBA. (c(Zr) = $8 \cdot 10^{-4}$ mol/L).

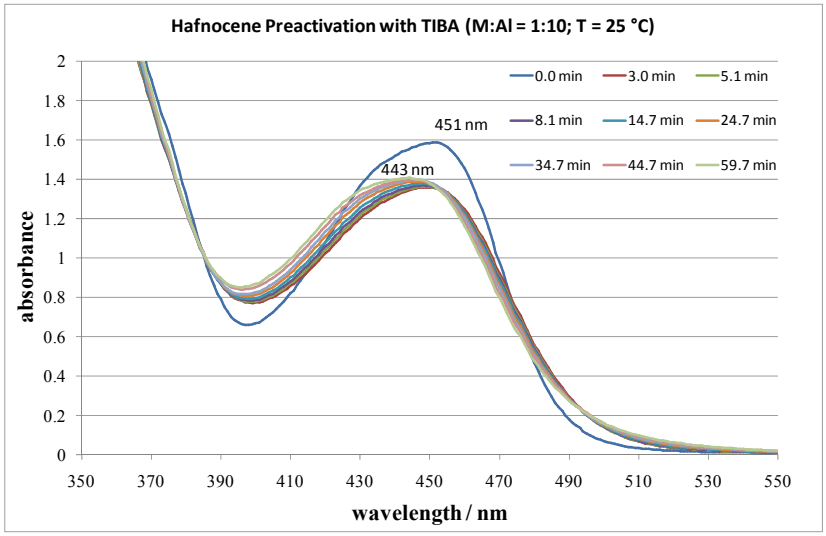

Figure 18: Preactivation of hafnocene **2** with TIBA. (c(Hf) = $8 \cdot 10^{-4}$ mol/L).

Another obvious difference between hafnocene **2** and zirconocene **1** is the wavelength of the LMCT-band, which is lower for the hafnium complex. As the ligands of these two complexes are identical and the HOMO is known to predominantly have the character of the Cp-based ligands, the relative position of the LUMOs for the different complexes can be directly determined. Higher electron density on the metal increases the LUMO energy of the metal. Therefore, the observed lower wavelength for the LMCT-band in case of hafnocene **2** is due to a higher HOMO-LUMO gap afforded by a higher electron density on the metal.

In order to obtain a significant shift of the LMCT-band for hafnocene **2** higher amounts of TIBA (Al:Hf = 200:1) and higher temperatures are necessary (Figure 19). NMR investigations for $Me_2Si(Ind)_2MCl_2$/ TIBA (M = Zr, Hf) also indicate the necessity of higher amounts of TIBA for a quantitative monoalkylation of the hafnocene compared to the zirconocene.[69]

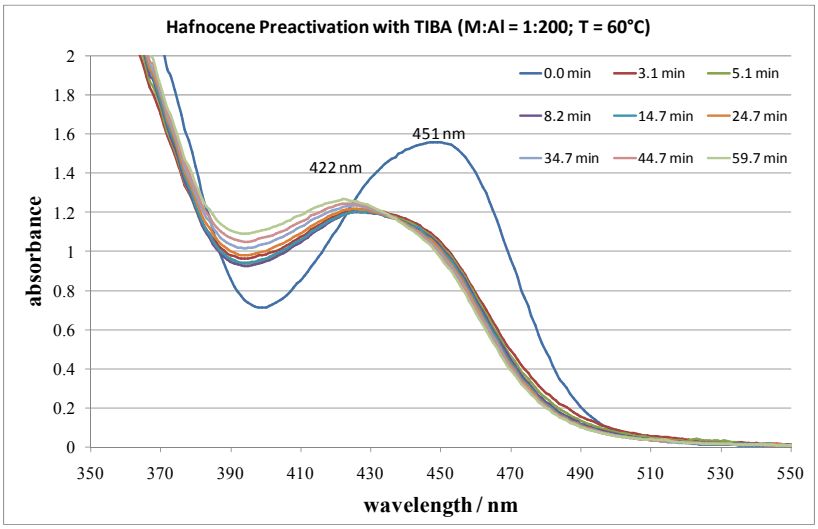

Figure 19: Preactivation of hafnocene **2** with TIBA. (c(Hf) = $8 \cdot 10^{-4}$ mol/L).

For polymerization reactions discussed in the previous chapter, both metallocenes were preactivated with 200 eq of TIBA at 60 °C. Consequently, the corresponding UV-Vis kinetics for the zirconocene **1** was recorded at the same conditions revealing completely different UV-Vis spectra (Figure 20). No isosbestic point could be observed, which leads to the conclusion that after the monoalkylation a fast and consecutive reaction occurs, affording a product with an absorption band below 400 nm.

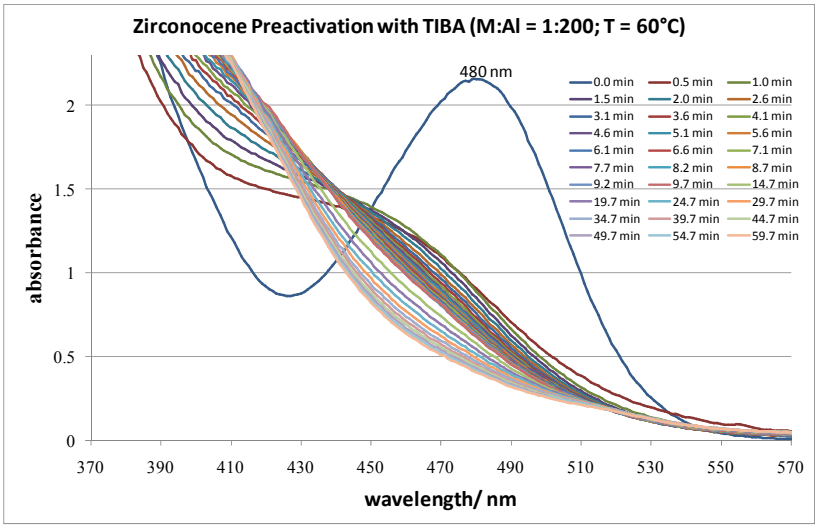

Figure 20: Preactivation of zirconocene **1** with TIBA. (c(Zr) = $9 \cdot 10^{-4}$ mol/L).

Commercially available TIBA contains low amounts of diisobutylaluminum hydride (DIBAL-H), normally below 2 %. In addition, due to the equilibrium between TIBA and the β-hydride elimination products DIBAL-H and isobutene, the amount of DIBAL-H is dependent on the temperature. Already at a temperature of 60 °C, partial decomposition of TIBA towards DIBAL-H was reported.[216] During the preactivation reaction of the

metallocene dichlorides with low concentrations of TIBA, the amount of DIBAL-H is by far not sufficient for an equimolar reaction. Increasing the amount of TIBA to 200 eq affords a quantity of DIBAL-H in the equimolar range. Recently performed NMR investigations concerning the reaction of different zirconocenes and low amounts of DIBAL-H showed the formation of different hydride-bridged complexes.[217, 218]

To elucidate a potential participation of DIBAL-H during the preactivation reaction of metallocenes **1** and **2** with TIBA and in order to find a fast and quantitative preactivation reaction for hafnocene **2**, further UV-Vis measurements were performed using DIBAL-H and mixtures of TIBA and DIBAL-H. For hafnocene **2** already with low amounts of DIBAL-H (7 eq), at 25 °C a fast reaction can be observed (Figure 21). Especially in the beginning of the reaction, two absorption bands, one around 450 nm (most presumably residual educt), the other at 410 nm, are detected. In addition, there are two more significant aspects apparent in the shown spectra. One is the absence of an isosbestic point in the recorded region and the other a hyperchromic shift (increasing absorbance) of the absorption band around 410 nm. A reasonable explanation for these observations can be a fast reaction towards a product absorbing in the region below 370 nm followed by at least one consecutive reaction which affords a product showing absorption above 370 nm. Another possible explanation is a fast reaction to the product with an absorption band at 410 nm followed by a consecutive reaction affording the observed hyperchromic shift.

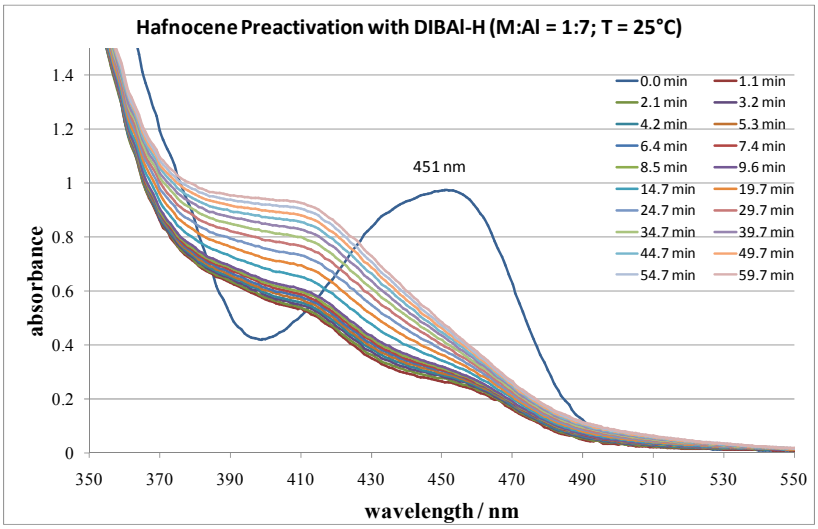

Figure 21: Preactivation of hafnocene **2** with DIBAL-H. (c(Hf) = $6 \cdot 10^{-4}$ mol/L).

Higher amounts of DIBAL-H (30 eq) resulted in a faster preactivation reaction (Figure 22). The absorption band of the newly formed species has its maximum at 405 nm, slightly lower than the one observed for the preactivation reaction with lower amounts of DIBAL-H. The obtained spectra look similar to that obtained with lower amounts of DIBAL-H showing both

a hypsochromic and a hyperchromic shift of the absorption band. The difference is the absence of the absorption band at around 450 nm, which was observed at lower amounts of DIBAL-H (7eq) in the beginning and assumed to be residual starting material. Hence, it can be concluded that conversion of hafnocene **2** is already complete after less than one minute if higher DIBAL-H concentrations are applied.

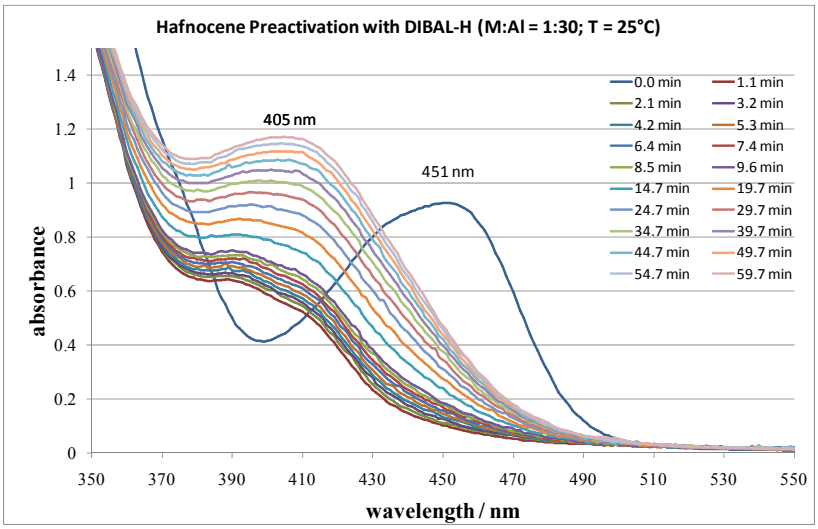

Figure 22: Preactivation of hafnocene **2** with DIBAL-H. (c(Hf) = $5 \cdot 10^{-4}$ mol/L).

In order to see if higher amounts of DIBAL-H can further increase the reaction rate also in presence of a high amount TIBA, a 1:1 mixture of TIBA and DIBAL-H with an Al: Hf ratio of 200:1 was used. The preactivation reaction was conducted at 60 °C, a temperature commonly applied for preactivation reactions. This resulted in a further acceleration of the reaction rate, accompanied by a hypsochromic and hyperchromic shift of the absorption band (Figure 23). Again, a slight shift to lower wavelengths than for the preactivation reaction with an Al: Hf ratio of 30:1 was observed. Absolute intensities of product absorption bands after one hour reaction time are similar for the last shown preactivation reactions (Figure 22; Figure 23). However, the experiment with neat DIBAL-H (Al:Hf = 30:1; Figure 22) has a slightly higher concentration of the dichloro precursor. This is expressed by the higher intensity of the absorbtion band before addition of the aluminum derivative (0.80 for TIBA:DIBAL-H = 1:1 and 200 eq and 0.93 for 30 eq of DIBAL-H). Therefore the reaction with 30 eq of DIBAL-H should afford a slightly higher intensity of the absorption band at 405 nm and is not completed after one hour for that reason.

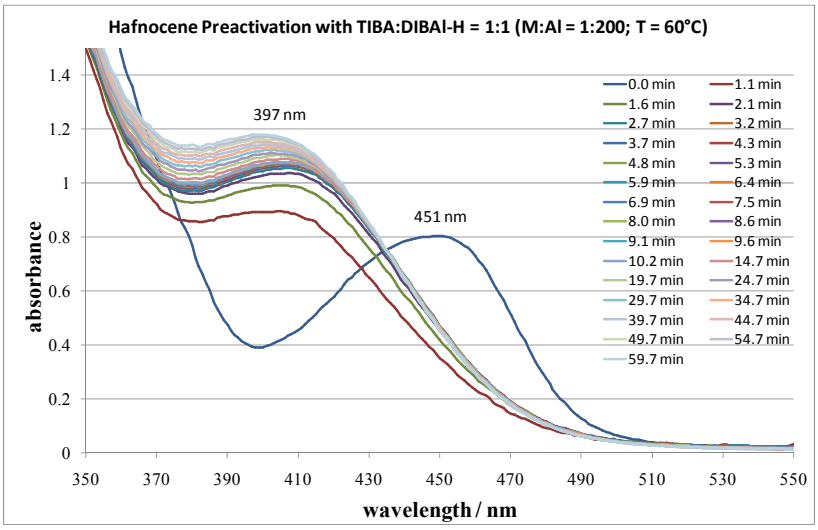

Figure 23: Preactivation of hafnocene **2** with TIBA and DIBAL-H. (c(Hf) = $5 \cdot 10^{-4}$ mol/L).

These results clearly indicate similar reaction products for all experiments where DIBAL-H was used. Additionally, the reaction with DIBAL-H is much faster as the reaction where TIBA was solely used. Hence, a participation of DIBAL-H during the activation of investigated metallocenes with high amounts of TIBA is very likely and cannot be ruled out as it was previously done by another group.[63]

Besides UV-Vis investigations reflecting the actual kinetic of the preactivation reactions also NMR experiments were conducted to gather further evidence for the different reaction products. Regarding these results, it should be noted, that higher concentrations are necessary for the NMR measurements, usually about two orders of magnitude higher, than in case of actual preactivation reactions or the UV-Vis measurements. The NMR spectrum of the preactivation reaction of hafnocene **2** with low amounts of TIBA (10 eq) is depicted in Figure 24. Besides the signals of TIBA and its impurities (isobutene, DIBAL-H), important signals are observed below 0 ppm and between 5.5 and 6.3 ppm (Figure 25). Three signals in the magnified region of the ^{1}H NMR spectrum have an integral ratio of about 1:1:1 (blue- and red-marked). Monoalkylation reaction of the dichloro precursor generates a metallocene with four different substituents. Hence the methylene group attached to the metal center is diastereotopic affording two different signals (red-marked) with a ^{2}J-coupling constant of 14 Hz and two different ^{3}J-coupling constants which are 4 and 8 Hz. These two signals always appear together with a singlet at 6.14 ppm (blue-marked) with identical integral which is therefore assigned to the hydrogen atom of the indenyl moiety. Additionally, the spectrum of hafnocene **2** with a M:Al ratio of 1:10 shows after a reaction time of one hour a residue of not

converted educt being roughly 10% (5.85 ppm). The compounds affording the signals at 5.92 and 5.97 ppm have not been identified so far.

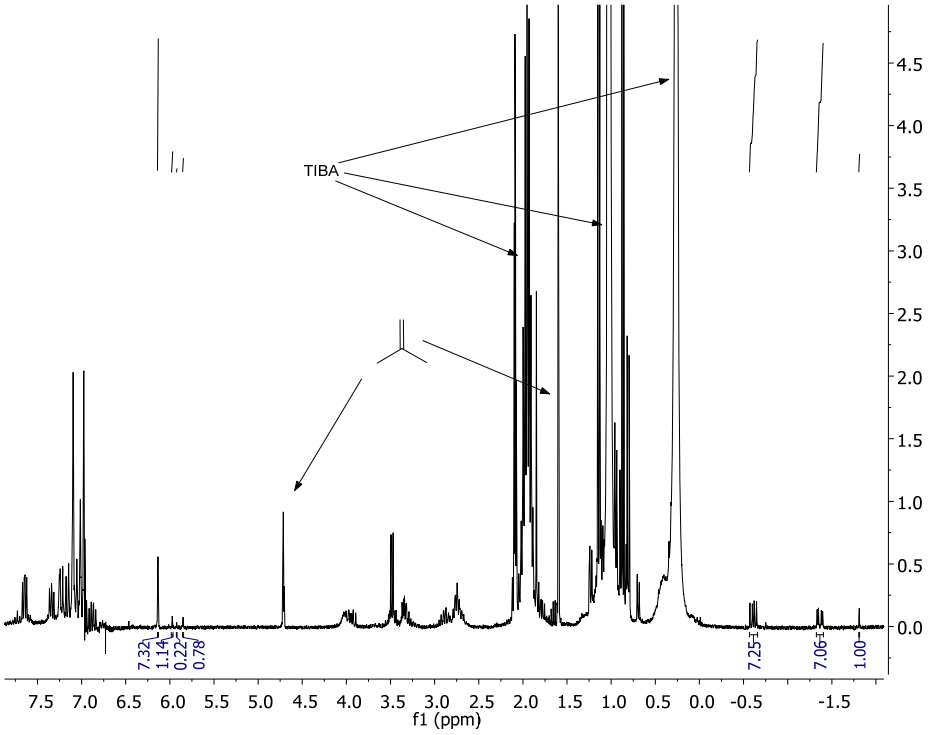

Figure 24: ^{1}H NMR spectrum of the preactivation reaction of TIBA with hafnocene **2** (M:Al = 1:10; T = 60 °C; c(Hf) = $2.6 \cdot 10^{-2}$ mol/L).

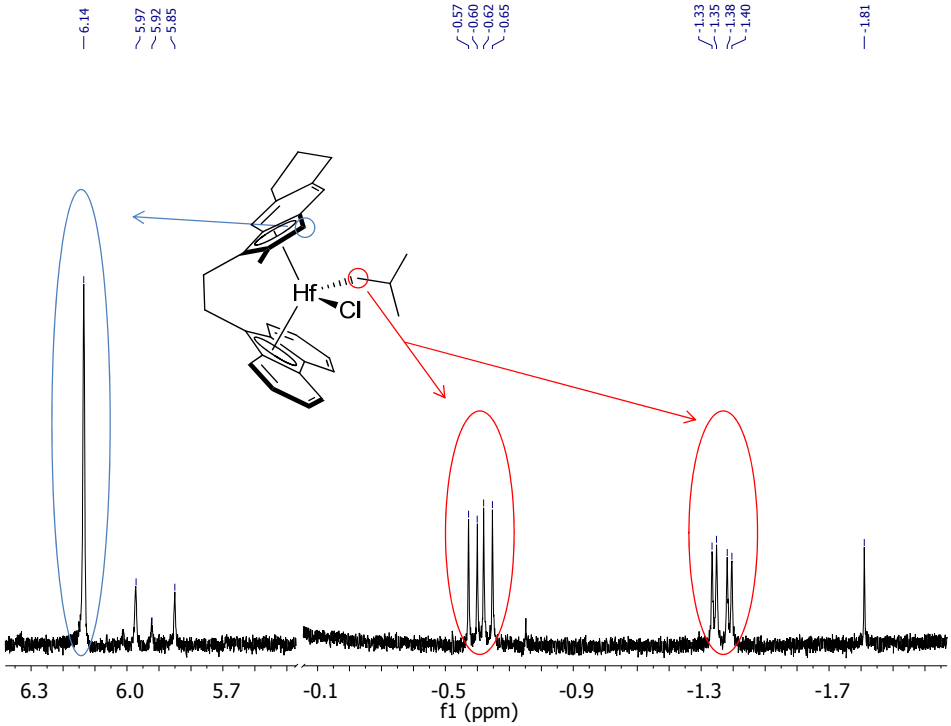

Figure 25: Magnified region of the ^{1}H NMR spectrum of the preactivation reaction of TIBA with hafnocene **2** (M:Al = 1:10; T = 60 °C; c(Hf) = $2.6 \cdot 10^{-2}$ mol/L).

Besides these signals an additional singlet at -1.81 ppm was observed (Figure 25). Recently *Baldwin et al*. investigated several bridged and unbridged metallocenes with respect to their reaction of DIBAL-H with and without addition of an cationization agent (e.g. $[CPh_3][B(C_6F_5)_4]$).[217, 218] In case of *ansa*-zirconocenes, reaction with DIBAL-H afforded neutral chloro dihydride complexes (Scheme 23). The chemical shift of the NMR signals of most of these bridged hydrides is reported in the range of -1 to -2 ppm, whereas terminal hydrides are known to have a chemical shift above 2 ppm.

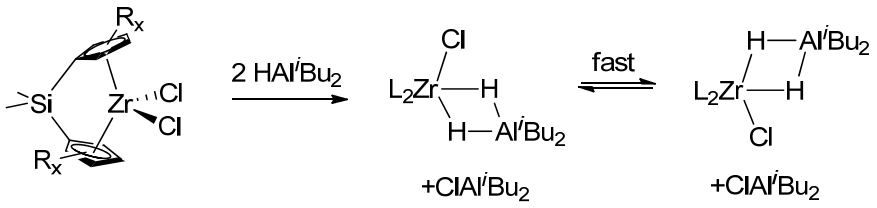

Scheme 23: Reported structures for several bridged zirconocenes after addition of DIBAL-H.

Bochmann and co-workers also used ^{1}H NMR spectroscopy to study the reaction of hafnocene **2** with TIBA and $[CPh_3][B(C_6F_5)_4]$. However, the reaction without addition of $[CPh_3][B(C_6F_5)_4]$ has not been reported so far. A clean reaction to one species was only found in case of higher applied amounts of TIBA (100 eq). For lower amounts more side products occurred after the addition of $[CPh_3][B(C_6F_5)_4]$. By usage of such high quantities of TIBA (100 eq) equimolarity of DIBAL-H and the metallocene can be assumed. Hence, this behavior is a further indication of the participation of DIBAL-H during the activation of hafnocene **2**. With high amounts of TIBA and addition of $[CPh_3][B(C_6F_5)_4]$ formation of a dihydrido-bridged complex (Scheme 24), which was approved to be an olefin polymerization catalyst was reported.

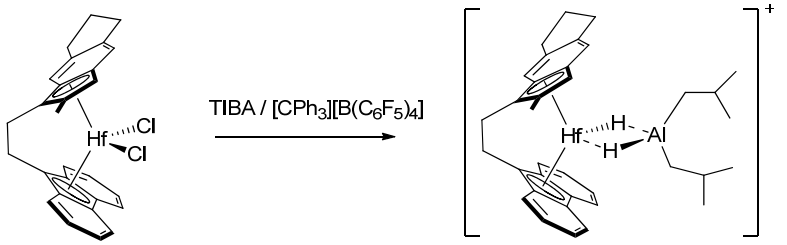

Scheme 24: Dihydrido-bridged complex reported by *Bochmann* and co-workers (counter anion: $B(C_6F_5)_4^-$).

With respect to the results shown above, the singlet observed at -1.81 ppm (Figure 25) in the ^{1}H NMR spectrum of the reaction of hafnocene **2** with a M:Al ratio of 1:10 at 60 °C can be assumed to be a hydrido-bridged complex. However, at this point a more detailed structure cannot be given.

At low amounts of TIBA (M: Al = 1:10), ^{1}H NMR spectra of zirconocene **1** and hafnocene **2** show similar reaction products (Figure 26). Thus, also the monoalkylation product together with the assumed hydrido-bridged complex seems to be present for the zirconocene **1**. In contrast to hafnocene **2**, zirconocene **1** shows a quantitative reaction. This can be recognized by the absence of the characteristic singlet from the dichloro precursor at 5.97 ppm. Similar observations were made by *Bochmann* and co-workers. They investigated the reaction of $Me_2Si(Ind)_2MCl_2$ (M = Zr, Hf) with TIBA and reported that higher amounts of TIBA are necessary for the monoalkylation reaction in case of the hafnocene.[63, 69] The additional signals between 6.1 and 6.2 ppm arise from species which have not been identified so far.

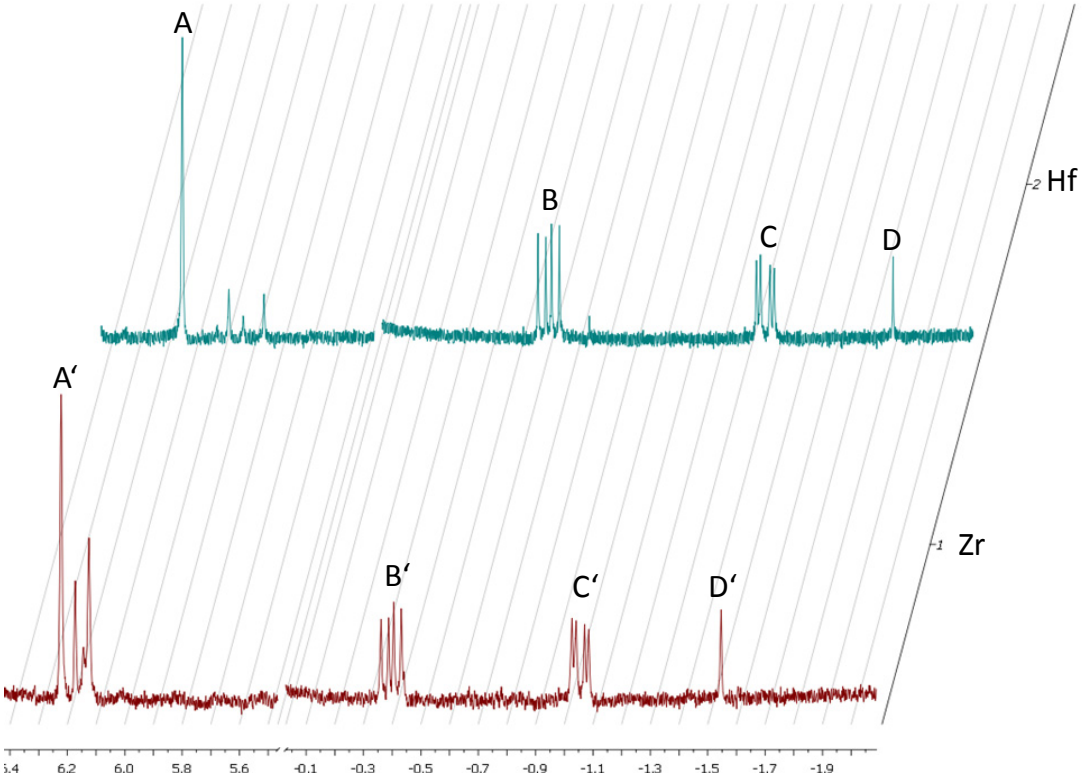

Figure 26: ^{1}H NMR spectra of the preactivation reaction of hafnocene **2** or zirconocene **1** with TIBA and an Al:M ratio of 10:1 (T = 60 °C (**2**) or rt (**1**))

In order to elucidate the influence of TIBA concentration and temperature on the formed reaction products, experiments with varying amounts of TIBA at different temperatures were conducted (Table 8). Error deviations of these measurements are about 10 to 20 %, and probably even higher for experiments with an increased amount of TIBA due to a worse signal to noise ratio. However, some general trends can be observed. By increasing the amount of TIBA the ratio of the signals C:D is decreased for hafnocene **2** (entries 1 and 2). In case of zirconocene **1** already low amounts of TIBA result in a lower ratio of C´:D´ which is

not significantly decreased with enhanced amount of TIBA (entries 5 and 6) and more or less in the region of the error deviation. Consequently, the assumed hydrido-bridged complex is more dominant for the zirconocene whereas in case of the hafnocene higher amounts of TIBA are necessary for its formation. A further obvious trend is the shift of the signals below 0 ppm. With increasing amount of TIBA, signals termed with the same letter are shifted in the same direction. C and C´ are shifted upfield, whereas the other signals below 0 ppm are shifted downfield. This could be a result of additional coordination of further aluminum derivatives to the formed complexes affording higher agglomerates. A major difference between hafnocene **2** and zirconocene **1** is the formation of an insoluble brown solid in case of zirconocene **1** at higher temperatures (entry 7), resulting in a worse signal to noise ratio. This behavior is in accordance with the literature, reporting the formation of a brown solid during the reaction of TIBA with $Ph_2C(CpFlu)ZrCl_2$ at higher temperatures (80°C).[214] In contrast, hafnocene **2** afforded similar results with 20 eq of TIBA for rt and 60 °C. Hence, with 20 eq of TIBA, one hour of reaction time and at the high concentrations applied during NMR investigations, results show no temperature induced limitation. However, NMR measurement itself was always conducted at rt after the reaction was performed for one hour at the specified temperature. Therefore, in case of a fast equilibrium reaction the temperature effect could also be missed.

Table 8: Ratio of the important signals and their chemical shifts of metallocenes **1, 2** after preactivation with TIBA to D, D‘ calibrated to 1.0.

				chemical shifts of the assigned signals/ ppm / integral of the assigned signals			
entry	**M**	**T[a]**	**Al:M**	**A; A’**	**B; B’**	**C; C’**	**D; D’**
1	Hf	60	10:1	6.14/ 7.3	-0.61/ 7.3	-1.36/ 7.1	-1.81/ 1.0
2	Hf	60	20:1	6.14/ 4.3	-0.58/ 3.9	-1.43/ 4.2	-1.82/ 1.0
3	Hf	60	50:1	6.12/ nd[b]	-0.55/ nd[b]	-1.66/ nd[b]	-1.94/ nd[b]
4	Hf	rt	20:1	6.14/ 4.2	-0.57/ 4.0	-1.44/ 4.1	-1.82/ 1.0
5	Zr	rt	10:1	6.22/ 5.0	-0.40/ 4.6	-1.06/ 4.3	-1.54/ 1.0
6	Zr	rt	20:1	6.22/ 4.5	-0.35/ 4.1	-1.12/ 3.7	-1.56/ 1.0
7	Zr	60	20:1	nd[b]	nd[b]	nd[b]	nd[b]

[a] In °C. [b] Signals are to small for a reasonable integration and/or picking.

For some alkylaluminum compounds such as TMA or TIBA, their reaction with a metallocene is reported to afford a direct formation of a polymerization active catalyst.[127, 219, 220] Even though a shift of the LMCT-band to wavelengths of about 500 nm (the reported region of a polymerization active catalyst) cannot be observed, it is interesting to test the products formed during NMR investigations for the polymerization of α-alkenes.[221] Based on the similarity of preactivation reaction products of hafnocene **2** and zirconocene **1**, experiments with hafnocene **2** are considered to be representative for both. 1-Hexene was added to the preactivated complex **2** at different M:Al ratios (1:10, 1:30 and 1:50) at 60 °C. ^{1}H NMR spectra were recorded after 5 h, but in all cases, no consumption of 1-hexene was observed. Even after 1 day, no 1-hexene was consumed whereas after the addition of $[CPh_3][B(C_6F_5)_4]$ to the reaction mixture, the monomer was completely polymerized to poly(1-hexene). Hence, the observed species of metallocenes **1** and **2** are not active for polymerization of α-olefins.

To sum up all abovementioned results (UV-Vis, NMR and polymerization), big differences for hafnocene **2** compared to zirconocene **1** during the preactivation reaction with TIBA can be seen. Even if NMR investigations can show contradicting results, the product formed, in case of concentrations used for the preactivation and polymerization reaction, was shown to be different for the two metallocenes **1** and **2**. This is also a proof that results obtained from NMR spectroscopy for such preactivation and activation reactions must be generally regarded with care. Finally, these different preactivation products are assumed to be the reason for the lower observed activity of the hafnocene **2** compared to the zirconocene **1**. This is due to the formation of a different active species or at least due to a different reaction pathway towards similar polymerization active species. In addition, for hafnocene **2**, the participation of DIBAL-H during activation was shown to be very likely.

4.1.3 *Influence of Polymerization Temperature on Molecular Weights of Produced ePPs*

The elastic behavior of ePP is known to be predominantly controlled by the amount of isolated stereoerrors and the molecular weight (2.9.3). Therefore, it is important to obtain polypropylenes with sufficiently high molecular weights to fulfill the mechanical demands of an ePP. For high propene concentrations at low polymerization temperatures, molecular weights of up to 5 000 000 g/mol are reported for polymers produced with the dimethylated hafnocene **2**, activated with $[CPh_3][B(C_6F_5)_4]$. In contrast, polymerization reactions performed

under identical conditions with the dimethylated zirconocene **1** afford ePPs with molecular weights below 1 000 000 g/mol.[68] Increasing the polymerization temperature led as expected, to polymers with lower molecular weights for both metallocenes. This is a consequence of increased chain release reaction rates at higher temperatures (Figure 27). For experiments concerning temperature effects, the propene concentration was kept as constant as possible.

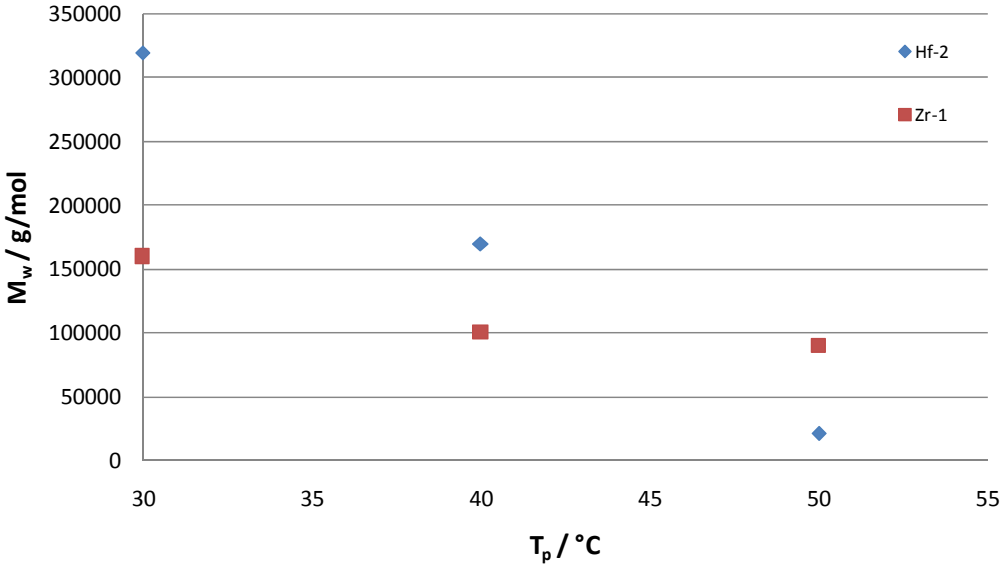

Figure 27: Influence of the polymerization temperature on the molecular weights of the PPs produced with complexes **1, 2** (5 µmol) activated with TIBA (200 eq)/$[CPh_3][B(C_6F_5)_4]$ (5 eq) at similar propene concentrations (1.2 ± 0.1 mol·L^{-1}) (propene concentrations were calculated using the equation reported by *Busico et al.*[222]).

Comparing the two metals, a significant difference for the decrease of the molecular weight upon increasing temperatures is observed. At lower temperatures, hafnocene **2** produces PP with much higher molecular weights than zirconocene **1**. At a specific temperature (in this case around 45 °C), the molecular weight of the polypropylene formed with zirconocene **1** becomes higher compared to the molecular weight of the polymer produced by hafnocene **2**. This much more pronounced drop of molecular weight with increasing polymerization temperature for hafnocene **2** must be a reason of different chain transfer reactions taking place for the two catalysts. The details therefore will be separately discussed in the subsequent sections.

4.1.4 *Chain Transfer Reactions to the Co-catalyst*

Chain transfer reactions to the co-catalyst are known to occur especially at high amounts of sterical less hindered alkylaluminum derivatives (e.g. TMA in MAO).[128] In case of a stable heterodinuclear complex, which is formed during the transfer of the polymer chain, also lower activities can be observed. The standard ternary catalyst used for the C_1-symmetric

complexes **1** and **2**, contains TIBA as a co-catalyst. Hence, due to the higher sterical hindrance less transfer reactions via aluminum should be obtained. As already discussed above, TIBA always contains DIBAL-H which influences not only the activation reaction but also acts as a transfer agent due to less steric hindrance compared to TIBA. Especially at temperatures above 60 °C more DIBAL-H is formed from TIBA via β-hydride transfer reaction.[216] Hence, polymers with lower molecular weights at higher polymerization temperatures could also be a result of a chain transfer reaction to DIBAL-H. However, due to the low amount of DIBAL-H, a significant participation as a chain transfer agent is only reasonable assuming a catalytic transfer mechanism. A theoretical chain transfer mechanism including DIBAL-H as a catalytic chain transfer agent is therefore proposed (Scheme 25). After the formation of the heterodinuclear complex and the transfer of the polymer chain to DIBAL-H it can be released in analogy to isobutene via β-hydride elimination. Due to the higher steric hindrance of the polymer chain compared to isobutyl, an increased selectivity for the release of the polymer chain would be reasonable. In order to clarify a possible participation of TIBA and DIBAL-H as chain transfer agents, reducing molecular weight of the polymers produced at elevated and high polymerization temperatures, different aluminum co-catalysts were synthesized.

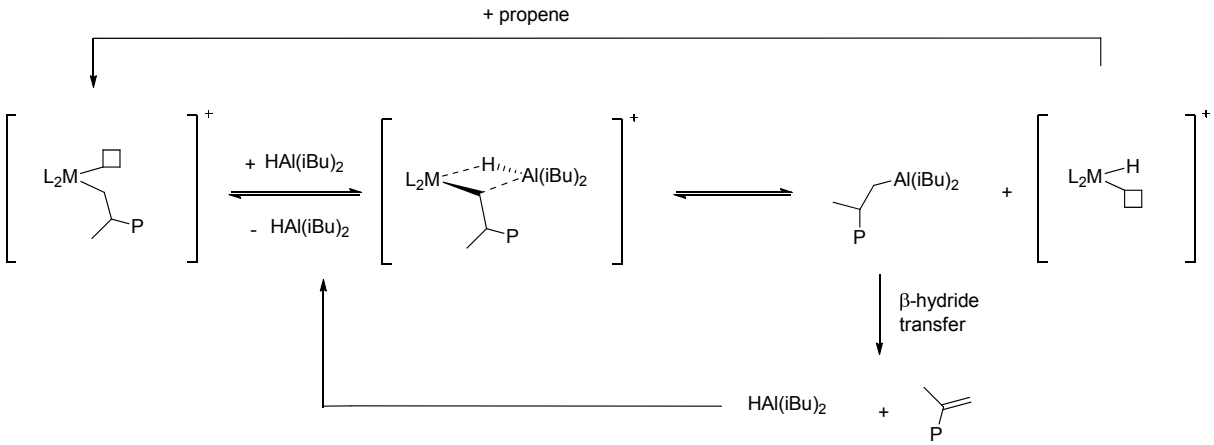

Scheme 25: Proposed catalytical chain transfer mechanism via DIBAL-H (counteranion is omitted for clarity).

For a successful suppression of a chain transfer to TIBA or DIBAL-H the co-catalyst can be modified in three different ways. First, an increased steric hindrance of the co-catalysts, second, a decrease of the *Lewis* acidity and third, addressing the catalytic chain transfer via DIBAL-H, is usage of aluminum co-catalysts with lack of β-hydrogen atom. The higher steric hindrance together with a lower *Lewis* acidity affords an aluminum compound with a lower probability for the formation of the heterodinuclear complex. Thus, transfer of the polymer chains to the co-catalyst is suppressed. Synthesized aluminum co-catalysts were trineopentylaluminum and $MeAl(BHT)_2$ (BHT = 2,6-di-*tert*-butyl-4-methylphenol). Both

were prepared via literature known synthesis routes.[223, 224] Latter is reported in particular as a noninteracting co-catalyst in the coordination-insertion polymerization of α-olefins with metallocenes.[224-227] However, due to the decreased reactivity of $MeAl(BHT)_2$ compared to TIBA, especial in case of the reaction with impurities such as water, the polymerization process was modified towards longer pre-stirring times of the aluminum co-catalyst in toluene before addition of the metallocene. Both aluminum derivatives cannot be used for the preactivation reaction of the dichloro precursor of **2**. Therefore the dimethylated precursor of **2** was synthesized via a literature known procedure.[68] A comparison of the results for the different co-catalysts during the polymerization of propene with hafnocene **2** indicates a slight increase of the molecular weight (Table 9, entries 1 → 2 → 3), being in accordance with a decreasing *Lewis* acidity. However, with an error deviation of about 10 % for the GPC device, the observed molecular weight difference is in the same range as error deviation. These results prove only minor influence of the co-catalyst on the molecular weights of produced PPs. Hence, the main reason for the observed significant decrease of the molecular weight of the polymers formed at increasing temperatures, especially for hafnocene **2**, cannot be a result of the chain transfer to TIBA or DIBAL-H.

Table 9: Polymerization of propene with hafnocene **2** and different co-catalysts.[a]

entry	complex	Al-compound	Hf/Al autoclave	$T_{preactivation}$ [b]	M_w [c]
1	$HfCl_2$ **2**	TIBA	1/310	60	35000
2	$HfMe_2$	Trineopentyl-aluminum	1/420	-	39000
3	$HfMe_2$	$MeAl(BHT)_2$	1/370	-	44000

[a] Polymerization conditions: $p = p_{Ar} + p_{propene} = 5.5$ bar, with $p_{Ar} = 1.9 \pm 0.2$ bar, $T_p = 60$ °C, $n_{complex} = 5$ µmol, 5 eq of $[CPh_3][B(C_6F_5)_4]$, preactivation for entry 1 : 200 eq of TIBA. [b] In °C. [c] In g/mol.

4.1.5 *Transfer Reactions: The Difference between Zr and Hf*

Polymers produced with complexes **1** and **2** at elevated temperatures were shown to have a low M_n. Therefore, the polymer chain end groups can be detected via ^1H NMR spectroscopy. These end groups can give further information on the transfer reactions taking place in case of zirconocene **1** and hafnocene **2**. The olefinic region of the ^1H NMR spectra of two polymers,

one produced with zirconocene **1**, the other with hafnocene **2** at the same conditions, are depicted in Figure 28.

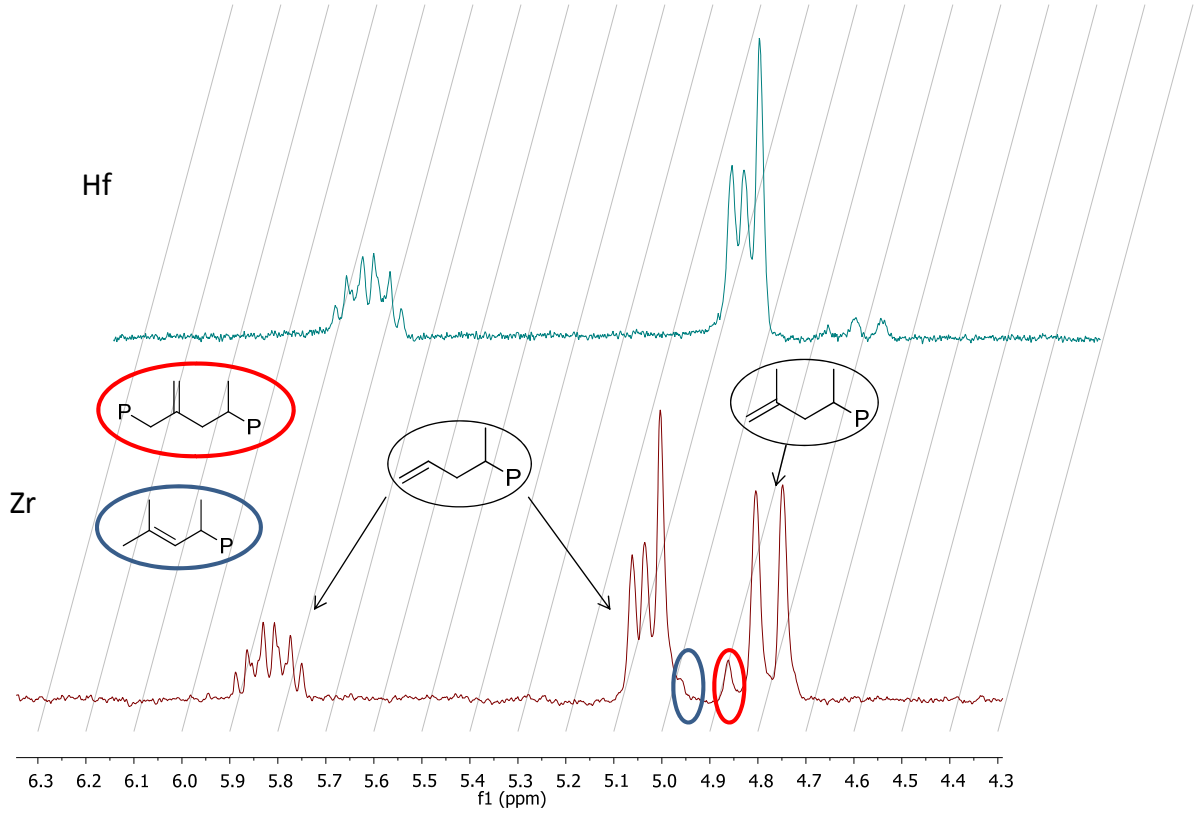

Figure 28: End group analysis via ^{1}H NMR spectroscopy (at 100 °C in C_6D_5Br) of two polymers, one produced with zirconocene **1** (bottom), the other with hafnocene **2** (top). ($n_{complex}$ = 5 µmol, 200 eq TIBA, 5 eq $[CPh_3][B(C_6F_5)_4]$, T_p = 80 °C, p = $p_{propene}$ + p_{Ar} = 7.6 bar, with p_{Ar} = 1.9 ± 0.2 bar)

Zirconocene **1** shows the formation of two main polymer chain end groups. These are vinylidene- and allyl-terminated chain ends with a ratio of 1:0.8 under applied conditions. Former end group is generated via a β-hydride, latter via a β-methyl transfer reaction. In addition two small singlets, one at 4.95 ppm, the other at 4.86 ppm are observable. These two signals can be assigned to polymer chains with internal double bonds and are reported to be formed via isomerization reactions.[100] In contrast to the polymer produced by zirconocene **1**, that produced by hafnocene **2**, shows a very selective chain transfer reaction towards polymers with an allylic chain end. Only minor amounts of vinylidene terminated polymer chains can be detected.

The β-hydride transfer reaction (2.7.1) is known to occur either unimolecular or bimolecular. A suppression of the bimolecular transfer mechanism is possible in case of C_2-symmetric bisindenyl-based metallocenes by introduction of a 2-methyl substituent (2.10.2.1). In contrast, for the β-methyl transfer reaction, predominantly a unimolecular reaction pathway is

reported. However, there are some reports on a bimolecular transfer reaction.[123-125] In order to investigate the molecularity of the β-methyl transfer reaction for studied C_1-symmetric complexes **1** and **2**, further polymerization experiments with increasing propene pressure were conducted at a constant temperature of 60 °C. The obtained polymers were analyzed by ^{1}H NMR spectroscopy and GPC. In case of polymers produced by hafnocene **2**, the degree of polymerization (P_n) was determined via ^{1}H NMR spectroscopy assuming all polymers to have an unsaturated chain end. For polymers produced by zirconocene **1**, the determination of P_n via end group analysis is too inaccurate. Hence, M_n determined by GPC was used for calculation of P_n. By plotting P_n over propene concentration, its influence on the obtained P_n and thus the influence of bimolecular transfer reactions can be elucidated. For comparison, $SiMe_2(BenzInd)_2ZrCl_2$, a complex known to predominantly undergo a bimolecular β-hydride transfer reaction is also plotted.[113] Values of propene concentration in case of complex **1** and **2** were calculated using *Busico´s* equation for the solubility of propene in toluene.[222] To get a better comparison, propene concentration values reported by *Stehling et al.* were also recalculated using *Busico´s* equation. For both complexes **1** and **2**, P_n is increased with propene concentration (Figure 29). In contrast, the C_2-symmetric complex $SiMe_2(BenzInd)_2ZrCl_2$ shows in particular at concentrations above 0.5 mol/L no significant increase of P_n with propene concentration. Hence, these results reveal no or only minor amount of bimolecular transfer reactions for complexes **1** and **2** under applied conditions.

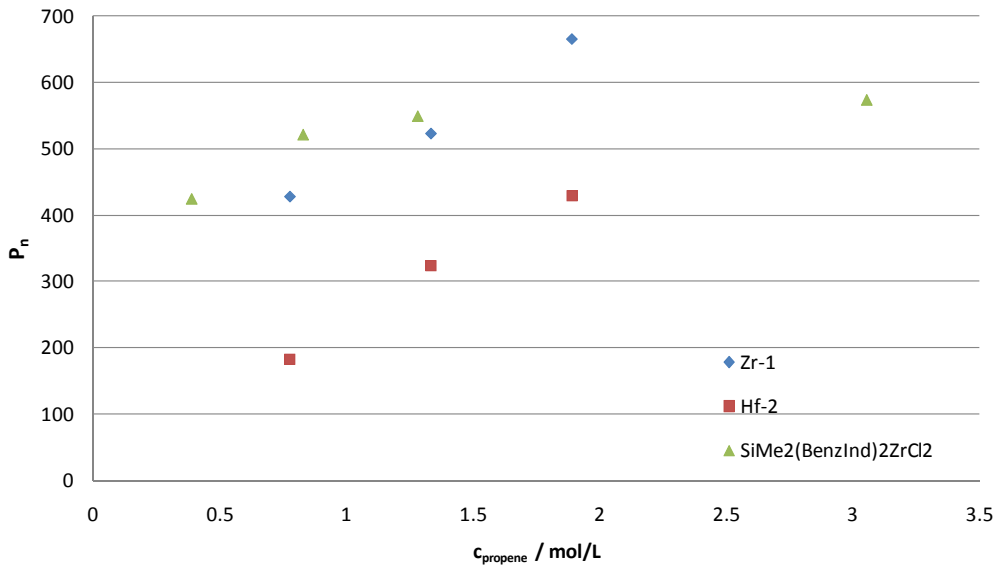

Figure 29: Dependency of P_n of the propene concentration in case of the polymerization of propene with complex **1** and **2** at T_p = 60 °C, ($n_{complex}$ = 5 µmol, 200 eq TIBA, 5 eq $[CPh_3][B(C_6F_5)_4]$) compared to a literature known metallocene at T_p = 50 °C.

For a more quantitative interpretation, the rate constants of the different chain transfer reactions can be calculated. In case of linear increase of catalyst activity with propene concentration equation 1.1 can be transformed into equation 1.2 (with [C] = concentration of the active catalyst; [M] = propene concentration; k_p = rate constant of the polymerization; k_{tu} = rate constant of the unimolecular transfer reaction and k_{tb} = rate constant of the bimolecular transfer reaction). For the investigated catalysts at the applied conditions, equation 1.2 can be used and transformed into equation 1.3 in order to determine different chain transfer rate constants by plotting $1/P_n$ against $1/c_{propene}$.

$$P_n = \frac{\sum R_p}{\sum R_t} \tag{1.1}$$

$$P_n = \frac{k_p \cdot [C] \cdot [M]}{k_{tu} \cdot [C] + k_{tb} \cdot [C] \cdot [M]} = \frac{k_p \cdot [M]}{k_{tu} + k_{tb} \cdot [M]} \tag{1.2}$$

$$\frac{1}{P_n} = \frac{k_{tu}}{k_p} \cdot \frac{1}{[M]} + \frac{k_{tb}}{k_p} \tag{1.3}$$

Polymerization experiments with complexes **1** and **2** were conducted with an argon system pressure of 1.9 bar with a deviation of about ± 0.2 bar. Therefore the partial pressure of propene and thus also propene concentration calculated by Busico´s equation is inaccurate. In order to account for this inaccuracy, error bars are included in the diagrams of the polymerization experiments of metallocenes **1** and **2** (conducted at a polymerization temperature of 60 °C after activation with TIBA and $[CPh_3][B(C_6F_5)_4]$, Figure 30 and Figure 31). For determination of chain transfer rate constants, the best fit straight lines using the calculated propene concentration with an argon system pressure of 1.9 bar, were plotted. In addition, propene concentration errors are considered by plotting two more straight line fits, one with highest, other with lowest slope. Especially the data points obtained with zirconocene **1** show a poor fitting. Therefore obtained absolute values for the different chain transfer rate constants must be regarded carefully, particularly these of zirconocene **1**. A qualitative interpretation of these values affording additional information, whether the β-methyl transfer is uni- or bimolecular is anyhow possible.

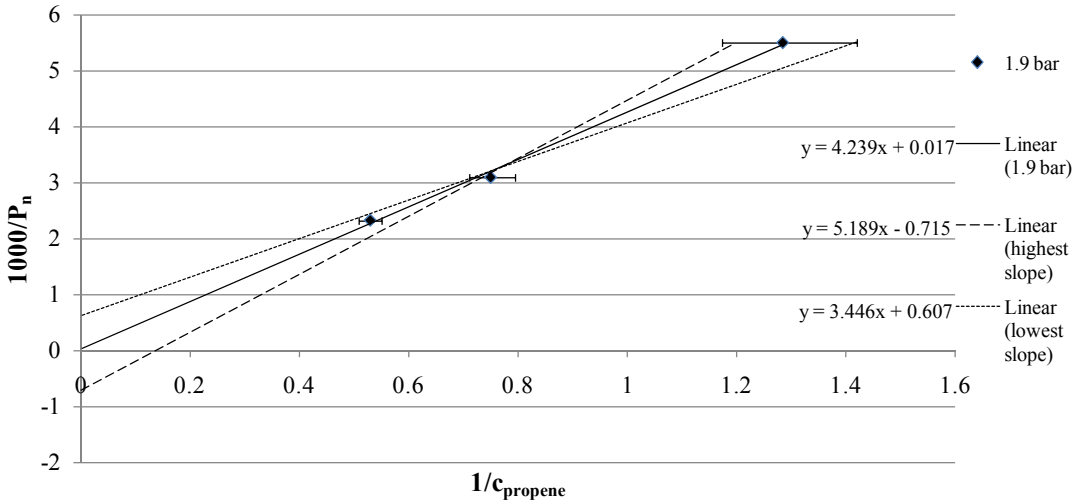

Figure 30: Plot for the determination of the uni and bimolecular transfer reaction rate constants relative to the rate of propagation for hafnocene **2** (T_p = 60°C).

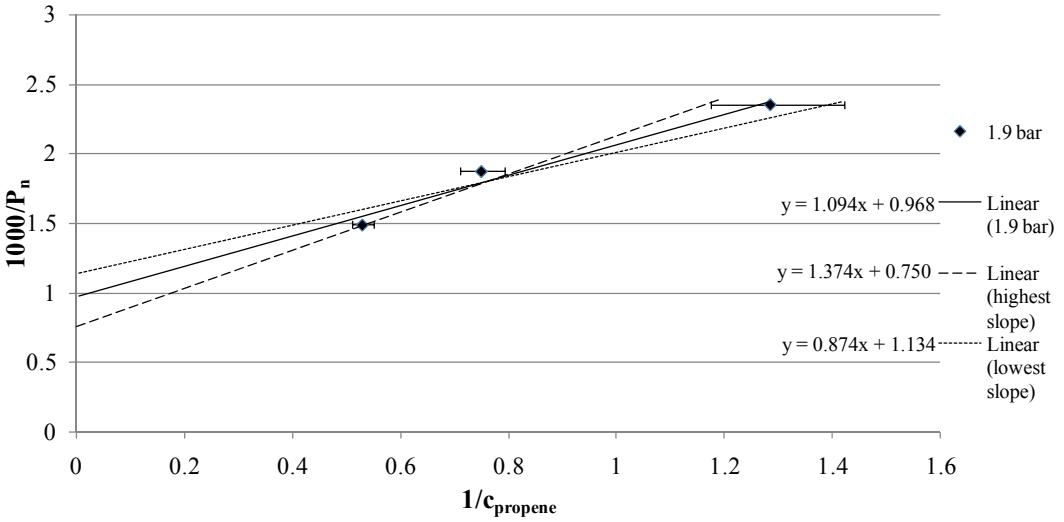

Figure 31: Plot for the determination of the uni and bimolecular transfer reaction rate constants relative to the rate of propagation for zirconocene **1** (T_p = 60°C).

For a better understanding, values of *Stehling et al*. were recalculated concerning the propene concentration for $SiMe_2(BenzInd)_2ZrCl_2$ and $SiMe_2$(2-Me-$BenzInd)_2ZrCl_2$ and also plotted.[113] Results are summarized together with the values of hafnocene **2** and zirconocene **1** in Table 10. Chain transfer for $SiMe_2(BenzInd)_2ZrCl_2$ is known to predominantly occur via a β-hydride transfer reaction to the monomer, thus the rate constant k_{tb} is found to be about five times the rate constant k_{tu}. The analog complex with an additional 2-Me substituent, known to suppress the bimolecular transfer reaction (2.10.2.1), affords a slightly higher rate constant for the unimolecular transfer reaction than for the bimolecular transfer reaction.

Table 10: Determined rate constants of uni- and bimolecular transfer reactions relative to rate constants of propagation for **1** and **2** compared to values of metallocenes reported in literature.

complex	$\frac{k_{tu}}{k_p}$ / 10^{-3}		$\frac{k_{tb}}{k_p}$ / 10^{-3}	
1	1.094	+ 0.280 - 0.220	0.968	- 0.218 + 0.166
2	4.239	+ 0.950 - 0.793	0.017	- 0.732 + 0.590
$SiMe_2(BenzInd)_2ZrCl_2$	0.282		1.615	
$SiMe_2(2\text{-}Me\text{-}BenzInd)_2ZrCl_2$	0.238		0.185	

As already mentioned, the absolute determined values have a relatively big error due to inaccuracy of the polymerization procedure, error of analysis and the low number of experiments. To get more precise data over a broader propene concentration range, more experiments, especially at higher and at very low propene concentration, have to be performed. So far, propene concentrations far above and below those applied, have not been accessible with the given polymerization set-up. The obtained rate constants for zirconocene **2** do not allow an interpretation concerning a preference of the uni or the bimolecular transfer reaction. However, hafnocene **2** shows, under applied conditions (range of propene concentration and T_p), a high preference for the unimolecular transfer reaction with a rate constant k_{tu} being at least six times higher than k_{tb}.

For hafnocene **2** a high selectivity towards the β-methyl transfer reaction was shown above. Therefore, a bimolecular pathway for the β-methyl transfer reaction in case of hafnocene **2** plays no or only minor role, at least for the applied conditions. In contrast zirconocene **1** has a lower selectivity for the β-methyl transfer, also showing a certain amount of β-hydride elimination. Hence, for zirconocene **1** a unimolecular β-methyl transfer reaction is most likely to occur alongside a β-hydride transfer reaction with at least a certain amount of a bimolecular transfer reaction.

4.1.6 *Postulated Transfer Mechanism: The Difference between Zr and Hf*

In the literature, there are unfortunately only few reports on an investigation of hafnocenes and zirconocenes with respect to their transfer reactions in combination with a molecular weight dependency of polymers produced at varying polymerization temperatures (Table 11). However, a comparison with these data will help to better understand the differences in the observed polymerization behavior of C_1-symmetric complexes **1** and **2**.[100, 156]

Table 11: Comparison of literature known metallocenes of Hf and Zr with regard to their polymerization behavior concerning polymer end groups and molecular weight dependency.[a]

entry	complex	co-catalyst	T_p[b]	P_n	β-Me[c]	β-H[c]	Al_t[c,d]
1	Cp_2ZrCl_2	MAO	50	17	-	100	-
2	Cp_2HfCl_2	MAO	50	140	-	100	-
3	$Cp^*_2ZrCl_2$	MAO	50	4.5	91.1	7.9	1
4	$Cp^*_2ZrCl_2$	MAO	0	95	81.8	7.1	11.1
5	$Cp^*_2HfCl_2$	MAO	50	3.4	98	2	traces
6	$Cp^*_2HfCl_2$	MAO	0	27	66.6	2.1	31.3
7	$Et(Flu)_2ZrCl_2$	MAO	50	1700	-	-	-
8	$Et(Flu)_2HfCl_2$	MAO	50	1600	-	-	-
9	$Et(Flu)_2ZrCl_2$	MAO	50	315	75	25	-
10	**1**	TIBA/**V**[e]	60	430[f]	64[h]	34[h]	-
11	**2**	TIBA/**V**[e]	60	180[g]	95[h]	4[h]	-

[a] Polymerization conditions: in liquid propene for entries 1-8; $p = p_{propene}$-a = 4 bar for entry 9; $p = p_{propene} + p_{Ar} = 4.0$ bar, with $p_{Ar} = 1.9 \pm 0.2$ bar for entries 10-11. [b] In °C. [c] In %. [d] Al_t: transfer to aluminum. [e] **V**: $[CPh_3][B(C_6F_5)_4]$. [f] Determined by GPC. [g] Determined by ^{1}H NMR spectroscopy. [h] Difference to 100 % is due to the formation of internal double bonds.

Metallocenes of Hf and Zr with a preference for β-hydride transfer reaction, show at a polymerization temperature of 50 °C the formation of polymers with a higher P_n for the respective hafnocene (entries 1 and 2). This behavior is in accordance with a β-hydride transfer rate, which is relative to this of propagation, higher in case of the zirconocene. More sterically hindered complexes such as $Cp^*_2MCl_2$ or $Et(Flu)_2MCl_2$ (M = Zr, Hf), are reported to have a higher selectivity for β-methyl compared to β-hydride transfer reactions. In contrast to the less sterically crowded metallocenes, the hafnocenes of these complexes are reported to produce PP with similar to slightly lower molecular weights at elevated polymerization

temperature (entries 3, 5, 7 and 8). In analogy to the polymerization behavior of metallocenes **1**, and **2** for reported catalysts a reversed behavior should also be obtained at low polymerization temperatures. Unfortunately, $Cp^*_2MCl_2$ (M = Zr, Hf) also produce at low temperatures polymers with lower molecular weight in case of the hafnocene (entries 4, 6). However, the reason for this behavior can be ascribed to the more significantly increased amount of chain transfer reactions to aluminum in case of the hafnocene compared to the zirconocene affording reduced molecular weights.

These reports demonstrate that metallocenes which show a preference for the β-methyl transfer reaction generate polymers with slightly lower molecular weights for the respective hafnocenes. Hence, this seems to be a general trend which is in accordance with observations of the polymerization behavior of metallocenes **1** and **2**. However, besides the generally similar behavior of metallocenes **1** and **2**, and already published metallocenes, a more pronounced difference of P_n and a higher selectivity towards the allylic chain ends for the hafnocene is obvious in case of metallocenes **1**, and **2** (entries 3, 5; 7, 8; 10, 11). One explanation for this behavior is a higher difference of the hafnocene´s activation barriers for the β-methyl and the β-hydride transfer reaction for metallocenes **1**, and **2**. In addition, for these C_1-symmetric metallocenes also a combination of their characteristic back skip polymerization mechanism and a site dependent transfer reaction could account for this behavior. In case of C_{2v}-symmetric complexes (entries 1-7) both active sites have a similar steric demand whereas the C_1-symmetric complexes are differently crowded on their active sites. Therefore, a different preference for the transfer reaction depending on the site of the complex is expected (Figure 32). A polymer chain situated on the less sterically hindered site (blue-marked) is assumed to undergo a β-hydride transfer reaction due to its similarity to *rac*-$SiMe_2(2\text{-Me-Ind})_2ZrCl_2$ and *rac*-$C_2H_4(Ind)_2ZrCl_2$, which are both known to afford predominantly a β-hydride transfer reaction.[100] In contrast, a polymer chain coordinated to the more sterically hindered site (red-marked) is assumed to have a high preference for a unimolecular β-methyl transfer reaction, analog to the depicted C_{2v}-symmetric complex.[100, 156]

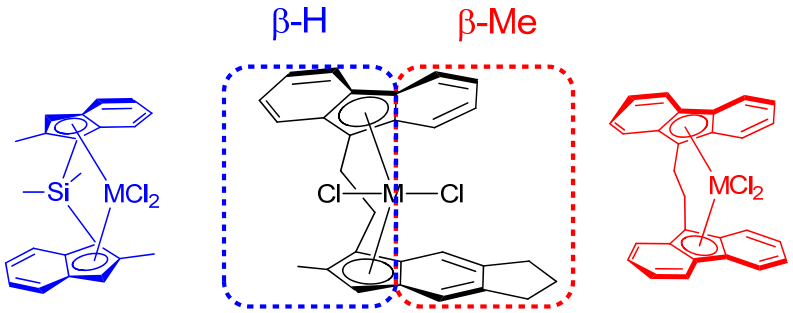

Figure 32: Proposed site dependency of the transfer reactions for metallocenes **1** and **2**.

The unexpectedly higher selectivity of hafnocene **2** towards allylic chain ends can be explained by a slower chain back skip of the polymer chain from the sterically more hindered to the opposite site of the complex. Consequently, the polymer chain has a longer resting time on the sterically more crowded site of the complex leading to an increased probability of the unimolecular β-methyl transfer reaction. The slower chain back skip for hafnocene **2** is also supported by investigations of *Bochmann* and coworkers. They studied the site epimerization of $[SBIMCH_2SiMe_3]^+[B(C_6F_5)_4]^-$ (M = Zr, Hf) and found a slower epimerization reaction for the hafnocene.[228] A further proof for the rate of the chain back skip can be given by polymerization experiments of complexes **1** and **2** (Table 12). Polymers produced by hafnocene **2** at different temperatures always have a lower amount of mmmm-pentad compared to polymers produced with zirconocene **1**. According to the underlying polymerization mechanism of these C_1-symmetric complexes (2.9.1) this observation is a result of a, relative to the rate of propagation, slower chain back skip of hafnocene **2.**

Table 12: Comparison of the amount of mmmm pentad for complexes **1** and **2**.[a]

complex	T_p[b]	p[c]	mmmm[d]
1	30	3.7	43
1	60	5.5	60
2	30	3.7	34
2	60	5.5	44

[a] Polymerization conditions: $n_{complex}$ = 5 µmol, 200 eq TIBA, 5 eq $[CPh_3][B(C_6F_5)_4]$. [b] In °C. [c] $p = p_{propene} + p_{Ar}$ with $p_{Ar} = 1.9 \pm 0.2$ bar. [d] In %.

4.1.7 *Modification of Ligand Structure of the C_1-symmetric Complexes for a Suppression of Transfer Reactions*

For the synthesis of high molecular weight ePP at high polymerization temperatures, the ligand structure of C_1-symmetric complexes used was modified with the aim to suppress the main transfer reactions. A position known to influence transfer reactions is the 2-position on the indenyl moiety. Higher steric hindrance on this position reduces the β-hydride transfer to the monomer (2.10.2.1). This substitution pattern could increase the molecular weight of polymers produced by zirconocene **1** where a certain amount of bimolecular β-hydride transfer reactions is present (4.1.5). With the intention to increase molecular weights of ePP produced at higher polymerization temperatures by hafnocene **2**, the activation barrier for β-methyl transfer has to be increased. This reaction is reported to proceed via a γ-agostic

interaction in the transition state.[122] In case of complexes **1**, and **2** the indenyl moiety is tilted towards the fluorenyl ligand with the 2-methyl-substituted cyclopentadienyl moiety. The introduction of higher steric hindrance in 2-position of the indenyl ligand can be assumed to reduce this tilt, additionally leading to increased steric hindrance on the already more encumbered site. In order to investigate if higher steric hindrance on both sites of the catalyst will influence bimolecular and unimolecular transfer reactions, the methyl group in 2-position was changed to a phenyl substituent. For the synthesis of the desired complex, the ligand was synthesized according to Scheme 26.

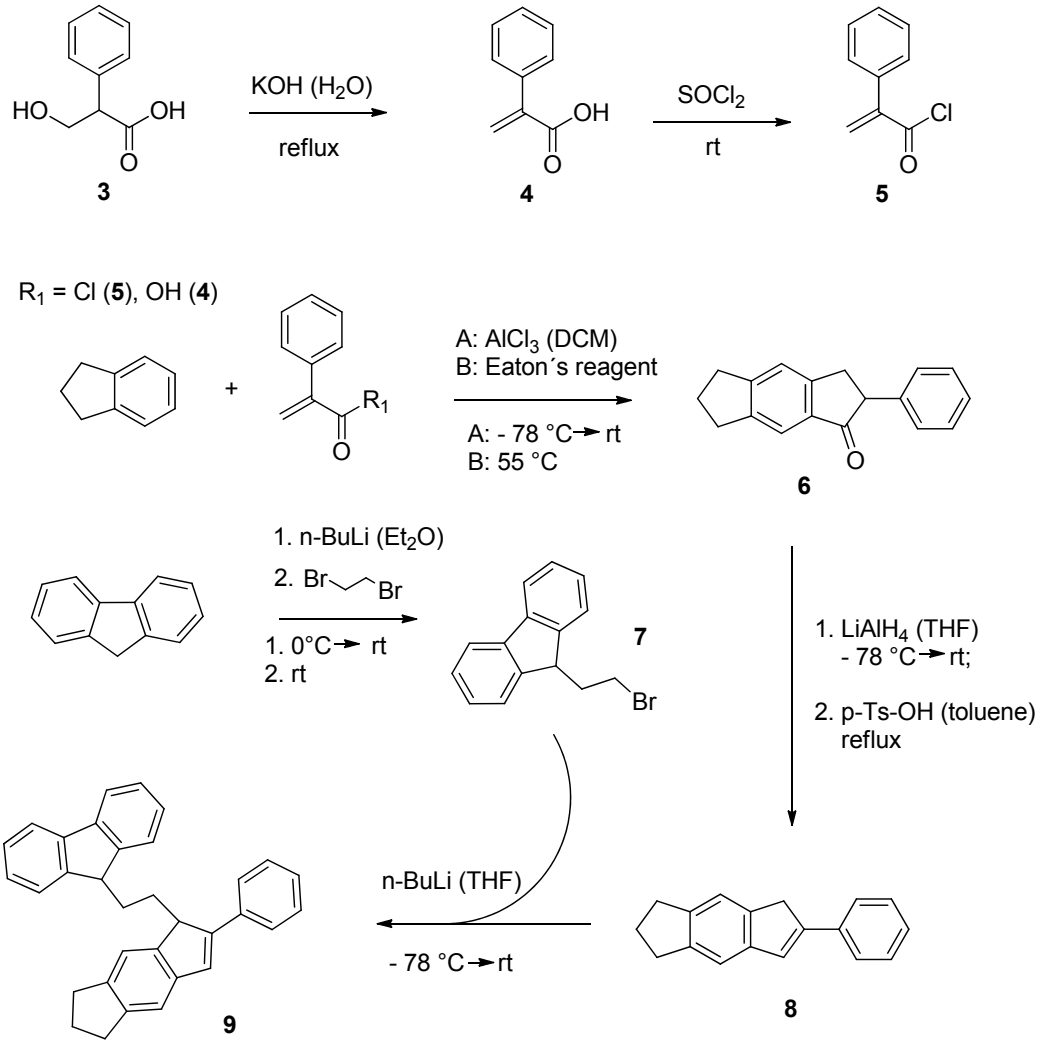

Scheme 26: Synthesis route of ligand **9**.

In a first step, tropic acid **(3)** is converted in an alkaline elimination reaction to atropic acid **(4)** using potassium hydroxide and a slightly modified version of the literature known synthesis route resulting in higher yield.[229, 230] Carboxylic acid **4** was either directly used in the next synthesis step or converted with thionylchloride in a further step to carboxylic acid chloride **5**. Latter was synthesized due to its higher electrophilicity and higher reactivity for

the subsequent nucleophilic attack of the indane. Unfortunately, the tendency for side reactions in case of the carboxylic acid chloride **5** led to a mixture of several products. Additionally, its handling is more complicated compared to carboxylic acid **4** due to its higher sensitivity towards moisture. Hence, the reaction with carboxylic acid **4** together with *Eaton´s* reagent (phosphorus pentoxide, 7.7 wt. % in methanesulfonic acid) and indane was preferred. The reaction mechanism for reaction of **4** and indane to indanone **6** is a two step mechanism. In a first step, a *Friedel Crafts* acylation is conducted, followed by a *Nazarov* cyclization reaction in the second step (Scheme 27).

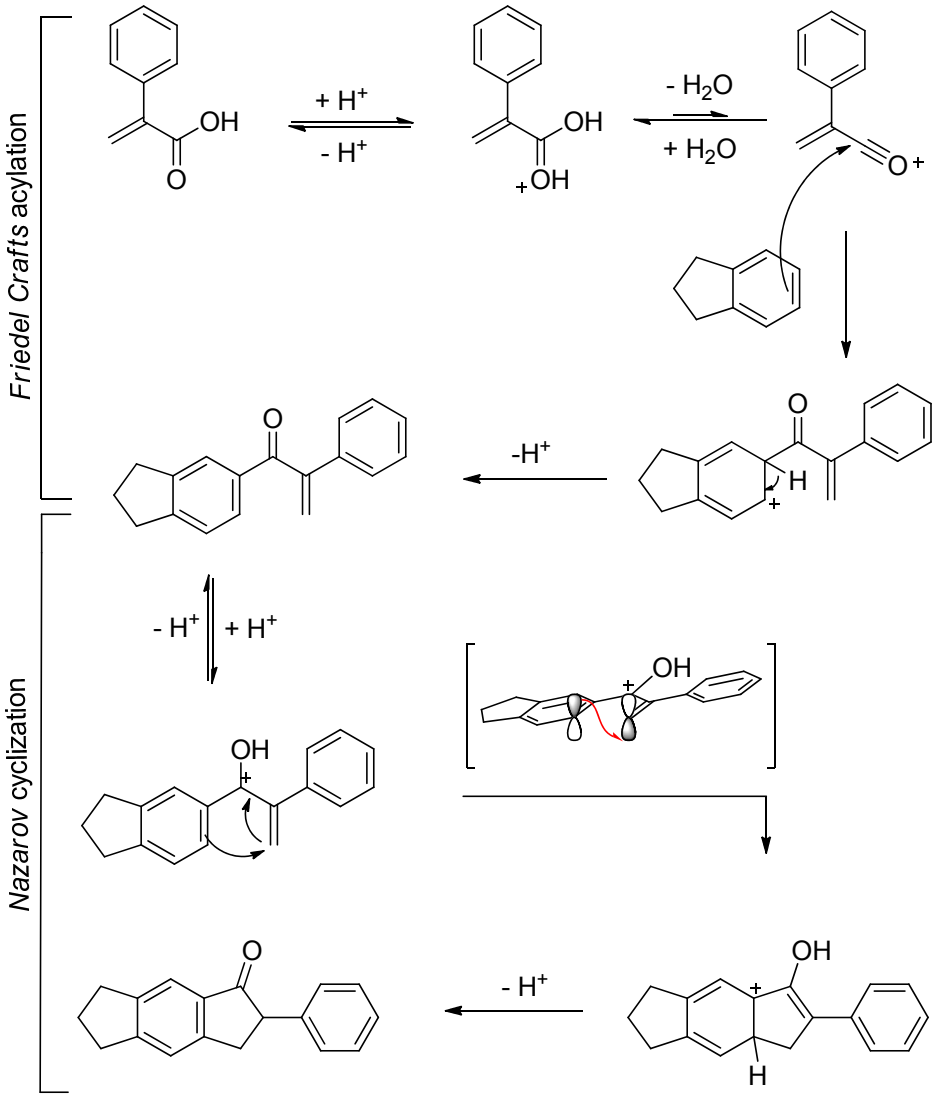

Scheme 27: Reaction mechanism of the two-step synthesis including *Friedel Crafts* acylation and *Nazarov* cyclization.

Eaton´s reagent activates the carboxylic acid and shifts equilibrium towards the more reactive acylium cation by reaction of phosphorus pentoxide with water. After electrophilic substitution of indane and the rearomatization the following *Nazarov* cyclization begins. Again, the intermediate is activated by protonation of the carbonyl oxygen atom. The 4π

electron system is known to undergo a 4π conrotatory electrocyclization reaction forming the indanone after rearomatization and transformation of the enol- to the keto-form.[231] Indanone **6** was reduced to a mixture of two isomers of the corresponding alcohol via a standard procedure with $LiAlH_4$ as reducing agent. After aqueous work-up this mixture was used without further purification for an acid-catalyzed elimination reaction with *p*-toluene sulfonic acid (*p*-Ts-OH) to indene **8**. Fluorenyl derivative **7**, already attached to the ethylene bridge, was obtained by reaction of excess dibromoethane with fluorenyllithium. Excess of dibromoethane is essential to suppress side reactions to difluorenylethane or spiro(cyclopropane-1,9′-fluorene). Deprotonation of indenylligand **8** with *n*-BuLi gave the lithium salt of **8**. Latter was reacted with ligand **7** in order to form the ethylene bridged ligand **9**. Unfortunately, only low yields of ligand **9** have been obtained so far. A major reason is the purification step affording moderate yields of pure product. First complexation reactions of $HfCl_4$ with ligand **9** and isolation of the desired complex have not been successful.

4.1.8 *Long-chain-branched (LCB) ePP*

During migratory insertion polymerization of propene catalyzed by metallocenes, different transfer reactions are known to occur, forming either saturated or unsaturated polymer chain ends, e.g. vinylidenic or allylic chain ends (2.7). As shown above, due to their higher selectivity for β-methyl transfer reaction, zirconocene **1** and particularly hafnocene **2** afford predominantly allylic in combination with a varying amount of vinylidenic polymer chain ends. In principle, both could be assumed to act as a macromonomer (MM) and thus be inserted during chain propagation. However, vinylidenic chain ends are hindered for coordination-insertion polymerization with metallocenes. The reason is an allyl-coordinated complex. Its formation is slower compared to the insertion of α-olefins, but faster than the insertion of a vinylidene macromonomer into the M-C bond of the growing polymer chain (Scheme 28). [50, 232-234] The insertion rate of α-olefins into such allyl-coordinated complexes is reported to be at least one to two order of magnitudes slower compared to typical insertion rates. Nevertheless, this reaction can take place in minor amounts and is reported as the reason for the formation of internal double bonds (Scheme 28), already discussed in section 4.1.5. Hence, significant amounts of macromonomer can only be incorporated if they exhibit an allylic chain end.

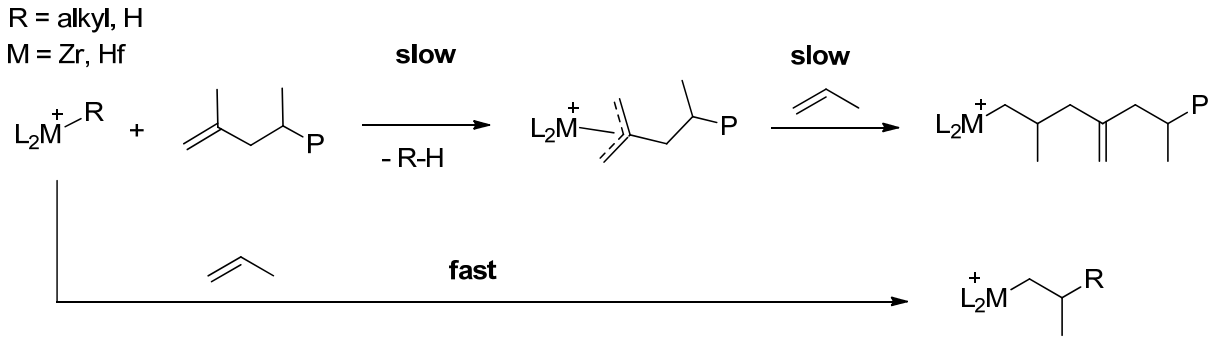

Scheme 28: Formation of $[L_2M\text{-allyl}]^+$ (M = Zr, Hf) complexes during the polymerization of propene (anion is omitted for clarity).

For a good elastic recovery of ePP produced with metallocenes **1** and **2**, a defined amount of stereoerrors and a high molecular weight are reported to be essential (2.9.3). In comparison to zirconocene **1**, hafnocene **2** produces polymers with higher molecular weights, but at the same time, these polymers have a higher amount of allylic chain ends. Therefore, besides the higher molecular weight, a higher quantity of long chain branches could also influence their mechanical behavior. Unfortunately, the amount of branches of ePP produced with metallocenes **1**, **2** is too low for a direct detection by ^{13}C NMR spectroscopy. In order to verify whether incorporation of PP macromonomers is theoretically possible for hafnocene **2**, a shorter macromonomer is separately produced at higher polymerization temperatures and afterwards copolymerized with ethene. In principle, this procedure can produce a mixture containing PE, PE with incorporated PP macromonomers and free macromonomer (Scheme 29).

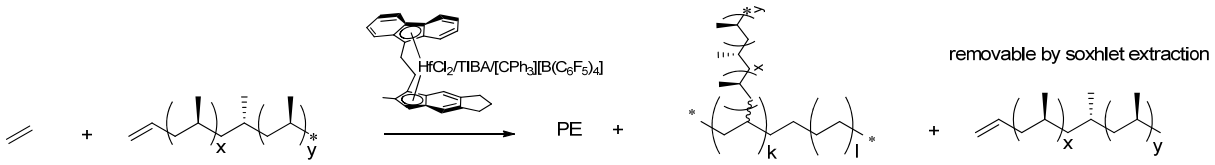

Scheme 29: Procedure for indirect proof of macromonomer incorporation during the formation of ePP by hafnocene **2**.

The high solubility of these PP macromonomers in pentane gives opportunity to remove not incorporated macromonomer after polymerization by soxhlet extraction. Hence, incorporated amount of macromonomer can easily be determined by ^1H NMR spectroscopy even at low incorporation levels. Therefore, the specific methine signal of the macromonomer, which is not overlayed with the methylene signals of the polymer backbone, was integrated (Figure 33). Before soxhlet extraction a low amount of olefinic signals from free macromonomer is detectable by ^1H NMR spectroscopy whereas afterwards they are absent. Together with

presence of methine and methyl signals after soxhlet extraction with pentane this proves copolymer formation.

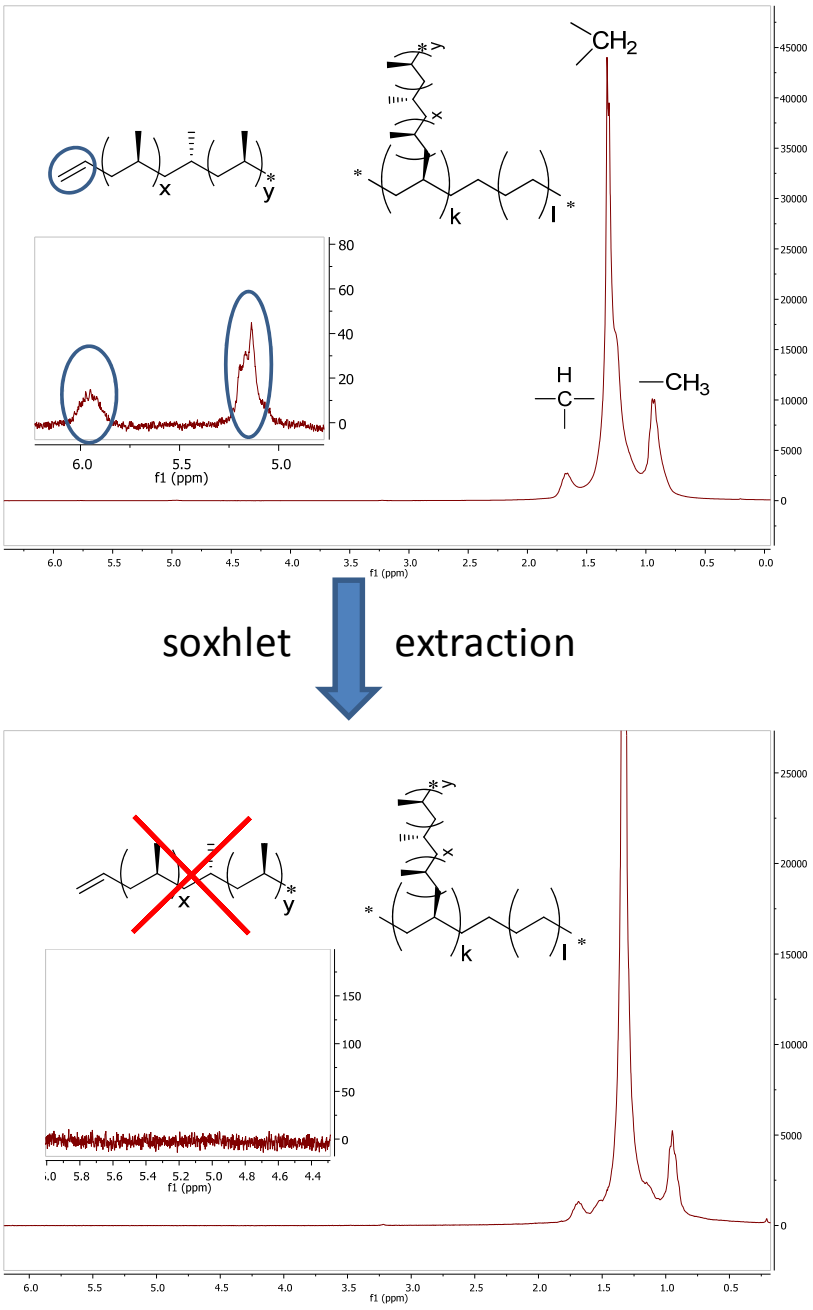

Figure 33: ^{1}H NMR spectra of a copolymer produced with hafnocene **1** using ethene and a PP macromonomer (M_n = 3900 g/mol) before (top) and after (bottom) soxhlet extraction with pentane.

An additional and more sensitive proof for quantitative removal of not incorporated macromonomer can be obtained from GPC traces of polymers before and after soxhlet extraction with pentane (Figure 34). A bimodal distribution is observed before and a monomodal distribution after extraction with pentane. Proof of purity by GPC analysis is especially important for copolymerization experiments using macromonomers with higher M_n

as the ratio of propene units to end groups is increased. Hence, small amounts of free macromonomer may not be detected by ^{1}H NMR spectroscopy.

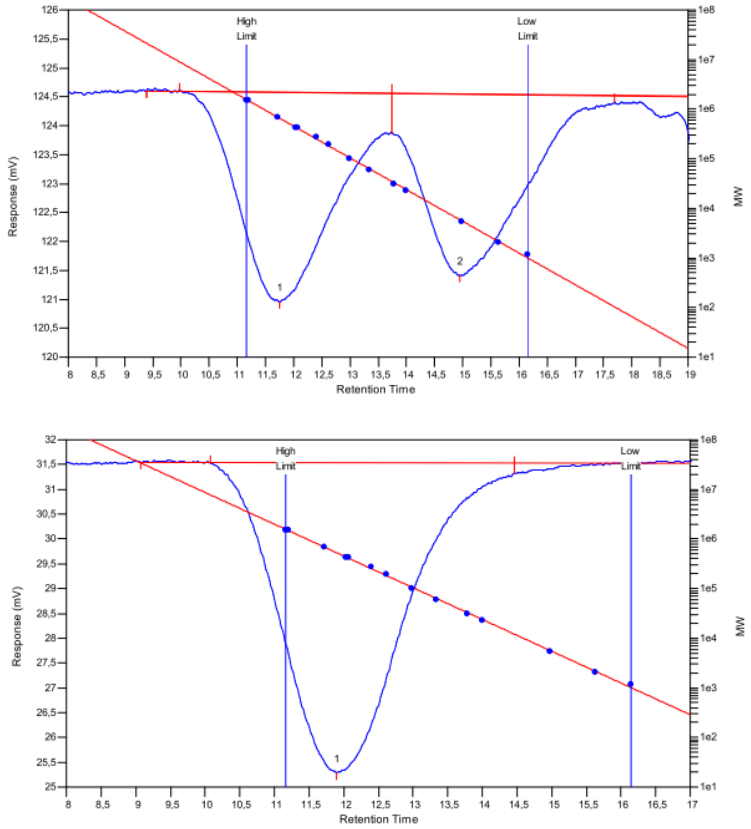

Figure 34: GPC traces (RI-detection) of a copolymer produced with hafnocene **2** using ethene and a PP macromonomer (M_n = 3900 g/mol) before (top) and after (bottom) soxhlet extraction with pentane.

These results show that the incorporation of PP macromonomers is possible during the polymerization of ethene by the C_1-symmetric complex **2**. Due to the higher propagation rate of ethene compared to propene, the incorporation of PP macromonomers during the polymerization of propene by hafnocene **2** is a reasonable assumption. Theoretically an enhanced chain release after incorporation of the macromonomer into a PP backbone compared to a PE backbone due to the increased steric hindrance is possible. However, with complex **2** also homopolymers of sterically more hindered α-olefins, i.e. 1-hexene or 4-methylpentene, were produced. Thus, a first hint for the formation of a LCB microstructure during the formation of ePP is given. In order to investigate the dependency of incorporation of these PP macromonomers on different parameters, e.g. polymerization temperature and macromonomer chain length, further polymerization experiments were conducted and will be discussed in the following section. Besides the indirect proof for the formation of LCB ePP, complex **2** will also be investigated regarding its application as a versatile catalyst for the formation of allylic macromonomers over a broad range of M_n and the formation of branched and long-chain-branched (LCB) copolymers.

4.1.9 *Formation of PP Macromonomers and their Copolymerization with Ethene*

The high selectivity of hafnocene **2** towards allylic polymer chain ends can be applied as a versatile tool for the production of PP macromonomers. These can be used for the formation of branched and long-chain-branched polymers. Latter are additives for metallocene-produced polymers to improve their poor melt processability (melt strength, shear thinning), being a result of their narrow MWD.[235-237] Macromonomers for the formation of LCB polymers are typically considered to be longer than 2.5 times the entanglement molecular weight (M_{ne}). For iPP and aPP, M_{ne} was determined to be 7000 g/mol, for syndiotactic PP below 3500 g/mol.[238, 239] PE macromonomers with high amount of allylic chain ends and sufficient molecular weight can be easily obtained by metallocenes due to the common β-hydride transfer reaction. However, for formation of PP macromonomers, only few examples are known fulfilling these requirements. Macromonomers with sufficient molecular weights and an increased amount of allylic chain ends were obtained for iPP and aPP (Scheme 30).[100, 156, 240, 241]

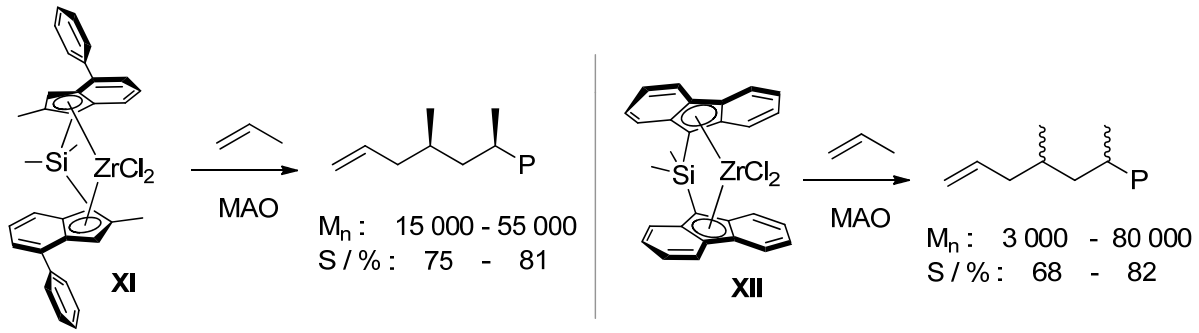

Scheme 30: Metallocenes reported for the formation of PP macromonomers with the highest allylic end group selectivity (S) for isotactic and atactic microstructures fulfilling at the same time requirements of polymer chain length for the formation of LCB polymers.

PP macromonomers with syndiotactic microstructures are available using bis(phenoxyimine)titanium dichloride catalysts. [242] These complexes produce suitable macromonomers due to an enhanced 2,1-insertion leading to α-olefinic chain ends after a β-hydride transfer reaction. However, under applied conditions necessary for the production of macromonomers with sufficient M_n and α-olefinic end group selectivity, these catalysts are less active compared to metallocenes **XI** and **XII**. Recently, a copolymer of ethene and propene produced with a $Cp^*_2ZrCl_2$/MAO catalyst was reported to have high amount of allylic chain ends.[243, 244] Molecular weights of these polymers are increased with increasing ethene concentration (8000 – 25 500 g/mol). A further advantage of these copolymers was shown to be their good solubility which ensures complete separation of unreacted

macromonomer from LCB copolymer. However, due to the lower solubility of PE domains, appreciable solubility is only obtained for macromonomers having a limited amount of ethylene units. Hence, to ensure sufficient solubility in organic solvents the molecular weight of these macromonomers is limited.

With hafnocene **2** macromonomers were produced at different polymerization temperatures (Table 13). Productivities of the polymerization reactions are in the same range of magnitude compared to complex **XII**. The M_n of the macromonomers produced could be adjusted over a broad range up to a M_n of 32 000 g/mol, however, even higher molecular weights are accessible. For all macromonomers produced higher selectivity towards allylic chain ends was observed compared to all catalysts discussed in this chapter which are able to form PP macromonomers. At decreased polymerization temperatures (50 °C), this selectivity is higher than 98 % (MM3). These polymerization experiments reveal that hafnocene **2** is a versatile tool for the formation of macromonomers with high selectivity towards allylic chain ends over a broad range of M_n. In addition, the obtained macromonomers exhibit good solubility in organic solvents.

Table 13: PP macromonomers produced by hafnocene **2**.[a]

macromonomer	T_p[b]	p[c]	M_n[d]	S_{allyl}[e]	productivity[f]
MM1	70	4.6	3900	93	19000
MM2	60	4.0	7200	91	5000
MM3	50	4.0	32000	> 98	5000

[a] $n_{complex}$ = 5 µmol, 200 eq TIBA, 5 eq $[CPh_3][B(C_6F_5)_4]$. [b] In °C. [c] $p = p_{propene} + p_{Ar,}$ with $p_{Ar} = 1.4 \pm 0.1$ bar. [d] In g/mol determined by ^{1}H NMR spectroscopy assuming all polymer chains with an unsaturated chain end. [e] Selectivity towards allylic polymer chain ends in %, determined by ^{1}H NMR spectroscopy and assuming all polymers to have an unsaturated chain end. [f] In kg (PP)/ (mol(Hf)·h).

Produced macromonomers were applied in a copolymerization reaction with ethene using the ternary catalyst hafnocene **2**/ TIBA/ $[CPh_3][B(C_6F_5)_4]$. Parameters such as polymerization temperature, amount of macromonomer and chain length of used macromonomers were varied in order to investigate their influence on the incorporation of macromonomer (Table 14). As a result of relatively low isotacticity of these PP macromonomers, solubility and thus separation from LCB copolymers is quantitative in all cases, either proved by ^{1}H NMR spectroscopy or GPC analysis (4.1.8). The copolymerization reaction was stopped after a total consumption of ethene ranging between 3000 and 5000 mL in order to reduce the influence of changing macromonomer concentration during the polymerization reaction. This procedure

afforded a consumption of 6 to 16 % of the initial amount of macromonomer. Productivities were calculated on the amount of LCB copolymer obtained after soxhlet extraction.

Table 14: Copolymerization of ethene and PP macromonomers (MM1 – MM3) by hafnocene **2**.[a]

entry	MM	amount of MM[b]	M_n (MM)[c]	c (MM)[d]	T_p[e]	M_w[f]	T_m[g]	MM content wt-%[h]	p[i]	branches/ 100000 C[j]
1	-	-	-	-	30	900	133	-	1000	-
2	-	-	-	-	50	600	135	-	1700	-
3	-	-	-	-	70	370	133	-	1100	-
4	1	2	3900	1.71	50	900	131	7	16000	26
5	1	2	3900	1.71	70	500	133	7	5000	28
6	1	5	3900	4.27	50	1100	130	10	4000	38
7	1	5	3900	4.27	70	600	131	11	2300	44
8	2	5	7200	2.31	30	900	129	16	400	37
9	2	5	7200	2.31	50	900	131	21	700	53
10	2	5	7200	2.31	70	600	129	19	1000	47
11	3	15	32000	1.56	30	1100	128	23	3200	13

[a] Polymerization conditions: $p = p_{ethene} + p_{Ar} = 2.0$ bar, with $p_{Ar} = 1.4 \pm 0.1$ bar; $n_{complex} = 5$ µmol, 200 eq TIBA, 5 eq $[CPh_3][B(C_6F_5)_4]$. [b] In g. [c] In g/mol, determined by ^{1}H NMR spectroscopy. [d] In mmol/L. [e] In °C. [f] In kg/mol. [g] In °C. [h] Determined by ^{1}H NMR spectroscopy. [i] Productivity in kg (copolymer)/ (mol(Hf)·h). [j] Branches per 100000 (backbone) carbon atoms.

A general observation for all copolymerization reactions are higher molecular weights for branched copolymers compared to PE homopolymers produced at the same conditions (entries 1 → 8 and 11; 2 → 4, 6 and 9; 3 → 5, 7 and 10). Melting transitions of branched copolymers are also lower compared to PE homopolymers as a result of the side chains disturbing intra- and intermolecular interactions of the PE backbone, and reducing crystallinity. However, the absolute amount of branches and the differences between copolymers is low, and therefore, a clear correlation between the amount of branches and T_m is not observed. As expected, the content (wt-%) of incorporated macromonomer and the amount of branches is increased for higher macromonomer concentrations (entries 4, 5 → 6, 7). In addition, the polymerization temperature also influences the amount of branches. At higher temperatures (50 to 70 °C) the amount of branches is also increased (entries 4, 6 → 5, 7). For macromonomers with slightly higher M_n an increasing temperature (30 to 50 °C) also afforded higher amounts of incorporated macromonomers (entries 8 → 9),

but a further temperature increase from 50 to 70 °C resulted in slightly decreased amounts of incorporated macromonomer (entries $9 \rightarrow 10$). This indicates a maximum polymerization temperature for a maximum amount of branches. Determining a trend concerning the M_n of the macromonomer is difficult with the so far conducted polymerization experiments, due to the shown temperature dependency and the different applied concentrations. This limits the comparison of the different used macromonomers. However, the polymerization experiment of the macromonomer with a M_n of 32000 g/mol, which is far above the entanglement molecular weight of PP, showed that also for increased macromonomer chain length the incorporation of these is possible and affords a relatively high content (wt-%) of incorporated macromonomer (entry 11).

The polymerization experiments discussed above reveal that hafnocene **2** is a versatile complex for the formation of branched and LCB copolymers over a broad range of macromonomer content. Depending on the conditions, the amount of incorporated macromonomer can be even higher compared to those obtained by complexes used by *Dekmezian* and coworkers.[241] Hence, hafnocene **2** affords a superior control of the microstructure of these branched and LCB copolymers and can thus produce branched copolymers for numerous applications, such as additives for low melt strength PE or for compatibilizer in PP/PE blends.

The hypothesis of a branched microstructure being essential for the superiority of ePPs produced by hafnocene **2** compared to those produced by zirconocene **1** is further supported by the shown possibility of macromonomer incorporation at low concentrations and at high M_n of the macromonomer. However, especially with respect to the influence on the mechanical behavior of those branches, further investigations are necessary.

4.2 C_2-symmetric Metallocenes for the Formation of ePP

Besides C_1-symmetric, additionally C_2-symmetric complexes were investigated aiming for a possible application as catalysts for the formation of ePP. These complexes are typically known to produce iPP. Nonetheless, at higher polymerization temperatures, the amount of stereoerrors important for the elastic behavior (2.9), is increased. In addition to the amount of stereoerrors, the molecular weight must be sufficiently high to guarantee elastic behavior of the polymer. With increasing polymerization temperature especially unimolecular chain transfer reactions becomes faster and molecular weights of polymers produced are decreased. In order to obtain PP with high molecular weight, metallocenes reported for formation of high

molecular weight PP were used. Besides the right choice of the substitution pattern of these complexes, a change of the metal from Zr to Hf, known to increase molecular weights (2.7.4), is necessary. The metallocene selected for this investigation was *rac*-Me_2Si(2-Me-BenzInd)$_2HfCl_2$ **(10)** (Figure 35). In order to obtain high productivities, TIBA and $[CPh_3][B(C_6F_5)_4]$ were used for the activation of the hafnocene (2.4.3). The corresponding zirconocene **(11)** is reported to produce iPP with high M_w.[191] Additionally, a catalyst with this substitution pattern generates iPP with more stereoerrors compared to other metallocenes, producing iPP with even higher molecular weights (e.g Me_2Si(2-Me-4-Ph-Ind)$_2ZrCl_2$). Reports on complex **10** are very rare and polymerization data is limited to one report of an ethene/ propene copolymerization.[245] Synthesis of metallocene **10** was performed in analogy to zirconocene **11** known in the literature.[191]

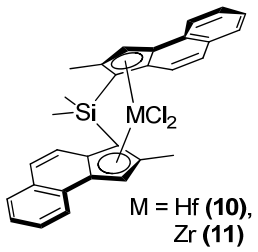

complex	T_p/ °C	$p_{propene}$/ bar	M_w/ g/mol	T_m/ °C
11	70	liquid	330 000	146
11	70	5	100 000	145

Figure 35: C_2-symmetric metallocenes **10** and **11** and some reported polymerization data of zirconocene **11** at high temperature.[191]

First polymerization reactions of propene with complex **10**, activated with TIBA/ $[CPh_3][B(C_6F_5)_4]$ were conducted in the temperature range of 30 to 80 °C (Table 15).
For a qualitative estimation of the amount of stereoerrors, melting transitions of produced PPs were measured by DSC. ePP reported by *Waymouth et al.* has the highest melting transitions with a value of up to 120 - 145 °C. [137] Due to their block-like structure, these polymers have a small amount of longer isotactic sequences at a generally low crystallinity, thus affording higher melting transitions compared to ePP with a similar amount, but random distribution of stereoerrors. For ePP with a random stereoerror distribution, isotactic sequences become shorter and melting transitions are typically below 100 °C.[18, 144, 145, 150]
As expected, melting transitions of polymers were decreased by increasing polymerization temperature. For a polymerization temperature of 80 °C, a melting transition of 135 °C was observed, being in the range of ePPs with block-like structure. However, according to a statistical distribution of the stereoerrors, the melting transition obtained is still too high, indicating high crystallinity and that leads to a more plastic than elastic behavior. Therefore, in order to obtain lower melting transitions, the polymerization temperature must be increased

further. Due to the fact that at 80 °C a polymer with moderate M_w is obtained that is already too low for good elastic behavior, higher polymerization temperatures were not applied. These findings limit the possibility of an ePP formation with complex **10** and analog C_2-symmetric bisindenyl metallocenes in the applied pressure and temperature range. In addition, metallocenes known to produce PP with higher molecular weight compared to complex **10** are little promising as they are in general more stereoselective. Consequently, even higher polymerization temperatures are necessary for the formation of a sufficient amount of stereoerrors most presumably resulting in low molecular weights.

Table 15: Polymerization of propene by ternary catalyst **10**/ TIBA/ $[CPh_3][B(C_6F_5)_4]$ at different temperatures.[a]

complex	T_p[b]	p[e]	T_m[f]	M_w[g]
10	30[c]	4.6	156.0	700000
10	45[c]	7.0	145.3	270000
10	60[c]	7.0	143.2	210000
10	80[d]	7.0	135.0	100000

[a] polymerization conditions: $n_{complex}$ = 0.5 µmol, 200 eq TIBA, 5 eq $[CPh_3][B(C_6F_5)_4]$. [b] Polymerization temperature in °C. [c] Temperature increase of 5 °C. [d] Temperature increase of 3 °C. [e] $p = p_{propene} + p_{Ar}$, with $p_{Ar} = 1.9 \pm 0.2$ bar. [f] Melting transition in °C. [g] In g/mol.

4.3 C_2-symmetric Metallocenes for the Formation of iPP

For formation of iPP, C_2-symmetric bisindenyl metallocene dichlorides, activated by MAO, boranes or borates, have proven to be suitable catalysts. Especially 2, 4 and 7-substituents on the indenyl moiety can influence the polymerization behavior towards iPP with a low degree of stereo- and regioerrors (2.10.2). Unfortunately, many of these complexes can afford these highly isotactic PPs only at low polymerization temperatures and there is no convenient and general synthesis route for complexes with this kind of substitution pattern. In particular, formation of a ligand with different substituents in these positions is difficult. Hence, in the following chapters, a versatile and convenient synthesis route towards these metallocenes will be discussed.

4.3.1 *Synthesis of Bis(7-alkoxy-4-aryl-2-methylindenyl)dimethyl silane from 4-Arylphenol and Methacryloylchloride*

A convenient synthesis route towards 4-aryl-7-hydroxy-2-methylindanones was patented by *Rieger et al.* in 1999.[246] Via this protocol, new indenes and new bridged ligands for the formation of *ansa*-metallocenes can be obtained (Scheme 31).

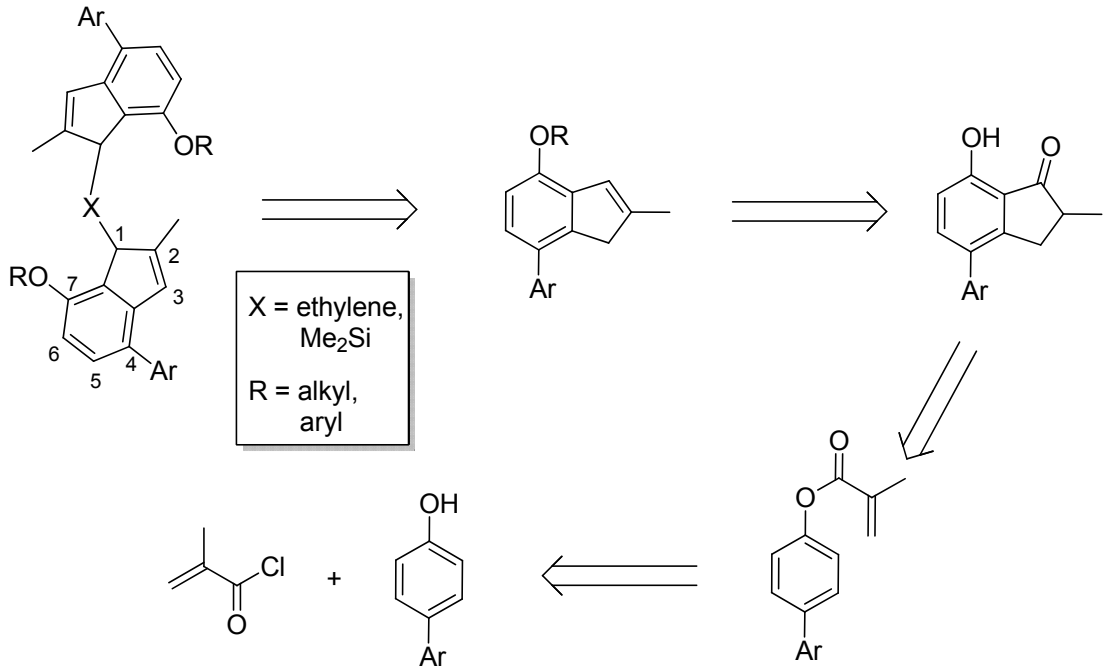

Scheme 31: Retrosynthetic analysis of (7-alkoxy-4-aryl-2-methylindenyl)dimethylsilanes.

In principle, formation of the bridged ligand can be achieved in analogy to standard protocols from respective indenes. Also, the reduction and elimination reaction from similar indanones to the corresponding indenes is a documented synthesis procedure. An additional protection of the hydroxy group is necessary to suppress a direct interaction with the catalytically active

metal center during the polymerization reaction. The indanone is formed in a *Fries* rearrangement reaction followed by a *Nazarov* cyclization from the respective ester which is synthesized from 4-arylphenol together with methacryloylchloride. This synthesis route allows a broad variety of new indene ligands with different 2, 4 and 7-substituents on the indenyl moiety and is only limited to the availability of corresponding phenols.

4.3.1.1 7-Hydroxy-2-methyl-4-phenylindanone (13)

Formation of 7-Hydroxy-2-methyl-4-phenylindanone **(13)** proceeds via the aforementioned synthesis route. In the first step, methacryloylchloride and 4-hydroxybiphenyl, both commercially available and cheap educts, are reacted to the corresponding ester **12** (Scheme 32).

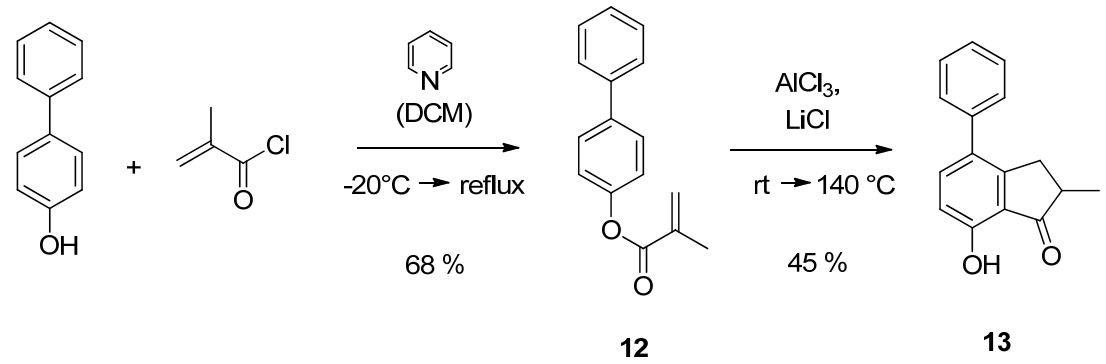

Scheme 32: Synthesis of 7-hydroxy-2-methyl-4-phenylindanone **(13)**.

The reaction proceeds with good yields. The second step, the *Fries* rearrangement and *Nazarov* cyclization, is a one-pot synthesis conducted in melt using $AlCl_3$ and LiCl with an eutectic point at around 110 °C.[247, 248] Depending on the reaction conditions, the *Fries* rearrangement can be *ortho*- or *para*-selective (Scheme 33). However, in parent case, only an *ortho*-substituted product can be formed. $AlCl_3$ acts as a *Lewis* acid, activating the ester and leading to an acylium cation, which reacts with the aromatic compound in an electrophilic substitution. The mechanism of this reaction is reported to be either intra- or intermolecular. Due to the fact that a substitution reaction was only observed on the hydroxyl-substituted phenyl moiety, an intramolecular route seems to be more likely for this ester. Evolution of gaseous HCl is indicative for the starting point of the reaction and was observed in the temperature range of 90 – 120 °C. The reaction was controlled by increasing the temperature stepwise to 140 °C. After the *Fries* rearrangement, the *Nazarov* cyclization takes place. This reaction proceeds via a 4π conrotatory electrocyclization reaction (4.1.7). Instead of a *Brønstedt* acid shown in section 4.1.7, the *Lewis* acid $AlCl_3$ was used. After aqueous work-up and keto-enol tautomerization reaction, the indanone is obtained.

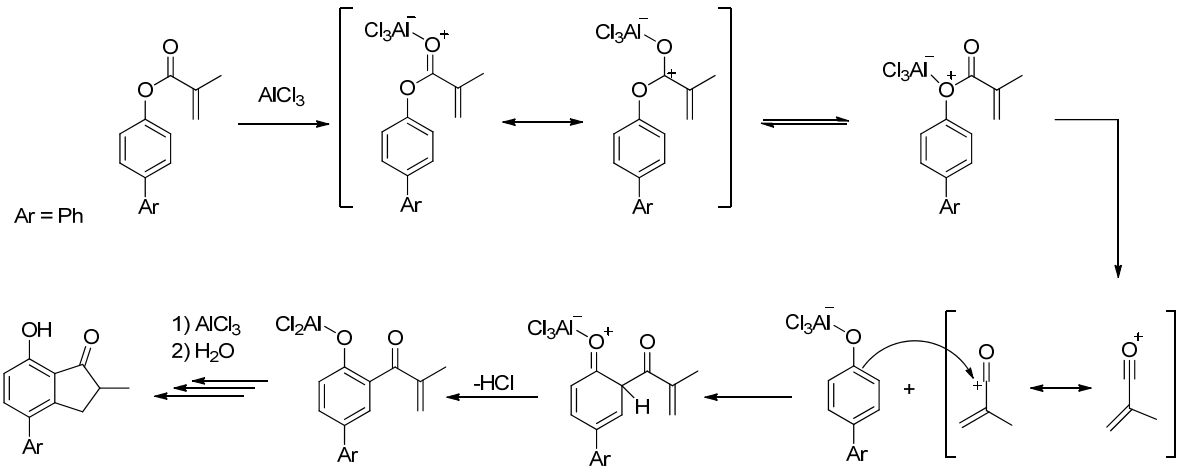

Scheme 33: Mechanism of the *Fries* rearrangement and the product of the following *Nazarov* cyclization.

Yields of this reaction were only moderate and can be explained by two facts. Firstly by a possible polymerization of the methacryloylic ester derivative **12** and secondly by formation of a highly viscous mixture during the reaction affording glassy solid and reducing yields. [249] Fine tuning of this reaction, e.g. applying different salt mixtures leading to a lower melting point and the addition of a radical scavenger will most presumably result in higher yields.

4.3.1.2 4-Methoxy-2-methyl-7-phenylindene (15)

Indanone **13** is reduced in a standard procedure by $LiAlH_4$ to the corresponding hydroxyl substituted indene **14**. Protection of the hydroxyl group affords indene **15** (Scheme 34).

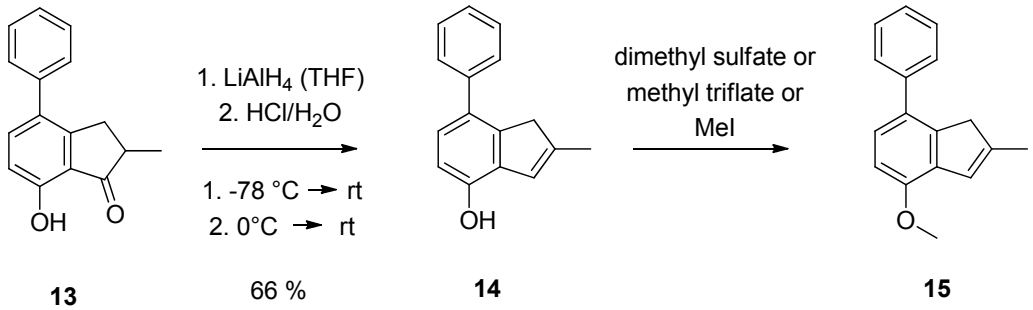

Scheme 34: Synthesis of 4-methoxy-2-methyl-7-phenylindene **(15)**.

The hydroxyl group is protected in order to avoid a deactivation reaction by σ-coordination of this group to the cationic metal center during the polymerization reaction. Therefore, different literature known synthesis routes with electrophiles such as dimethyl sulfate, methyl trifluoromethanesulfonate or methyl iodide were used.[250, 251] Standard procedures typically used for analog phenols were applied (Scheme 35). In case of synthesis route **B)**, especially

the very polar solvent afforded insufficient solubility of indene **14**, which finally resulted in low yields. Using route **C)** with methyl trifluoromethanesulfonate, improved yield was obtained. However, the third alternative, route **A)**, was proven to be most successful. The pure product crystallized from the reaction mixture in good yields. In all cases, basic conditions also led to an isomerization reaction of the double bond to corresponding isomers with a ratio of 1:1.

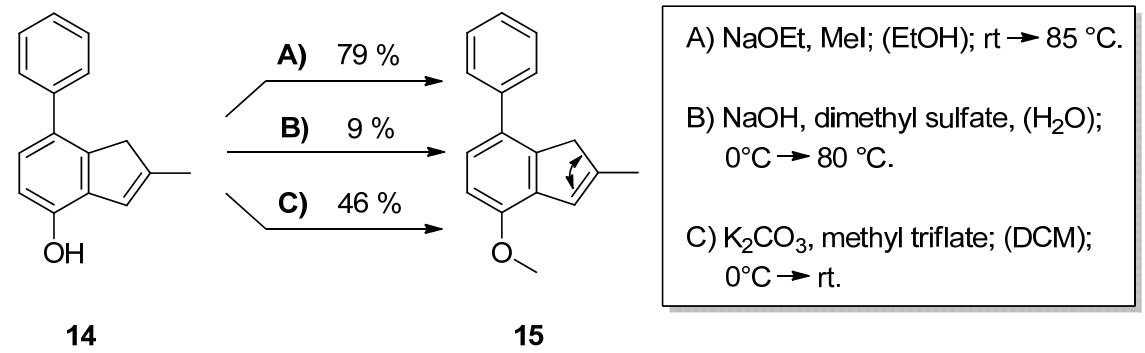

Scheme 35: Protection of the hydroxyl group by different synthesis procedures.

4.3.1.3 Bis(7-methoxy-2-methyl-4-phenylindene)dimethyl silane (16)

One of the standard bridging units for metallocene dichlorides is the Me_2Si-bridge. This bridging unit was chosen as it generally affords high activities and higher stereo- and regioselectivities compared to bridging units like ethylene (2.3, 2.10.2.1). For deprotonation of the indene derivative **15**, a standard procedure with *n*-BuLi as base was used. Due to the fact that organo lithium compounds are known to form higher adducts depending on the polarity of the solvent, besides a very unpolar solvent such as toluene, also Et_2O or the addition of TMEDA was investigated (Scheme 36).

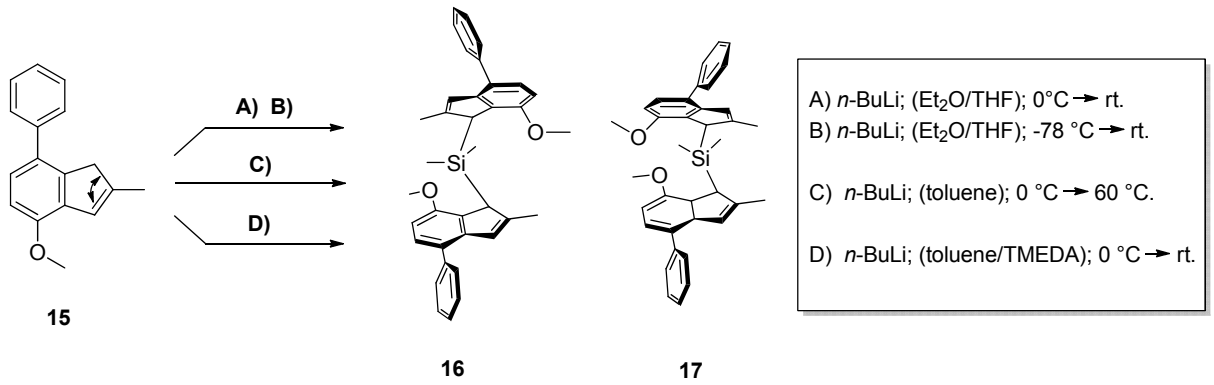

Scheme 36: Synthesis of bis(7-methoxy-2-methyl-4-phenylindene)dimethyl silane **(16)** and **(17)** via different synthesis procedures.

Besides different reactivities of the formed lithium organyls which should be increased going from toluene to Et_2O and toluene/TMEDA, a non-regioselective reaction can occur for these

unsymmetrically substituted indenes. After deprotonation of indene **15**, the lithium organyl formed can react with added Me_2SiCl_2 via carbon atom one or three, producing two additional regioisomers based on the *rac*-form of the complex and two additional regioisomers based on the *meso*-form (Scheme 37).

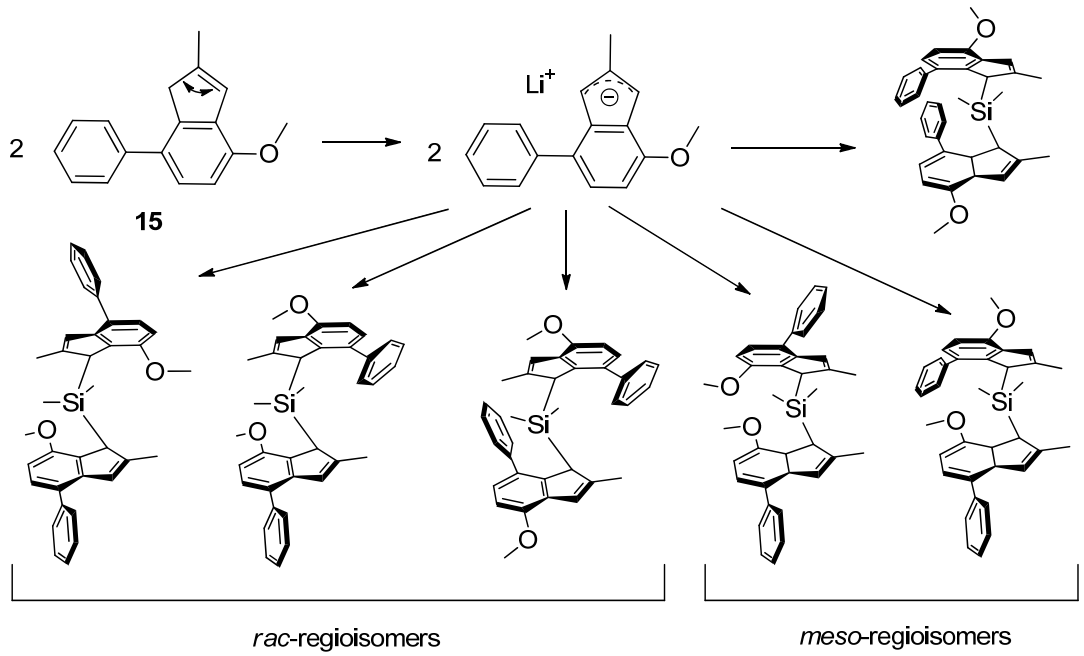

Scheme 37: Formation of the lithium organyl from indene **15,** and theoretically available regioisomers after addition of Me_2SiCl_2.

Products obtained via synthesis route **A)** and **B)** (Scheme 36) show the mass of the desired bridged compounds **16** and **17** in ESI-MS spectra after purification by column chromatography. However, ^{1}H NMR spectra reveal a broad multiplett in the region of the methyl groups on the silicon atom (Figure 36). Normally, this region should contain three signals, two from the *meso*- and one from the *rac*-form. Hence, formation of different regioisomers is assumed.

A potential coordination of the lithium cation to the methoxy group of the indenyl anion could be weakened by stronger coordinating solvents. Thus, THF and TMEDA were investigated concerning their influence on the regioselectivity. For products obtained via synthesis routes **C)** and **D)**, ESI-MS and ^{1}H NMR spectra were directly recorded after the reaction without purification by column chromatography. Observed ^{1}H NMR signals for the region of the methyl groups on the silicon atom are similar to those obtained from the product mixture formed via synthesis route **A)** (Figure 36).

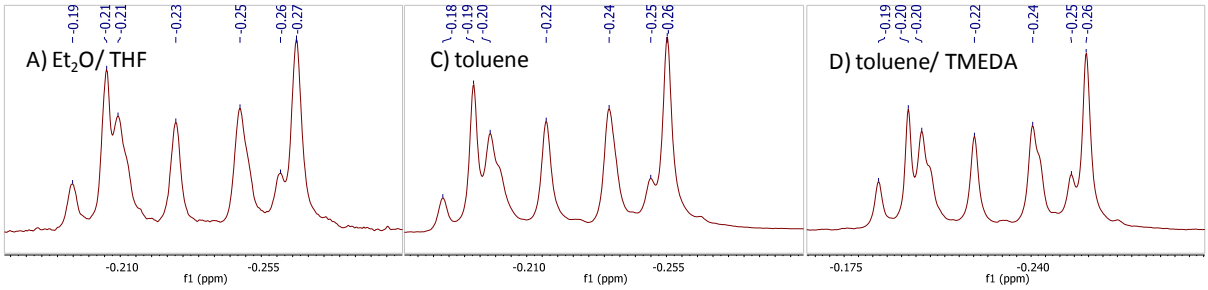

Figure 36: Region of the methyl groups on the silicon atom of the ^{1}H NMR spectra of product mixtures formed via synthesis routes **A)**, **C)** and **D)**.

ESI-MS spectra show the mass of the desired bridged compound **16** and **17** as a main product, together with some educt. In addition, two further signals were identified which can be assigned to disubstituted derivatives (Figure 37). This observation further underlines the formation of different regioisomers due to similar reactivities of the two positions on the indenyl moiety.

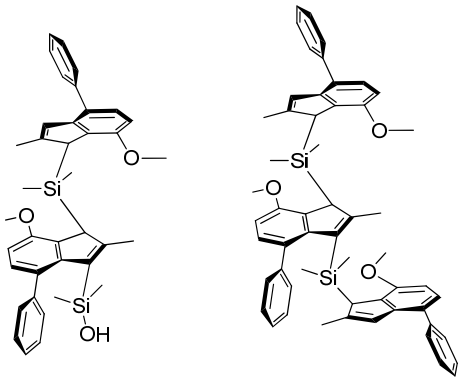

Figure 37: Assumed structures being in accordance with the masses found for additional peaks in the ESI-MS spectra of the raw product mixture formed via synthesis routes **C)** and **D)**.

A further error during the reaction could be inexact stoichiometry of the lithium organyls. However, NMR investigations revealed a fast and quantitative formation of the lithium organyls. Additionally, synthesis routes **C)** and **D)** were conducted with an excess of *n*-BuLi which was removed afterwards to isolate the lithium organyl of indene **15**. Hence, inexact stoichiometry can be neglected as the main reason for the formation of side products. These results show that a regioselective synthesis of these bridged ligands is not possible under the applied conditions.

4.3.2 *Synthesis of Bis(7-alkoxy-4-aryl-2-methylindenyl)dimethyl silane from 4-Bromophenol and Methacryloylchloride*

In the previous chapter, a regioselective bridging process and thereby a synthesis of the desired bridged ligand was shown to be impossible by the used procedure. In order to increase regioselectivity, steric hindrance on one side of the indene has to be increased. Therefore, the

synthesis route discussed above is modified towards a more versatile synthesis route with the possibility to introduce bulky aryl ligands in a late stage (Scheme 38). The synthesis steps are similar to those already described (4.3.1). Introduction of bulky aryl substituents is achieved by an additional C-C coupling reaction.

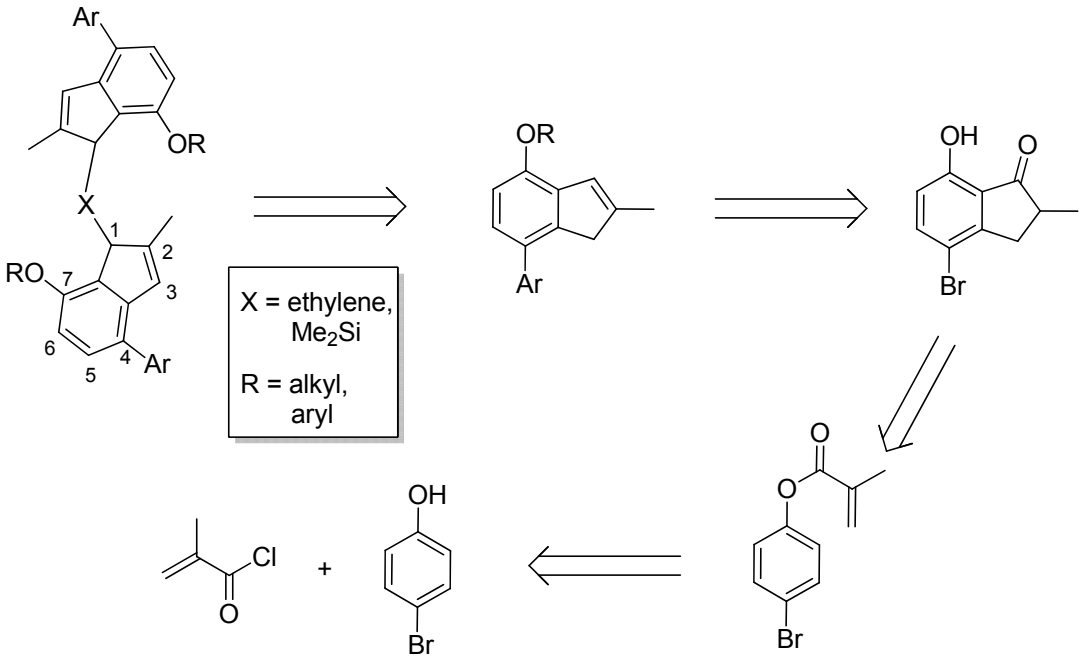

Scheme 38: Retrosynthetic analysis of (7-alkoxy-4-aryl-2-methylindenyl)dimethyl silanes.

4.3.2.1 4-Bromo-7-hydroxy-2-methylindanone (19)

Formation of ester **18** is conducted in analogy to the formation of ester **12** (4.3.1.1) affording similar yields (Scheme 39). In the second step, the *Fries* rearrangement and *Nazarov* cyclization were conducted without addition of LiCl, as ester **18** is a liquid educt which can completely dissolve added $AlCl_3$ at elevated temperatures. At around 90 °C, gaseous HCl is observed indicating the start of the reaction. When the temperature was kept at 90 - 100 °C during the whole reaction, ester **18** was not completely converted. Formed indanone **19** and ester **18** have similar boiling points and are difficult to separate from each other. Hence, the reaction temperature was increased during the reaction stepwise to 120 °C affording elimination of unreacted ester **18**. Independent from the reaction temperature, in all cases, a highly viscous to glassy solid was obtained during the reaction. In analogy to the synthesis of indanone **13** (4.3.1.1), the yield may be improved by modifying the temperature program or by adding a radical scavenger in order to prevent a possible polymerization of the methacrylate derivative.

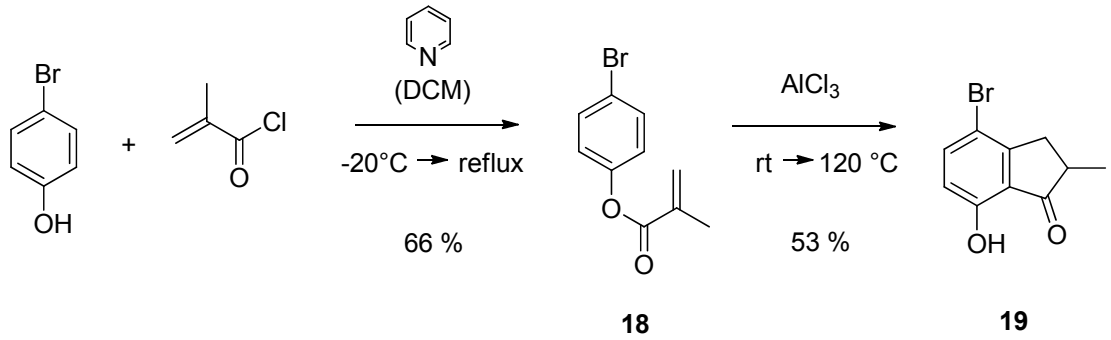

Scheme 39: Synthesis of 4-bromo-7-hydroxy-2-methylindanone **(19)**.

4.3.2.2 7-Bromo-4-methoxy-2-methylindene (21)

In analogy to synthesis of indene **15** (4.3.1.2), two more steps are necessary to form indene **21** from indanone **19** (Scheme 40). The hydroxyl group must be protected to avoid its σ-coordination to the active center of the catalyst leading to a deactivation during the polymerization reaction. Following reduction and elimination reactions of indanone **20** afford the desired indene **21**. For indanone **19**, these two steps were conducted in a different order than previously, due to an improved work-up procedure of the methoxy-substituted indanone compared to the hydroxyl-substituted derivative.

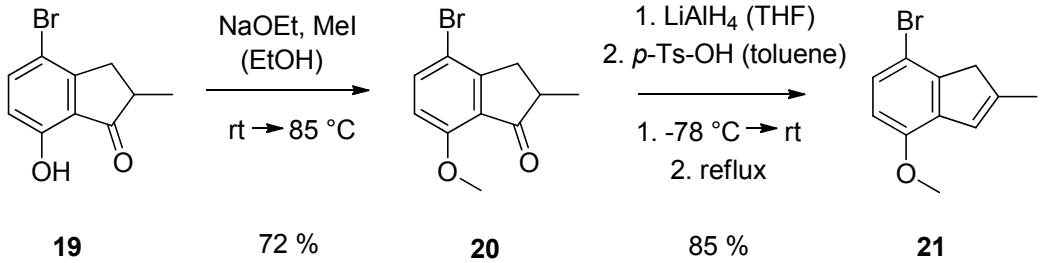

Scheme 40: Synthesis of 7-bromo-4-methoxy-2-methylindene **(21)**.

4.3.2.3 4-Aryl-7-methoxy-2-methylindenes via C-C Coupling Reaction

Indene **21** can be used for C-C coupling reactions leading to new 2,4,7-substitituted indenes (Scheme 41). Selected aromatic compounds were varied concerning their steric hindrance to investigate their influence on the regioselectivity during the introduction of the $SiMe_2$-bridge. For all coupling reactions, a *Suzuki* reaction was used. Boronic acids (3,5-di-*tert*-butylphenyl-, 3,5-dimethylphenyl- and 9-anthracenyl-boronic acid (**22-24**)) necessary for this type of C-C coupling reaction were synthesized via standard procedures. Therefore, either a Grignard compound or the lithium organyl was prepared from respective bromo-substituted derivatives

and converted with trimethyl borate followed by acidic work-up.[252] All coupling reactions gave moderate to high yields (53-81 %).

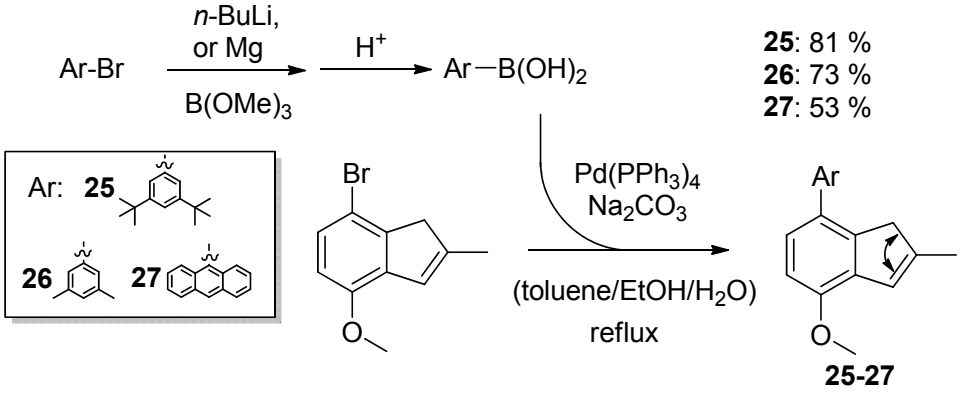

Scheme 41: C-C coupling reaction to the indenes **25 – 27**.

The applied *Suzuki* coupling reaction requires the addition of a boronic acid, together with a base (Na_2CO_3). Latter activates the boronic acid and thus facilitates the transmetallation reaction. In addition to the coupling reaction, an isomerization of the double bond was observed and the different isomers were determined by 2-D NMR spectroscopy. The degree of isomerization was shown to vary depending on the concentration of the base in the reaction mixture. First experiments during the introduction of the bridging unit in the following step seemed to show an influence of the different isomers. For this reason varying base concentrations were applied in order to improve the selective formation of indene derivatives **A**, the products without isomerization (Table 16).

Table 16: Influence of base on the formation of isomers during *Suzuki* coupling reaction.

indene	Na_2CO_3	isomer A	isomer B
25	2N (5 eq)	80	20
25	4N (10 eq)	35	65
26	2N (2 eq)	100	0
26	8N (5 eq)	25	75
27	2N (2 eq)	40	60

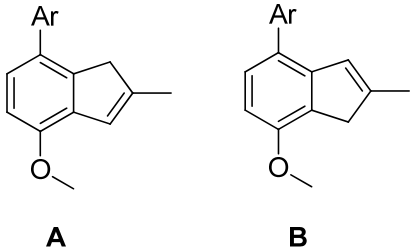

There is a clear trend towards an isomerization of isomer **A** to **B** for higher concentrations of base. For indenes **25** and **26**, little or even no isomerization was observed during the C-C coupling reaction with lower amounts of Na_2CO_3. The synthesis of indene **27** afforded significant isomerization to isomer **B** even at low base concentrations. The reason for that is a higher amount of EtOH, which had to be used to dissolve 9-anthracenyl-boronic acid **24**.

Hence, polarity of the organic phase was increased affording a higher concentration of Na_2CO_3 in the organic phase. An additional parameter influencing the base concentration in the organic phase is the structure of the boronic acid. Depending on the reaction conditions and the structure of the aromatic compound itself, the boronic acid was obtained either in its monomeric form, or by condensation reaction in its trimeric or oligomeric form or in mixtures thereof. However, for simplification, the amount of added boronic acid was always calculated with the molar mass of the monomeric form. Hence, especially for higher condensed boronic acids a higher amount of acid was added reducing the residual amount of base. For a clean coupling reaction with only minor amounts of isomerization reaction, concentration of base has to be adjusted in each case separately.

4.3.2.4 Synthesis of $SiMe_2$-bridged Ligands

As a regioselective bridging process was not possible in case of indene **15** (4.3.1.3), synthesized indenes **25-27** were investigated concerning the influence of the different substituents on the regioselectivity of the silylation reaction. First experiments with indene **25** under standard reaction conditions (*n*-BuLi, -20 °C to rt) resulted in the selective formation of a monosubstituted derivative of Me_2SiCl_2, leading to R-($SiMe_2$)-O-($SiMe_2$)-R after aqueous work-up via condensation (Scheme 42). Reactions in more polar solvents, such as THF, which generally increase reactivity of lithium organyls, afforded many side products which were not analyzed in detail. The successful synthesis of the desired ligand was achieved in a toluene/dioxane mixture by heating the reaction mixture to 60 °C during the silylation reaction. NMR investigations showed that the first reaction of a lithium organyl with Me_2SiCl_2 already occurs below room temperature. However, the substitution of second chlorine atom is hindered, most presumably due to the high steric encumbrance and thus higher temperatures are necessary for the second substitution reaction. For synthesis of ligands **29** and **30**, conditions successfully affording ligand **28** were used without further investigations. Hence, for those, the substitution reaction of the second chlorine atom could already occur at lower reaction temperatures. For all of these ligands, a regioselective silylation reaction was achieved. Thus, already the small methyl substituents on the phenyl moiety introduce sufficient steric hindrance.

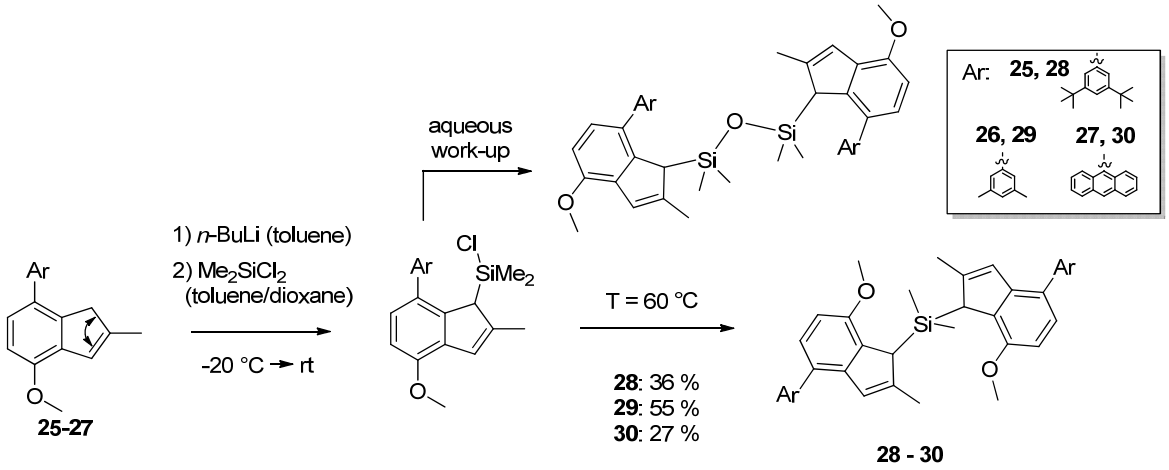

Scheme 42: Synthesis of desired *ansa*-ligands **28-30**.

4.3.3 *Synthesis of Bis[4-(3′,5′-di-tert-butylphenyl)-2-methylindenyl]dimethyl silane (33) from 1-Bromo-2-(bromomethyl)benzene*

In 2002, bridged indene **33** and metallocenes thereof were patented (Scheme 43).[253] However, only the synthesis and polymerization results of the respective zirconocene are reported in this patent application. For comparison to synthesized ligand **28** with an additional 7-methoxy substituent and to reveal its influence on the polymerization behavior of the respective catalyst, ligand **33** and the corresponding hafnocene were synthesized. 7-bromo-2-methylindanone (**30**) was synthesized in analogy to the modified route of *Spaleck* (Scheme 18, Scheme 19; p. 39 f). The following steps were performed similar to synthesis of bridged ligand **28** (Scheme 43). An isomerization reaction during the *Suzuki* coupling reaction also occurred for indene **32**. However, in this case, besides depicted isomer of indene **32** only 5 % of its double bond isomer was obtained.

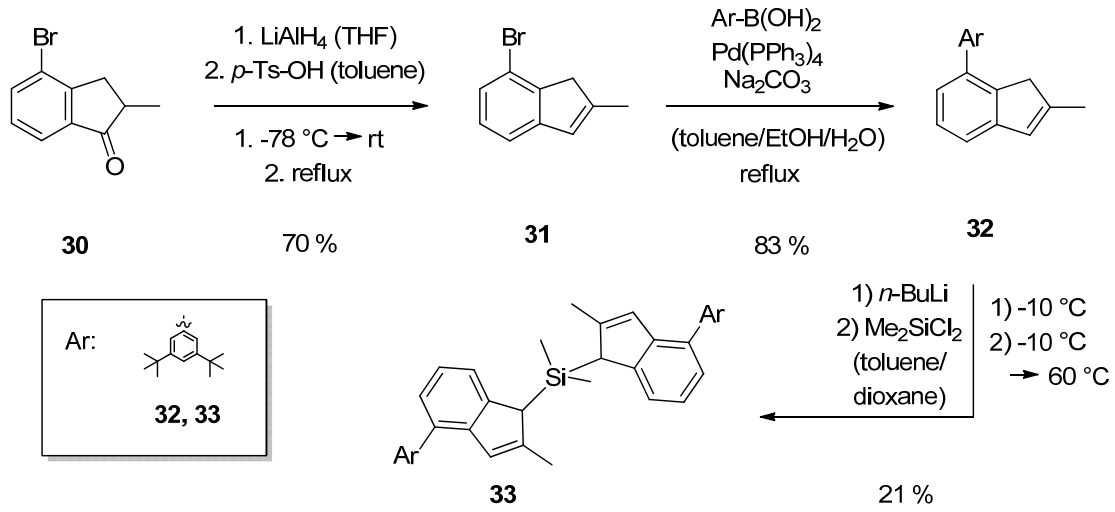

Scheme 43: Synthesis of ligand **33** without 7-substituent**.**

4.3.4 *Complex Synthesis and Crystal Structures*

4.3.4.1 Synthesis of Zirconocene 34 and Hafnocene 35 from Bis[4-(3´,5´-di-*tert*-butylphenyl)-7-methoxy-2-methylindenyl] dimethyl silane

Metallocenes **34** and **35** were obtained in a standard procedure via deprotonation of the *ansa*-bisindenyl ligand **28** with *n*-BuLi and subsequent reaction with the corresponding metal chloride (Scheme 44).

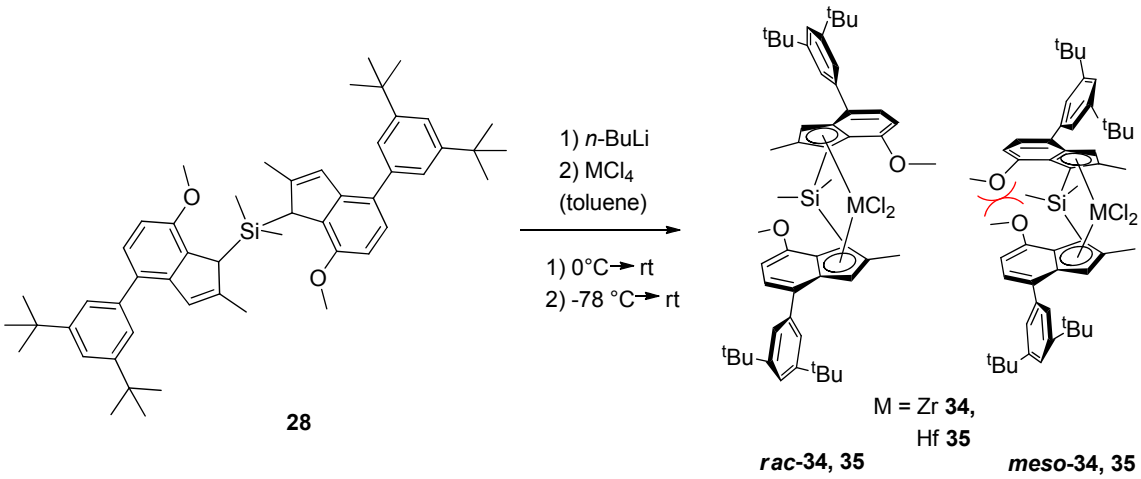

Scheme 44: Synthesis of the 2,4,7-substituted *ansa*-bisindenyl metallocenes **34** and **35**.

In all cases, a preferred formation of the *rac*- over the *meso*-form was observed, with a *rac* to *meso* ratio of up to 9:1. The predominant formation of the desired *rac*-form of the complexes is most presumably due to repulsive interactions of the methoxy groups in the *meso* isomer, increasing the activation barrier for its formation. Such racemoselective synthesis of *ansa*-bisindenyl metallocenes was claimed recently for highly hindered and symmetrically 4,7-substituted bisindenyl metallocenes with substituents like naphthyl or *p*-*tert*-butylphenyl (2.10.2.3).[202] Isolated yields of the pure *rac*-form after crystallization from toluene/pentane have been only low (11 - 27 %) so far. However, in analogy to improvements for the synthesis of complex **36** (see following chapter), higher yields may be obtained by tuning the reaction conditions.

4.3.4.2 Synthesis of Hafnocene 36 from Bis[4-(3´,5´-di-*tert*-butylphenyl)-2-methylindenyl]dimethyl silane

Hafnocene **36** was synthesized via a standard procedure in analogy to above discussed complexes **34** and **35 (**Scheme 45). When the complexation reaction was conducted from -78 °C to rt, conversion was incomplete. Due to high solubility of the desired complex in pentane, it was impossible to separate the unreacted ligand. Increasing temperature to the boiling point of toluene during complexation led to higher conversions. The metallocene was obtained as a mixture of the *rac*- and *meso*-form. The pure *rac*-form could be isolated by crystallization from pentane with a yield of 39 %.

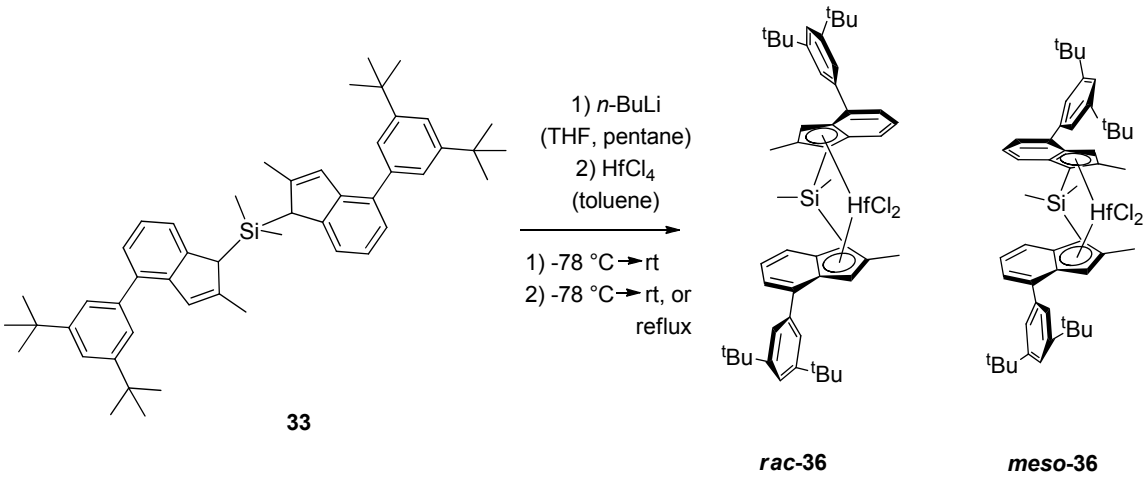

Scheme 45: Synthesis of the 2,4-substituted *ansa*-bisindenyl metallocene **36**.

4.3.4.3 Comparison of Crystal Structures of *rac*-34-36

Crystallization from a toluene/pentane mixture yielded crystals suitable for X-ray structure analysis. As expected, crystal structures of zirconocene *rac*-**34** and hafnocene *rac*-**35** are similar (Figure 38). They show high steric encumbrance with a short distance of the *tert*-butyl groups of the different indenes. However, both chlorine atoms representing the two active sites during polymerization, are easily accessible. For better understanding, important structural parameters already discussed in section 2.3 are compared to complexes known in the literature, such as *Spaleck´s* 2-methyl-4-phenyl-substituted bisindenyl-based metallocene (Table 17). In comparison to the synthesized metallocenes *rac*-**34** and *rac*-**35** the crystal structure of Spaleck´s complex is the most similar which is reported in the literature. Crystals of complex *rac*-**36**, suitable for X-ray structure analysis were obtained via crystallization from

n-pentane by slow evaporation of the solvent. Due to its similarity to complexes *rac*-**34** and *rac*-**35,** it will be compared with these and the *Spaleck* metallocene.

Compared to *Spaleck´s* metallocene, the other complexes shown have a shorter M-Cp bond length. Hafnocene *rac*-**35** has a shorter M-Cp bond length than the zirconocene *rac*-**34** and the 2,4-disubstituted hafnocene *rac*-**36**. Hafnocene *rac*-**36** has an M-Cp bond length in between these of *rac*-**34** and *rac*-**35**. Hence, an influence on the M-Cp bond length is obvious by both the metal and the substitution pattern (2,4- vs. 2,4,7-substitution).

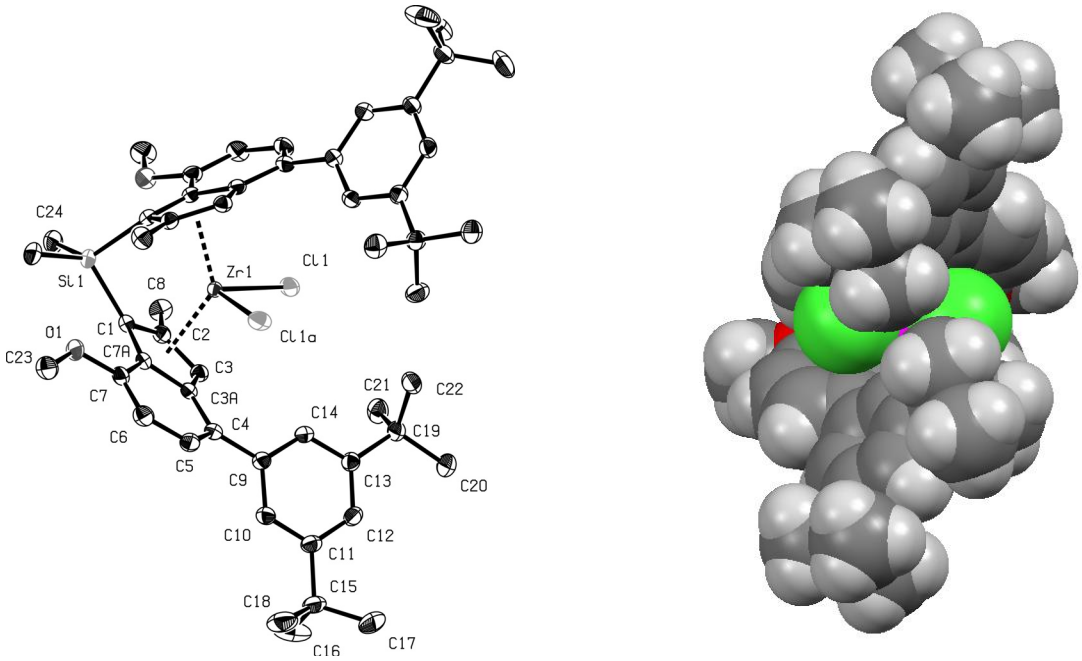

Figure 38: Ortep style plot of compound *rac*-**34** in the solid state (left). Hydrogen atoms are omitted for clarity. Thermal ellipsoids are drawn at the 50% probability level. Space filling plot (right) of compound *rac*-**35** with typical *van-der-Waals* (vdW) radii.

Table 17: Important structural parameters of the metallocenes **34** – **36** in comparison to literature-known. [191]

complex	bite angle β	M-Cp/ Å	D/ Å	dihedral angle Ph-Ind
rac-**34**	58.1°	2.234[a]	0.941	40.6°
$SiMe_2$(2-Me-4-Ph-Ind)$_2ZrCl_2$	59.2°	2.247	0.975	44.8°
rac-**35**	57.8°	2.219[a]	0.926	40.2°
rac-**36**	59.1°	2.228[a]	0.959	47.2°, 80.0°

[a] arithmetic average of the two M-Cp distances (ΔM-Cp = 0.001 Å for *rac*-**34**, *rac*-**35** and 0.003 Å for *rac*-**36**).

Besides the M-Cp bond length, the bite angle and parameter D are influenced by both the metal and the substitution pattern. Hafnocene *rac*-**35** shows the smallest value of D. Nevertheless, in this case, the effect of the substitution pattern seems to be more important, as

D is larger for hafnocene *rac*-**36** than for zirconocene *rac*-**34**. Along with shorter M-Cp bond lengths, smaller values of D indicate a more stable M-Cp bond. Also the bite angle is majorly dependent on the substitution pattern, showing smaller bite angles for the 2,4,7-substituted metallocenes and only minor effects of the metal center. Thus, the bite angle is significantly reduced by a methoxy substituent in 7-position of the indenyl moiety.

The dihedral angle Ph-Ind is the angle between the two planes defined by the 4-phenyl-substituent and the plane of the phenyl ring of the indene. Smaller dihedral angles for metallocenes *rac*-**34** and *rac*-**35** compared to *Spaleck´s* complex were found. Metallocene *rac*-**36** is not comparable to the other complexes as two different angles are formed as a result of package effects in the crystal. Due to steric repulsion, the dihedral angle between the indenyl- and the phenyl-group in 4-position would have a theoretical optimum at 90 °, whereas the contribution of the delocalization effect of the π-electrons would lead to a coplanar structure. Therefore, the expected dihedral angle of complexes *rac*-**34** and *rac*-**35** should be slightly larger compared to Spaleck´s complex due to the repulsive contribution of the *tert*-butyl groups and the indenyl fragment. The smaller observed angle may be explained by a steric interaction of the *tert*-butyl groups of opposite phenyl substituents, at least in the solid state. In addition, the smaller bite angle of *rac*-**34** and *rac*-**35** increases this repulsion and thus, the dihedral angle is even further reduced.

In complexes *rac*-**34** and *rac*-**35**, the silicon methyl groups are in close contact to the 7-methoxy oxygen atom, resulting in a repulsive interaction.[254] This leads to a distortion of the $SiMe_2$ group out of plane, defined by the $SiMe_2$ and MCl_2 fragments (Figure 39). An additional proof for the steric interaction of the methoxy- and the $SiMe_2$ group is the position of carbon atom C-7 relative to the indenyl plane. This carbon atom is slightly shifted out of the indenyl plane compared to the unsubstituted complex *rac*-**36** that does not show such a shift. These observations show that the smaller bite angles of complexes *rac*-**34** and *rac*-**35** are a result of steric interaction between the methoxy substituent and $SiMe_2$. In addition, as already mentioned above, the *tert*-butyl-groups of the different 4-phenyl substituents generate high steric hindrance on the front side of the complex. These two structural elements indicate a high steric rigidity of the *ansa*-metallocene frame for metallocenes *rac*-**34** and *rac*-**35**.

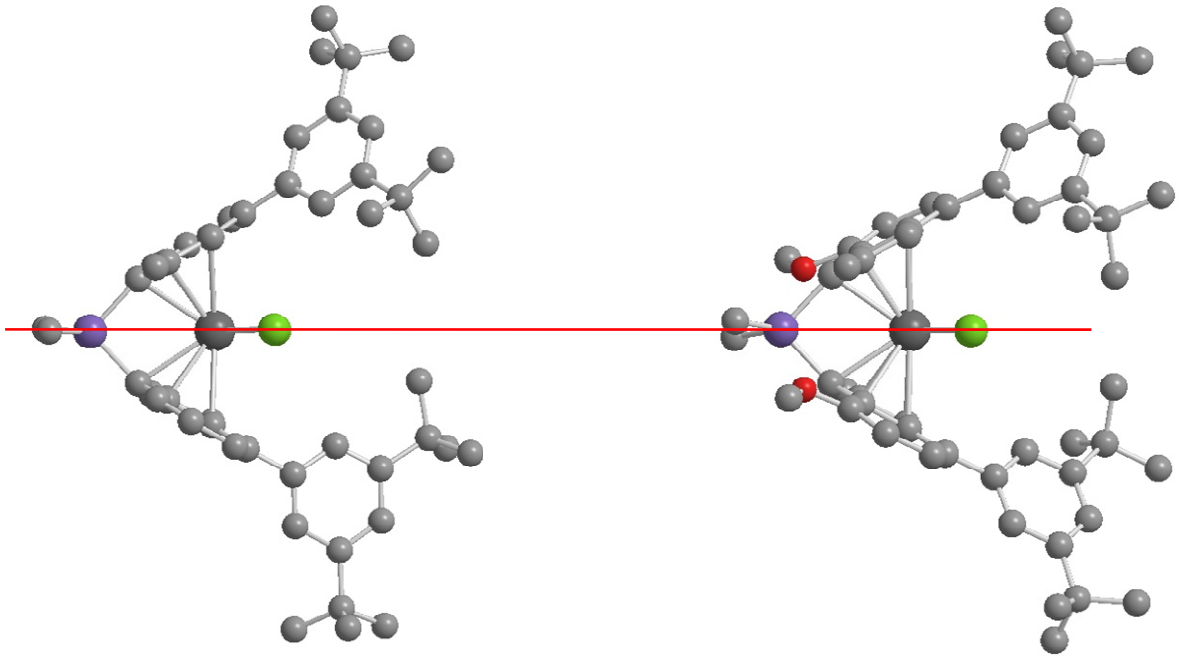

Figure 39: Influence of the 7-methoxy group on the crystal structure of metallocene **35** (*rac*-**35** (right) and *rac*-**36** (left))

4.3.5 *Solution Polymerization of Propene with rac-34-36*

According to the known and accepted *Cossée* and *Modified Green-Rooney* mechanisms (2.5) in chain migratory insertion polymerization, the polymer chain has to migrate from one site of the complex to the other. On a first glance the high steric hindrance on the front side of the shown complexes *rac*-**34**-**36** seems to block migration of the polymer chain. Nonetheless, the 4-phenyl substituents could rotate in order to facilitate this process.

Hence, a possible influence of the rotation of the 4-phenyl substituents of produced metallocene *rac*-**34** on the polymerization behavior was qualitatively investigated by temperature dependent NMR spectroscopy. Therefore ^{1}H NMR spectra of complex ***rac*-34** were recorded in the temperature range of – 80 to 0 °C (Figure 40). Significant changes are observed for the signal originating from H-Ar-2´and H-Ar-6´, both marked in red. Decreasing temperature leads to broadening of the signal starting below -10 °C. Hence, the rate of rotation of the 4-phenyl substituents is in the range of the NMR detection time scale at temperatures lower than -10 °C.

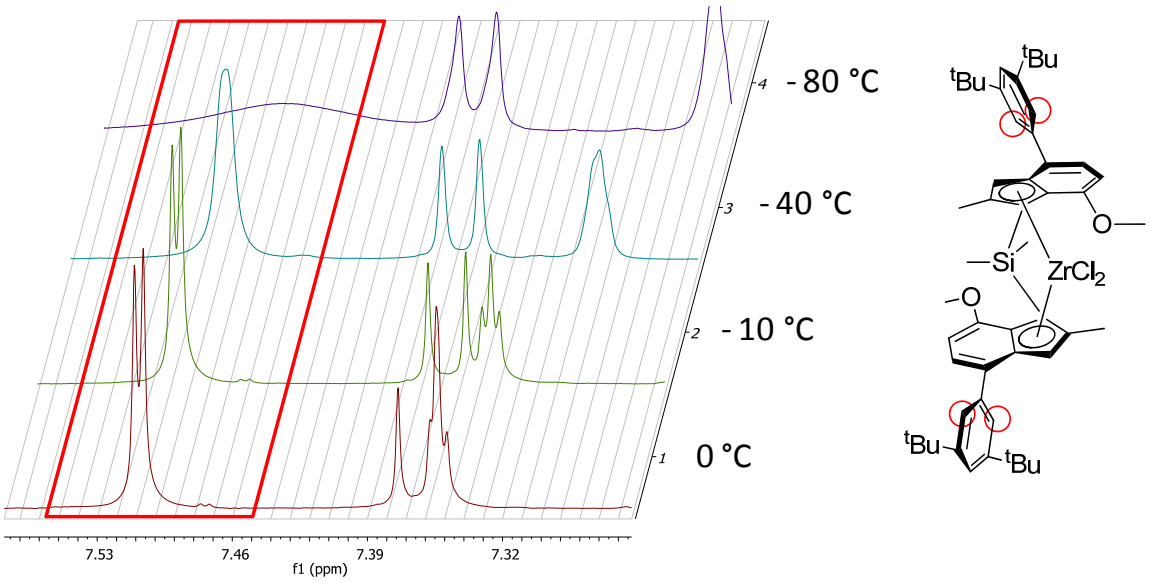

Figure 40: Variable temperature NMR investigations for qualitative determination of the 4-phenyl rotation.

Unfortunately, -80 °C was not low enough to obtain two separate signals for protons H-Ar-2´and H-Ar-4´. This information would have given the opportunity to estimate the rotation rate constant of the 4-phenyl substituents. A comparison of this rate constant with that of propagation could reveal if rotation of the phenyl rings can limit the polymerization. However, at these low temperatures at which rotation of the phenyl substituents occurs, the propagation rate is assumed to be very slow. As a consequence, a limiting effect of the rotation is unlikely. Nonetheless, these measurements were conducted with the dichloro precursor of the polymerization active catalyst. Hence, higher steric hindrance induced by the polymer chain could slow down the 4-phenyl rotation during polymerization.

Temperature-dependent NMR spectroscopy showed that a limiting effect of the rotation of the 4-phenyl substituents on the propagation rate is unlikely and thus it will be neglected for the following discussion of the polymerization experiments. In order to investigate the influence of the different substitution patterns of complexes *rac*-**34**-**36** on their propene polymerization behavior concerning productivity, stereo- and regioselectivity, solution polymerization experiments in toluene were conducted. The applied polymerization procedure was identical to polymerization experiments with C_1-symmetric complexes. Dichloro precursors were preactivated by reaction with TIBA at 60 °C. The formation of the polymerization active species was achieved by addition of $[CPh_3][B(C_6F_5)_4]$ **V**. TIBA was also used as scavenging agent for the polymerization experiments. Complexes *rac*-**34** - **36** show, depending on the polymerization conditions, productivities between 1800 and 129 000 kg(PP)·(mol(metal)·h)$^{-1}$ (Table 18). The polymers produced are highly isotactic polypropylenes with melting

transitions ranging between 141 and 171 °C and a polydispersity index of 1.2 - 2.2 which is typical for metallocene produced PP. In the following chapters, the specific differences of complexes *rac*-**34-36** and the influence of process parameters, e.g. propene concentration and polymerization temperature, on the molecular weight, amount of stereo- and regioerrors and the melting transitions of the resulting polymers will be discussed in more detail.

Table 18: Polymerization of propene with complexes *rac*-**34** (Zr), *rac*-**35** (Hf) and *rac*-**36** (Hf) activated by TIBA / $[CPh_3][B(C_6F_5)_4]$ in toluene.

entry	complex	n[a]	p[b]	T_p[c]	T_m[d]	mmmm[e]	2,1 e[e]	3,1[e]	M_w[f]	product.[g]
1	*rac*-**34**	2	4	30[h]	165	99.6	0.09	nd[j]	700	61 000
2	*rac*-**34**	1	4	50[i]	163	99.4	0.17	nd[j]	480	103 000
3	*rac*-**34**	1	6	70[h]	158	99.0	0.23	0.04	420	129 000
4	*rac*-**34**	1	4	90	141, 153	nm[k]	nm[k]	nm[k]	130	23 000
5	*rac*-**35**	2	3	0	171	99.9	nd[j]	nd[j]	5 800	1 800
6	*rac*-**35**	2	4	30[h]	170	99.5	nd[j]	nd[j]	1 700	27 000
7	*rac*-**35**	2	4	50	165	99.3	0.06	0.02	1 100	17 000
8	*rac*-**35**	2	6	70	163	99.0	0.04	0.03	600	54 000
9	*rac*-**35**	2	4	70	160	98.4	0.04	0.06	410	33 000
10	*rac*-**35**	2	4	90[h]	152	95.2	0.01	0.15	44	51 000
11	*rac*-**36**	4	3	0	170	nm[k]	nm[k]	nm[k]	2 300	3 900
12	*rac*-**36**	1	4	30[h]	168	nm[k]	nm[k]	nm[k]	2 000	18 000
13	*rac*-**36**	1	4	50	164	nm[k]	nm[k]	nm[k]	800	21 000
14	*rac*-**36**	1	4	70	157	nm[k]	nm[k]	nm[k]	230	95 000

[a] In µmol. [b] Pressure in bar, with $p = p_{Ar} + p_{propene}$ ($p_{Ar} = 1.4 \pm 0.1$ bar).
[c] Polymerization temperature in °C ± 1°C. [d] In °C. [e] In % from ^{13}C NMR (100 MHz); determined assuming the enantiomorphic site model.[94] [f] In kg/ mol. [g] Productivity in kg(PP)/ (mol(metal)·h). [h] ± 2 °C. [i] ± 5 °C.
[j] nd = not detected. [k] nm = not measured.

4.3.5.1 Productivity of Complexes *rac*-34-36

Productivities of complexes *rac*-**34-36** are in the same order of magnitude as complexes reported in the literature (e.g. *Spaleck´s* complex). Due to different applied activation methods which significantly influence the productivities of respective catalysts detailed comparison with literature reported values is not reasonable. Within complexes *rac*-**34-36**, zirconocene *rac*-**34** reveals the highest productivities (entries 1-3, 5-9, 11-14 for *rac*-**34**, *rac*-**35** and *rac*-**36**, respectively). Lower productivities in comparison to the corresponding zirconocenes can be found in the literature for many hafnocenes (2.4.5) and are often explained by a stronger Hf-carbon bond, resulting in slower propagation rates. But differences during the activation reaction of zirconocenes and hafnocenes must be also considered. This can result from a different or an incomplete reaction, during preactivation-/activation, affording either different catalytic active centers, or lower concentrations of those. Especially a different precursor after preactivation with TIBA is very likely, considering the results of preactivation investigations with C_1-symmetric complexes (4.1.2).

At high polymerization temperatures (90 °C), the trend is inverted for metallocenes *rac*-**34** and *rac*-**35** (entries 4 and 10) and therefore, higher productivities are obtained for the hafnocene (51 000 vs. 23 000 kg(PP)·(mol(metal)·h)$^{-1}$ for *rac*-**35** and *rac*-**34**, respectively). The lower productivity of zirconocene *rac*-**34** at 90 °C must be a result of a degradation reaction of the active species. This is confirmed by further polymerizations experiments at 90 °C with complex *rac*-**34** affording no or only low yields. Productivities observed for hafnocene *rac*-**35** are increased by raising the polymerization temperature from 50 to 90 °C (entries 7 and 10, with 17 000 to 51 000 kg(PP)·(mol(metal)·h)$^{-1}$), whereas those of zirconocene *rac*-**34** are decreased (entries 2 and 4, with 103 000 to 23 000 kg(PP)·(mol(metal)·h)$^{-1}$). Consequently, hafnocene *rac*-**35** is more temperature stable than zirconocene *rac*-**34**. This is in accordance with the M-Cp bond distances and parameter D which indicate a more stable complex in case of the hafnocene.

In particular at lower temperatures, complexes *rac*-**35** and *rac*-**36** afford similar productivities. However, at a polymerization temperature of 70 °C, productivity of hafnocene *rac*-**36** is significantly higher compared to that of hafnocene *rac*-**35** (entries 9, 14 33 000 vs. 95 000 kg(PP)·(mol(metal)·h)$^{-1}$). A possible explanation is a stronger influence of the counteranion in case of hafnocene *rac*-**36**, due to the larger bite angle (4.3.4.3). At higher polymerization temperatures, this influence becomes smaller due to a weaker coordination of the counteranion. In case of hafnocene *rac*-**35**, the counteranion is assumed to be also better

separated at lower polymerization temperatures. Thus, a smaller temperature influence on the productivity is proposed for hafnocene *rac*-**35**.

Literature-known *ansa*-bisindenyl metallocenes with alkoxy substituents on the indenyl moiety often afford decreased productivities which are explained by a reaction of the co-catalyst with the alkoxy group destabilizing the catalyst (2.10.2.4). In contrast, for metallocenes *rac*-**34** and *rac*-**35** moderate to high activities are obtained. Hence, a reaction of the co-catalyst (TIBA) affording reduced productivities is unlikely.

4.3.5.2 Determination of Stereo- and Regioregularity via ^{13}C NMR Spectroscopy

The polymer products produced with metallocenes *rac*-**34-36** are highly isotactic polypropylenes with ultrahigh molecular weights and melting transitions (*ex reactor*) up to 171 °C (Table 18, entry 5, Figure 41). So far, this is the highest reported melting transition for untreated (not extracted or annealed) iPP. The stereo- and regioregularity of these polypropylenes is extraordinarily high and was determined by ^{13}C NMR spectroscopy for the samples 1-3 and 5-10 (Table 18). Given the extremely high stereoregularity observed by ^{13}C NMR spectroscopy, the experimental conditions of the NMR experiment itself limit the precision of the determined isotacticity. When only isolated stereo defects are observed, the detection threshold of the mmrr signal limits the accuracy of the quantification.

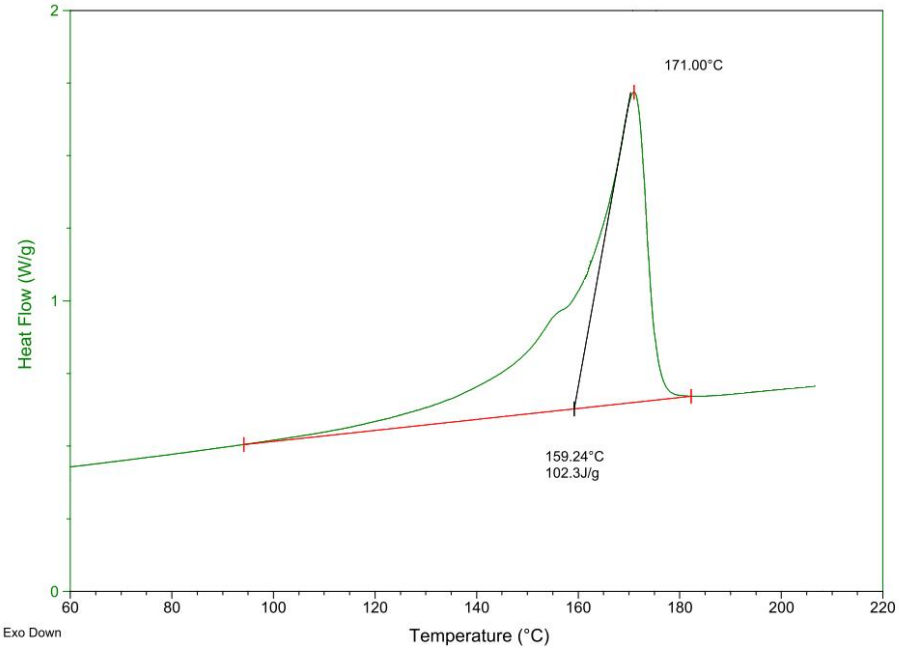

Figure 41: DSC: 2nd heating run of iPP produced with complex *rac*-**35** at 0°C.

For the extremely isotactic materials, where no stereo defects were observed under standard NMR conditions (8k/NOE/3s), a pentad isotacticity of 100.0 % is observed by inspection (Figure 42). However, using automated spectral analysis non-zero baseline and phasing issues, result in non-zero integrals and thus pentad isotacticities < 100.0 %. With the signal-to-noise ratio of the mmmm signal known and a signal-to-noise ratio of 2.5 assumed as the detection threshold of the mmrr signal, the minimum pentad isotacticity of sample 5 in Table 18 can be estimated to be at least 99.90 % using the enantiomorphic site control model (7.1, NMR).

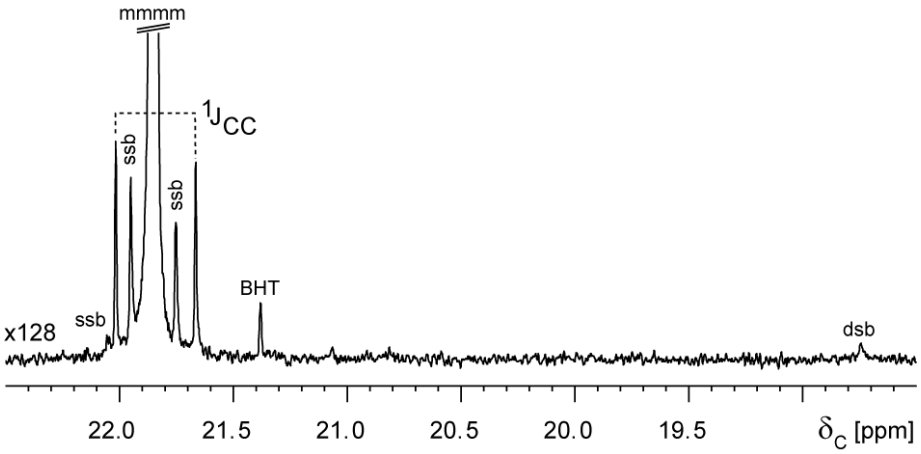

Figure 42: Quantitative $^{13}C\{^1H\}$ NMR spectrum of iPP produced with complex *rac*-**35** at 0 °C including BHT as stabilizer, illustrating no detectable stereo defects and only the expected ^{13}C satellites and artifacts (spinning/decoupling sidebands) under standard measurement conditions.

4.3.5.3 Comparison of Stereo- and Regioregularity of iPP Produced with Complexes *rac*-34-36 and Literature-known Catalysts

2,4- and 2,4,7-substituted bisindenyl metallocenes were previously reported (2.10.2.2, 2.10.2.3) to produce iPP with very high melting transitions of up to 169 °C. However, extremely low polymerization temperatures (-78 °C) are necessary. With increasing polymerization temperature the reported stereoregularities and melting transitions of polymers produced with these metallocenes are significantly lower than those obtained with complex *rac*-**34** and *rac*-**35** at similar conditions. For polymers produced with these complexes, the stereoregularity and therefore also melting transitions stay quite high (163 °C) also at increased polymerization temperatures (70 °C; Table 19, entry 8). This underlines the temperature stability of these complexes with respect to stereoselectivity based on their high rigidity.[191, 255, 256]

Regarding the polymerization results of hafnocene *rac*-**35**, a clear correlation between melting transition and tacticity can be observed (entries 5-10, Table 19). As the amount of regioerrors for entries 7-9 and 5, 6 is similar, the change of T_m is only influenced by the mmmm-pentad concentration. A nearly linear increase of T_m is obvious in the case of lower tacticities (entries 7-9). For lower polymerization temperatures (entries 6, 7), the amount of the mmmm-pentad is increased in a similar extent, whereas T_m is increased stronger. This change of the so far linear correlation can be explained by a perfect regioregular polymerization behavior at these temperatures. For highest tacticities (entries 5 and 6), a further increase in stereoregularity results in an only slight increase of T_m reaching a maximum value of about 171 °C, which is assumed to be kinetically controlled by the conditions applied during the DSC measurement. This is underlined by annealing experiments which resulted in fractions of the polymer melting close to the so far expected equilibrium melting point of 186 °C (4.3.6.2).[257, 258]

Table 19: Abbreviation of **Table 18**.

entry	complex	n[a]	p[b]	T_p[c]	T_m[d]	mmmm[e]	2,1 e[e]	3,1[e]	M_w[f]	product.[g]
5	*rac*-**35**	2	3	0	171	99.9	nd[j]	nd[j]	5 800	1 800
6	*rac*-**35**	2	4	30[h]	170	99.5	nd[j]	nd[j]	1 700	27 000
7	*rac*-**35**	2	4	50	165	99.3	0.06	0.02	1 100	17 000
8	*rac*-**35**	2	6	70	163	99.0	0.04	0.03	600	54 000
9	*rac*-**35**	2	4	70	160	98.4	0.04	0.06	410	33 000
10	*rac*-**35**	2	4	90[h]	152	95.2	0.01	0.15	44	51 000

[a] In µmol. [b] Pressure in bar, with $p = p_{Ar} + p_{propene}$ ($p_{Ar} = 1.4 \pm 0.1$ bar).
[c] Polymerization temperature in °C ± 1°C. [d] In °C. [e] In % from ^{13}C NMR (100 MHz); determined assuming the enantiomorphic site model.[94] [f] In kg/ mol. [g] Productivity in kg(PP)/ (mol(metal)·h). [h] ± 2 °C. [i] ± 5 °C.
[j] nd = not detected. [k] nm = not measured.

A comparison of the two metals (Hf and Zr) reveals higher melting transitions for iPP produced with hafnocene *rac*-**35** than with zirconocene *rac*-**34** at the same polymerization conditions. This general trend is interrupted by polymers produced at 90 °C. At this temperature the polymer produced with the zirconocene *rac*-**34** shows two melting transitions during DSC measurement (Table 18, entry 4). One is slightly higher (153 °C), other

significantly lower (142 °C) than the T_m of the polymer produced with *rac*-**35** at 90 °C (152 °C). The two melting transitions indicate different polymer phases and are most presumably a result of the deactivation reaction observed for zirconocene *rac*-**34** at high polymerization temperatures.

As described above, both a high mmmm-pentad concentration as well as a low amount of 2,1- and 3,1-regioerrors are necessary to obtain polymers with high T_m. As the mmmm-pentad level is almost identical for zirconocene *rac*-**34** and hafnocene *rac*-**35**, the observed T_m differences are a result of the two latter parameters. Whereas iPP formed by zirconocene *rac*-**34** shows a low amount of 2,1- and 3,1-regioerrors (Table 18, entries 1-4), for polymers produced with hafnocene *rac*-**35**, these regioerrors are only present in very minor amounts or even below the detection limit (Table 18, entries 5-10). Very recently, theoretical calculations showed the same trend for Cp_2MCl_2 (M = Zr, Hf). The authors reported this effect as a result of a higher energy difference between the transition states of a 1,2 and a 2,1-insertion for the hafnocene compared to the corresponding zirconocene.[108] Calculations for $SiMe_2$-bridged Cp_2MCl_2 (M = Ti, Zr, Hf) complexes showed the differences of the regioselectivity for the different metals to be mainly sterically induced.[259] With respect to these investigations, higher regioselectivities for metallocenes *rac*-**34**-**36** compared to complexes known in the literature are assumed to be a result of the steric influence of the indenyl fragments. This effect is more pronounced for complexes with a closer contact of the metal to the indenyl moiety. Hence, hafnocene *rac*-**35** afford higher regioselectivity due to its shortened M-Cp distance, its smaller parameter D and bite angle, compared to zirconocene *rac*-**34** and hafnocene *rac*-**36**. However, as these parameters are also influenced by the electronic nature of the ligand and the metal, the regioslectivity is indirectly also influenced by electronic effects.

A comparison of iPP produced by hafnocenes *rac*-**35** and *rac*-**36** with respect to T_m show slightly lower melting transitions for hafnocene *rac*-**36.** Unfortunately, the reason for the lower melting transitions cannot be clarified in detail, as ^{13}C NMR analysis for these polymers was not possible within the frame of this work. Consequently, the difference results of a lower stereo- or regioselectivity or a combination of both. Nevertheless, it is clear that the high rigidity introduced by the *tert*-butyl groups on the phenyl substituents improve stereo- and regioselectivity. In addition, the 7-methoxy-group in hafnocene *rac*-**35** further increases rigidity and thus also regio- and steresoselectivity, which affords iPP with increased melting transitions compared to those of iPP produced with hafnocene *rac*-**36**.

In particular, the combination of high stereo- and regioselectivity of complexes *rac*-**34**-**36** was shown to be important for the formation of polymers with high T_m. Hence, their stereo- and regioselectivity will be briefly compared to literature known 2,4-substituted *ansa*-bisindenyl based metallocenes known for the formation of highly iPP (2.10.2). *rac*-Me_2Si[2-Me-4-(1-naphthyl)Ind]$_2ZrCl_2$ or *rac*-Me_2Si[2-n-Pr-4-(9-phenanthryl)Ind]$_2ZrCl_2$, are among the most stereoselective metallocenes so far and produce iPP (50 °C, 1 bar propene pressure) with a total amount of regioerrors (2,1- + 3,1-regioerrors) of 0.34 % and 0.22 %, respectively.[192] Thus, the obtained regioselectivities with both rac-**34** and rac-**35** are significantly higher.
The comparison of different 2-, 4- and 7- substituted *ansa*-bisindenyl metallocenes (2.10.2.3) did not show a straightforward trend for the effect of the substituents. Especially the influence of the 4- and 7-substituent on the indenyl moiety on the polymerization behavior of corresponding metallocenes is unclear. Complexes *rac*-**34** and *rac*-**36** can both produce iPP with high melting transitions; slightly higher T_m is hereby obtained for the hafnocene bearing a 7-methoxy substituent. However, besides the 7-methoxy substituents particularly the *tert*-butyl groups on the 4-aryl fragment improve stereo- and especially regioselectivity.

Besides metallocenes, very recently a titan salalen complex was reported to produce iPP with high melting transitions up to 170 °C. Molecular weights of these polymers were not reported but concerning to the applied conditions they can be assumed as moderate to low (below 200 000 g/mol, 2.10). Compared to commonly industrially used ZN catalysts with reported melting transitions of up to 168 °C (2.10.1) complexes *rac*-**34** and *rac*-**35** can afford polypropylenes with even higher melting transitions.

4.3.5.4 Influence of Propene Concentration on Molecular Weight and Microstructure of iPP Produced by Metallocenes *rac*-34-36

A significant increase of molecular weight, independent on the ligand substitution pattern, is found for iPP produced with hafnocenes. This effect is known as the hafnium effect and is most presumably due to a more stable Hf-C bond compared to the Zr-C bond (2.7.4).[66, 133] However, at a polymerization temperature of 90 °C molecular weights of polypropylene produced with zirconocene *rac*-**34** (M_w = 130000 g/mol) are higher than those formed with hafnocene *rac*-**35** (M_w = 44000 g/mol) at the same conditions. This behavior is in analogy to investigations with the C_1-symmetric complexes (4.1.3). Additionally, end group analysis by ^{13}C NMR spectroscopy shows a higher amount of isobutyl compared to *n*-propyl end groups (74:26). This can be either a result of the first insertion of propene into an M-CH_3 bond or due

to a transfer reaction to TIBA (2.7). Former can only occur after a β-methyl transfer reaction. With respect to results obtained for the C_1-symmetric complexes, the reason of the inverted trend concerning the molecular weight at high polymerization temperatures is a fast β-methyl transfer reaction in case of hafnocene *rac*-**35**.

In general, complexes *rac*-**34-36** show decreased molecular weights with higher polymerization temperature. This is a known effect for metallocene catalysts, as solubility of propene and thus the propagation rate is decreased, whereas the rate of the termination reaction is increased (Table 18, entries 1-4, 5-10, 11-14). Besides these observations, hafnocene complexes *rac*-**35** and *rac*-**36** produce polymers with similar molecular weights at moderate polymerization temperatures, but differ especially at low (0 °C) and high (70 °C) polymerization temperatures (Table 18, entries 5, 11: 5800000 vs. 2300000 g/mol; and entries 9, 14: 410000 vs. 230000 g/mol). At these polymerization temperatures hafnocene *rac*-**35** produces PP with higher molecular weights as hafnocene *rac*-**36**.

Besides the molecular weight of produced iPP, also the amount of stereoerrors is influenced by propene concentration. The formation of a stereoerror is known to proceed either via choice of the "wrong" enantioface of the propene monomer or due to a chain end epimerization process (CEP) (2.6.1).[96] A key step of the CEP is the β-hydride transfer to the metal and therefore the amount of stereoerrors and the molecular weight of the produced polypropylenes are both directly influenced by propene concentration. A direct effect of the propene concentration on stereoselectivity was observed for hafnocene *rac*-**35** at a polymerization temperature of 70 °C (Table 18, entries 8, 9; 6 bar: mmmm = 99.0 %, 4 bar: mmmm = 98.4 %). Higher propene concentration suppresses β-hydride elimination due to a faster coordination and insertion reaction and results therefore in iPP with higher stereoregularity and higher molecular weights (M_w(4 bar) = 410000 g/mol, M_w(6 bar) = 600000 g/mol). A crucial difference of complexes *rac*-**34** and *rac*-**35** to metallocenes known for the production of highly isotactic PP is the combination of high stereo- and regioselectivity of complexes *rac*-**34** and *rac*-**35** even at elevated polymerization temperatures. The effect of Hf in combination with the presented ligand structure particularly increases the regioselectivity of complex *rac*-**34** at elevated temperatures. Hence, polypropylenes with high melting transitions can be obtained at high polymerization temperatures by increasing the propene concentration (Table 18, entries 8, 9) due to a decreased rate of CEP.

In order to obtain further information about the influence of propene concentration on the CEP of complexes *rac*-**34**-**36**, polymerization experiments with varying propene pressure between 0.7 and 8 bar were conducted (leading to propene concentrations of 0.2 - 2.1 mol/L, as calculated by the equation reported by *Busico et al.* Figure 43).[222] The total amount of 2,1- and 3,1-units is independent of propene concentration. Therefore, DSC analysis can be used as a tool for a qualitative determination of the amount of stereoerrors and thus the amount of CEP.

Both hafnocenes show a significant influence of the propene concentration on T_m. Hereby, hafnocene *rac*-**35** is slightly stronger affected by the propene concentration affording lower T_m at low propene concentration and higher T_m at elevated propene concentration. Hence, CEP seems to be more important for hafnocene *rac*-**35** in comparison to hafnocene *rac*-**36**. In contrast to these results, the stereoselectivity of zirconocene *rac*-**34** is not significantly affected by the propene concentration.

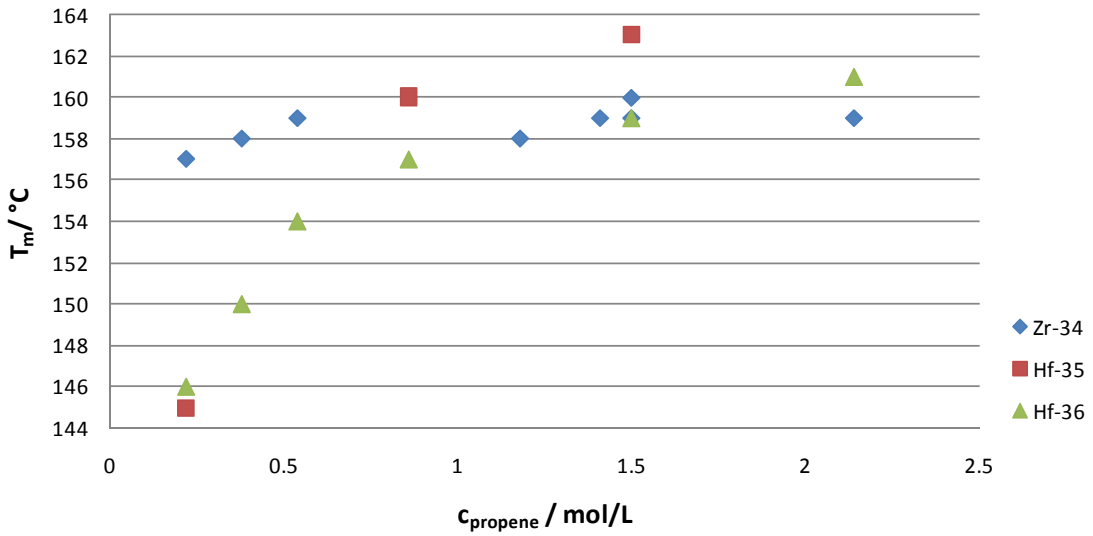

Figure 43: Dependency of T_m with increasing propene concentration for complexes *rac*-**34**-**36** ($n_{complex}$ = 0.5 - 2.0 µmol, 200 eq TIBA, 5 eq $[CPh_3][B(C_6F_5)_4]$, T_p = 70 °C).

Besides the amount of stereoerrors, in accordance with an unimolecular isomerization reaction of 2,1- to 3,1-units (2.6.1), also the ratio of 2,1- to 3,1-units is decreased for decreasing propene concentration. 3,1-units were obtained with complexes *rac*-**34** and *rac*-**35** only at elevated polymerization temperatures (50-90 °C) for which the solubility of propene is reduced (Table 18, entries 3 and 7-10, with an amount of 3,1-units of 0.04, 0.02, 0.03, 0.06 and 0.15 %, respectively). At a polymerization temperature of 90 °C, hafnocene *rac*-**35** nearly affords a complete conversion of 2,1-regioerrors to 3,1-units (Table 18, entry 10, with 2,1/3,1 = 0.01/0.15). In addition, a significant difference is observed in the ratio of 2,1- to

3,1-regioerrors for the two metals. Hafnocene *rac*-**35** produces iPPs with a lower ratio of 2,1- to 3,1-units compared to zirconocene *rac*-**34** (Table 18, entries 2,7 and 3,8 with 2,1/3,1 = 0.17/0 (Zr), 0.06/0.02 (Hf) and 0.23/0.04 (Zr), 0.04/0.03 (Hf), respectively). This tendency may be explained by a higher activation barrier for the propagation reaction after a 2,1-insertion in case of hafnocene *rac*-**35**. Hence, compared to zirconocene *rac*-**34**, hafnocene *rac*-**35** affords a slower propagation after regiomisinsertion which results in a higher probability for an unimolecular 1,3-isomerization reaction.

4.3.6 *Stability, Melting, Crystallization, and Mechanical Properties of the Highly Regio- and Isospecific PP*

For further information besides the microstructure, the melting transition, and the molecular weight of produced iPP, annealing experiments and dynamic mechanical thermal analysis (DMTA) were performed. Unfortunately, during standard analytical methods, e.g. GPC or the determination of the melting transition by DSC, these polymers differed in their behavior from commercial iPP. Especially for polymers with high M_w, degradation processes could be observed. In order to prevent these, and to obtain reproducible and reliable results, analysis of polymers already presented and discussed above was slightly modified.

4.3.6.1 Stability of the Highly Regio- and Isospecific PP

Occasionally, first DSC measurements of highly isotactic samples afforded an exothermic signal during the first heating run directly after the melting transition (Figure 44). During the second run, a significantly lower melting transition was obtained for these polymers. This specific behavior was mainly observed for polymers with high isotacticity and high molecular weight. The introduction of a small whole into the lid of the pan ensured an almost oxygen-free atmosphere during the measurement as the DSC chamber is purged with nitrogen. This procedure afforded the elimination of the exothermic signal and an almost identical second heating run. These observations lead to the conclusion that under specific conditions, high temperature and oxygen atmosphere, an oxidative degradation process can take place. This was proven by GPC analysis, conducted after DSC analysis for polymers with an observed exothermic peak, showing reduced molecular weights (e.g. from 1 100 000 g/mol to 200 000 g/mol).

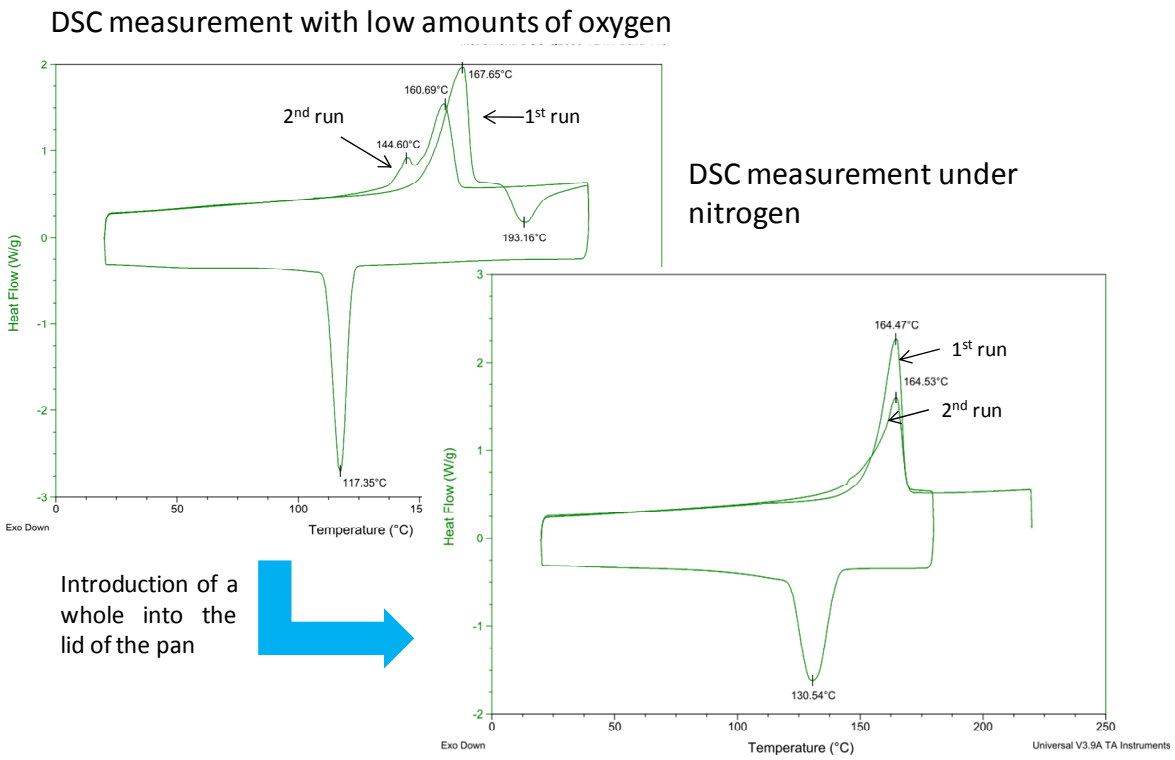

Figure 44: Stability of the highly stereo- and regioregular PP under standard DSC measurement conditions (left) and under almost oxygen-free conditions (right) (polymer: Table 18, entry 7).

A second problem for highly isotactic samples with ultrahigh molecular weights occurred during GPC measurements. Molecular weights of polymer samples measured directly after their preparation were significantly higher than after storage for several days or weeks. In particular the sample with the highest obtained M_w, produced with hafnocene *rac*-**35** at 3 bar and 0 °C, showed a strongly reduced molecular weight of only 2 200 000 g/mol after storage. Stabilizing the same directly after its formation with BKF, a radical scavenger, afforded reproducible and ultrahigh molecular weights above 5 000 000 g/mol even after storage for several weeks. With the partly degraded polymer, an additional experiment concerning its temperature stability was performed. Therefore, three samples of this polymer were heated to 160 °C in the auto-sampler of a high temperature GPC device and measured after heating for 0, 1 and 2 h, respectively (Figure 45). In order to exclude an inhomogeneous distribution of the polymer, 15 mg of the polymer were dissolved in 15 mL of stabilized (BHT) TCB at 140 °C (1 h) and the resulting solution was divided into six samples. A decrease of the molecular weight of the polymer from 2 200 000 g/mol to 1 700 000 g/mol within two hours at 160 °C was evident (1st measurement of Figure 45). In order to exclude inaccurate measurement of the molecular weight, the experiment was conducted twice affording similar results (Figure 45).

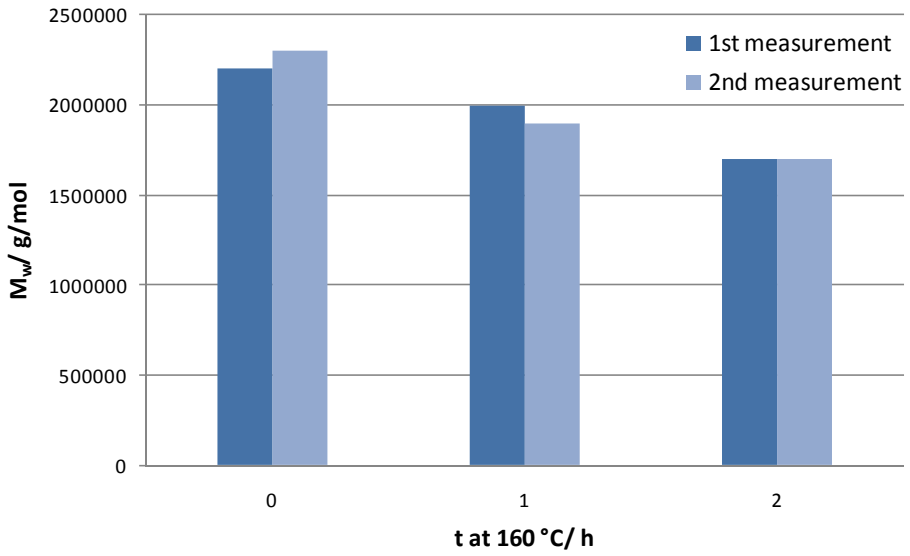

Figure 45: Degradation of a highly isotactic and ultrahigh molecular weight PP (polymer: Table 18, entry 5 already partly degraded).

These observations reveal a reduced stability of high molecular weight highly isotactic PP at high temperatures. In addition, in absence of a radical scavenger, degradation already occurs at room temperature. This degradation process could be catalyzed by impurities from catalyst or cocatalyst which were coprecipitated and remained in the polymer due to its low solubility. In order to prevent this degradation process of highly isotactic and ultrahigh M_w PPs, samples described above (4.3.5) were measured shortly after the polymerization reaction with minimum sample preheating during GPC analysis.

4.3.6.2 Annealing Experiments

To get further insight into the melting and crystallization behavior of highly stereo- and regioregular polypropylenes, annealing experiments were performed with a DSC device. Owing to degradation reactions shown above, the experiments were conducted in analogy to DSC measurements described in the previous chapter. Chosen temperatures for annealing (T_c) were above those of crystallization determined during standard DSC measurements. The experiments for iPP produced with hafnocene *rac*-**35** at 3 bar and 0 °C show a shift of the melting transition towards the equilibrium melting transition reported to be 186 °C. [257, 258] The higher the annealing temperature, the stronger is the shift of the melting transition. At the two highest annealing temperatures (160 °C and 163 °C), crystallinity was lower and thus curves are plotted separately. This effect is expected as a result of the slower crystallization process at higher temperatures.

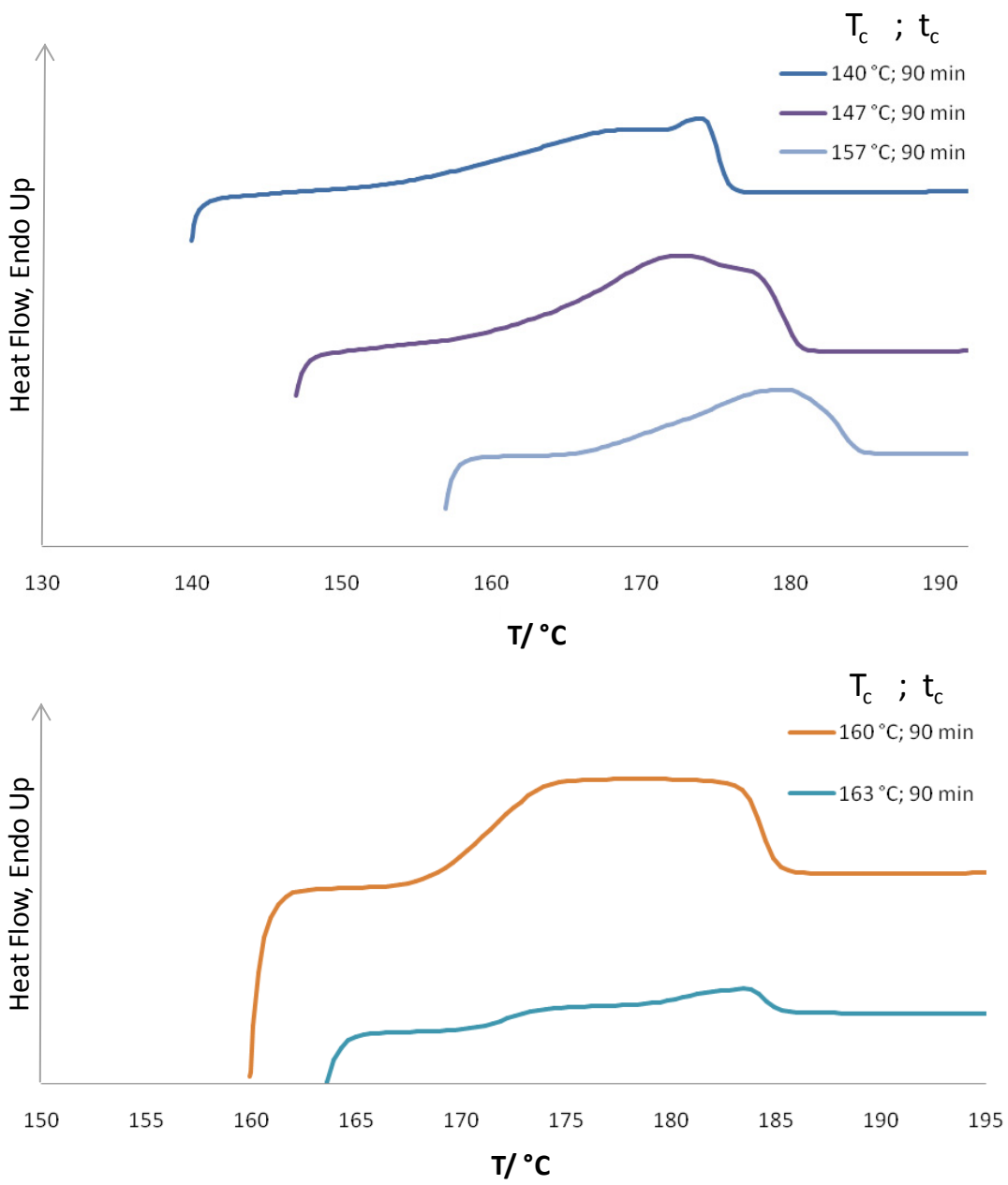

Figure 46: Annealing experiments of a highly isotactic and ultrahigh molecular weight PP (polymer: Table **18**, entry 5, already partly degraded, temperature program see 7.1).

These results and especially kinetics of the crystallization process must be regarded with care as a melt with small crystals or slightly preordered structures cannot be ruled out. Both could significantly influence the crystallization kinetics if present. Additionally, already observed degradation processes can also have a severe influence on the crystallization behavior.

4.3.6.3 Mechanical Investigations

First mechanical investigations were conducted with a DMTA device under standard conditions (Table 20). Based on the limited amount of available polymer, smaller samples were prepared (7.1, DMTA). In order to exclude influences of the reduced sample size, a commercially available iPP from Borealis (HC600TF, T_m = 164 °C) was prepared accordingly and compared to the standard sample geometry showing good agreement.

Table 20: DMTA-measurements with reduced sample size for some of the highly isotactic polypropylenes produced with the hafnocene **35**.

entry	mmmm[a]	2.1e[a]	3.1[a]	T_m[b]	G´(23 °C)[c]	G´(120 °C)[c]
1	98.4	0.04	0.06	160	859	140
2	99.0	0.04	0.03	163	906	150
3	99.5	nd[d]	nd[d]	170	886	162
4	99.9	nd[d]	nd[d]	171	902	195
5 (HC600TF)	nm[e]	nm[e]	nm[e]	164	919	131

[a] In %. [b] In °C. [c] In MPa [d] nd = not detected. [e] nm = not measured.

At 23 °C, the stiffness of the highly isotactic polypropylenes are lower or similar compared to the commercial iPP (entries 1-4 and 5). However, at a temperature of 120 °C all samples produced with hafnocene *rac*-**35** (entries 1-4) afforded higher values of G´ compared to the commercial iPP (entry 5). Hereby, a stiffness increase of up to 50% with respect to the commercial iPP was observed. Additionally, highly iPP formed by hafnocene *rac*-**35** show increasing values of G´ for higher melting transitions. For the two most stereo- and regioregular polypropylenes (entries 3 and 4), the observed difference in the mechanical behavior is significant although T_m is very similar.

Besides DMTA measurements, also stress-strain measurements with larger standard samples were conducted. Unfortunately, compression molding produced slightly colored samples. Hence, GPC and DSC measurements were made after the preparation in order to verify if degradation had occurred (Table 21). DSC curves of the samples before and after compression molding show a significant difference. The main melting transition is slightly reduced and an additional second melting transition appeared at 152 °C. This indicates a different phase composition of the samples before and after compression molding. Degradation during compression molding was further confirmed by GPC analysis.

Mechanical investigations have revealed increased stiffness at high temperatures for high-molecular weight highly stereo- and regioregular PPs. However, due to the shown difficulties during the sample preparation, the absolute values must be regarded carefully.

Table 21: iPP prepared by hafnocene *rac*-**35** at 0°C before and after compression molding.[a]

compression molding	$\mathbf{M_w}$[b]	**PDI**	$\mathbf{T_m}$[c]	$\mathbf{T_c}$[c]
before	4 200 000	1.4	170	133
after	3 400 000	1.7	152; 168	119

[a] $n_{complex}$ = 4.0 µmol, 200 eq TIBA, 5 eq $[CPh_3][B(C_6F_5)_4]$, T_p = 0 °C, $p = p_{propene} + p_{Ar}$ with $p_{Ar} = 1.4 \pm 0.1$. [b] In g/mol. [c] In °C.

5 Summary

Although metallocenes are known for a long time, especially high temperature processes usually used for the industrial production of PP are often problematic for metallocenes. The advantage of homogeneous metallocenes over heterogeneous *Ziegler-Natta* catalysts is their superior control over the microstructure of the PPs formed. However, at higher polymerization temperatures especially the good control over microstructure becomes significantly affected. As a result moderate or low molecular weights together with uncontrolled microstructures are often obtained. Hence, in this work different metallocenes were investigated with respect to their temperature stability and their polymerization behavior at high temperatures. Therefore both, complexes known in the literature were used and new structures were synthesized via convenient and versatile synthesis routes. The thesis concentrates on two main microstructures, namely the variable isotactic and the highly isotactic structure.

The variable isotactic structure of PP (viPP) can afford polymers with an elastic behavior. For good elastic properties two main factors must be in the right range. First is the amount of stereoerrors regulating the length of the isotactic segments and thus controlling the crystallization behavior, second is molecular weight. For the formation of ePP several catalysts are reported in the literature. However, as the most promising candidate the C_1-symmetric metallocenes developed by *Rieger* and coworkers were chosen for the determination of their high temperature polymerization behavior (Figure 47).

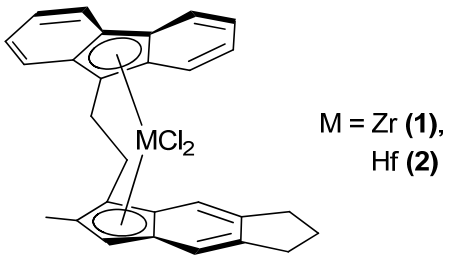

Figure 47: Investigated C_1-symmetric complexes for the formation of ePP at elevated and high temperatures.

Especially the hafnocene of these C_1-symmetric metallocenes can produce viPP with elastic behavior comparable to commercially available thermoplastic elastomers like Kraton a SBS copolymer. For the determination of the temperature stability polymerization experiments were conducted up to 100 °C. The polymerization apparatus used for the polymerization reactions allowed an online recording of the propene consumption. A constant propene flow

was observed for both metallocenes also at high temperatures (Zr (80 °C) and Hf (100 °C)) and therefore both catalysts were proven to be temperature stable under applied conditions.
Besides temperature stability the hafnocene showed lower productivities, which was not expected due to the fact that polymerization experiments with the dimethylprecursors of metallocenes **1** and **2** activated with $[CPh_3][B(C_6F_5)_4]$ revealed similar productivities for both. For the polymerization reactions in this thesis always a ternary catalysts of metallocene/TIBA/$[CPh_3][B(C_6F_5)_4]$ was applied. Hence, especially the preactivation reaction of the dichloroprecursors **1** and **2** with TIBA was investigated by ^{1}H NMR and UV-Vis spectroscopy. These studies revealed especially concerning the kinetics of the preactivation reaction a severe difference of the two metals. At usually applied preactivation conditions, the zirconocene afforded a different precursor compared to the hafnocene. Thus a different active species of the hafnocene or at least a different reaction pathway to the same or similar active species was assumed as the reason for the lower productivity observed for the hafnocene.
A second and unexpected result was the lower molecular weight of polymers produced by the hafnocene at elevated and high temperatures. End group analysis of produced polymers and determination of rate constants of the different chain transfer reactions proved a fast and unimolecular β-methyl transfer reaction to be the reason for these low molecular weights at elevated temperatures. A comparison with investigations of other metallocenes known to predominantly undergo a β-methyl transfer reaction, reported in literature, also showed at higher polymerization temperatures similar or lower molecular weights of polymers produced with corresponding hafnocenes. Hence, this behavior was concluded to be a general and valid trend in case of hafnocenes undergoing predominantly a β-methyl instead of a β-hydrid transfer reaction. Compared to zirconocene **1**, hafnocene **2** showed a higher selectivity towards the β-methyl transfer reaction. For the increased selectivity of the C_1-symmetric hafnocene compared to respective zirconocene a mechanism considering the special chain back skip mechanism, which was postulated for these catalysts, was proposed.
So far, the improved elastic behavior of hafnocene produced ePP has been traced back to higher molecular weights. Due to the higher selectivity of hafnocene **2** towards the β-methyl transfer reaction more polymer chains with an allylic chain end are generated. These can be theoretically incorporated during the homopolymerization of propene. Hence, besides the higher molecular weights of the hafnocene produced polymers there is also a higher probability for a branched structure which can significantly influence the elastic behavior of these polymers. Unfortunately the amount of branches is only low and thus not detectable by ^{1}H NMR spectroscopy. Copolymerization reactions using hafnocene **2** at different

temperatures with ethene and separately prepared macromonomers afforded depending on the conditions a high level of incorporation. This result is indicative for the formation of a long chain branched microstructure also in case of hafnocene **2** produced ePP. In addition the C_1-symmetric hafnocene **2** was also shown to be a versatile tool for the formation of branched and long chain branched PE-*g*-PP copolymers which can be used for example as compatibilizers.

A second approach applied for the formation of ePP by C_1-symmetric complexes at high temperatures was the synthesis of similar complexes with a slightly modified ligand structure. In order to suppress transfer reactions, the 2-methyl group of the investigated C_1-symmetric metallocenes was substituted by a phenyl substituent. Unfortunately, the clean complex has not been obtained so far.

The third and last approach for the formation of ePP was the use of C_2-symmetric complexes at high polymerization temperatures. At these an increased amount of stereoerrors is expected, reducing the length of the isotactic segments. For this investigation the catalyst chosen was $SiMe_2$(2-Me-BenzInd)$_2HfCl_2$/TIBA/$[CPh_3][B(C_6F_5)_4]$. As expected, polymerization experiments showed decreased crystallinity with increasing temperature, but obtained molecular weights of produced PP was too low. Hence, these investigations revealed that at least for similar C_2-symmetric complexes the formation of ePP is unlikely.

The second main topic of this work was the synthesis of C_2-symmetric metallocenes for the formation of highly iPP also at elevated polymerization temperatures. For the formation of these highly isotactic PP, in literature, especially bisindenyl-based metallocenes with a 2,4,7-substitution pattern are reported. So far there is no versatile and convenient synthesis route towards these 2,4,7-substituted indenes with the possibility to change the substituents independently of each other. A convenient and versatile synthesis strategy was developed based on a patent application of *Rieger et al.* (Scheme 46).

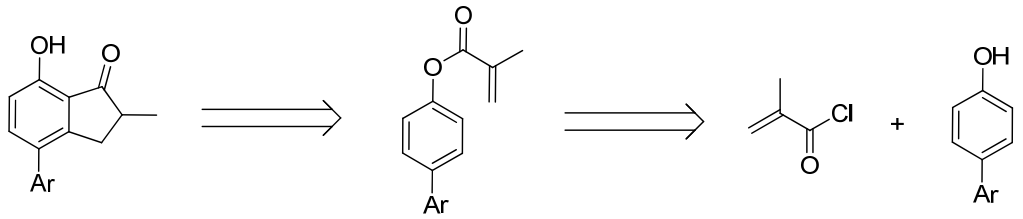

Scheme 46: Synthesis route towards new indanones patented by *Rieger et al.* in 1999.

Via this synthesis route the indanone and finally the indene with a methyl protecting group on the hydroxyl and a phenyl substituent for the aryl group was successfully synthesized. The

formation of respective $SiMe_2$-bridged ligand failed due to similar reactivities of carbon atoms C-1 and C-3 forming a mixture of different regioisomers which were not separable from each other anymore. A more versatile synthesis route was developed allowing the introduction of more sterically demanding aryl substituents in the last step before silylation (Scheme 47). Different aryl substituents were introduced and even a phenyl ring with two methyl groups in 3´- and 5´-postion led to a regioselective introduction of a $SiMe_2$ group.

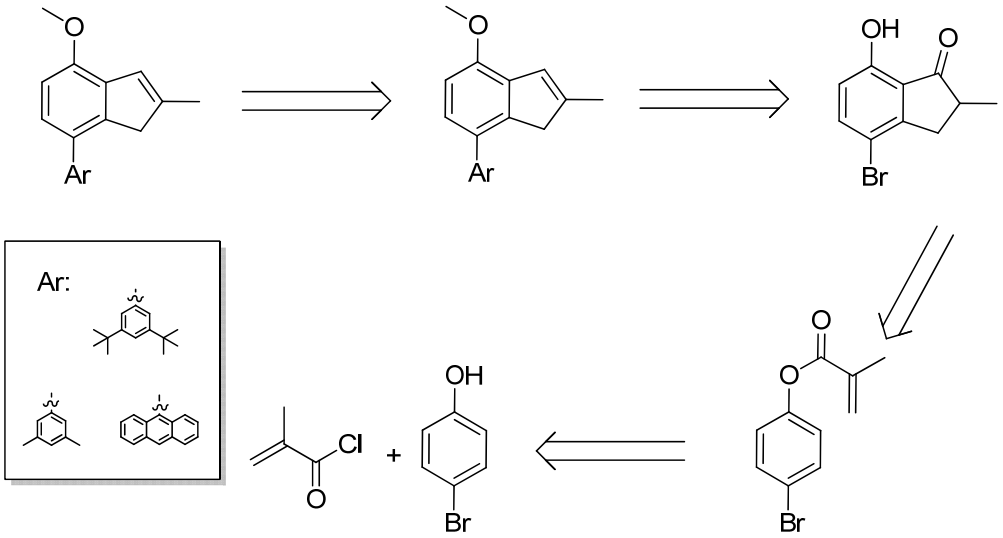

Scheme 47: Versatile and convenient synthesis route towards new 2,4,7-indenes.

A successful synthesis of the zirconocene **34** and hafnocene **35** has been achieved from the 3´,5´-di-*tert*-butylphenyl substituted and $SiMe_2$-bridged ligand so far. For comparison and to reveal the influence of the methoxy group, the corresponding hafnocene **36** without 7-methoxy substituent was synthesized in analogy to a literature known synthesis route (Figure 48). All complexes were characterized by standard analytical methods such as NMR, EA and X-ray structure analysis. Variable temperature NMR demonstrated the high flexibility of the two phenyl groups on the indenyl moiety. Polymerization experiments were conducted in the temperature range of 0 to 90 °C. Especially hafnocene **35** revealed that iPPs with extraordinarily high stereo- and regioselectivities and ultrahigh molecular weights which have not been obtained from any other catalyst up to date are accessible. Together with these high stereo- and regioselectivities also the melting transition of the produced polymers (ex reactor) reached values of up to 171 °C which have been unrivaled so far for not extracted or not annealed iPP. This melting transition is assumed to be a kinetically observed melting transition formed during DSC measurement due to the conditions of standard DSC analysis. This was underlined by annealing experiments which shifted the melting transition close to the so far expected equilibrium melting transition of 186 °C. In addition to these highly

melting iPP with ultrahigh molecular weights produced at low temperature stereo- and regioregularity of the formed polymers stood also high at high polymerization temperatures. This result is most presumably due to the high rigidity of the complexes which is achieved by the steric demand of the *tert*-butyl and the methoxy groups.

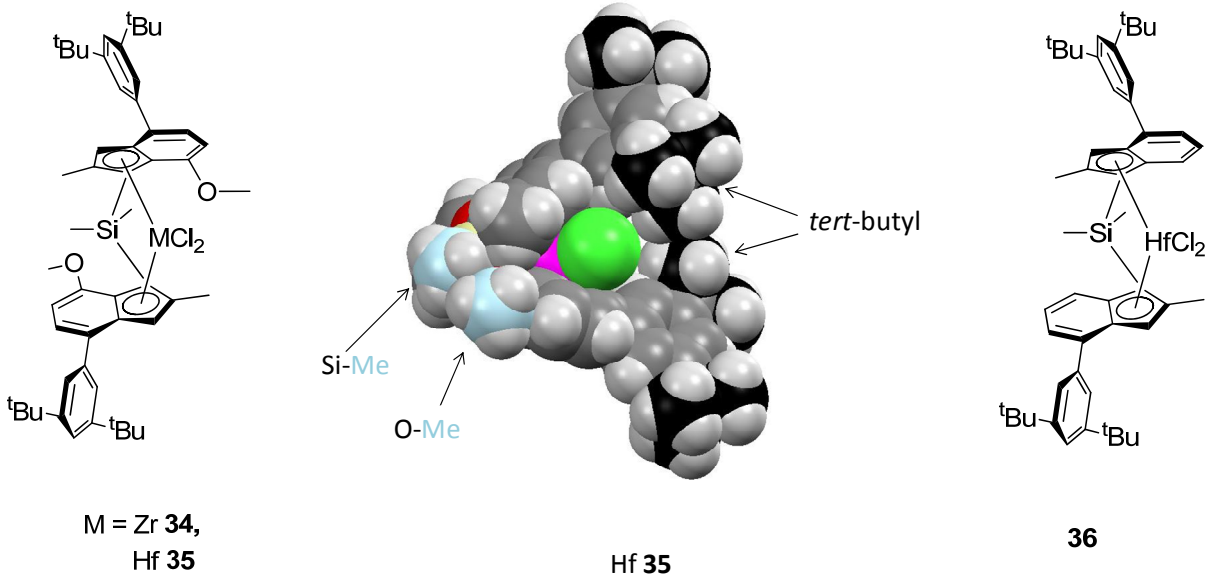

Figure 48: Synthesized and investigated C_2-symmetric metallocene structures **34**-**36** (left and right), and the crystal structure of hafnocene **35** (middle) plotted with the typical vdW radii of the respective atoms illustrating the close contact of the $SiMe_2$ fragment with the methoxy group (blue-marked) and the close contact of the *tert*-butyl groups (black-marked).

Hafnocene *rac*-**35** showed higher regioselectivies and similar stereoselectivities compared to zirconocene *rac*-**34** and slightly higher stereo- and regioselectivities compared to hafnocene *rac*-**36**. By a detailed analysis of the structural parameters of metallocenes **34**-**36** the observed stereo- and regioslectivities were assumed to be predominantly influenced by the steric influence of the indenyl ligands. As the steric influence of the lingands (e.g. M-Cp distance) is also indirectly controlled by the electronical factors of the substituents and the metal, analog structures must be synthesized in order to decide whether the influence is of electronic or steric nature. For this purpose a ligand with an ethyl instead of a methoxy group in 7-position could help.

Preliminary investigations concerning the stability and the mechanical performance of the highly iPP showed significant differences to commercially available iPP. Especially polymers with ultrahigh molecular weight and high stereo- and regioregularity tended to degradation processes especially in presence of oxygen and at high temperature. Despite the difficult handling of the polymers, mechanical investigations with dynamic mechanical thermal

analysis (DMTA) proved higher stiffness of these polymers at higher temperature (120 °C) compared to commercial iPP.

Within the frame of measurement precision (^{13}C NMR), especially complex **35**, already affords the formation of perfect isotactic polypropylene helices. A solution to the question how the extreme molecular parameters of the present polymer products allow a technical processing will decide on the future of this new polypropylene family.

6 Zusammenfassung

Obwohl Metallocene schon seit langer Zeit bekannt sind gibt es dennoch, speziell bei hohen Temperaturen, welche für die industrielle Polymerisation von Propen verwendet werden, oftmals Probleme. Im Vergleich zu den heterogenen *Ziegler-Natta* Katalysatoren liegt der Vorteil der homogenen Metallocene vor allem in Ihrer besseren Kontrolle über die Mikrostruktur der produzierten Polypropylene. Bei hohen Polymerisationstemperaturen verschlechtert sich die Kontrolle über die Mikrostruktur jedoch oftmals erheblich. Als Resultat daraus kann sich Polypropylen mit moderatem bzw. geringem Molekulargewicht zusammen mit einer unerwünschten Mikrostruktur ergeben. Aus diesem Grund wurden in dieser Arbeit unterschiedliche Metallocene bezüglich ihrer Temperaturstabilität und ihrem Polymerisationsverhalten bei hohen Temperaturen untersucht. Hierzu wurden zum Einen literaturbekannte Metallocene verwendet, und zum Anderen neue Strukturen über eine einfache und variable Syntheseroute hergestellt. Der Fokus in dieser Arbeit lag auf zwei unterschiedlichen Mikrostrukturen, hoch isotaktischem PP und variabel isotaktischem PP.
Variabel isotaktisches PP kann elastisches Verhalten aufweisen. Hierzu sind vor allem zwei Parameter entscheidend, die Menge der Stereofehler, welche die Länge der isotaktischen Blöcke und somit das Kristallisationsverhalten reguliert, und das Molekulargewicht des Polymers. Für die Herstellung von elastischem PP (ePP) sind in der Literatur einige Beispiele erwähnt. Hierbei sind die vielversprechendsten Komplexe, die von *Rieger* und Mitarbeiter entwickelten C_1-symmetrischen Metallocene, welche deshalb auf ihr Polymerisationsverhalten bei hohen Temperaturen hin untersucht wurden (Abbildung 1).

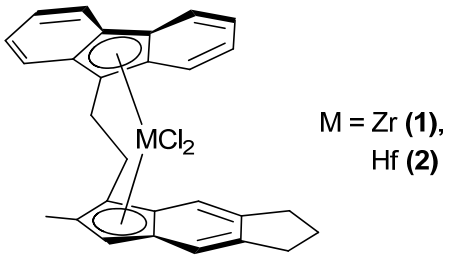

Abbildung 1: Untersuchte C_1-symmetrische Komplexe für die Herstellung von ePP bei erhöhten und hohen Temperaturen.

Speziell das Hafnocen dieser C_1-symmetrischen Metallocene kann variabel isotaktisches PP mit elastischen Eigenschaften generieren. Dieses ist in seinen elastischen Eigenschaften vergleichbar mit kommerziell erhältlichen thermoplastischen Elastomeren wie beispielsweise Kraton®, ein SBS Copolymer. Für die Bestimmung der Temperaturstabilität wurden Polymerisationsexperimente bis zu 100 °C durchgeführt. Mittels des verwendeten

Polymerisationsaufbaus konnte der Gasfluss und somit der Verbrauch des Propens während der Polymerisation aufgenommen werden. Hierbei wurde auch bei hohen Temperaturen ein konstanter Gasfluss für beide untersuchten Metallocene (Zr (80 °C), Hf (100 °C)) beobachtet, weshalb unter diesen Bedingungen die Katalysatoren als temperaturstabil angesehen werden können.

Neben der beobachteten Temperaturstabilität wurde für das Hafnocen **2** im Vergleich zum Zirkonocen **1** eine geringere Produktivität erhalten. Dies war aufgrund von Polymerisationsexperimenten mit den Dimethylprecursoren der Metallocene **1** und **2**, welche mit $[CPh_3][B(C_6F_5)_4]$ aktiviert wurden und ähnliche Produktivitäten für beide Metalle zeigten nicht zu erwarten. In dieser Arbeit wurde der ternäre Katalysator, bestehend aus dem jeweiligen Metallocen und TIBA/$[CPh_3][B(C_6F_5)_4]$ verwendet. Aus diesem Grunde wurde speziell die Voraktivierungsreaktion der Dichloroprecursoren **1** und **2** mit TIBA mittels ^{1}H-NMR und UV-Vis Spektroskopie näher untersucht. Diese Studien verdeutlichten einen signifikanten Unterschied der beiden Metalle speziell im Hinblick auf die Geschwindigkeit der Voraktivierungsreaktion. Im Vergleich zum Hafnocen **2**, zeigte sich bei den üblich verwendeten Voraktivierungsbedingungen beim Zirkonocen **1** die Bildung einer anderen Vorstufe. Aus diesem Grund wurde die beobachtete geringere Produktivität des Hafnocens auf eine andere polymerisationsaktive Spezies, bzw auf einen anderen Reaktionsweg zu der gleichen oder einer ähnlichen aktiven Spezies, zurückgeführt.

Das zweite unerwartete Ergebnis der Polymerisationen bei hohen Temperaturen war ein geringeres Molekulargewicht der Polymere, die mit dem Hafnocen **2** hergestellt wurden. Endgruppen Analytik dieser Polymere und die Bestimmung der Ratenkonstanten für die unterschiedlichen Abbruchsreaktionen offenbarten als Grund für die geringen Molekulargewichte bei hohen Temperaturen eine schnelle und unimolekulare β-methyl Übertragungsreaktion. Ein Vergleich mit literaturbekannten Daten von Metallocenen, bei denen hauptsächlich eine β-methyl Übertragungsreaktion vorliegt, zeigt bei erhöhten Polymerisationstemperaturen ebenfalls die Bildung von Polymeren mit ähnlichen oder geringeren Molekulargewichten für die entsprechenden Hafnocenene. Deshalb kann das beobachtete Verhalten der Hafnocene, die anstelle einer β-Hydrid hauptsächlich einer β-Methyl Übertragungsreaktion unterliegen, einem generell gültigen Trend zugeschrieben werden. Im Vergleich zum Zirkonocen **1** zeigte das Hafnocen **2** eine höhere Selektivität bezüglich der β-Methyl Übertragungsreaktion. Für diese höhere Selektivität wurde unter Berücksichtigung des für diese Metallocene berichteten chain back skip Mechanismus ein seitenabhängiger Abbruchmechanismus vorgeschlagen.

Bis heute wurde das bessere elastische Verhalten von ePP das mit dem Hafnocen **2** hergestellt wurde auf ein höheres Molekulargewicht zurückgeführt. Aufgrund der höheren Selektivität des Hafnocen **2** bezüglich der β-Metyl Übertragungsreaktion entstehen mehr Polymerketten mit einer allylischen Endgruppe. Diese können theoretisch während der Hompolymerisation von Propen mit in das Polymerrückgrat eingebaut werden. Deshalb liegt neben dem höheren Molekulargewicht für diese Polypropylene ebenfalls eine höhere Wahrscheinlichkeit für eine verzweigte Struktur vor, welche das elastische Verhalten dieser Polymere entscheidend beeinflussen kann. Allerdings ist die Anzahl dieser Verzweigungen zu gering, um sie mittels ^{1}H-NMR Spektroskopie nachzuweisen. Copolymerisationsreaktionen von Ethen und separat hergestellten PP-Makromonomeren wurden mit dem Hafnocen **2** bei unterschiedlichen Temperaturen durchgeführt. Hierbei konnten abhängig von den Bedingungen teilweise hohe Einbaugrade dieser Makromonomere erreicht werden. Dieses Ergebnis unterstützt die Hypothese einer langkettenverzweigten Struktur auch während der Herstellung des ePP´s mit Hafnocen **2**. Zudem wurde gezeigt, dass das C_1-symmetrische Hafnocen **2** ebenfalls als ein sehr variabler Komplex für die Herstellung von verzweigten und langkettenverzweigten PE-*g*-PP Copolymeren verwendet werden kann. Diese können beispielsweise als Compatibilizer eingesetzt werden.

Ein weiterer Ansatz zur Herstellung von ePP mit C_1-symmetrischen Komplexen bei hohen Temperaturen war die Synthese von analogen Metallocenen durch eine Modifikation der Ligandenstruktur. Um die Übertragungsreaktionen zu unterdrücken wurde hierzu die 2-Methylgruppe der untersuchten C_1-symmetrischen Komplexe durch einen Phenylsubstituenten ersetzt. Der saubere Komplex konnte bisher jedoch nicht isoliert werden.

Beim dritten und letzten Ansatz zur Herstellung von ePP bei hohen Polymerisationstemperaturen kamen C_2-symmetrische Metallocene zum Einsatz. Bei hohen Polymerisationstemperaturen wird eine erhöhte Anzahl von Stereofehlern erwartet, wodurch die Länge der isotaktischen Blöcke verkürzt wird. Für diese Untersuchungen wurde ein ternärer Katalysator, bestehend aus $SiMe_2$(2-Me-BenzInd)$_2HfCl_2$/TIBA/$[CPh_3][B(C_6F_5)_4]$, verwendet. Mit zunehmender Polymerisationstemperatur wurde, wie erwartet, PP mit abnehmender Kristallinität erhalten, jedoch waren die erhaltene Molekulargewichte des PP bei höheren Temperaturen zu gering. Aufgrund dieser Ergebnisse ist die Herstellung von ePP, zumindest mit ähnlichen C_2-symmetrischen Metallocenen, unwahrscheinlich.

Das zweite Hauptthema dieser Arbeit war die Synthese von C_2-symmetrischen Metallocenen für die Herstellung von hoch isotaktischem PP bei hohen Polymerisationstemperaturen. Für die Herstellung von diesem PP sind vor allem Bis(indenyl)metallocene mit einem

2,4,7-Substistitutionsmuster bekannt. Jedoch gibt es bisher keine variable und praktische Syntheseroute für diese 2,4,7-substituierten Indene, bei der diese Substituenten unabhängig voneinander variiert werden können. Basierend auf einem Patent von *Rieger et al.* (Schema 1) wurde eine praktische und variable Syntheseroute für diese 2,4,7-substituierten Indene entwickelt.

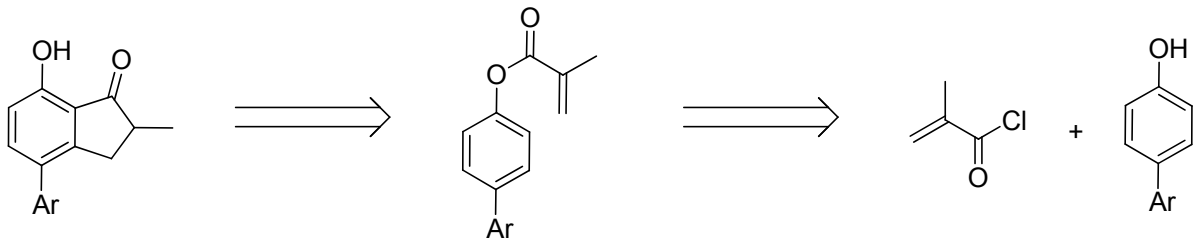

Schema 1: Von *Rieger et al*. im Jahre 1999 patentierte Syntheseroute für neue Indanone.

Über diese Syntheseroute konnte das Indanon und letztendlich das Inden mit einer methylgeschützten Hydroxyfunktion und einem Phenylsubstituenten erfolgreich synthetisiert werden. Die Synthese des entsprechenden $SiMe_2$-verbrückten Liganden gelang aufgrund der ähnlichen Reaktivitäten der Kohlenstoffattome C-1 und C-3 nicht, da dies zu der Bildung einer Mischung der verschiedenen Regioisomere führte, die nicht mehr voneinander zu trennen waren. Es wurde eine noch variablere Syntheseroute entwickelt, welche die Einführung eines sterisch anspruchsvolleren Arylsubstituenten im letzten Schritt vor der Silylierungsreaktion ermöglicht (Schema 2).

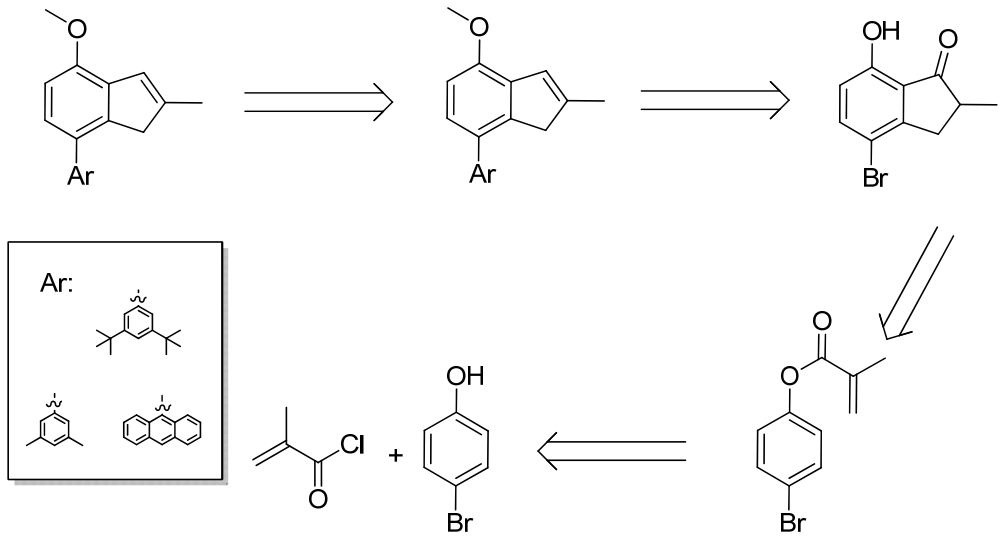

Schema 2: Praktische und variable Syntheseroute für neue 2,4,7-substituierte Indene.

Hierbei wurden verschiedene Arylsubstituenten eingeführt, wobei ein Phenylrest mit zwei Methylgruppen in 3´- und 5´-Position genügte, um eine regioselektive Verbrückung mit $SiMe_2$ zu gewährleisten.

Bisher gelang die Synthese des entprechenden Zirconocens **34** und des Hafnocens **35** mit dem 3´,5´-di-*tert*-butylphenyl substituierten und $SiMe_2$ verbrückten Liganden. Zum Vergleich und um den Einfluss des Methoxysubstituenten bestimmen zu können wurde das entsprechende Hafnocen **36** ohne den 7-Methoxysubstituenten synthetisiert (Abbildung 2). Die Synthese erfolgte analog zu einer literaturbekannten Route. Alle Komplexe wurden mittels Standardanalytik, wie NMR, EA und Röntgenstrukturanalyse, charakterisiert. Tieftemperatur NMR Messungen zeigten die hohe Flexibilität der beiden Phenylsubstituenten am Inden.

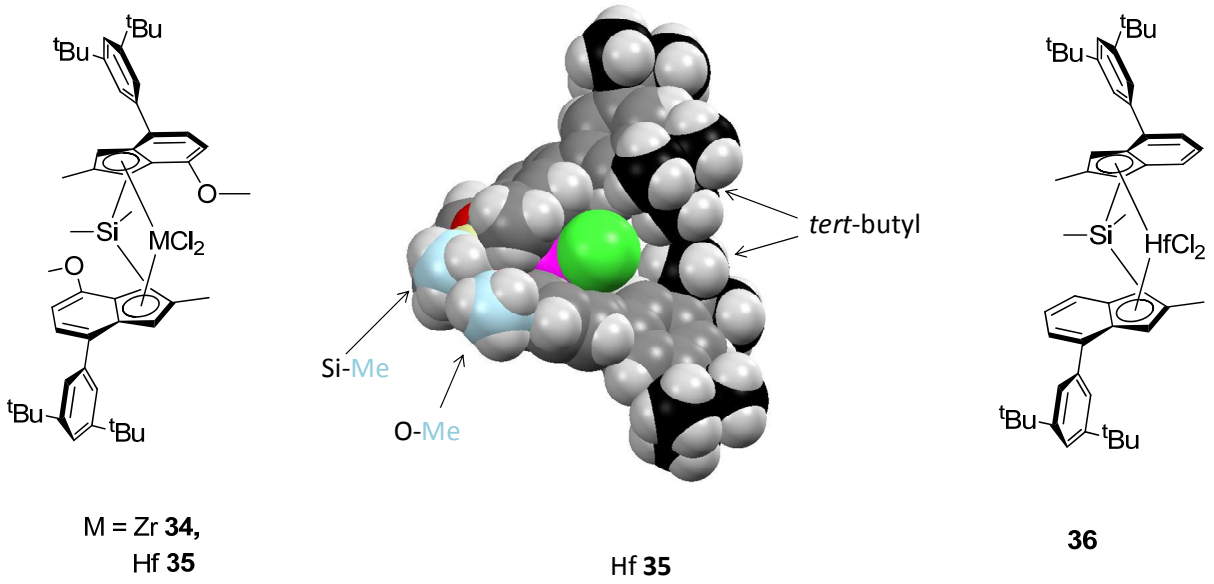

Abbildung 2: Synthestiesierte und untersuchte C_2-symmetrische Metallocenstrukturen **34-36** (links und rechts), und die Kristallstruktur des Hafnocens **35** (Mitte), dargestellt mit den typischen vdW Radien der entsprechenden Atome. Die Kristallstruktur verdeutlicht den nahen Kontakt der $SiMe_2$-Fragmente zu den Methoxygruppen (blau markiert), sowie den der *tert*-butylgruppen (schwarz markiert).

Polymerisationsexperimente mit den Metallocenen *rac*-**34-36** wurden im Bereich von 0 bis 90 °C durchgeführt. Speziell das Hafnocen **35** zeigte hierbei, dass iPP mit ungemein hohen Stereo- und Regioselektivitäten und ultrahohen Molekulargewichten, die bis heute von keinem anderen Katalysator erreicht wurden, zugänglich sind. Zusammen mit diesen hohen Stereo- und Regioslektivitäten wurden auch für die Schmelzübergange der Polymere (*ex reactor*) Werte von bis zu 171 °C erreicht, was bisher für nicht extrahiertes oder nicht getempertes iPP unereicht war. Es wird angenommen, dass der Schmelzübergang aufgrund der Standard DSC Bedingungen ein kinetisch kontrollierter Schmelzübergang ist. Dies wurde durch Temperexperimente bekräftigt, die den Schmelzübergang nahe zu dem bisher angenommenen Equilibriumschmelzpunkt von iPP (186 °C) verschoben haben. Neben diesem hochschmelzenden iPP mit ultrahohen Molekulargewichten, das bei niedrigen Temperaturen

entstand, wurde im Allgemeinen auch bei hohen Polymerisationstemperaturen eine hohe Stereo- und Regioselektivität erhalten. Dies ist höchstwahrscheinlich das Ergebnis der hohen Rigidität dieser Komplexe welche sowohl durch die *tert*-butylgruppen als auch durch die Methoxygruppen erhalten wird.

Hafnocen *rac*-**35** zeigte höhere Regioselektivitäten und ähnliche Stereoselektivitäten im Vergleich zum Zirkonocen *rac*-**34**. Im Vergleich zu dem Hafnocen *rac*-**36,** wurden für das Hafnocen *rac*-**35** etwas höhere Stereo- und Regioselektivitäten erhalten. Mittels einer detailierten Analyse der Strukturparameter der Metallocene **34-36** wurden die unterschiedlichen Stereo- und Regioselektivitäten dieser Metallocene hauptsächlich auf den sterischen Einfluss der Liganden zurückgeführt. Da der sterische Einfluss der Liganden (z.B. M-Cp Abstand) auch indirekt über die elektronischen Faktoren der Substituenten und des Metalls kontrolliert wird, müssen weitere analoge Strukturen synthestisiert werden um entscheiden zu können ob der Einfluss eher sterischer oder elektronsicher Natur ist. Hierfür bietet sich beispielsweise die Synthese eines Indens mit einem Ethyl- anstelle eines Methoxysubstituenten in 7-Position an. Vorläufige Untersuchungen bezüglich der Stabilität und der mechanischen Eigenschaften des hoch isotaktischen PP zeigte signifikante Unterschiede im Vergleich zu kommerziellem iPP. Vor allem die Polymere mit ultrahohem Molekulargewicht und hoher Stereo- und Regioregularität neigten unter Anwesenheit von Sauerstoff und bei hohen Temperaturen zu Abbauprozessen. Trotz dem schwierigen Handling dieser Polymere zeigten mechanische Untersuchungen mittels Dynamisch-mechanischer Thermoanalyse (DMTA) im Vergleich zu kommerziellem iPP eine höhere Festigkeit bei höheren Temperaturen (120 °C).

Innerhalb der Grenzen der Messgenauigkeit (^{13}C-NMR) wird mit dem Hafnocen **35** schon die perfekte iotaktische Polypropylenhelix erhalten. Die Antwort auf die Frage wie die extremen molekularen Parameter eine technische Prozessierung dieser Polymere erlauben, wird über die Zukunft dieser neuen Polypropylene entscheiden.

7 Experimental Part

7.1 General Procedures

Solvents and Chemicals

All manipulations with air and moisture sensitive compounds were carried out either under argon using standard *Schlenk* techniques or in an argon (4.8) filled glove box from *MBraun*. If not otherwise mentioned all used chemicals are commercially available, purchased from *Aldrich*, *Acros*, *ABCR* or *VWR*, and used without further purification. All deuterated solvents for NMR measurements were obtained from *Deutero*. Dry solvents like toluene, diethyl ether, tetrahydrofurane, *n*-pentane and dichloromethane were obtained from an *MBraun* solvent purification system (MB-SPS-800). Dioxane and *n*-hexane have been dried prior use by filtration over Al_2O_3 and were stored over molecular sieve 3 Å. Ethanol was dried and stored over molecular sieve 3 Å. The concentration of *n*-BuLi solutions was determined by a convenient and known titration method.[260]

Substances synthesized via published procedures

2-Methylbenz[e]indene[18], bis(2-methylbenz[e]indenyl)dimethyl silane[191], $Pd(PPh_3)_4$[261], *rac*-[1-(9-η^5-fluorenyl)-2-(5,6-cyclopenta-2-methyl-1-η^5-indenyl)ethane]zirconium dichloride **(1)**,[18, 159, 262] *rac*-[1-(9-η^5-fluorenyl)-2-(5,6-cyclopenta-2-methyl-1-η^5-indenyl)ethane]hafnium dichloride **(2)**,[18, 159, 262] *rac*-[1-(9-η^5-fluorenyl)-2-(5,6-cyclopenta-2-methyl-1-η^5-indenyl)ethane]dimethylhafnium,[68] $(BHT)_2AlMe$,[224] trineopentylaluminum,[223] and $[CPh_3][B(C_6F_5)_4]$[263] were prepared according to published procedures.

Thin layer chromatography (TLC)

For thin layer chromatography plates coated with siliga gel from *Roth* (Polygram SIL G/UV_{254}) were used. For detection of the signals either UV light (254 nm) was applied or the TLC plate was dipped into a solution of potassium permanganate and subsequently heated.

Column chromatography

Column chromatography was either manually performed or with a column chromatography device from *Varian* (IntelliFlash 310, Varian Flash Purification System) applying a solvent gradient.

For the manual column chromatography silica gel from *Fluka* (grain size 0.040-0.063 mm) with an excess of 50-100 times referred to the mass of the substance separated was used. For the column chromatography device already packed standard columns from *Varian* were applied. For both methods technical solvents have been distilled prior to use.

Gel permeation chromatography (GPC)

GPC was performed using a *Polymer Laboratories* PL-GPC 220 high temperature chromatograph, equipped with two *Olexis* 300·7.5 mm columns and triple detection by a differential refractive index detector, a PL-BV 400 HT viscosimeter and a Precision Detectors Model 2040 Light Scattering Detector (15 °, 90°). As solvent BHT stabilized 1,2,4-trichlorobenzene was used. About 1 mg of the polymer was dissolved in 1 ml of stabilized TCB for 1 hour. Afterwards the samples were transferred into the auto sampler where they were kept for a maximum of five hours at 140 °C and a maximum of three hours at 160 °C prior injection. For the very highly isotactic und ultrahigh molecular weight polypropylenes the samples were directly measured after sample preparation at 140 °C after keeping them some minutes at 160 °C. The measurements were performed at 160 °C with PE standards for calibration and a solvent flow of 1 mL/min. The used dn/dc value was 0.097 for highly isotactic PP, for the elastic PP and the ethylene propylene copolymers a dn/dc value of 0.1 was used.[264]

Nuclear magnetic resonance spectroscopy (NMR)

NMR spectra of ligand precursors and complexes were recorded on a *Bruker* AMX-300. As internal standard for calibration, the residual proton signal of deuterated solvents was used. For detected multiplicity of the signals typical abbreviations were used (s = singlet, d = doublet, t = triplet, m = multiplet).

Chloroform ^{1}H (δ = 7.26 ppm), ^{13}C (δ = 77.16 ppm); toluene ^{1}H (δ = 2.08, 6.97, 7.01, 7.09 ppm), ^{13}C (δ = 137.48, 128.87, 127.96, 125.13, 20.43 ppm); benzene ^{1}H (δ = 7,16 ppm), ^{13}C (δ = 128.06 ppm); CD_2Cl_2 ^{1}H (δ = 5.32 ppm), ^{13}C (δ = 53.84 ppm).

Polymer NMR:

The polypropylenes and the copolymers produced with the C_1-symmetric complexes were measured on a Bruker AMX-300 at 100 °C in bromobenzene. As internal standard for calibration the residual proton signal of deuterated bromobenzene was used: bromobenzene ^{1}H (furthest upfield peak, δ = 7.00 ppm), ^{13}C (δ = 123.00 ppm).

Determination of the percentaged amount of the mmmm pentad:

In case of the elastic PP signals which can be assigned to saturated end groups, or regiodefects (2,1e, 2,1t or 3,1) could not be observed, at least by the obtained precision of measurement.[5] Hence the percentaged amount of the mmmm pentad was directly determined by dividing the integral of the methyl-signal of the mmmm-pentad by the sum of the integrals of the methyl-signals of all pentads.

Quantitative NMR-spectroscopy of the highly isotactic polypropylenes was performed by the analytical department of *Borealis Polyolefine* GmbH, Linz and used to quantify the isotacticity, tacticity distribution, content of regiodefects and degree of unsaturation of the polymers.

Quantitative ^{13}C{^{1}H} NMR spectra were recorded in the solution-state using a Bruker Advance III 400 NMR spectrometer operating at 400.15 and 100.62 MHz for ^{1}H and ^{13}C respectively. All spectra were recorded using a ^{13}C optimized 10 mm selective excitation probehead at 125°C using nitrogen gas for all pneumatics. Approximately 200 mg of material was dissolved in 1,2-tetrachloroethane-d_2 (TCE-d_2). This setup was chosen primarily for the high resolution needed for tacticity distribution quantification.[265, 266] Standard single-pulse excitation was employed utilizing the NOE and bi-level WALTZ16 decoupling scheme.[267, 268] A total of 8192 (8k) transients were acquired per spectra. Quantitative ^{13}C{^{1}H} NMR spectra were processed, integrated and relevant quantitative properties determined from the integrals using proprietary computer programs developed by *Borealis*. All chemical shifts were internally referenced to the methyl signal of the isotactic pentad mmmm at 21.85 ppm.

The tacticity distribution was quantified through integration of the methyl region between 23.6 and 19.7 ppm correcting for any sites not related to the stereo sequences of interest e.g. those from regiodefects, end-groups, artifacts, stabilizer etc.[265, 266] With characteristic signals corresponding to regiodefects observed the influence of regiodefects on the quantification of the tacticity distribution was corrected for by subtraction of representative integrals from integrals corresponding to specific steric n-ad sequences.[5] The pentad tacticity distribution was determined through direct separate integration of each methyl signal from a given steric

pentad followed by normalization to the sum of methyl signals from all steric pentads. The relative content of a specific steric pentad was reported as the mole fraction or percentage of a given steric pentad xxxx with respect to all steric pentads:

$$[xxxx] = xxxx / (mmmm + mmmr + rmmr + mmrr + xmrx + mrmr + rrrr + mrrr + mrrm)$$

where xmrx represents the combined integral of both mmrm and rmrr as signal from these steric pentads are not commonly resolved.

The pentad isotacticity was given by fitting the experimentally determined steric pentad distribution to the enantiomorphic site control model. Specifically the integral region for mmmm and mmmr were combined and termed mmmx, by doing so the need for further error inducing corrections was eliminated. Thus the relationship between the probability of primary insertion on the favored enantio-face (σ) and the mole fraction of mmmx is as follows:

$$[mmmx] = [mmmm] + [mmmr] = \sigma^5 + (1- \sigma)^5 + 2((\sigma^4(1- \sigma)^1) + 2((\sigma^1(1- \sigma)^4)$$

Relationships for other pentad sequence can be commonly found in the literature. Through linear least-squares fitting the value of σ which gave the best fit to this model was obtained. The pentad isotacticity was then predicted from the fitted value of σ according to the standard relationship:

$$[mmmm] = \sigma^5 + (1- \sigma)^5$$

Table 22: Predicted values for the mmmm-pentad.

entry	[mmmm]	σ
1	99.64	0.9993
2	99.44	0.9989
3	99.00	0.9980
5	99.89	0.9998
6	99.49	0.9990
7	99.29	0.9986
8	99.04	0.9981
9	98.35	0.9967

Due to the extreme nature of some of the highly isotactic polypropylenes (e.g. Table 18, entry 5) manual adjustment of phase, baseline and integrals was undertaken to increase precision at the expense of repeatability. Raw data extracted from the spectra is given in the following (Table 23)

Table 23: SNR calculated on the real part of the spectum only (Bruker sino real command).

signal	δ ppm	experimental %	experimental SNR	ES fit %
mmmx	22.50 – 21.25	99.95185	19393.70	99.95213
mmrr	21.00 – 20.65	0.03075	6.28	0.03190
mrrm	19.95 – 19.65	0.01740	2.92	0.01595

Fitting to the enantiomorphic site control model results in a defining probably σ of 0.99984, a pentad isotacticy of 99.920 % with the sum of the least squares of 3.5×10^{-10}.

The presence of secondary inserted propene in the form of 2,1 erythro regiodefects was indicated by the presence of the two methyl signals at 17.7 and 17.2 ppm and confirmed by the presence of other characteristic signals. The amount of 2,1 erythro regiodefects was quantified using the average integral (e) of the two methyl signals at 17.7 and 17.2 ppm termed e6 and e8 respectively, i.e. e = (e6 + e8)/2.

The presence of tertiary inserted propene in the form of 3,1 isomerization regiodefects was indicated by the presence of the signals at 37.5 and 27.6 ppm and confirmed by the presence of other characteristic signals. The amount of 3,1 isomerization regiodefects was quantified using the average integral (i) of the two characteristic signals at 37.5 and 27.6 ppm termed i3 and i4, i.e. i = (i3 + i4)/2.

Characteristic signals corresponding to other types of regiodefects were not observed.[5]

The amount of primary inserted propene (p) was quantified based on the integral of all signals in the methyl region from 23.6 to 19.7 ppm with correction for other species included in the integral not related to primary insertion as well as for primary insertion signals excluded from this region.

The relative content of a specific type of regiodefect was reported as the mole fraction of said regiodefect with respect to all observed forms of propene insertion i.e. sum of all primary (1,2), secondary (2,1) and tertiary (3,1) inserted propene units:

$$[21e] = e / (p + e + i) \qquad \text{and} \qquad [31] = i / (p + e + i)$$

With only 2,1 erythro regiodefects observed the total amount of secondary inserted propene in the form of either erythro or threo regiodefects was identical to the content of 2,1 erythro regiodefects:

$$[21] = [21e]$$

For some systems neither stereo nor regioerrors were observed under standard measurement conditions (8k transients). From such spectra the detection threshold of SNR = 2.5 may be used to estimate the minimum pentad isotacticy by assuming the presence of only signals from mmmr, mmrr and mrrm stereo sequences i.e. enantiomorphic site control only, with similar line shape as that of the observed mmmm signal. Thus the defining probability of the enatimorophic site control model can be determined from the signal to noise ratios of observed SNR of the mmmm signal (SNR_{mmmm}) and the detection threshold of the mmrr signal ($SNR_{mmrr} = 2.5$) from the following relationship:

$$SNR_{mmmm} / [\sigma^5 + (1- \sigma)^5] = SNR_{mmrr} / [2(\sigma^4(1- \sigma)) + 2(\sigma (1- \sigma)^4)]$$

The pentad isotacticy may then predicted from the determined value of σ in the usual manner.

Differential scanning calorimetry (DSC)

DSC measurements were performed either using a DSC-device of the *Wacker-Chair of Macromolecular Chemistry* or at the *Borealis GmbH* in Linz.

Measurements at the *Borealis* were performed on a DSC200 *TA Instrument*, by placing a 5-7 mg polymer sample into a closed DSC aluminum pan, heating the sample from -10 °C to 210 °C at 10 °C/min, holding for 5 min at 210 °C, cooling from 210 °C to -10 °C, holding for 5 min at -10 °C, heating from -10 °C to 210 °C at 10 °C/min. The reported values are those determined from the second heating scan.

Measurements at the *Wacker-Chair of Macromolecular Chemistry* were performed using a DSC device from *TA Instruments* (Q2000). 2-3 mg of the polymer sample were placed in a closed DSC aluminum pan. As discussed, for the highly isotactic polypropylenes a whole was made into the lid of the pan. Sample were measured using the following program: heating from rt to 180 °C at 10 °C/min, holding for 1 min at 180 °C, cooling from 180 °C to rt at 10 °C/min, holding for 1 min at rt, heating from rt to 200 °C at 10 °C/min. The reported values are those determined from the second heating scan.

Annealing experiments

The annealing investigations were performed using a DSC device from *TA Instrument* (Q2000). In analogy to DSC analysis, between 2 and 3 mg of the polymer sample were placed into a closed aluminum pan. To prevent observed degradation processes a whole was made into the lid of the pan. The annealing experiment was performed using the following procedure:

1) Heating with 50 °C/min to 180 °C
2) Equilibrating for 2 minutes at 180 °C
3) Cooling to T_c with 50 °C/min
4) Holding at T_c for t_c
5) Heating with 10 °C/min to 200 °C (depicted run)

Dynamic mechanical thermal analysis (DMTA)

DMTA measurements and the preparation of the samples were performed at the *Borealis* GmbH using the following procedure:

Sample preparation:

Compression molding (on samples stabilized with standard antioxidant) was done in two steps. In the first step thin plaques (~ 0.3 mm) were pressed. Then the thin plaques were cut into small pieces (approx. 1x1 mm) which were used to fill the frame.

1) PC-lab press at 200°C/ 2 minutes

2) Collin P200M
   Dosing: 0.12 g
   Temp.: 200 °C
   A) 240s//8bar//0bar/s
   B) 300s//50bar//3bar/s
   C) 300s//200bar//10bar/s
   D) 780s//200bar//-15K/min//0bar/s

Conditioning: for 96 h at room temperature.

Test method:

DMTA according to ISO 6721-7 Torsion mode
Sample geometry: 30 x 5 x 0.6 mm
Test setup:

normal force: 20g/ +-10
rate: 2K/ min
Initial temp.: -50°C, end temp.: 165°C
Strain: 0.15%, 0.5/ 3 s cycle

Electrospray ionization mass spectrometry (ESI-MS)

For the determination of the masses an ESI-MS device from *Varian* (Varian LC-MS 500; 50 – 2000 Da) was used. The measurement was performed either in the positive or in the negative mode.

Elemental analysis (EA)

EA were performed in the micro analysis lab of the institute of anorganic chemistry of the Technischen Universität München. Water and oxygen sensitive substances were weighed and stored in the glove box until their measurement. The combustion analysis of C, H and N was done using an elemental analysis device from *Elementar* (Vario EL).

Single crystal X-ray structure determinations

Data were collected on an X-ray single crystal diffractometer equipped with a CCD detector (APEX II, κ–CCD), a rotating anode (Bruker AXS, FR591) with MoK_α radiation (λ = 0.71073 Å), and a graphite monochromator by using the SMART software package.[269] The measurements were performed on single crystals coated with perfluorinated ether. The crystals were fixed on the top of a glass fiber and transferred to the diffractometer. Crystals were frozen under a stream of cold nitrogen. A matrix scan was used to determine the initial lattice parameters. Reflections were merged and corrected for Lorenz and polarization effects, scan speed, and background using SAINT.[270] Absorption corrections, including odd and even ordered spherical harmonics were performed using SADABS.[270] Space group assignments were based upon systematic absences, *E* statistics, and successful refinement of the structures. Structures were solved by direct methods with the aid of successive difference Fourier maps, and were refined against all data using WinGX[271] based on SIR-92.[272] The hydrogen positions

were refined with individual isotropic displacement parameters (***rac*-34**). Hydrogen atoms were assigned to ideal positions and refined using a riding model with an isotropic thermal parameter 1.2 times that of the attached carbon atom (1.5 times for methyl hydrogen atoms) (***meso*-34**). If not mentioned otherwise, non-hydrogen atoms were refined with anisotropic displacement parameters. Full-matrix least-squares refinements were carried out by minimizing $\Sigma w(F_o^2-F_c^2)^2$ with SHELXL-97[273] weighting scheme. Neutral atom scattering factors for all atoms and anomalous dispersion corrections for the non-hydrogen atoms were taken from *International Tables for Crystallography*.[274]

7.2 **UV-Vis Investigations**

For the UV-Vis measurements a device from *Varian* (Cary 50) equipped with a peltier thermostated cell holder, allowing temperature control and stirring with a magnetic stirring bar, was used. In order to perform the kinetic investigations under Argon, a 3.5 mL modified quartz glass cell equipped with a *Schlenk* connection was used (Figure 49). The cell was heated to 80 °C and directly transferred into the antechamber of the glove box and dried in vacuum for at least 30 min. The catalyst was weighed in the glove box and dissolved in 3 mL of dry toluene. After equilibration of the complex solution at the desired temperature, the preactivation agent (TIBA, DIBAL-H) was added via the septum of the cell while at the same time the measurement was started. The addition of the TIBA or DIBAL-H solution was performed with a gastight *Hamilton* syringe with a teflon tipped plunger. TIBA and DIBAL-H were used as a 1.1 and 1.2 M toluene solution respectively. Concentrations of the reaction solutions after addition of TIBA or DIBAL-H solution were in the range of $5\cdot10^{-4}$ - $9\cdot10^{-4}$ mol/L and are mentioned in the figure captions of the corresponding UV-Vis spectra.

Figure 49: Modified quartz glass cell for UV-Vis investigations.

7.3 NMR Investigations

The NMR investigations of the preactivation reaction of complexes **1**, **2** with TIBA and DIBAL-H were performed in screw cap NMR tubes equipped with a Teflon sealing. Prior use the NMR tubes were heated to 80 °C and subsequently dried in vacuum. The complex was weighed in the glove box and dissolved in deuterated toluene. A 2.0 M solution of TIBA or a 1.2 M solution of DIBAL-H in deuterated toluene was prepared separately. After addition of the alkylaluminum compound, complex solutions had a concentration in the range of $1.9 \cdot 10^{-2}$ to $2.9 \cdot 10^{-2}$ mol/L. The NMR tube was placed into an oil bath already heated to the desired temperature for one hour. Subsequently a ^{1}H NMR spectrum was recorded.

7.4 Polymerization procedure

All polymerization reactions were conducted in a similar manner. Hence a general description of the procedure will be given here. Differences to the general procedure will be mentioned afterwards and in addition information such as changed procedures or the precise conditions are given below each table depicted in chapter 4.

Polymerization assembly (Figure 50):

All polymerization reactions were conducted in a 1.1 L *Büchi* steel autoclave equipped with a paddle mixer. Ethene (2.7) and propene (2.6) were fed continuously into the autoclave during the polymerization reaction. Before their injection both gases were purified by a *BASF* catalyst (R3-11) and molecular sieve 3-4 Å. The propene or ethene consumption was measured with a gas flow meter (*Bronkhorst* F-111C-HA-33P). Pressure (*Bronkhorst* pressure controller P-602C-FAC-33P) and temperature (*Thermo Scientific* HAAKE DynaMax) were kept constant during the entire polymerization procedure. Pressure, temperature and propene or ethene consumption were also monitored and recorded online during the whole polymerization process via the connected PC.

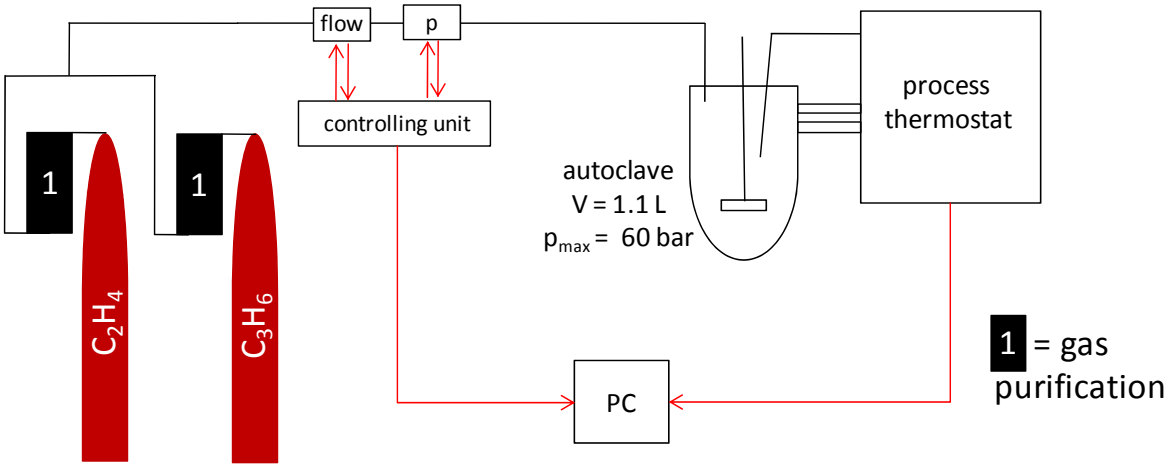

Figure 50: Schematic presentation of the polymerization assembly.

Polymerization process:

In order to remove water and residual polymer of former polymerization reactions the autoclave was charged with 300 ml of dry toluene and 3 mL of a 1.1 M TIBA solution in toluene and stirred for 1 h at 90 °C. For polymerization reactions the autoclave was charged with 280 mL of dry toluene and between 0.5 and 2 mL of of a 1.1 M TIBA solution in toluene depending on the amount of used complex (for 5 µmol of metallocene 0.5 mL of TIBA solution, for 2 µmol 1 mL and for 1 µmol 2 mL).

For the preactivation the metallocene was dissolved in 10 mL of dry toluene and if not otherwise mentioned 200 eq of a 1.1 M TIBA solution in toluene was added. The reaction mixture was stirred for 1 h at 60 °C. The preactivated complex solution was added via syringe into the autoclave which was filled before with 280 mL of dry toluene and the desired amount of the TIBA solution. A stirring rate of 1000 rpm and the desired temperature was adjusted. Just before pressurizing the autoclave with propene or ethene the argon system pressure was adjusted. In case of the propene homopolymerization reactions with complexes **1** and **2** (4.1.2 - 4.1.6) and the C_2 symmetric complex for the formation of ePP (4.2) the argon system pressure was set to 1.9 ± 0.2 bar, in case of the macromonomers and the copolymers produced with complex **2** (4.1.8, 4.1.9) and the highly isotactic polypropylenes (4.3) the argon system pressure was adjusted to 1.4 ± 0.1 bar. Afterwards the autoclave was pressurized with ethene or propene up to the desired polymerization pressure. After equilibration of pressure and temperature the polymerization reaction was started by adding the trityl tetrakis(pentafluorophenyl)borate solution (5 eq, in 10 mL of dry toluene) via a pressure burette into the autoclave. During the entire polymerization reaction the propene or ethene consumption and the temperature was recorded online. The polymerization reaction was stopped by adding a few mL of methanol via the pressure burette into the autoclave and

closure of the gas inlet valve. Subsequently the residual propene or ethene pressure was slowly reduced by opening an additional valve. The autoclave content was poured into acidified methanol. The polymer was filtered off, washed exhaustively with methanol and dried in vacuum at 80 °C for several hours.

Additional information for the production of the macromonomers and the copolymerization reactions of these, using complex **1**:

The polymerization procedure of the macromonomer itself was conducted analog to the procedure mentioned above. However, due to the good solubility of the macromonomer after pouring the content of the autoclave into acidified methanol it took some time until the polymer settled down to the bottom of the beaker. The solution was decanted and the polymer was washed with methanol. Afterwards it was dissolved in toluene and transferred into a *Schlenk* flask. The solvent was removed at reduced pressure and dry toluene was added to the polymer which was again removed under vacuum. The polymer was dried at 80 °C under vacuum (*Schlenk* line) for several hours.
For the copolymerization reactions with ethene the macromonomer was added into the autoclave after addition of TIBA but before the catalyst and stirred for some time. The used amount of TIBA for these polymerization reactions was 2 mL. Afterwards the polymerization reaction was performed in the usual described manner. The obtained polymer contained besides the real copolymer also not incorporated macromonomer. Latter was quantitatively separated from the copolymer by soxhlet extraction with *n*-pentane, which was conducted for 24 h.

7.5 Ligand Synthesis

7.5.1 *1-(9-Fluorenyl)-2-(5,6-cyclopentyl-2-phenyl-1-indendyl)-ethane*

7.5.1.1 Atropic Acid (4)

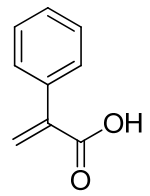

M = 148.16 g/mol

16.6 g (100 mmol) of tropic acid were dissolved in 200 mL of an aqueous solution of KOH (30.3 g KOH, 540 mmol) and refluxed over night. The solution was cooled, acidified with 10 % HCl to precipitate the product as a white solid. The solid was separated by filtration and washed with H_2O. The white solid was dissolved in DCM, washed with saturated sodium chloride solution and dried over Na_2SO_4. After filtration and evaporation of the solvent atropic acid was obtained as a white crystalline powder.

Yield: 11.8 g (80 mmol, 80 %).

^{1}H NMR (300 MHz, $CDCl_3$): δ [ppm] = 7.49 - 7.32 (m, 5H, H-Ar),
6.55 (d, ^{1}J = 1.1 Hz, 1H, C=CH_2), 6.04 (d, ^{1}J = 1.1 Hz, 1H, C=CH_2).

^{13}C NMR (75 MHz, $CDCl_3$): δ [ppm] = 172.33, 140.57, 136.04, 129.54, 128.44, 128.34, 128.12.

R_f-value: (n-pentane:ethyl acetate = 90:10) = 0.20.

Elemental analysis:
calculated: C 72.96 %; H 5.44 %.
found: C 72.57 %; H 5.54 %.

7.5.1.2 Atropic Acid Chloride (5)

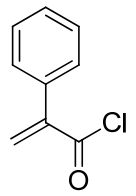

M = 166.60 g/mol

To 1.96 g (13.5 mmol) of atropic acid and a small amount of BHT as stabilizer 2 mL of $SOCl_2$ (3.28 g, 27.6 mmol) were added and stirred over night at room temperature. Residual $SOCl_2$ was removed at rt and reduced pressure. The product, a clear liquid, was condensed into a flask cooled with liquid nitrogen by increasing the oil bath temperature stepwise up to 70 °C at a reduced pressure of $1 \cdot 10^{-1}$ mbar.

Yield: 0.98 g (5.9 mmol, 44 %).

^{1}H NMR (300 MHz, $CDCl_3$): δ [ppm] = 7.41 – 7.36 (m, 5H, H-Ar), 6.77 (s, 1H, C=CH_2), 6.32 (s, 1H, C=CH_2).

7.5.1.3 5,6-Cyclopenta-2-phenylindane-1-one (6)

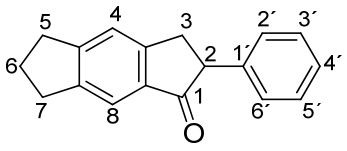

23.6 g (200 mmol) of indane were dissolved in 45 mL of *Eaton's* reagent. A separately prepared solution of 3.0 g (20 mmol) atropic acid **(4)** in 35.5 g (300 mmol) indane was slowly added over a period of one hour to the atropic acid at 55 °C. The reaction mixture was stirred for additional 4 h at 55 °C. Afterwards it was cooled to rt and poured into ice-water. The organic phase was separated and the aqueous phase was extracted several times with Et_2O. The combined organic phases were washed with an aqueous solution of potassium carbonate and afterwards with water and a saturated sodium chloride solution. The organic phase was

dried over Na_2SO_4. After filtration and removal of solvent and excess indane at reduced pressure the product was chromatographically obtained (*n*-hexane:ethyl acetate) as a slightly yellow solid.

Yield: 3.0 g (12 mmol, 60 %).

^{1}H NMR (300 MHz, $CDCl_3$): δ [ppm] = 7.63 (s, 1H, H-8),
7.37 – 7.14 (m, 6H, H-2´, H-3´, H-4´, H-5´, H-6´), 3.93 – 3.85 (m, 1H, H-2),
3.68 – 3.52 (m, 1H, H-3), 3.23 – 3.13 (m, 1H, H-3), 3.03 – 2.90 (m, 4H, H-5, H-7),
2.23 - 2.09 (m, 2H, H-6).

^{13}C NMR (75 MHz, $CDCl_3$): δ [ppm] = 205.76, 153.63, 153.10, 144.76, 140.27, 135.17,
128.88, 127.89, 126.98, 122.03, 119.88, 54.04, 35.77, 33.27, 32.18, 25.93.

R_f-value: (*n*-hexane:ethyl acetate = 90:10) = 0.42.

Elemental analysis:
calculated: C 87.06 %; H 6.49 %.
found: C 87.34 %; H 6.13 %.

7.5.1.4 1-(9-Fluorenyl)-2-bromoethane (7)

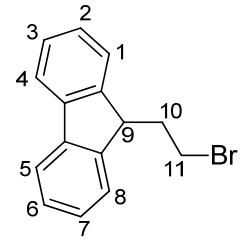

M = 273.17 g/mol

3.33 g (20.0 mmol) of fluorene were dissolved in 100 mL Et_2O. 8.0 mL (20.0 mmol) of a 2.5 M solution of *n*-BuLi in hexane were added at 0 °C and stirred for an additional hour at room temperature. A 10-fold excess of 1,2-dibromoethane (17.3 mL, 200.0 mmol) was added at rt and the reaction mixture was stirred for 4h at rt. 100 mL of water were added to the reaction mixture. The organic phase was separated from the aqueous phase, which was

extracted twice with Et_2O. The combined organic phases were washed with water, saturated sodium chloride solution and dried over Na_2SO_4. After filtration the solvent and excess of 1,2-dibromoethane was removed under reduced pressure. Crystallization from *n*-pentane gave the product as an orange solid.

Yield: 4.15 g (15.2 mmol, 76 %).

^{1}H NMR (300 MHz, $CDCl_3$): δ [ppm] = 7.76 (d, ^{3}J = 7.0 Hz, 2H, H-4, H-5),
7.54 (d, ^{3}J = 7.3 Hz, 2H, H-1, H-8,), 7.42-7.30 (m, 4H , H-2, H-3, H-6, H-7),
4.18 (t, ^{3}J = 6.1 Hz, 1H, H-9), 3.30 (t, ^{3}J = 7.6 Hz, 2H, H-11),
2.55-2.48 (m, 2H, H-10).

^{13}C NMR (75 MHz, $CDCl_3$): δ [ppm] = 145.89, 141.18, 127.56, 127.30, 124.45, 120.22,
46.45, 36.70, 30.55.

R_f-value: (*n*-pentane:ethyl acetate = 95:5) = 0.81.

7.5.1.5 5,6-Cyclopenta-2-phenyl-1-indene (8)

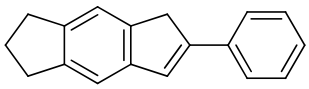

M = 232.32 g/mol

0.25 g (6.6 mmol) $LiAlH_4$ were dispersed in 10 mL THF and cooled to -78 °C. Subsequently a separately prepared solution of 2.72 g (11 mmol) of 2-phenylindanone **6** was added slowly over a period of time of 60 minutes. The reaction mixture was slowly heated to rt and stirred over night. Afterwards it was carefully hydrolyzed at 0 °C with 20 ml HCl (10% aq.). The THF/H_20 phase was extracted several times with Et_2O and the combined organic phases were washed three times with water, and saturated sodium chloride solution and dried over Na_2SO_4. After filtration the solvent was removed at reduced pressure and a mixture of the diasteriomeric alcohols was obtained as a yellow solid.
2.75 g (11 mmol) of the mixture of the diastereomeric alcohols were dissolved in 30 mL toluene and 0.065 g (0.38 mmol) *p*-toluene sulfonic acid were added. The yellow solution was heated under reflux in a *Dean-Stark* apparatus, until no further water was produced

(about 2 h). The mixture was neutralized with aqueous KOH (1 M), washed with water, saturated sodium chloride solution and dried over Na_2SO_4. After filtration the solvent was removed under reduced pressure and the product was obtained by crystallization from toluene/ *n*-pentane as a white crystalline solid.

Yield: 1.55 g (6.7 mmol, 61 %).

^{1}H NMR (300 MHz, $CDCl_3$): δ [ppm] = 7.65 – 7.61 (m, 2H, H-Ar),
7.41 – 7.33 (m, 3H, H-Ar), 7.28 – 7.24 (m, 2H, H-Ar), 7.20 (s, 1H, CH-olefinic),
3.74 (s, 1H, CH_2 - indene), 2.94 (t, ^3J = 7.3 Hz, 4H, CH_2-cyclopentyl),
2.18 (m, 2H, CH_2 - cyclopentyl).

^{13}C NMR (75 MHz, $CDCl_3$)δ [ppm] = 145.45, 143.81, 142.64, 141.64, 141.22, 136.25, 128.61, 127.17, 126.58, 125.41, 119.89, 116.88, 38.41, 32.77, 32.68, 25.87.

R_f-value: (*n*-pentane:ethyl acetate = 95:5) = 0.82.

Elemental analysis:
calculated: C 87.06 %; H 6.49 %.
found: C 87.34 %; H 6.13 %.

7.5.1.6 1-(9-Fluorenyl)-2-(5,6-cyclopentyl-2-phenyl-1-indenyl)-ethane (9)

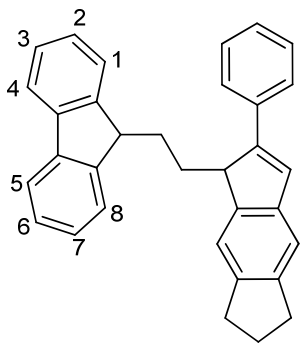

M = 424.58 g/mol

1.0 g (4.3 mmol) of 5,6-cyclopenta-2-phenylindene **8** were dissolved in 75 mL THF. At -78 °C, 3.5 mL (8.8 mmol) of a 2.5 M solution of *n*-BuLi in *n*-hexane were added. The reaction mixture was stirred for 30 min at -78 °C. Afterwards the mixture was heated to rt and stirred for an additional hour at rt. The formed lithium salt of **8** was isolated by removing the solvent at reduced pressure. Unreacted *n*-BuLi and organic impurities were removed by washing the residue twice with 10 mL of *n*-hexane. A red solution was obtained by dissolving the lithium salt of **8** in 50 mL THF. A separately prepared solution of 1.2 g (4.3 mmol) 1-(9-fluorenyl)-2-bromoethane **7** in 20 mL THF was added slowly to the lithium salt at rt. The reaction mixture was stirred over night at rt and at 40 °C for additional 4.5 h. Afterwards it was added to a saturated aqueous solution of NH_4Cl and the organic phase was separated. The aqueous phase was extracted with a mixture of THF and Et_2O and the combined organic phases were washed with water, and saturated sodium chloride solution and dried over Na_2SO_4. After filtration the solvent was removed at reduced pressure. The crude product was obtained by washing the residue with hot *n*-hexane. After chromatographic purification (*n*-hexane:ethyl acetate), the ligand was obtained as a white, crystalline solid.

Yield: 0.90 g (2.1 mmol, 49 %).

^{1}H NMR (300 MHz, $CDCl_3$): δ [ppm] = 7.79 – 7.76 (m, 2H, H-Ar-fluorene),
7.61 – 7.57 (m, 2H, H-Ar-fluorene), 7.43 – 7.30 (m, 10 H, H-Ar),
7.09 (s, 1H, H-Ar-indene), 4.17 (t, ^3J = 4.7 Hz, 1H, 9-H-fluorene),
3.64 (s, 2H, CH_2-indene), 2.99 – 2.91 (2 t, ^3J = 7.4 Hz, 4H, CH_2 – cyclopentyl),
2.55 – 2.45 (m, 2H, CH_2-bridge), 2.40 – 2.32 (m, 2H, CH_2-bridge),
2.19 – 2.07 (m, 2H, CH_2-cyclopentyl).

^{13}C NMR (75 MHz, $CDCl_3$): δ [ppm] = 21.39, 25.97, 31.22, 32.72, 32.84, 40.52, 47.42,
115.13, 119.66, 119.92, 124.23, 126.44, 126.91, 127.08, 127.72, 128.27, 137.47, 138.96,
139.53, 141.08, 141.13, 141.41, 142.28, 145.00, 146.64.

R_f-value: (*n*-pentane:ethyl acetate = 95:5) = 0.70.

7.5.2 *Bis(7-alkoxy-4-aryl-2-methylindenyl)dimethyl silane*

7.5.2.1 (1,1´-Biphenyl)-4-yl methacrylate (12)

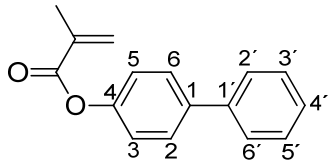

M = 238.28 g/mol

20.43 g (120.0 mmol) of 4-hydroxybiphenyl were diluted in 650 mL of dry DCM and 9.49 g (120.0 mmol) pyridine. At -20 °C 12.57 g (120.3) of methacryloylchloride were added dropwise over a period of time of 20 minutes. Afterwards the reaction mixture was refluxed for further 1.5 hours to complete the reaction. The mixture was washed with H_2O, aqueous NaOH solution (0.4 M), again with H_2O and finally with saturated sodium chloride solution. The organic phase was dried over Na_2SO_4. After filtration the organic solvent was removed at reduced pressure and the obtained solid was washed several times with cold methanol. After removal of the solvent a white solid was obtained.

Yield: 19.5 g (81.8 mmol, 68 %)

^{1}H NMR (300 MHz, CD_2Cl_2): δ [ppm] = 7.66 – 7.59 (m, 4H, H-2´, H-3´, H-5´, H-6´), 7.48 – 7.42 (m, 2H, H-2, H-6), 7.39 – 7.33 (m, 1H, H-4´), 7.22 – 7.18 (m, 2H, H-3, H-5), 6.36 – 6-43 (m, 1H, =CH_2), 5.80 – 5.77 (m, 1H, =CH_2), 2.08 – 2.06 (m, 3H, CH_3).

^{13}C NMR (75 MHz, CD_2Cl_2): δ [ppm] = 166.24, 150.87, 140.60, 139.13, 136.35, 129.19, 128.40, 127.75, 127.45, 127.40, 122.37, 18.55.

Elemental analysis:
calculated: C 80.65 %; H 5.92 %.
found: C 80.39 %; H 5.97 %.

7.5.2.2 7-Hydroxy-2-methyl-4-phenylindanone (13)

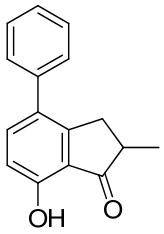

M = 238.28 g/mol

20.07 g (150.5 mmol) of powdered $AlCl_3$, 7.61 g (179.5 mmol) LiCl and 10.0 g (42.0 mmol) of (1,1´-biphenyl)-4-yl methacrylate **(12)** were mixed in a flask and stirred. The reaction was conducted using the following temperature steps: from room temperature to 80 °C in 15 min, from 80 °C to 100 °C in 45 min (the temperature was slowly increased to control the intensive reaction). Afterwards the temperature was increased to 140 °C and the mixture was stirred for further 3 hours. The reaction mixture turned to a highly viscous and black material during the reaction. After completion it was cooled to 120 °C and diluted in 200 mL of chlorobenzene. After cooling to 60 °C, 200 mL of H_2O were added slowly. The solid $AlOH_3$ was diluted by adding 15 mL of concentrated H_2SO_4. The organic phase was separated and the aqueous phase extracted with DCM. The combined organic phases were washed with aqueous K_2CO_3, H_2O and saturated sodium chloride solution. The organic phase was dried over Na_2SO_4 and filtered. Toluene was added to the filtrate affording a slightly grey solid. After filtration this solid was washed several times with small portions of toluene leading to the product as a white solid, pure enough for further use.

Yield: 4.47 g (18.7 mmol, 45 %).

^{1}H NMR (300 MHz, CD_2Cl_2): δ [ppm] = 7.74 (d, ^{3}J = 8.0 Hz, 1H, H-Ar),
7.65 – 7.62 (m, 1H, H-Ar´), 7.59 – 7.52 (m, 3H, H-Ar, H-Ar´), 6.99 – 6.93 (m, 2H, H-Ar´),
5.63 (s, 1H, -OH), 3.44 (dd, ^{2}J = 18.0 Hz, ^{3}J = 8.7 Hz, 1H, -CH_2), 2.76 (m, 2H, -CH, -CH_2),
1.30 (d, ^{3}J = 7.2 Hz, 3H, -CH_3).

^{13}C NMR (75 MHz, CD_2Cl_2): δ [ppm] = 210.00, 157.04, 155.09, 147.79, 134.91, 132.67,
129.12, 126.55, 124.64, 124.46, 116.26, 42.77, 35.35, 16.49.

Elemental analysis:
calculated: C 80.65 %; H 5.92 %.
found: C 79.64 %; H 5.89 %.

7.5.2.3 4-Hydroxy-2-methyl-7-phenylindene (14)

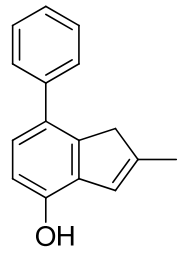

M = 222.28 g/mol

1.04 g (27.4 mmol) $LiAlH_4$ were suspended in 300 mL of dry THF. At -78 °C a solution of 6.52 g (27.4 mmol) 7-hydroxy-2-methyl-4-phenylindanone **(13)** in 70 ml of dry THF was added dropwise. The reaction mixture was allowed to warm up to room temperature and was stirred over night. Afterwards 60 mL H_2O were carefully added at 0°C. Subsequently 30 mL of concentrated HCl were added and the mixture was stirred for further 2 hours at room temperature. After completion of the reaction the organic phase was separated and the aqueous phase was extracted twice with Et_2O. The combined organic phases were washed with aqueous K_2CO_3, H_2O and a saturated Na_2SO_4 solution. After filtration the organic solvents were removed under reduced pressure. The raw material was purified by column chromatography over silica gel (pentane/EtOAc = 6:1) affording a white solid.

Yield: 4.05 g (18.2 mmol, 66 %)

^{1}H NMR (300 MHz, CD_2Cl_2): δ [ppm] = 7.48 – 7.46 (m, 1H, H-Ar´),
7.43 – 7.37 (m, 2H, H-Ar´), 7.30 (dd, ^3J = 7.8 Hz, ^5J = 1.7 Hz, 1H, H-Ar),
7.18 (d, ^3J = 7.8 Hz, 1H, H-Ar), 6.84 – 6.78 (m, 2H, H-Ar´), 6.44 – 6.40 (m, 1H, =CH-),
4.91 (s, 1H, -OH), 3.28 – 3.26 (m, 2H, -CH_2-), 2.10 – 2.06 (m, 3H).

^{13}C NMR (75 MHz, CD_2Cl_2): δ [ppm] = 155.18, 147.10, 145.12, 144.59, 136.42, 134.85,
128.45, 126.95, 125.09, 122.06, 120.05, 115.86, 43.09, 16.93.

Elemental analysis:
calculated: C 86.45 %; H 6.35 %.
found: C 86.41 %; H 6.33 %.

7.5.2.4 4-Methoxy-2-methyl-7-phenylindene, 7-Methoxy-2-methyl-4-phenylindene (15)

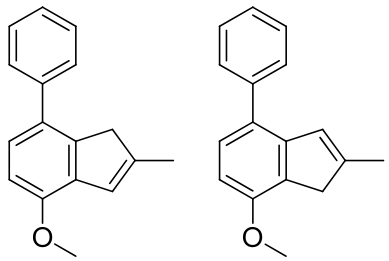

M = 236.31 g/mol

A) Methyl iodide procedure:

1.97 g (8.9 mmol) 4-hydroxy-2-methyl-7-phenylindene **(14)** were dissolved in 40 mL of dry EtOH. 0.98 g (14.4 mmol) NaOEt were dissolved in 16 mL of dry EtOH and added to the alcohol **14**. 2.03 g (14.3 mmol) MeI were added and the reaction mixture was stirred at a temperature of 85 °C for 2.5 hours. Subsequently the mixture was allowed to warm up to room temperature and was stirred over night. At -20 °C a yellow crystalline solid was directly obtained from the reaction mixture. The product was isolated after filtration and washing with H_2O as a slightly yellow and crystalline solid. The ratio of the two isomers in the product was 1:1.

Yield: 1.66 g (7.0, 79 %).

^{1}H NMR (300 MHz, CD_2Cl_2): δ [ppm] = 7.59 – 7.50, 7.44 – 7.37 (2 m, 3H H-Ar´, 1H H-Ar), 7.31 – 7.24 (m, 1H, H-Ar), 7.00 – 6.93 (m, 2H, H-Ar´), 6.55 – 6.48 (m, 1H, =CH-), 3.83 (s, 1H, -OCH_3), 3.36, 3.34 (2 s, 2H, -CH_2-), 2.17 (s, 3H, -CH_3).

^{13}C NMR (75 MHz, CD_2Cl_2): δ [ppm] = 159.29, 159.16, 147.48, 147.02, 147.00, 145.06, 144.56, 142.37, 139.28, 136.45, 134.65, 134.60, 128.36, 128.17, 127.24, 126.94, 125.07, 123.74, 122.44, 122.03, 120.03, 118.26, 114.41, 114.37, 55.60, 43.06, 42.70, 16.90, 16.89.

ESI-MS (isopropanol + KOH): m/z = 235.3 (100%, $[M-H]^-$).

Elemental analysis:
calculated: C 86.40 %; H 6.82 %.
found: C 85.91 %; H 6.90 %.

B) Dimethyl sulfate procedure:

0.50 g (2.25 mmol) 7-hydroxy-2-methyl-4-phenylindene **(14)** were suspended in 3.25 ml of a 7 % NaOH solution. Dimethyl sulfate was added to the mixture at 0°C and stirred for further 2 h at 0 °C. Afterwards the reaction mixture was allowed to warm up to room temperature and it was stirred over the weekend. The reaction mixture was heated to 80 °C for further 2 hours to destroy unreacted dimethyl sulfate. Toluene was added and the mixture was washed with a 10% NaOH solution, with H_20 and with a saturated sodium chloride solution. The organic phase was dried over Na_2SO_4. After filtration and removal of the organic solvent at reduced pressure a slightly yellow solid containing educt and product in a ratio of 9:1was obtained.

Yield: (calculated): 49 mg (0.21 mmol, 9 %)

C) Methyl trifluoromethanesulfonate procedure:

0.42 g (1.89 mmol) 7-Hydroxy-2-methyl-4-phenylindene **(14)** and 1.28 g (9.26 mmol) K_2CO_3 were placed in a flask and 5 mL of dry DCM were added. At 0°C 0.49 g (2.99 mmol) methyl trifluoromethanesulfonate were added dropwise. Afterwards the reaction mixture was allowed to warm up to room temperature and was stirred over night. DCM was added and the organic phase was washed with H_2O, saturated NH_4Cl solution, H_2O and saturated sodium chloride solution. The product was obtained via column chromatography over silica gel (*n*-pentane/EtOAc = 95:5) as a slightly yellow solid.

Yield: 205 mg (0.87 mmol, 46 %).

7.5.2.5 bis(7-Methoxy-2-methyl-4-phenylindenyl)dimethyl silane (16)

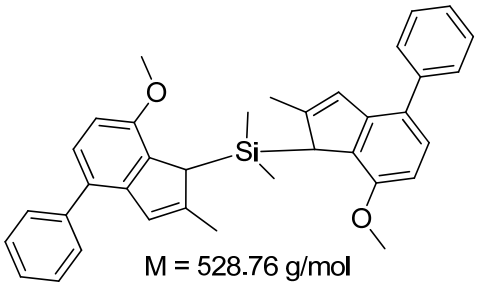

A) Et_2O/THF (0 °C to rt):

0.170 g (0.72 mmol) indene **15** were dissolved in 8 mL of dry Et_2O. 0.200 g of a 2.5 M *n*-BuLi solution in *n*-hexane were added dropwise to the indene at 0 °C. The reaction mixture was stirred for 1.5 h at room temperature. Subsequently one mL of dry THF was added to dissolve the lithium salt of indene **15** and the mixture was stirred for further 0.5 h. 0.046 g (0.36 mmol) of $SiCl_2Me_2$ were added at 0°C and the reaction mixture was stirred over night at room temperature. Afterwards the reaction mixture was washed twice with H_2O, saturated sodium chloride solution, and dried over Na_2SO_4. After filtration the organic solvent was removed under reduced pressure. The product was isolated by column chromatography (*n*-pentane/EtOAc = 9/1) as a mixture of different regioisomers.

Yield: 96 mg (0.18 mmol, 25 %)

^{1}H NMR spectroscopy: As one characteristic of the different regioisomers especially the broad multiplett for the dimethylsilane group shall be mentioned. Usually 3 singlets (one for the *rac*- and two for the *meso*-form) are expected. After column chromatography, reaction products other than the different regioisomers are unlikely due to the clean mass spectrum.

ESI-MS (isopropanol + KOH): m/z = 527.8 (100%, $[M-H]^-$).

B) Et_2O/THF (-78 °C to rt):

0.219 g (0.93 mmol) indene **15** were dissolved in 10 mL of dry Et_2O. 0.255 g (0.92 mmol) of a 2.5 M *n*-BuLi solution in *n*-hexane were added to the indene dropwise at 0 °C. The reaction mixture was stirred for 4 h at room temperature. Subsequently the mixture was cooled to

-78 °C and one mL of dry THF was added to dissolve the lithium salt of indene **15**. 0.060 g (0.47 mmol) of $SiCl_2Me_2$ were diluted in one mL of dry THF and added to the reaction mixture at -78 °C. The mixture was allowed to slowly warm up to room temperature and was stirred for further 24 h at room temperature. Afterwards the organic phase was washed twice with H_2O, saturated sodium chloride solution, and dried over Na_2SO_4. After filtration the organic solvent was removed under reduced pressure. The raw product was directly analyzed using ^1H NMR and ESI-MS spectroscopy, both showing the formation of the different regioisomers analog to synthesis route A).

C) Toluene (0 to 60 °C):

0.390 g (1.65 mmol) indene **15** were dissolved in 15 mL of dry toluene. 0.570 g (2.06 mmol) of a 2.5 M *n*-BuLi solution in *n*-hexane were added dropwise to the indene at 0 °C. The reaction mixture was stirred for one hour at room temperature. 10 mL of dry *n*-hexane were added in order to precipitate the lithium salt of indene **15**. The solvent was removed by filtration and the residue was washed with dry *n*-hexane. The lithium salt was suspended in 15 mL of dry toluene and 0.107 g (0.83 mmol) of $SiCl_2Me_2$ in 15 mL of dry toluene were added to the reaction mixture at 0 °C. The mixture was allowed to warm up to room temperature and was stirred over night. Afterwards the mixture was stirred at 60 °C for 5 h. The organic phase was washed twice with H_2O, saturated sodium chloride solution, and dried over Na_2SO_4. After filtration the organic solvent was removed under reduced pressure. The raw product was directly analyzed using ^1H NMR and ESI-MS spectroscopy, both showing the formation of the different regioisomers analog to synthesis route A).

D) Toluene/TMEDA (0 °C to rt)

0.315 g (1.33 mmol) indene **15** were dissolved in 15 mL of dry toluene. 0.372 g (1.34 mmol) of a 2.5 M n-BuLi solution in n-hexane were added dropwise to the indene at room temperature. The reaction mixture was stirred for 12 h at room temperature. 10 mL of dry *n*-hexane were added in order to precipitate the lithium salt of indene **15**. The solvent was removed by filtration and the residue was washed with dry *n*-hexane. The lithium salt was dissolved in 15 mL of dry toluene and 0.310 g (2.67 mmol) of TMEDA. 0.08 g (0.62 mmol) of $SiCl_2Me_2$ (being 0.5 eq of the produced lithium salt) in 13 mL of dry toluene were added to the reaction mixture at 0 °C. The mixture was allowed to warm up to room temperature and

was stirred for 22 h. The organic phase was washed twice with H_2O, saturated sodium chloride solution, and dried over Na_2SO_4. After filtration the organic solvent was removed under reduced pressure. The raw product was directly analyzed using ^{1}H NMR and ESI-MS spectroscopy, both showing the formation of the different regioisomers analog to synthesis route A).

7.5.2.6 4-Bromophenyl methacrylate (18)

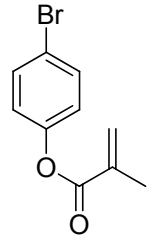

M = 241.08 g/mol

56.29 g (325.4 mmol) of 4-bromophenol were dissolved in a mixture of 400 mL DCM and 25.74 g (325.4 mmol) of pyridine. The solution was cooled to -20 °C and 34.02 g (325.4 mmol) of methacryloylchloride were added dropwise. After complete addition the resulting suspension was stirred at reflux for 2 h. The mixture was extracted with water, aqueous sodium hydroxide, again with water and saturated sodium chloride solution. The organic phase was dried over Na_2SO_4. After filtration the solvent was removed under reduced pressure. Fractional distillation (bp 88 °C/ 0.1 mbar) afforded a colorless oil.

Yield: 51.78 g (214.8 mmol, 66 %).

^{1}H NMR (300 MHz, CD_2Cl_2): δ [ppm] = 7.53 (m, 2H, H-Ar), 7.04 (m, 2H, H-Ar), 6.33 (m, 1H, =CH_2), 5.78 (m, 1H, =CH_2), 2.04 (m, 3H, CH_3).

^{13}C NMR (75 MHz, CD_2Cl_2): δ [ppm] = 165.83, 150.49, 136.09, 132.76, 127.75, 123.94, 119.01, 18.48.

Elemental analysis:
calculated: C 49.82 %; H 3.76 %.
found: C 49.93 %; H 3.71 %.

7.5.2.7 4-Bromo-7-hydroxy-2-methylindanone (19)

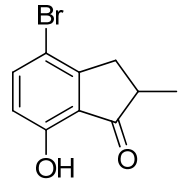

M = 241.08 g/mol

39.33 g (163.1 mmol) of 4-bromophenyl methacrylate **(18)** were placed in a flask together with 54.38 g (407.8 mmol) of powdered $AlCl_3$. The mixture was heated stepwise to 120 °C during 1 h. The black solid formed was dissolved in DCM and poured into ice water. The resulting solid was dissolved by adding 15 mL conc. H_2SO_4. The organic phase was separated and the aqueous phase was extracted with DCM. The combined organic phases were washed with water and saturated sodium chloride solution, dried over Na_2SO_4. After filtration the solvent was removed under reduced pressure. Fractional distillation (bp 105 °C/ 0.1 mbar) afforded a yellow oil.

Yield: 20.87 g (86.2 mmol, 53 %).

^{1}H NMR (300 MHz, CD_2Cl_2): δ [ppm] = 8.97 (s, 1H, OH), 7.58 (d, ^{3}J = 8.6 Hz, 1H, H-Ar), 6.70 (d, ^{3}J = 8.6 Hz, 1H, H-Ar), 3.30 (m, 1H, -CH_2-), 2.81 (m, 1H, -CH-),
2.62 (m, 1H, -CH_2-), 1.31 (d, ^{3}J = 7.5 Hz, 3H, CH_3).

^{13}C NMR (75 MHz, CD_2Cl_2): δ [ppm] = 212.35, 157.04, 153.32, 140.16, 123.61, 116.26, 110.37, 42.23, 36.42, 16.06.

Elemental analysis:
calculated: C 49.82 %; H 3.76 %.
found: C 49.76 %; H 3.71 %.

7.5.2.8 4-Bromo-7-methoxy-2-methylindanone (20)

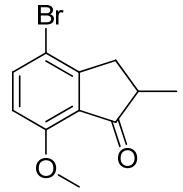

M = 255.11 g/mol

To a solution of 49.80 g (206.6 mmol) 4-bromo-7-hydroxy-2-methylindanone **(19)** in 250 ml of dry ethanol, 33.73 g (237.6 mmol) methyl iodide and a solution of 15.46 g (227.2 mmol) NaOEt in 250 ml of dry ethanol were added. The mixture was stirred for 16 h at 85 °C. Subsequently 2 M sodium hydroxide solution was added to destroy residual methyl iodide. Afterwards 500 ml H_2O was added and the mixture was extracted several times with DCM. The combined organic phases were washed with saturated sodium chloride solution, dried with sodium sulfate and evaporated to dryness. The product was isolated as a white crystalline solid by crystallization from cyclohexane.

Yield: 37.67 g (147.7 mmol, 72 %).

^{1}H NMR (300 MHz, $CDCl_3$): δ [ppm] = 7.65 (d, ^3J = 8.7 Hz, 1H, H-Ar),
6.73 (d, ^3J = 8.7 Hz, 1H, H-Ar), 3.94 (s, 3H, -OCH_3), 3.27 (m, 1H, -CH_2-),
2.67 (m, 2H, -CH-, -CH_2-), 1.31 (d, ^3J = 7.3 Hz, 3H, -CH_3).

^{13}C NMR (75 MHz, $CDCl_3$): δ [ppm] = 229.53, 181.10, 178.70, 162.18, 149.89, 135.27, 135.08, 79.63, 65.87, 59.50, 39.83.

Elemental analysis:
calculated: C 51.79 %; H 4.35 %.
found: C 51.27 %; H 4.43 %.

7.5.2.9 7-Bromo-4-methoxy-2-methylindene (21)

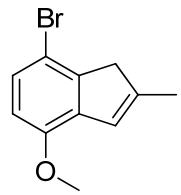

M = 239.11 g/mol

3.69 g (14.5 mmol) of 4-bromo-7-methoxy-2-methylindanone **(20)** were dissolved in 27 mL of dry THF and added dropwise at -78 °C to a suspension of 0.36 g (9.5 mmol) of $LiAlH_4$ in 11 mL of dry THF. Afterwards the reaction mixture was allowed to warm up to room temperature and stirred over night. Subsequently remaining $LiAlH_4$ was carefully hydrolyzed at 0 °C with 40 ml of water and 4 mL conc. HCl. The mixture was extracted several times with Et_2O. The combined organic phases were washed with saturated sodium chloride solution and dried over sodium sulfate. After filtration and evaporation of the solvent the solid was dissolved in 40 mL toluene and 92 mg of *p*-toluene sulfonic acid were added. The mixture was stirred at reflux for 1 h using a *Dean-Stark* apparatus. The resulting solution was washed with aqueous potassium hydroxide, water, saturated sodium chloride solution, and dried over Na_2SO_4. Filtration and evaporation of the solvent gave a slightly yellow solid.

Yield: 2.93 g (12.3 mmol, 85 %).

^{1}H NMR (300 MHz, CD_2Cl_2): δ [ppm] = 7.16 (d, ^{3}J = 8.6 Hz, 1H, H-Ar),
6.68 (d, ^{3}J = 8.6 Hz, 1H, H-Ar), 6.63 (m, 1H,=CH-), 3.83 (s, 3H, OCH_3), 3.28 (s, 2H, -CH_2-), 2.16 (m, 3H, CH_3).

^{13}C NMR (75 MHz, CD_2Cl_2): δ [ppm] = 151.92, 145.73, 144.97, 135.91, 127.55, 123.57, 111.14, 109.72, 56.00, 45.10, 16.75.

Elemental analysis:
calculated: C 55.25 %; H 4.64 %.
found: C 55.69 %; H 4.99 %.

7.5.2.10 (3,5-Di-*tert*-butylphenyl)boronic acid (22)

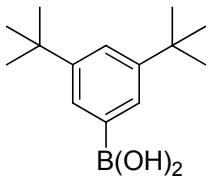

M = 234.14 g/mol

10.0 g (37.1 mmol) of 1-bromo-3,5-di-*tert*-butylbenzene in 20 ml of dry THF was added dropwise to a suspension of 1.26 g (51.9 mmol) Mg turnings and a catalytic amount of iodine in 30 ml of dry THF. The temperature was kept below 50 °C by the rate of addition. After complete addition the mixture was stirred at reflux for 2.5 h. Subsequently the warm *Grignard* solution was transferred *via canula* into a dropping funnel and added dropwise to a solution of 5.77 g (55.6 mmol) trimethyl borate in 100 mL of dry Et_2O. During addition the temperature was kept below - 60 °C. After complete addition the mixture was allowed to warm up to room temperature and stirred over night. The reaction was quenched by adding 55.8 ml H_2O and 5.6 mL conc. HCl. The organic phase was separated and the aqueous phase was extracted several times with Et_2O. The combined organic phases were washed with saturated sodium chloride solution and dried over sodium sulfate. Filtration and evaporation of the solvent gave a white solid. The boronic acid was obtained as a mixture of its monomeric and oligomeric form and used without further purification.

Yield: 7.59 g (88 %).

7.5.2.11 (3,5-Dimethylphenyl)boronic acid (23)

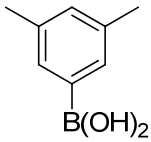

M = 149.98 g/mol

34.88 g (189.6 mmol) 1-bromo-3,5-dimethylbenzene in 100 mL dry Et_2O were added dropwise to a suspension of 5.529 g (227.5 mmol) Mg turnings and 26.1 mg (0.184 mmol) methyl iodide in 250 mL of dry Et_2O. The reaction mixture was kept at reflux by the rate of addition. After complete addition the reaction mixture was heated to reflux and stirred for further 6 h. Subsequently the warm *Grignard* solution was transferred *via canula* into a dropping funnel and added dropwise to a solution of 19.70 g (189.6 mmol) trimethyl borate in

250 mL of dry Et_2O. During the addition the temperature was kept below - 60 °C. After complete addition the reaction mixture was allowed to warm up to room temperature over night. The white suspension was added to aqueous H_2SO_4 (20 wt-%). The organic phase was separated, and the aqueous phase was extracted several times with Et_2O. The combined organic phases were washed several times with H_2O and saturated sodium chloride solution and dried over Na_2SO_4. After filtration the organic solvent was removed under reduced pressure. The raw product was washed with cold pentane and a white solid was obtained. The boronic acid was obtained as a mixture of its monomeric and oligomeric form and used without further purification.

Yield: 19.35 g (129.0 mmol, 68 %).

7.5.2.12 (9-Anthracenyl)boronic acid (24)

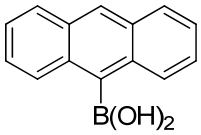

M = 222.05 g/mol

15.77 g (61.59 mmol) 9-bromoanthracene were dissolved in 500 mL of dry THF and cooled to -78 °C. 36.96 mL (92.39 mmol) of a 2.5 M solution of *n*-BuLi in hexane were added dropwise. The reaction mixture was stirred for further 3 h at -78 °C. Subsequently 9.60 g (92.39 mmol) of $B(OMe)_3$ were added at once at -78 °C and the reaction mixture was allowed to warm up to room temperature over night. The reaction was quenched by adding 200 mL of water. Afterwards the mixture was acidified by a 6 M HCl solution. The reaction mixture was extracted several times with DCM. The combined organic phases were washed with saturated sodium chloride solution and dried over Na_2SO_4. After filtration the organic solvent was removed under reduced pressure. The raw product, a yellow oil, was digerated with boiling cyclohexane affording a yellow solid. The boronic acid was obtained in its monomeric form.

Yield: 5.30 g (23.86 mmol, 39 %).

^{1}H NMR (300 MHz, DMSO): δ [ppm] = 8.81 (s, 2H, -OH), 8.52 (s, 1H, H-10),
8.07 (m, 2H, H-1, H-8), 8.02 – 7.96 (m, 2H, H-4, H-5),
7.55 – 7.46 (m, 4H, H-2, H-3, H-6, H-7).

^{13}C NMR (75 MHz, DMSO): δ [ppm] = 132.77; 130.82; 129.09; 128.48; 125.97; 125.19; 125.05. (C-9 is not resolved due to the coupling with the boron atom)

7.5.2.13 7-(3´,5´-Di-*tert*-butylphenyl)-4-methoxy-2-methylindene (25 A) 4-(3´,5´-di-*tert*-butylphenyl)-7-methoxy-2-methylindene (25 B)

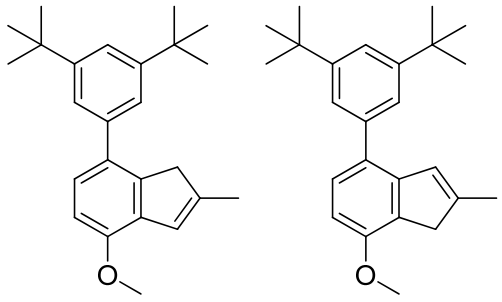

25 A **25 B**

M = 348.52 g/mol

0.72 g (3.0 mmol) of 7-bromo-4-methoxy-2-methylindene **(21)** and 0.42 g (0.36 mmol) of $Pd(PPh_3)_4$ were dissolved in 18 mL toluene. 7.5 mL (7.5 mmol) of a 2 N sodium carbonate solution and 0.77 g (3.3 mmol) of 3,5-di-*tert*-butylphenyl boronic acid **(22)** in 5 mL EtOH were added in one portion. The mixture was stirred at reflux for 3 d. Afterwards the yellow mixture was neutralized with aqueous NH_4Cl solution and extracted several times with toluene. The combined organic phases were washed with saturated sodium chloride solution and dried over sodium sulfate. Filtration and evaporation of the solvent and subsequent column chromatography (hexane/EtOAc) gave a white solid. (As an alternative to column chromatography, the raw product dissolved in toluene can be filtered over silica gel, and the product can be isolated by crystallization from methanol.)

Yield: 0.85 g (2.44 mmol, 81 %).

Mixture of Isomers: **25 A / 25 B** = 80 / 20

Using the same procedure but instead of a 2 N (5 eq) aqueous solution of Na_2CO_3 a 4 N (10 eq) resulted in the formation of the indene with a mixture of the isomers:
25 A / 25 B = 34 / 66.

25 A:

^{1}H NMR (300 MHz, $CDCl_3$): δ [ppm] = 7.39 (t, ^{4}J = 1.8 Hz, 1H, H-Ar-4´),
7.34 (d, ^{4}J = 1.8 Hz, 2H, H-Ar-2´, H-Ar-6´), 7.14 (d, ^{3}J = 8.3 Hz, 1H, H-Ar),
6.87 (d, ^{3}J = 8.3 Hz, 1H, H-Ar), 6.71 – 6.68 (m, 1H, =CH-), 3.91 (s, 3H, -OCH_3),
3.40 (s, 2H, -CH_2-), 2.15 – 2.13 (m, 3H, -CH_3), 1.38 (s, 18H, -CMe_3).

^{13}C NMR (75 MHz, $CDCl_3$): δ [ppm] = 151.59, 150.68, 144.71, 142.85, 140.39, 134.70,
132.11, 125.52, 123.38, 122.94, 120.71, 109.35, 55.74, 43.59, 35.08, 31.71, 16.89.

25 B:

^{1}H NMR (300 MHz, $CDCl_3$): δ [ppm] = 7.39 (t, ^{4}J = 1.8 Hz, 1H, H-Ar-4´),
7.32 (d, ^{4}J = 1.8 Hz, 2H, H-Ar-2´,H-Ar-6´), 7.29 (d, ^{3}J = 8.4 Hz 1H, H-Ar),
6.77 (d, ^{3}J = 8.4 Hz 1H, H-Ar), 6.64 – 6.61 (m, 1H,=CH-), 3.92 (s, 3H, -OCH_3),
3.34 (s, 2H, -CH_2-), 2.17 – 2.15 (m, 3H, -CH_3), 1.37 (s, 18H, -CMe_3).

^{13}C NMR (75 MHz, $CDCl_3$): δ [ppm] = 154.23, 150.67, 146.85, 145.32, 140.11, 130.30,
129.01, 128.49, 126.50, 123.41, 120.44, 106.87, 55.47, 40.55, 35.05, 31.71, 17.08.

Elemental analysis:
calculated: C 86.15 %; H 9.25 %.
found: C 86.47 %; H 9.47 %.

7.5.2.14 7-(3´,5´-Dimethylphenyl)-4-methoxy-2-methylindene (26 A) 4-(3´,5´-dimetylphenyl)-7-methoxy-2-methylindene (26 B)

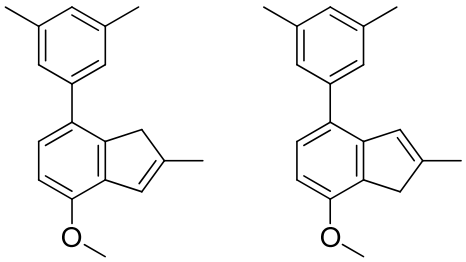

26 A **26 B**

M = 264.36 g/mol

9.09 g (38.0 mmol) of 7-bromo-4-methoxy-2-methylindene **(21)** and 5.27 g (4.56 mmol) of $Pd(PPh_3)_4$ were dissolved in 250 ml of degased toluene. 76.0 mL (76.0 mmol) of a 2 N sodium carbonate solution and 6.28 g (41.9 mmol) of 3,5-dimethylphenyl boronic acid **(23)** in 60 mL degased EtOH were added in one portion. The mixture was stirred at reflux for 3 d. The palladium spezies was slowly oxidized during the work up procedure in air and the mixture turned to black. Further H_2O was added and the aqueous phase was extracted several times with toluene. The combined organic phases were washed with saturated sodium chloride solution, dried over Na_2SO_4, filtrated and the organic solvent was removed under reduced pressure. The palladium species was removed by filtration over silica gel and the organic compounds were eluted with further toluene. After removal of toluene at reduced pressure the product was isolated by crystallization from methanol as a white solid. The procedure afforded the clean isomer **26 A**.

Yield: 7.36 g (27.8 mmol, 73 %).

Using the same procedure but instead of a 2 N (2 eq) aqueous solution of Na_2CO_3 a 8 N (5 eq), resulted in a lower yield (37 %) and a mixture of the isomers: **26 A** / **26 B** = 25 / 75.

26 A:

^{1}H NMR (300 MHz, CD_2Cl_2): δ [ppm] = 7.19 (d, ^{3}J = 8.3 Hz, 1H, H-Ar),
7.15 (s, 2H, H-Ar-2´, H-Ar-6´), 7,04 (s, 1H, H-Ar-4´), 6.89 (d, ^{3}J = 8.3 Hz, 1H, H-Ar),
6.75 (s, 1H, =CH-), 3.93 (s, 3H, -OCH_3), 3.46 (s, 2H, -CH-), 2.43 (s, 6H, Ar-CH_3´),
2,20 (s, 3H, -CH_3)

^{13}C NMR (75 MHz, CD_2Cl_2): δ [ppm] = 152.05, 145.28, 143.04, 141.52, 138.40, 134.95, 131.42, 128.72, 126.66, 125.76, 123.46, 109.66, 55.97, 43.96, 21.68, 16.93.

26 B:

^{1}H NMR (300 MHz, CD_2Cl_2): δ [ppm] = 7.23 (d, ^{3}J = 8,3 Hz, 1H, H-Ar), 7.09 (s, 2H, H-Ar-2´, H-Ar-6´), 6.98 (s, 1H, H-Ar-4´), 6.76 (d, ^{3}J = 8.3 Hz, 1H, H-Ar), 6.65 (s, 1H, =CH-), 3.91 (s, 3H, -OCH_3), 3.33 (s, 2H, -CH_2-), 2.39 (s, 6H, Ar-CH_3´), 2.17 (s, 3H, -CH_3).

Elemental analysis:
calculated: C 86.32 %; H 7.63 %.
found: C 86.50 %; H 7.55 %.

7.5.2.15 7-(9´-Anthracenyl)-4-methoxy-2-methylindene (27 A) 4-(9´-anthracenyl)-7-methoxy-2-methylindene (27 B)

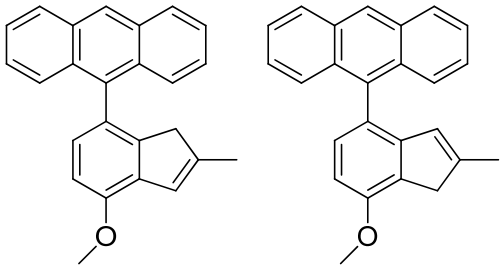

27 A **27 B**

M = 336.43 g/mol

7.34 g (30.7 mmol) of 7-bromo-4-methoxy-2-methylindene **(21)** and 4.26 g (3.7 mmol) of $Pd(PPh_3)_4$ were dissolved in 200 ml of degased toluene. 61.4 mL (61.4 mmol) of a 2 N sodium carbonate solution and 7.50 g (33.8 mmol) of (9-anthracenyl)boronic acid **(24)** in 150 mL degased EtOH were added in one portion. The mixture was stirred at reflux for 3 d. The palladium spezies was slowly oxidized during the work up procedure in air and the mixture turned to black. Further H_2O was added and the aqueous phase was extracted several times with toluene. The combined organic phases were washed with saturated NH_4Cl solution, H_2O, saturated sodium chloride solution, dried over Na_2SO_4, filtrated and the organic solvent was removed under reduced pressure. Subsequent column chromatography (*n*-pentane/EtOAc) gave a yellow solid.

Yield: 5.46 g (16.2 mmol, 53 %).

Mixture of isomers: **27 A / 27 B** = 40 / 60

27 A:

^{1}H NMR (500 MHz, CD_2Cl_2): δ [ppm] = 8.56 (s, 1H, H-Ar-10´),
8.11 (d, ^{3}J = 8.5 Hz, 2H, H-Ar-4´, H-Ar-5´),
7.65 (ddd, J = 8.8, 2.0, 1.0 Hz, 2H, H-Ar-1´, H-Ar-8´),
7.51 (dt, J = 8.5, 1.2 Hz, 2H, H-Ar-3´, H-Ar-6´),
7.36 (dd, J = 8.8, 1.3 Hz, 2H, H-Ar-2´, H-Ar-7´), 7.12 (d, ^{3}J = 8.2 Hz, 1H, H-Ar),
7.05 (d, ^{3}J = 8.2 Hz, 1H, H-Ar), 6.77 (dd, J = 3.1, 1.5 Hz, 1H, =CH-), 4.04 (s, 3H, -OCH_3),
2.82 – 2.80 (m, 2H, -CH_2-); 2.02 – 2.01 (m, 3H, -CH_3).

27 B:

^{1}H NMR (500 MHz, CD_2Cl_2): δ [ppm] = 8.56 (s, 1H, H-Ar-10´),
8.11 (d, ^{3}J = 8.5 Hz, 2H, H-Ar-4´, H-Ar-5´),
7.67 (ddd, J = 9.0, 1.9, 1.0 Hz, 2H, H-Ar-1´, H-Ar-8´),
7.49 (dt, J = 6.5, 1.2 Hz, 2H, H-Ar-3´, H-Ar-6´),
7.37 (dd, J = 8.8, 1.3 Hz, 2H, H-Ar-2´, H-Ar-7´), 7.25 (d, ^{3}J = 8.2 Hz, 1H, H-Ar),
6.95 (d, ^{3}J = 8.2 Hz, 1H, H-Ar), 5.69 (dd, J = 3.1, 1.5 Hz, 1H, =CH-), 4.04 (s, 3H, -OCH_3),
3.49 – 3.43 (m, 2H, -CH_2-); 2.04 – 2.02 (m, 3H, -CH_3).

Elemental analysis:
calculated: C 89.25 %; H 5.99 %.
found: C 89.35 %; H 6.03 %.

7.5.2.16 Bis[4-(3′,5′-di-*tert*-butylphenyl)-7-methoxy-2-methylindenyl]dimethyl silane (28)

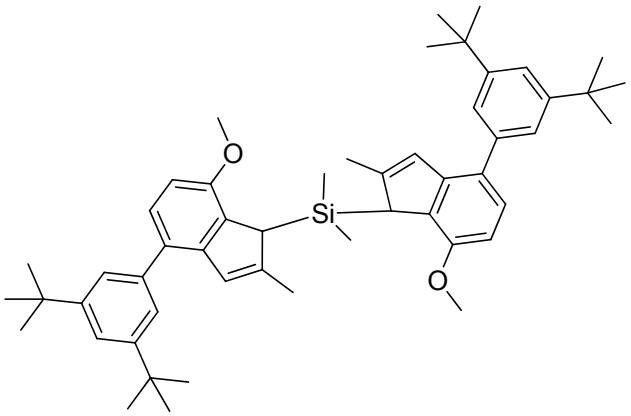

M = 753.18 g/mol

1.87 g (5.4 mmol) of 7-(3′,5′-di-*tert*-butylphenyl)-4-methoxy-2-methylindene **(25 A)** (and its isomer **25 B** with a ratio of 8:2) were dissolved in 50 ml of dry toluene/dioxane (1:1). 2.22 mL (5.4 mmol) of a 2.43 M solution of *n*-BuLi in *n*-hexane were added at - 20 °C. The solution was warmed to room temperature and stirred for 2 h. The resulting yellow solution was cooled to -20 °C and 0.35 g (2.7 mmol) $SiMe_2Cl_2$ were added. After complete addition the mixture was heated to 60 °C and stirred over night. Diethylether was added to the yellow suspension. The organic phase was washed with water, saturated sodium chloride solution and dried over Na_2SO_4. Filtration and evaporation of the solvent, followed by column chromatography (*n*-hexane/ethylacetate) and washing with hot methanol gave a white solid. A mixture of the *rac*- **28 A** and *meso*-form **28 B** of the ligand was obtained.

Yield: 0.72 g (1.0 mmol, 36 %).

Mixture of two isomers:
^{1}H NMR (300 MHz, $CDCl_3$): δ [ppm] = 7.39 – 7.33 (m, 6H, H-Ar′),
7.25 (d, ^{3}J = 7.9 Hz, 2H, H-Ar), 6.76 – 6.67 (m, 4H, H-Ar, =CH-), 4.22, 4.04 (2s, 2H, -CH-),
3.91, 3.84 (2 s, 6H, $-OCH_3$), 2.28, 2.15 (2s, 6H, $-CH_3$), 1.39, 1.38 (2s, 36H, $-CMe_3$),
0.19, 0.26, 0.35 (3s, 6H, $SiMe_2$).

Due to the low amount of **28 B**, only **28 A** is resolved and depicted:
^{13}C NMR (75 MHz, $CDCl_3$): δ [ppm] = 153.54, 150.57, 149.43, 144.38, 140.50, 133.50, 128.85, 126.84, 125.26, 123.41, 120.31, 105.27, 54.80, 47.07, 35.05, 31.72, 17.87, -3.73.

Elemental analysis:

calculated: C 82.92 %; H 9.10 %.

found: C 82.61 %; H 8.89 %.

7.5.2.17 Bis[4-(3´,5´-dimethylphenyl)-7-methoxy-2-methylindenyl]dimethyl silane (29)

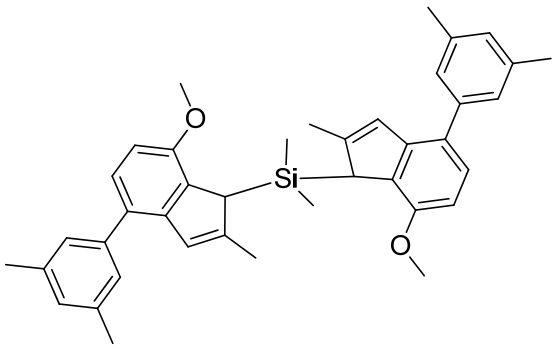

M = 584.86 g/mol

12.08 g (45.7 mmol) 7-(3´,5´-dimethylphenyl)-4-methoxy-2-methylindene **(26 A)** were dissolved in 200 mL of dry toluene/dioxane (1:1). 18.29 mL (45.7 mmol) of a 2.5 M solution of *n*-BuLi in *n*-hexane were added at - 10 °C. The solution was warmed to room temperature and stirred for 45 min. Afterwards 2.95 g (22.9 mmol) $SiMe_2Cl_2$ were added at -10 °C. After complete addition the reaction mixture was heated to 60 °C and stirred for 40 h forming a white suspension. Diethyl ether was added to the suspension. The organic phase was washed with water, saturated sodium chloride solution and dried over Na_2SO_4. Filtration and evaporation of the solvent at reduced pressure gave a brown oil, containing the *rac*- **29 A** and *meso*-isomer **29 B**. The oil was stirred in boiling methanol for 2 h, forming a white solid which was separated by filtration at -20 °C. The white solid is the isomer **29 A**. Methanol of the residual solution was removed in vacuum and the resulting oil was crystallized from *n*-hexane. This afforded a white solid containing the isomers **29 A** and **29 B**. Further purification of the brown residue which was formed after evaporation of *n*-hexane was performed by column chromatography and afforded after digestion in hot methanol further product (mixture of **29 A** and **B**).

Yield: 7.41 g (12.7 mmol 55 %).

29 A:

^{1}H NMR (300 MHz, $CDCl_3$): δ [ppm] = 7.20 (d, ^{3}J = 8.2 Hz, 2H, H-Ar),
7.13 (s, 4H, H-Ar-2´, H-Ar-6´), 6.97 (s, 2H, H-Ar-4´), 6.71 (d, ^{3}J = 8.1 Hz, 2H, H-Ar),
6.70 (s, 2H, =CH-), 4.23 (s, 2H, -CH-), 3.91 (s, 6H, $-OCH_3$), 2.39 (s, 12H, Ar-CH_3´),
2.28 (s, 6H, $-CH_3$), -0.38 (s, 6H, $SiMe_2$).

^{13}C NMR (75 MHz, $CDCl_3$): δ [ppm] = 153.58, 149.41, 144.27, 141.41, 137.87, 133.49, 128.05, 127.97, 126.86, 126.74, 125.19, 105.27, 54.78, 47.09, 21.60, 17.81, -3.81.

29 B:

^{1}H NMR (300 MHz, CD_2Cl_2): δ [ppm] = 7.18 (d, ^{3}J = 8.2 Hz, 2H, H-Ar),
7.10 (s, 4H, H-Ar-2´, H-Ar-6´), 6.96 (s, 2H, H-Ar-4´), 6.71 (d, ^{3}J = 8.3 Hz, 2H, H-Ar),
6.67 (s, 2H, =CH-), 4.02 (s, 2H, -CH-), 3.84 (s, 6H, $-OCH_3$), 2.36 (s, 12H, Ar-CH_3´),
2.15 (s, 6H, $-CH_3$), -0.26, -0.24 (2 s, 6H, $SiMe_2$).

^{13}C NMR: Due to the low amount of the *meso*-form signals were poorly resolved.

Elemental analysis:
calculated: C 82.14 %; H 7.58 %.
found: C 81.79 %; H 7.53 %.

7.5.2.18 Bis[4-(9´-anthracenyl)-7-methoxy-2-methylindenyl]dimethyl silane (30)

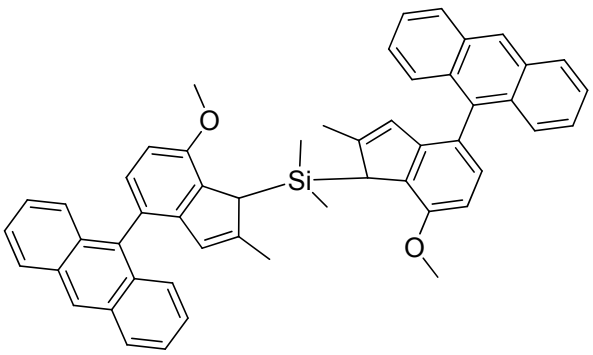

M = 728.99 g/mol

5.18 g (15.4 mmol) of 7-(9′-anthracenyl)-4-methoxy-2-methylindene **(27 A)** (and its isomer **27 B** with a ratio of 4:6) were dissolved in 150 ml of dry toluene/dioxane (1:1). 6.17 mL (15.4 mmol) of 2.5 M solution of *n*-BuLi in *n*-hexane were added at - 10 °C. The solution was warmed to room temperature and stirred for 45 min. Afterwards 0.99 g (7.7 mmol) $SiMe_2Cl_2$ were added at -10 °C. After complete addition the reaction mixture was heated to 60 °C and stirred for 40 h forming a white suspension. Diethyl ether was added to the suspension. The organic phase was washed with water, saturated sodium chloride solution and dried over Na_2SO_4. Filtration and evaporation of the solvent at reduced pressure afforded a brown oil, which contained *rac*-**30 A**, and *meso*-**30 B**. The oil was stirred for 2 h in boiling methanol forming a white solid. This solid was separated by filtration, at -20 °C. The white solid was further purified by digestion in boiling *n*-hexane.

Yield: 2.99 g (4.1 mmol, 27 %).

30 A:

^{1}H NMR (300 MHz, $CDCl_3$): δ [ppm] = 8.51 (s, 2H, H-Ar-10′),
8.07 (d, ^{3}J = 8.3 Hz, 4H, H-Ar-4′, H-Ar-5′), 7.75 – 7.60 (m, 4H, H-Ar-1′, H-Ar-8′),
7.46 (dd, J = 13.8, 6.8 Hz, 4H, H-Ar-3′, H-Ar-6′), 7.38 – 7.28 (m, 4H, H-Ar-2′, H-Ar-7′),
7.20 (d, ^{3}J = 8.1 Hz, 2H, H-Ar), 6.88 (d, ^{3}J = 8.2 Hz, 2H, H-Ar), 5.79 (s, 2H, =CH-),
4.47 (s, 2H, -OCH_3), 4.00 (s, 6H, -CH-), 2.16 (s, 4H, -CH_3), -0.30 (s, 6H, $SiMe_2$).

30 B:

^{1}H NMR (300 MHz, $CDCl_3$): δ [ppm] = 8.51 (s, 2H, H-Ar-10′),
8.07 (d, ^{3}J = 8.3 Hz, 4H, H-Ar-4′, H-Ar-5′), 7.75 – 7.60 (m, 4H, H-Ar-1′, H-Ar-8′),
7.46 (dd, J = 13.8, 6.8 Hz, 4H, H-Ar-3′, H-Ar-6′), 7.38 – 7.28 (m, 4H, H-Ar-2′, H-Ar-7′),
7.22 (d, ^{3}J = 8.2 Hz, 2H, H-Ar), 6.89 (d, ^{3}J = 8.2 Hz, 2H, H-Ar), 5.79 (s, 2H, =CH-),
4.30 (s, 2H, -OCH_3), 4.00 (s, 6H, -CH-), 2.10 (s, 4H, -CH_3), -0.16 (s, 3H, $SiMe_2$),
-0.27 (s, 3H, $SiMe_2$).

Elemental analysis:
calculated: C 85.67 %; H 6.08 %.
found: C 85.61 %; H 6.31 %.

7.5.3 *Bis(4-aryl-2-methylindenyl)dimethyl silane*

7.5.3.1 7-Bromo-2-methylindene (31)

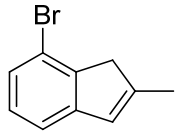

M = 209.08 g/mol

5.57 g (24.7 mmol) of 4-bromo-2-methylindanone **(30)** were dissolved in 45 mL of dry THF and added dropwise at -78 °C to a suspension of 0.56 g (14.8 mmol) of $LiAlH_4$ in 18 mL of dry THF. Afterwards the reaction mixture was allowed to warm up to room temperature and stirred over night. Subsequently remaining $LiAlH_4$ was carefully hydrolyzed at 0 °C with 60 ml of H_2O and 6 mL conc. HCl. The mixture was extracted several times with Et_2O. The combined organic phases were washed with saturated sodium chloride solution and dried over Na_2SO_4. After filtration and evaporation of the solvent, the obtained solid was dissolved in 60 mL toluene and 150 mg of *p*-toluene sulfonic acid were added. The mixture was stirred at reflux for 1 h. The resulting solution was washed with H_2O, aqueous KOH, H_2O and saturated sodium chloride solution and dried over Na_2SO_4. Filtration and evaporation of the solvent gave a slightly yellow solid. Its analytic data are consistent with literature.[194] Hence the indene could be used in the next step without further purification.

Yield: 3.61 g (17.3 mmol, 70 %).

^{1}H NMR (300 MHz, $CDCl_3$): δ [ppm] = 7.22 (d, ^3J = 8.8 Hz, 1H, H-6),
7.18 (d, ^3J = 7.2 Hz, 1H, H-4), 7.12 – 7.05 (m, 1H, H-5), 6.51 (m, 1H,=CH-),
3.29 (s, 2H, -CH_2-), 2.17 (s, 3H, CH_3).

^{13}C NMR (75 MHz, $CDCl_3$): δ [ppm] = 147.3, 146.8, 143.3, 128.2, 127.1, 126.6, 118.7, 118.3, 44.2, 16.7.

7.5.3.2 7-(3′,5′-Di-*tert*-butylphenyl)-2-methylindene (32 A), 4-(3′,5′-di-*tert*-butylphenyl)-2-methylindene (32 B)

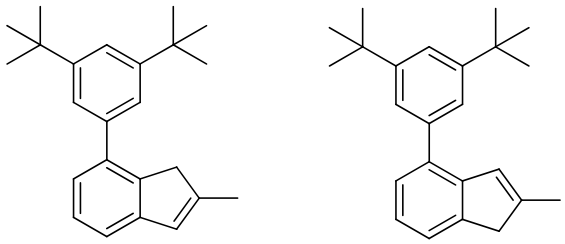

32 A **32 B**

M = 318.50 g/mol

3.61 g (17.3 mmol) of 7-bromo-2-methylindene **(31)**, and 2.40 g of $Pd(PPh_3)_4$ (2.08 mmol) were dissolved in 90 mL toluene. 43.25 mL of a 2 N (43.25 mmol) sodium carbonate solution, and 4.45 g of (3,5-di-*tert*-butylphenyl)boronic acid **(22)** in 23 mL EtOH were added in one portion. The mixture was stirred at reflux for 3 d. Afterwards it was neutralized with aqueous NH_4Cl and extracted several times with toluene. The combined organic phases were washed with saturated sodium chloride solution and dried over Na_2SO_4. Filtration over silica gel and evaporation of the solvent gave the raw product. Crystallization from MeOH gave a white solid containing the two isomers **32 A**, and **32 B** with a ratio of 95:5.

Yield: 4.58 g (83 %).

Mixture of two isomers:
^{1}H NMR (CD_2Cl_2): δ [ppm] = 7.43 (t, ^{4}J = 1.8 Hz, 1H, H-Ar-4′),
7.38, 7.34 (2 d, ^{4}J = 1.8 Hz, 2H, H-Ar-2′,H-Ar-6′), 7.30, 7.27 (2 d, ^{3}J = 7.4 Hz, 1H, H-Ar-6),
7.25 – 7.19 (m, 1H, H-Ar-5), 7.15 – 7.10 (m, 1H, H-Ar-4),
6.65 – 6.62, 6.57 – 6.52 (m, 1H,=CH-), 3.38 (s, 2H, -CH_2-), 2.15 (s, 3H, -CH_3),
1.37 (s, 18H, -CCH_3).

Due to the low amount of **32 B** only **32 A** is resolved and depicted:
^{13}C-NMR (75 MHz, CD_2Cl_2): δ [ppm] = 151.19, 146.98, 146.91, 141.24, 140.84, 138.81,
127.38, 127.27, 124.66, 123.19, 121.43, 119.03, 43.24, 35.26, 31.70, 16.85.

Elemental analysis:

calculated: C 90.51 %; H 9.49 %.

found: C 89.93 %; H 9.55 %.

7.5.3.3 Bis[4-(3´,5´-di-*tert*-butylphenyl)-2-methylindenyl]dimethyl silane (33)

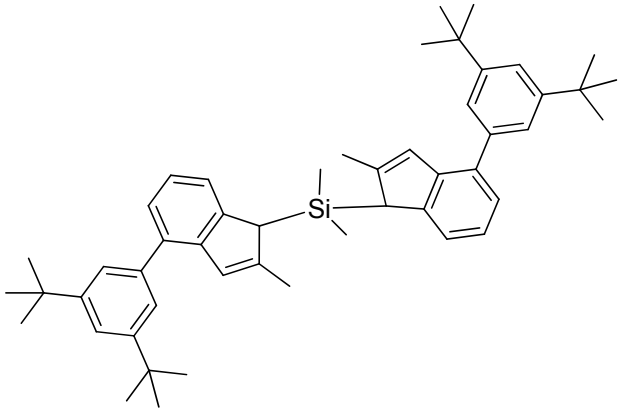

M = 693.13 g/mol

4.00 g (12.6 mmol) of 7-(3´,5´-di-*tert*-butylphenyl)-2-methylindene (**32 A)** (and ist isomer **32 B** with a ratio of 95:5) were dissolved in 100 ml toluene/dioxane (1:1). 5.04 mL (12.6 mmol) of a 2.5 M solution of *n*-BuLi in *n*-hexane were added at 0 °C. The solution was warmed to room temperature and stirred for 2 h. The resulting yellow solution was cooled to 0 °C and 0.81 g (6.3 mmol) $SiMe_2Cl_2$ were added. After complete addition the mixture was stirred at rt over night. Diethyl ether was added to the yellow suspension. The organic phase was washed with H_2O, saturated sodium chloride solution and dried over Na_2SO_4. Filtration and evaporation of the solvent, followed by column chromatography (*n*-hexane/ethylacetate) gave a slightly yellow solid which was suspended in hot methanol. This afforded after filtration at room temperature a white solid containing the *rac*- **33 A** and *meso*-isomer **33 B** of the ligand.

Yield: 0.9 g (1.3 mmol, 21 %).

Mixture of two isomers:

^{1}H NMR (CD_2Cl_2):

δ [ppm] = 7.52-7.37 (m, 8H, H-Ar-2´, H-Ar-4´, H-Ar-6´, H-Ar), 7.32 – 7.25 (m, 2H, H-Ar), 7.22 – 7.14 (m, 2H, H-Ar), 6.84 – 6.78 (m, 2H, =CH-), 3.88, 3.84 (2s, 2H, -CH-), 2.27 (s, 6H, $-CH_3$), 1.40 (s, 36H, $-CMe_3$), -0.15, -0.20, -0.22 (3s, 6H, $SiMe_2$).

33 A:

^{13}C NMR (75 MHz, CD_2Cl_2): δ [ppm] = 151.18, 148.30, 145.96, 143.35, 140.79, 135.42, 126.30, 125.90, 123.65, 123.41, 122.42, 121.18, 48.02, 35.22, 31.67, 18.32, -5.99.

33 B:

^{13}C NMR (75 MHz, CD_2Cl_2): δ [ppm] = 151.18, 148.40, 146.00, 143.35, 140.79, 135.40, 126.23, 125.87, 123.65, 123.35, 122.47, 121.18, 47.98, 35.22, 31.67, 18.25, -5.62, -5.63.

Elemental analysis:
calculated: C 86.64 %; H 9.31 %.
found: C 86.30 %; H 9.37 %.

7.6 **Complex Synthesis**

7.6.1 ***Rac-dimethylsilanediylbis(2-methyl-1-benz[e]indenyl) hafnium dichloride (10)***

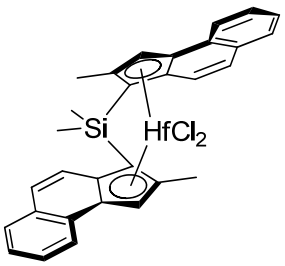

M = 668.04 g/mol

0.83 g (2.0 mmol) bis(2-methyl-4,5-benz[e]indenyl)dimethyl silane were dissolved in 40 mL toluene and cooled to -15 °C. 1.6 mL (4.0 mmol) of a 2.5 M solution of *n*-BuLi in hexane were added at -15 °C. Afterwards the mixture was stirred for further 2 h at rt. 0.64 g (2.0 mmol) $HfCl_4$ were added at -15 °C to the suspension. The reaction mixture was stirred over night at rt and a yellow suspension was obtained. The yellow solution was separated from the residue which was extracted twice with toluene and subsequently twice with DCM. The organic phases were combined and the solvent was removed under reduced pressure. The

residue was washed several times with pentane and the *rac*-form of the complex was obtained after crystallization from toluene as a yellow crystalline solid.

Yield: 48 mg (0.07 mmol, 4 %).

^{1}H NMR (300 MHz, $CDCl_3$): δ [ppm] = 7.92 (d, ^{3}J = 7.4 Hz, 2H, H-Ar),
7.77 (d, ^{3}J = 6.86 Hz, 2H, H-Ar), 7.63 (d, ^{3}J = 9.17 Hz, 2H, H-Ar),
7.45-7.56 (m, 4H, H-Ar), 7.33 (d, ^{3}J = 9.25 Hz, 2H, H-Ar), 7.19 (s, 2H, CH-indene),
2.45 (s, 6H, 2-Me), 1.35 (s, 6H, $SiMe_2$).

The observed signals are in good accordance with reported values of the corresponding zirconocene. Hence, and due to the low amount of product no further analysis was conducted.

7.6.2 *Rac-dimethylsilanediylbis[4-(3′,5′-di-tert-butylphenyl) - 7-methoxy-2-methylindenyl]zirconium dichloride (34)*

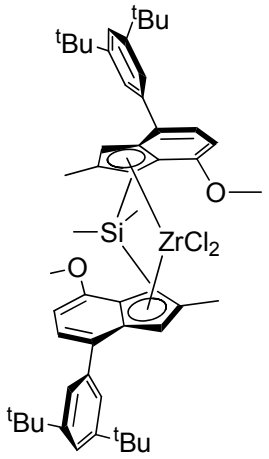

M = 913.29 g/mol

2.37 g (3.15 mmol) of bis[4-(3′,5′-di-*tert*-butylphenyl)-7-methoxy-2-methylindenyl]dimethyl silane **(28)** were dissolved in 110 mL of dry toluene. 2.52 mL (6.3 mmol) of a 2.5 M solution of *n*-BuLi in hexane were added at 0 °C. The solution was stirred for 24 h at room temperature. Afterwards the solution was cooled to -78 °C and 0.73 g (3.14 mmol) of zirconium tetrachloride were added. The suspension was allowed to warm up to room temperature and stirred over night. The red toluene solution was separated from the solid and latter was extracted several times with toluene. The solvent was removed in vacuum and the

resulting solid was washed several times with dry *n*-pentane. Crystallization from toluene/*n*-pentane gave the pure racemic form of the metallocene as a crystalline orange solid.

Yield: 0.79 g (0.87 mmol, 28 %).

^{1}H NMR (CD_2Cl_2): δ [ppm] = 7.51 (d, ^{4}J = 1.7 Hz, 4H, H-Ar-2′, H-Ar-6′), 7.36 (m, 4H, H-Ar, H-Ar-4′), 6.95 (s, 2H, CH-indene), 6.45 (d, ^{3}J = 7.9 Hz, 2H, H-Ar), 3.91 (s, 6H, -OCH_3), 2.17 (s, 6H, -CH_3), 1.31 (s, 36H, -CMe_3) 1.22 (s, 6H, -$SiMe_2$).

^{13}C NMR (75 MHz, CD_2Cl_2): δ [ppm] = 155.79, 151.49, 139.05, 135.40, 133.47, 131.79, 128.01, 123.70, 123.66, 121.87, 121.19, 103.50, 84.08, 54.34, 35.36, 31.65, 17.72, 6.12.

Elemental analysis:
calculated: C 68.38 %; H 7.28 %.
found: C 68.47 %; H 7.42 %.

X-Ray structure analysis: Crystals were obtained by crystallization from toluene/*n*-pentane. Structure is deposited at the Cambridge Crystallographic Data Center: CCDC-841805 (*rac*-**34**), CCDC-841804 (*meso*-**34**)

7.6.3 *Rac-dimethylsilanediylbis[4-(3′,5′-di-tert-butylphenyl)-7-methoxy-2-methylindenyl]hafnium dichloride (35)*

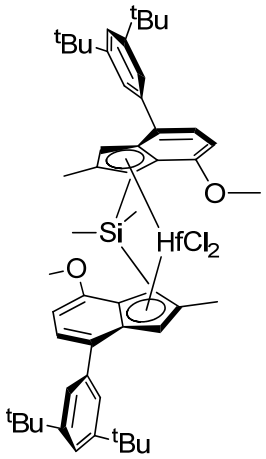

M = 1000.56 g/mol

2.74 g (3.64 mmol) of bis[4-(3´,5´-di-*tert*-butylphenyl)-7-methoxy-2-methylindenyl]dimethyl silane **(28)** were dissolved in 120 mL of dry toluene. 2.91 mL (7.28 mmol) of a 2.5 M solution of *n*-BuLi in *n*-hexane were added at 0 °C. The solution was stirred for 24 h at room temperature. Afterwards the solution was cooled to -78 °C and 1.16 g (3.62 mmol) of hafnium tetrachloride were added to the reaction mixture. The suspension was allowed to warm up to room temperature and stirred over night. The brown toluene solution was separated from the solid and latter was extracted several times with toluene. Afterwards toluene was removed in vacuum. The obtained solid was washed several times with *n*-pentane. Crystallization from toluene/*n*-pentane afforded the pure *rac*-form as a yellow crystalline solid.

Yield: 0.35 g (0.35 mmol, 10 %).

^{1}H NMR (C_6D_6): δ [ppm] = 7.94 (d, ^{4}J = 1.4 Hz, 4H, H-Ar-2´, H-Ar-6´),
7.66 – 7.61 (m, 2H, H-Ar-4´), 7.37 (d, ^{3}J = 7.7 Hz, 2H, H-Ar), 7.10 (s, 2H, CH-indene),
6.04 (d, ^{3}J = 7.8 Hz, 2H, H-Ar), 3.26 (s, 6H, -OCH_3), 2.12 (s, 6H, -CH_3), 1.46 (s, 36H, -CMe_3)
1.05 (s, 6H, -$SiMe_2$).

^{13}C NMR (75 MHz, C_6D_6): δ [ppm] = 155.40, 151.37, 140.13, 133.49, 132.29, 132.07,
124.29, 122.56, 120.98, 120.20, 103.20, 84.81, 53.27, 35.38, 31.90, 17.42, 5.97. (one signal is beneath the solvent signal)

Elemental analysis:
calculated: C 62.42 %; H 6.65 %.
found: C 62.73 %; H 6.77 %.

X-Ray structure analysis: Crystals were obtained by crystallization from toluene/*n*-pentane. Structure is deposited at the Cambridge Crystallographic Data Center: CCDC-841806 (*rac*-**35**)

7.6.4 *Rac-dimethylsilanediylbis[4-(3′,5′-di-tert-butylphenyl)-2-methylindenyl]hafnium dichloride (36)*

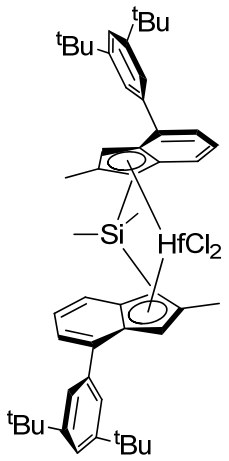

M = 940.51 g/mol

0.68 g (0.98 mmol) of bis[4-(3′,5′-di-*tert*-butylphenyl)-2-methylindenyl]dimethyl silane **(33)** were dissolved in a mixture of 7 mL dry THF and 1 mL dry *n*-pentane. 0.81 mL (2.03 mmol) of a 2.5 M solution of *n*-BuLi in *n*-hexane were added at -78 °C. The solution was allowed to warm up to - 60 °C during 30 minutes, afterwards up to rt and was stirred for a further 1 h. The solvent was removed in vacuum, 3 mL of dry toluene were added and again removed in vacuum. The residue was dissolved in 8 mL of dry toluene. Afterwards the solution was cooled to -78 °C and 0.317 g (0.99 mmol) of hafnium tetrachloride were added. The suspension was allowed to warm up to room temperature within 2 h and was refluxed for further 6 h. Toluene was removed in vacuum and the yellow residue was stirred in 10 ml of dry *n*-pentane over night. The yellow solution was separated from the yellow residue, which was again extracted with further 6 mL of dry *n*-pentane. The combined *n*-pentane solutions were reduced and the pure racemic form of the complex was obtained as a yellow crystalline solid.

Yield: 0.363 g (0.39 mmol, 39 %).

^{1}H NMR (CD_2Cl_2): δ [ppm] = 7.74 (d, ^{3}J = 8.7 Hz, 2H, H-Ar-5),
7.53 (d, ^{4}J = 1.8 Hz, 4H, H-Ar-2′, H-Ar-6′), 7.42 (t, ^{4}J = 1.8 Hz, 2H, H-Ar-4′),
7.38 (dd, ^{3}J = 7.0 Hz, ^{4}J = 0.7 Hz, 2H, H-Ar-7),
7.10 (dd, ^{3}J = 8.7 Hz, ^{3}J = 7.0 Hz, 2H, H-Ar-6), 6.86 (s, 2H, CH-indene),
2.35 (s, 6H, -CH_3), 1.35 (s, 6H, $SiMe_2$), 1.31 (s, 36 H, -CMe_3).

^{13}C NMR (75 MHz, CD_2Cl_2): δ [ppm] = 151.59, 139.44, 138.97, 133.74, 131.92, 126.77, 126.55, 125.91, 124.65, 123.60, 121.88, 121.29, 85.10, 35.36, 31.63, 18.68, 2.68.

Elemental analysis:

calculated: C 63.85 %; H 6.64 %.

found: C 63.60 %; H 6.91 %.

X-Ray structure analysis: Crystals were obtained by crystallization from *n*-pentane

Table S1 - Crystal Data and Details of the Structure Determination for: **SCHD 6257-123**

Crystal Data

Formula			C50 H62 Cl2 Hf Si
Formula Weight			940.48
Crystal System			Monoclinic
Space group		P21/c	(No. 14)
a, b, c [Angstrom]	10.6003(3)	15.4403(4)	27.7996(7)
alpha, beta, gamma [deg]	90	90.3077(11)	90
V [Ang**3]			4550.0(2)
Z			4
D(calc) [g/cm**3]			1.373
Mu(MoKa) [/mm]			2.469
F(000)			1928
Crystal Size [mm]		0.20 x	0.25 x 0.30

Data Collection

Temperature (K)			123
Radiation [Angstrom]		MoKa	0.71073
Theta Min-Max [Deg]			1.5, 25.4
Dataset		-12: 12 ; -18: 18 ; -33: 33	
Tot., Uniq. Data, R(int)		120868,	8356, 0.025
Observed data [I > 0.0 sigma(I)]			7978

Refinement

Nref, Npar			8356, 502
R, wR2, S		0.0201,	0.0491, 1.04
w = 1/[\s^2^(Fo^2^)+(0.0192P)^2^+8.0608P] where P=(Fo^2^+2Fc^2^)/3			
Max. and Av. Shift/Error			0.00, 0.00
Min. and Max. Resd. Dens. [e/Ang^3]			-1.12, 1.29

Table S2 - Bond Distances (Angstrom) for: **SCHD 6257-123**

Hf1	-Cl1	2.3949(6)	C13	-C14	1.402(3)
Hf1	-Cl2	2.3873(6)	C13	-C19	1.536(4)
Hf1	-C1	2.453(2)	C15	-C16	1.468(8)
Hf1	-C2	2.511(2)	C15	-C17	1.469(6)
Hf1	-C3	2.584(2)	C15	-C18	1.515(7)
Hf1	-C3A	2.623(2)	C19	-C20	1.535(4)
Hf1	-C7A	2.513(2)	C19	-C21	1.536(4)
Hf1	-C25	2.477(2)	C19	-C22	1.534(4)
Hf1	-C26	2.509(2)	C25	-C26	1.446(3)
Hf1	-C27	2.561(2)	C25	-C31A	1.451(3)
Hf1	-C27A	2.619(2)	C26	-C27	1.412(3)
Hf1	-C31A	2.540(2)	C26	-C32	1.504(3)
Si1	-C1	1.887(2)	C27	-C27A	1.418(3)
Si1	-C23	1.869(3)	C27A	-C28	1.429(3)
Si1	-C24	1.865(2)	C27A	-C31A	1.446(3)
Si1	-C25	1.890(2)	C28	-C29	1.368(3)
C1	-C2	1.441(3)	C28	-C33	1.498(3)
C1	-C7A	1.447(3)	C29	-C30	1.424(3)
C2	-C3	1.409(3)	C30	-C31	1.362(4)
C2	-C8	1.511(3)	C31	-C31A	1.432(3)
C3	-C3A	1.420(3)	C33	-C34	1.393(3)
C3A	-C4	1.436(3)	C33	-C38	1.392(3)
C3A	-C7A	1.445(3)	C34	-C35	1.388(3)
C4	-C5	1.370(3)	C35	-C36	1.404(3)
C4	-C9	1.485(3)	C35	-C39	1.539(3)
C5	-C6	1.419(4)	C36	-C37	1.389(3)
C6	-C7	1.365(4)	C37	-C38	1.400(3)
C7	-C7A	1.429(3)	C37	-C43	1.539(3)
C9	-C10	1.396(3)	C39	-C40	1.532(4)
C9	-C14	1.394(3)	C39	-C41	1.537(4)
C10	-C11	1.390(3)	C39	-C42	1.533(4)
C11	-C12	1.399(4)	C43	-C44	1.500(5)
C11	-C15	1.544(4)	C43	-C45	1.495(5)
C12	-C13	1.398(3)	C43	-C46	1.501(5)

Table S3 - Bond Angles (Degrees) for: **SCHD 6257-123**

Cl1	-Hf1	-Cl2	96.76(2)	C3A	-C4	-C5	117.2(2)
Cl1	-Hf1	-C1	121.34(6)	C3A	-C4	-C9	121.2(2)
Cl1	-Hf1	-C2	87.98(6)	C5	-C4	-C9	121.6(2)
Cl1	-Hf1	-C3	78.73(5)	C4	-C5	-C6	122.3(2)
Cl1	-Hf1	-C3A	102.88(5)	C5	-C6	-C7	121.7(2)
Cl1	-Hf1	-C7A	132.23(5)	C6	-C7	-C7A	119.2(2)
Cl1	-Hf1	-C25	123.02(6)	Hf1	-C7A	-C1	70.81(13)
Cl1	-Hf1	-C26	133.86(6)	Hf1	-C7A	-C3A	77.88(13)
Cl1	-Hf1	-C27	104.77(5)	Hf1	-C7A	-C7	119.45(16)
Cl1	-Hf1	-C27A	80.69(5)	C1	-C7A	-C3A	109.0(2)
Cl1	-Hf1	-C31A	89.85(6)	C1	-C7A	-C7	132.5(2)
Cl2	-Hf1	-C1	124.55(6)	C3A	-C7A	-C7	118.55(19)
Cl2	-Hf1	-C2	132.46(5)	C4	-C9	-C10	119.4(2)
Cl2	-Hf1	-C3	102.63(5)	C4	-C9	-C14	121.3(2)
Cl2	-Hf1	-C3A	79.76(5)	C10	-C9	-C14	119.3(2)
Cl2	-Hf1	-C7A	90.82(5)	C9	-C10	-C11	121.4(3)
Cl2	-Hf1	-C25	124.14(5)	C10	-C11	-C12	117.8(2)
Cl2	-Hf1	-C26	90.61(5)	C10	-C11	-C15	120.7(3)
Cl2	-Hf1	-C27	79.53(5)	C12	-C11	-C15	121.5(2)

Cl2	-Hf1	-C27A	102.66(5)	C11	-C12	-C13	122.7(2)
Cl2	-Hf1	-C31A	132.78(5)	C12	-C13	-C14	117.7(2)
C1	-Hf1	-C2	33.73(8)	C12	-C13	-C19	123.0(2)
C1	-Hf1	-C3	54.95(7)	C14	-C13	-C19	119.3(2)
C1	-Hf1	-C3A	55.12(7)	C9	-C14	-C13	121.1(2)
C1	-Hf1	-C7A	33.85(7)	C11	-C15	-C16	110.9(5)
C1	-Hf1	-C25	68.64(7)	C11	-C15	-C17	109.1(4)
C1	-Hf1	-C26	89.49(7)	C11	-C15	-C18	112.5(3)
C1	-Hf1	-C27	120.80(7)	C16	-C15	-C17	113.2(6)
C1	-Hf1	-C27A	120.72(7)	C16	-C15	-C18	105.5(5)
C1	-Hf1	-C31A	89.29(7)	C17	-C15	-C18	105.5(4)
C2	-Hf1	-C3	32.07(7)	C13	-C19	-C20	112.5(2)
C2	-Hf1	-C3A	53.27(7)	C13	-C19	-C21	110.0(2)
C2	-Hf1	-C7A	54.50(8)	C13	-C19	-C22	108.8(2)
C2	-Hf1	-C25	90.08(7)	C20	-C19	-C21	108.0(2)
C2	-Hf1	-C26	119.22(7)	C20	-C19	-C22	108.2(2)
C2	-Hf1	-C27	144.62(7)	C21	-C19	-C22	109.4(2)
C2	-Hf1	-C27A	124.71(7)	Hf1	-C25	-Si1	97.82(9)
C2	-Hf1	-C31A	94.33(7)	Hf1	-C25	-C26	74.37(12)
C3	-Hf1	-C3A	31.64(7)	Hf1	-C25	-C31A	75.60(12)
C3	-Hf1	-C7A	53.65(7)	Si1	-C25	-C26	126.01(18)
C3	-Hf1	-C25	120.95(7)	Si1	-C25	-C31A	124.58(16)
C3	-Hf1	-C26	143.52(7)	C26	-C25	-C31A	105.42(19)
C3	-Hf1	-C27	175.74(7)	Hf1	-C26	-C25	71.93(12)
C3	-Hf1	-C27A	148.96(7)	Hf1	-C26	-C27	75.86(13)
C3	-Hf1	-C31A	124.47(7)	Hf1	-C26	-C32	121.04(15)
C3A	-Hf1	-C7A	32.59(7)	C25	-C26	-C27	109.5(2)
C3A	-Hf1	-C25	120.51(7)	C25	-C26	-C32	127.4(2)
C3A	-Hf1	-C26	123.25(7)	C27	-C26	-C32	123.1(2)
C3A	-Hf1	-C27	147.05(7)	Hf1	-C27	-C26	71.83(13)
C3A	-Hf1	-C27A	175.51(7)	Hf1	-C27	-C27A	76.39(13)
C3A	-Hf1	-C31A	143.87(7)	C26	-C27	-C27A	108.95(19)
C7A	-Hf1	-C25	88.91(7)	Hf1	-C27A	-C27	71.86(13)
C7A	-Hf1	-C26	92.90(8)	Hf1	-C27A	-C28	124.67(15)
C7A	-Hf1	-C27	122.97(7)	Hf1	-C27A	-C31A	70.74(12)
C7A	-Hf1	-C27A	143.05(7)	C27	-C27A	-C28	131.9(2)
C7A	-Hf1	-C31A	118.26(7)	C27	-C27A	-C31A	107.2(2)
C25	-Hf1	-C26	33.70(7)	C28	-C27A	-C31A	120.9(2)
C25	-Hf1	-C27	55.16(7)	C27A	-C28	-C29	117.8(2)
C25	-Hf1	-C27A	55.00(7)	C27A	-C28	-C33	120.9(2)
C25	-Hf1	-C31A	33.58(8)	C29	-C28	-C33	121.3(2)
C26	-Hf1	-C27	32.31(7)	C28	-C29	-C30	121.8(2)
C26	-Hf1	-C27A	53.32(8)	C29	-C30	-C31	121.9(2)
C26	-Hf1	-C31A	54.30(7)	C30	-C31	-C31A	119.1(2)
C27	-Hf1	-C27A	31.75(7)	Hf1	-C31A	-C25	70.82(12)
C27	-Hf1	-C31A	53.72(7)	Hf1	-C31A	-C27A	76.75(12)
C27A	-Hf1	-C31A	32.51(7)	Hf1	-C31A	-C31	121.23(16)
C1	-Si1	-C23	113.34(12)	C25	-C31A	-C27A	108.87(19)
C1	-Si1	-C24	113.62(11)	C25	-C31A	-C31	132.6(2)
C1	-Si1	-C25	94.81(10)	C27A	-C31A	-C31	118.5(2)
C23	-Si1	-C24	104.62(13)	C28	-C33	-C34	119.7(2)
C23	-Si1	-C25	115.75(11)	C28	-C33	-C38	120.60(19)
C24	-Si1	-C25	115.02(11)	C34	-C33	-C38	119.7(2)
Hf1	-C1	-Si1	98.72(9)	C33	-C34	-C35	121.0(2)
Hf1	-C1	-C2	75.33(13)	C34	-C35	-C36	117.9(2)
Hf1	-C1	-C7A	75.35(13)	C34	-C35	-C39	122.0(2)
Si1	-C1	-C2	126.35(17)	C36	-C35	-C39	120.1(2)
Si1	-C1	-C7A	124.71(17)	C35	-C36	-C37	122.7(2)

C2	-C1	-C7A	105.60(18)	C36	-C37	-C38	117.7(2)
Hf1	-C2	-C1	70.94(12)	C36	-C37	-C43	121.8(2)
Hf1	-C2	-C3	76.84(13)	C38	-C37	-C43	120.5(2)
Hf1	-C2	-C8	118.99(16)	C33	-C38	-C37	121.0(2)
C1	-C2	-C3	109.5(2)	C35	-C39	-C40	109.8(2)
C1	-C2	-C8	128.00(19)	C35	-C39	-C41	109.9(2)
C3	-C2	-C8	122.5(2)	C35	-C39	-C42	111.7(2)
Hf1	-C3	-C2	71.10(13)	C40	-C39	-C41	109.0(2)
Hf1	-C3	-C3A	75.68(13)	C40	-C39	-C42	108.2(2)
C2	-C3	-C3A	109.0(2)	C41	-C39	-C42	108.2(2)
Hf1	-C3A	-C3	72.69(13)	C37	-C43	-C44	108.4(2)
Hf1	-C3A	-C4	123.99(15)	C37	-C43	-C45	111.7(3)
Hf1	-C3A	-C7A	69.53(12)	C37	-C43	-C46	111.6(2)
C3	-C3A	-C4	132.1(2)	C44	-C43	-C45	108.7(4)
C3	-C3A	-C7A	106.88(18)	C44	-C43	-C46	108.4(3)
C4	-C3A	-C7A	121.0(2)	C45	-C43	-C46	108.1(3)

Figure F1 – Ortep drawing with 50% ellipsoids for: **SCHD 6257-123**

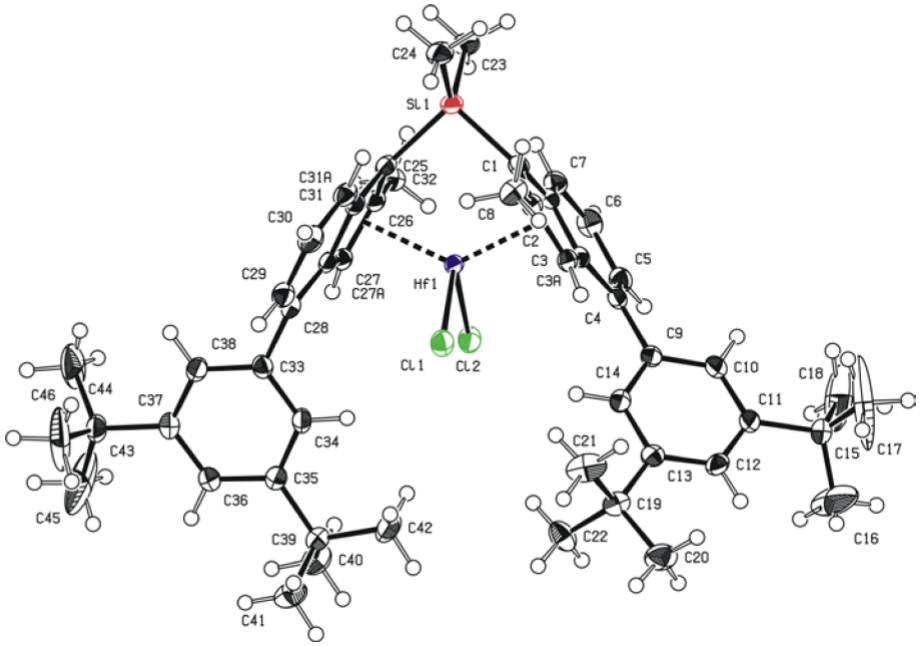

8 Literature

1. http://www.plasticseurope.de/Document/plastics---the-facts-2011.aspx?Page=DOCUMENT&FolID=2. , status march 2012.
2. http://www.plasticseurope.de/Document/visions-in-polymers.aspx?Page=DOCUMENT&FolID=2. , status march 2012.
3. Ziegler, K.; Holzkamp, E.; Breil, H.; Martin, H., *Angew. Chem. Int. Ed. Engl.* **1955,** 67, (19-2), 541-547.
4. Natta, G., *Angew. Chem. Int. Ed. Engl.* **1956,** 68, (12), 393-403.
5. Resconi, L.; Cavallo, L.; Fait, A.; Piemontesi, F., *Chem. Rev.* **2000,** 100, (4), 1253-1345.
6. Jordan, R. F., *Adv. Organomet. Chem.* **1991,** 32, 325-387.
7. Natta, G.; Pino, P.; Mazzanti, G.; Giannini, U., *J. Am. Chem. Soc.* **1957,** 79, (11), 2975-2976.
8. Breslow, D. S.; Newburg, N. R., *J. Am. Chem. Soc.* **1957,** 79, (18), 5072-5073.
9. Breslow, D. S.; Newburg, N. R., *J. Am. Chem. Soc.* **1959,** 81, (1), 81-86.
10. Long, W. P.; Breslow, D. S., *J. Am. Chem. Soc.* **1960,** 82, (8), 1953-1957.
11. Wild, F.; Zsolnai, L.; Huttner, G.; Brintzinger, H. H., *J. Organomet. Chem.* **1982,** 232, (3), 233-247.
12. Ewen, J. A., *J. Am. Chem. Soc.* **1984,** 106, (21), 6355-6364.
13. Long, W. P.; Breslow, D. S., *Liebigs Ann. Chem.* **1975**, (3), 463-469.
14. Sinn, H.; Kaminsky, W.; Vollmer, H. J.; Woldt, R., *Angew. Chem., Int. Ed. Engl.* **1980,** 19, (5), 390-392.
15. Sinn, H.; Kaminsky, W., *Adv. Organomet. Chem.* **1980,** Volume 18, 99-149.
16. Wild, F.; Wasiucionek, M.; Huttner, G.; Brintzinger, H. H., *J. Organomet. Chem.* **1985,** 288, (1), 63-67.
17. Kaminsky, W.; Kulper, K.; Brintzinger, H. H.; Wild, F., *Angew. Chem., Int. Ed. Engl.* **1985,** 24, (6), 507-508.
18. Dietrich, U.; Hackmann, M.; Rieger, B.; Klinga, M.; Leskelä, M., *Journal of the American Chemical Society* **1999,** 121, (18), 4348-4355.
19. Wang, B. Q., *Coord. Chem. Rev.* **2006,** 250, (1-2), 242-258.
20. Hortmann, K.; Brintzinger, H. H., *New J. Chem.* **1992,** 16, (1-2), 51-55.
21. Möhring, P. C.; Coville, N. J., *Coord. Chem. Rev.* **2006,** 250, (1-2), 18-35.

22. Brintzinger, H. H.; Fischer, D.; Mülhaupt, R.; Rieger, B.; Waymouth, R. M., *Angew. Chem., Int. Ed. Engl.* **1995,** 34, (11), 1143-1170.
23. Shaltout, R. M.; Corey, J. Y.; Rath, N. P., *J. Organomet. Chem.* **1995,** 503, (2), 205-212.
24. Karttunen, V. A.; Linnolahti, M.; Turunen, A.; Pakkanen, T. A.; Severn, J. R.; Maaranen, J.; Kokko, E.; Pitkänen, P., *J. Organomet. Chem.* **2008,** 693, (1), 155-163.
25. Linnolahti, M.; Pakkanen, T. A., *Macromolecules* **2000,** 33, (25), 9205-9214.
26. Piemontesi, F.; Camurati, I.; Resconi, L.; Balboni, D.; Sironi, A.; Moret, M.; Zeigler, R.; Piccolrovazzi, N., *Organometallics* **1995,** 14, (3), 1256-1266.
27. Smith, J. A.; Vonseyerl, J.; Huttner, G.; Brintzinger, H. H., *J. Organomet. Chem.* **1979,** 173, (2), 175-185.
28. Linnolahti, M.; Pakkanen, T. A.; Leino, R.; Luttikhedde, H. J. G.; Wilen, C. E.; Nasman, J. H., *Eur. J. Inorg. Chem.* **2001**, (8), 2033-2040.
29. Rieger, B., *J. Organomet. Chem.* **1992,** 428, (3), C33-C36.
30. Dang, V. A.; Yu, L. C.; Balboni, D.; Dall'Occo, T.; Resconi, L.; Mercandelli, P.; Moret, M.; Sironi, A., *Organometallics* **1999,** 18, (19), 3781-3791.
31. Zachmanoglou, C. E.; Docrat, A.; Bridgewater, B. M.; Parkin, G.; Brandow, C. G.; Bercaw, J. E.; Jardine, C. N.; Lyall, M.; Green, J. C.; Keister, J. B., *J. Am. Chem. Soc.* **2002,** 124, (32), 9525-9546.
32. Wang, B. Q.; Mu, B.; Deng, X. B.; Cui, H. L.; Xu, S. S.; Zhou, X. Z.; Zou, F. L.; Li, Y.; Yang, L.; Li, Y. F.; Hu, Y. L., *Chemistry-a European Journal* **2005,** 11, (2), 669-679.
33. Zakharov, I. I.; Zakharov, V. A., *Macromol. Theory Simul.* **2001,** 10, (2), 108-116.
34. Babushkin, D. E.; Semikolenova, N. V.; Panchenko, V. N.; Sobolev, A. P.; Zakharov, V. A.; Talsi, E. P., *Macromol. Chem. Phys.* **1997,** 198, (12), 3845-3854.
35. Bryant, P. L.; Harwell, C. R.; Mrse, A. A.; Emery, E. F.; Gan, Z. H.; Caldwell, T.; Reyes, A. P.; Kuhns, P.; Hoyt, D. W.; Simeral, L. S.; Hall, R. W.; Butler, L. G., *J. Am. Chem. Soc.* **2001,** 123, (48), 12009-12017.
36. Stellbrink, J.; Niu, A. Z.; Allgaier, J.; Richter, D.; Koenig, B. W.; Hartmann, R.; Coates, G. W.; Fetters, L. J., *Macromolecules* **2007,** 40, (14), 4972-4981.
37. Chen, E. Y. X.; Marks, T. J., *Chem. Rev.* **2000,** 100, (4), 1391-1434.
38. Pédeutour, J. N.; Radhakrishnan, K.; Cramail, H.; Deffieux, A., *Macromol. Rapid Commun.* **2001,** 22, (14), 1095-1123.

39. Wieser, U.; Brintzinger, H. H., Uv/Vis Studies on the Activation of Zirconocene-Based Olefin-Polymerization Catalysts. In *Organomateallic Catalysts and Olefin Polymerization*, Blom, R.; Follestad, A.; Rytter, A.; Tilset, M.; Ystenes, M., Eds. Springer: Berlin, 2001; p 3.
40. Babushkin, D. E.; Panchenko, V. N.; Timofeeva, M. N.; Zakharov, V. A.; Brintzinger, H. H., *Macromol. Chem. Phys.* **2008,** 209, (12), 1210-1219.
41. Seraidaris, T.; Löfgren, B.; Makela-Vaarne, N.; Lehmus, P.; Stehling, U., *Macromol. Chem. Phys.* **2004,** 205, (8), 1064-1069.
42. Coevoet, D.; Cramail, H.; Deffieux, A., *Macromol. Chem. Phys.* **1998,** 199, (7), 1459-1464.
43. Coevoet, D.; Cramail, H.; Deffieux, A., *Macromol. Chem. Phys.* **1999,** 200, (5), 1208-1214.
44. Pédeutour, J. N.; Coevoet, D.; Cramail, H.; Deffieux, A., *Macromol. Chem. Phys.* **1999,** 200, (5), 1215-1221.
45. Pédeutour, J. N.; Cramail, H.; Deffieux, A., *J. Mol. Catal. A: Chem.* **2001,** 176, (1-2), 87-94.
46. Pédeutour, J. N.; Cramail, H.; Deffieux, A., *J. Mol. Catal. A: Chem.* **2001,** 174, (1-2), 81-87.
47. Yang, X.; Stern, C. L.; Marks, T. J., *J. Am. Chem. Soc.* **1994,** 116, (22), 10015-10031.
48. Bochmann, M.; Lancaster, S. J.; Hursthouse, M. B.; Malik, K. M. A., *Organometallics* **1994,** 13, (6), 2235-2243.
49. Chien, J. C. W.; Song, W.; Rausch, M. D., *Macromolecules* **1993,** 26, (12), 3239-3240.
50. Bochmann, M., *Organometallics* **2010,** 29, (21), 4711-4740.
51. Bochmann, M.; Lancaster, S. J., *Angew. Chem., Int. Ed. Engl.* **1994,** 33, (15-16), 1634-1637.
52. Chien, J. C. W.; Xu, B. P., *Makromol. Chem., Rapid Commun.* **1993,** 14, (2), 109-114.
53. Chien, J. C. W.; Song, W.; Rausch, M. D., *J. Polym. Sci., Part A: Polym. Chem.* **1994,** 32, (12), 2387-2393.
54. Bochmann, M.; Sarsfield, M. J., *Organometallics* **1998,** 17, (26), 5908-5912.
55. Mathis, D. b.; Couzijn, E. P. A.; Chen, P., *Organometallics* **2011,** 30, (14), 3834-3843.
56. Beck, S.; Brintzinger, H. H.; Suhm, J.; Mülhaupt, R., *Macromol. Rapid Commun.* **1998,** 19, (5), 235-239.

57. Coevoet, D.; Cramail, H.; Deffieux, A., *Macromol. Chem. Phys.* **1998,** 199, (7), 1451-1457.
58. Giannetti, E.; Nicoletti, G. M.; Mazzocchi, R., *J. Polym. Sci., Part A: Polym. Chem.* **1985,** 23, (8), 2117-2134.
59. Kenney, J. W.; Boone, D. R.; Striplin, D. R.; Chen, Y. H.; Hamar, K. B., *Organometallics* **1993,** 12, (9), 3671-3676.
60. Bruce, M. R. M.; Kenter, A.; Tyler, D. R., *J. Am. Chem. Soc.* **1984,** 106, (3), 639-644.
61. Seraidaris, T.; Löfgren, B.; Helaja, T.; Vanne, T.; Makela-Vaarne, N., *J. Polym. Sci., Part A: Polym. Chem.* **2005,** 43, (24), 6455-6464.
62. Kaminsky, W.; Steiger, R., *Polyhedron* **1988,** 7, (22-23), 2375-2381.
63. Bryliakov, K. P.; Talsi, E. P.; Semikolenova, N. V.; Zakharov, V. A.; Brand, J.; Alonso-Moreno, C.; Bochmann, M., *J. Organomet. Chem.* **2007,** 692, (4), 859-868.
64. Beck, S.; Brintzinger, H. H., *Inorg. Chim. Acta* **1998,** 270, (1-2), 376-381.
65. Hollemann, A. F.; Wiberg, E., *Lehrbuch Der Anorganischen Chemie*. 101 ed.; Walter de Gruyter: Berlin, 1995; p 1399-1417.
66. Ewen, J. A.; Haspeslagh, L.; Atwood, J. L.; Zhang, H. M., *J. Am. Chem. Soc.* **1987,** 109, (21), 6544-6545.
67. Kaminsky, W.; Engehausen, R.; Zoumis, K.; Spaleck, W.; Rohrmann, J., *Makromol. Chem., Macromol. Chem. Phy.* **1992,** 193, (7), 1643-1651.
68. Rieger, B.; Troll, C.; Preuschen, J., *Macromolecules* **2002,** 35, (15), 5742-5743.
69. Bryliakov, K. P.; Talsi, E. P.; Voskoboynikov, A. Z.; Lancaster, S. J.; Bochmann, M., *Organometallics* **2008,** 27, (23), 6333-6342.
70. Busico, V.; Cipullo, R.; Pellecchia, R.; Talarico, G.; Razavi, A., *Macromolecules* **2009,** 42, (6), 1789-1791.
71. Cossee, P., *Tetrahedron Lett.* **1960,** 1, (38), 12-16.
72. Cossee, P., *Tetrahedron Lett.* **1960,** 1, (38), 17-21.
73. Cossee, P., *J. Catal.* **1964,** 3, (1), 80-88.
74. Arlman, E. J.; Cossee, P., *J. Catal.* **1964,** 3, (1), 99-104.
75. Dawoodi, Z.; Green, M. L. H.; Mtetwa, V. S. B.; Prout, K., *J. Chem. Soc., Chem. Commun.* **1982**, (24), 1410-1411.
76. Brookhart, M.; Green, M. L. H., *J. Organomet. Chem.* **1983,** 250, (1), 395-408.
77. Laverty, D. T.; Rooney, J. J., *J. Chem. Soc., Faraday Trans. 1* **1983,** 79, 869-878.
78. Krauledat, H.; Brintzinger, H.-H., *Angewandte Chemie International Edition in English* **1990,** 29, (12), 1412-1413.

79. Piers, W. E.; Bercaw, J. E., *J. Am. Chem. Soc.* **1990,** 112, (25), 9406-9407.
80. Brookhart, M.; Green, M. L. H.; Parkin, G., *Proc. Nat. Acad. Sci. USA* **2007,** 104, (17), 6908-6914.
81. Jordan, R. F.; Bradley, P. K.; Baenziger, N. C.; LaPointe, R. E., *J. Am. Chem. Soc.* **1990,** 112, (3), 1289-1291.
82. Venditto, V.; Guerra, G.; Corradini, P.; Fusco, R., *Polymer* **1990,** 31, (3), 530-537.
83. Resconi, L.; Abis, L.; Franciscono, G., *Macromolecules* **1992,** 25, (25), 6814-6817.
84. Naga, N.; Mizunuma, K., *Polymer* **1998,** 39, (13), 2703-2708.
85. Castonguay, L. A.; Rappé, A. K., *J. Am. Chem. Soc.* **1992,** 114, (14), 5832-5842.
86. Cavallo, L.; Guerra, G.; Oliva, L.; Vacatello, M.; Corradini, P., *Polymer Communications* **1989,** 30, (1), 16-19.
87. Longo, P.; Grassi, A.; Pellecchia, C.; Zambelli, A., *Macromolecules* **1987,** 20, (5), 1015-1018.
88. Dahlmann, M.; Erker, G.; Nissinen, M.; Fröhlich, R., *J. Am. Chem. Soc.* **1999,** 121, (12), 2820-2828.
89. Kawamura-Kuribayashi, H.; Koga, N.; Morokuma, K., *J. Am. Chem. Soc.* **1992,** 114, (22), 8687-8694.
90. Yoshida, T.; Koga, N.; Morokuma, K., *Organometallics* **1996,** 15, (2), 766-777.
91. Guerra, G.; Cavallo, L.; Moscardi, G.; Vacatello, M.; Corradini, P., *J. Am. Chem. Soc.* **1994,** 116, (7), 2988-2995.
92. Guerra, G.; Longo, P.; Cavallo, L.; Corradini, P.; Resconi, L., *J. Am. Chem. Soc.* **1997,** 119, (19), 4394-4403.
93. Corradini, P.; Guerra, G., *Prog. Polym. Sci.* **1991,** 16, (2-3), 239-257.
94. Resconi, L.; Fait, A.; Piemontesi, F.; Colonnesi, M.; Rychlicki, H.; Zeigler, R., *Macromolecules* **1995,** 28, (19), 6667-6676.
95. Leclerc, M. K.; Brintzinger, H. H., *J. Am. Chem. Soc.* **1995,** 117, (5), 1651-1652.
96. Busico, V.; Cipullo, R., *J. Am. Chem. Soc.* **1994,** 116, (20), 9329-9330.
97. Resconi, L., *J. Mol. Catal. A: Chem.* **1999,** 146, (1-2), 167-178.
98. Yoder, J. C.; Bercaw, J. E., *J. Am. Chem. Soc.* **2002,** 124, (11), 2548-2555.
99. Kawamura-Kuribayashi, H.; Koga, N.; Morokuma, K., *J. Am. Chem. Soc.* **1992,** 114, (7), 2359-2366.
100. Resconi, L.; Camurati, I.; Sudmeijer, O., *Top. Catal.* **1999,** 7, (1-4), 145-163.
101. Cheng, H. N.; Ewen, J. A., *Die Makromolekulare Chemie* **1989,** 190, (8), 1931-1943.

102. Grassi, A.; Zambelli, A.; Resconi, L.; Albizzati, E.; Mazzocchi, R., *Macromolecules* **1988,** 21, (3), 617-622.

103. Zhou, Z.; Stevens, J. C.; Klosin, J.; Kummerle, R.; Qiu, X. H.; Redwine, D.; Cong, R. J.; Taha, A.; Mason, J.; Winniford, B.; Chauvel, P.; Montanez, N., *Macromolecules* **2009,** 42, (6), 2291-2294.

104. Rieger, B.; Mu, X.; Mallin, D. T.; Rausch, M. D.; Chien, J. C. W., *Macromolecules* **1990,** 23, (15), 3559-3568.

105. Prosenc, M. H.; Brintzinger, H. H., *Organometallics* **1997,** 16, (18), 3889-3894.

106. Pilmé, J.; Busico, V.; Cossi, M.; Talarico, G., *J. Organomet. Chem.* **2007,** 692, (20), 4227-4236.

107. Ewen, J. A.; Zambelli, A.; Longo, P.; Sullivan, J. M., *Macromol. Rapid Commun.* **1998,** 19, (1), 71-73.

108. Laine, A.; Linnolahti, M.; Pakkanen, T. A.; Severn, J. R.; Kokko, E.; Pakkanen, A., *Organometallics* **2010,** 29, (7), 1541-1550.

109. Caporaso, L.; de Rosa, C.; Talarico, G., *J. Polym. Sci., Part A: Polym. Chem.* **2010,** 48, (3), 699-708.

110. Woo, T. K.; Fan, L.; Ziegler, T., *Organometallics* **1994,** 13, (6), 2252-2261.

111. Resconi, L.; Piemontesi, F.; Camurati, I.; Balboni, D.; Sironi, A.; Moret, M.; Rychlicki, H.; Zeigler, R., *Organometallics* **1996,** 15, (23), 5046-5059.

112. Cavallo, L.; Guerra, G., *Macromolecules* **1996,** 29, (8), 2729-2737.

113. Stehling, U.; Diebold, J.; Kirsten, R.; Roll, W.; Brintzinger, H. H.; Jungling, S.; Mülhaupt, R.; Langhauser, F., *Organometallics* **1994,** 13, (3), 964-970.

114. Talarico, G.; Budzelaar, P. H. M., *Organometallics* **2008,** 27, (16), 4098-4107.

115. Eshuis, J. J. W.; Tan, Y. Y.; Teuben, J. H.; Renkema, J., *J. Mol. Catal.* **1990,** 62, (3), 277-287.

116. Eshuis, J. J. W.; Tan, Y. Y.; Meetsma, A.; Teuben, J. H.; Renkema, J.; Evens, G. G., *Organometallics* **1992,** 11, (1), 362-369.

117. Resconi, L.; Piemontesi, F.; Franciscono, G.; Abis, L.; Fiorani, T., *J. Am. Chem. Soc.* **1992,** 114, (3), 1025-1032.

118. Guo, Z. Y.; Swenson, D. C.; Jordan, R. F., *Organometallics* **1994,** 13, (4), 1424-1432.

119. Hajela, S.; Bercaw, J. E., *Organometallics* **1994,** 13, (4), 1147-1154.

120. Resconi, L.; Piemontesi, F.; Camurati, I.; Sudmeijer, O.; Nifant'ev, I. E.; Ivchenko, P. V.; Kuz'mina, L. G., *J. Am. Chem. Soc.* **1998,** 120, (10), 2308-2321.

121. Yang, X. M.; Stern, C. L.; Marks, T. J., *J. Am. Chem. Soc.* **1994,** 116, (22), 10015-10031.
122. Chirik, P. J.; Dalleska, N. F.; Henling, L. M.; Bercaw, J. E., *Organometallics* **2005,** 24, (11), 2789-2794.
123. Yang, P.; Baird, M. C., *Organometallics* **2005,** 24, (24), 6005-6012.
124. Yang, P.; Baird, M. C., *Organometallics* **2005,** 24, (24), 6013-6018.
125. Suzuki, Y.; Yasumoto, T.; Mashima, K.; Okuda, J., *J. Am. Chem. Soc.* **2006,** 128, (39), 13017-13025.
126. Chien, J. C. W.; Wang, B. P., *J. Polym. Sci., Part A: Polym. Chem.* **1988,** 26, (11), 3089-3102.
127. Resconi, L.; Bossi, S.; Abis, L., *Macromolecules* **1990,** 23, (20), 4489-4491.
128. Naga, N.; Mizunuma, K., *Polymer* **1998,** 39, (21), 5059-5067.
129. Pino, P.; Cioni, P.; Wei, J., *J. Am. Chem. Soc.* **1987,** 109, (20), 6189-6191.
130. Busico, V.; Cipullo, R.; Chadwick, J. C.; Modder, J. F.; Sudmeijer, O., *Macromolecules* **1994,** 27, (26), 7538-7543.
131. Zintl, M.; Rieger, B., *Angew. Chem. Int. Ed. Engl.* **2007,** 46, (3), 333-335.
132. Arriola, D. J.; Carnahan, E. M.; Hustad, P. D.; Kuhlman, R. L.; Wenzel, T. T., *Science* **2006,** 312, (5774), 714-719.
133. Ewen, J. A.; Jones, R. L.; Razavi, A.; Ferrara, J. D., *J. Am. Chem. Soc.* **1988,** 110, (18), 6255-6256.
134. Gauthier, W. J.; Corrigan, J. F.; Taylor, N. J.; Collins, S., *Macromolecules* **1995,** 28, (11), 3771-3778.
135. Razavi, A.; Peters, L.; Nafpliotis, L., *J. Mol. Catal. A: Chem.* **1997,** 115, (1), 129-154.
136. Ewen, J. A.; Elder, M. J.; Jones, R. L.; Haspeslagh, L.; Atwood, J. L.; Bott, S. G.; Robinson, K., *Makromol. Chem., Macromol. Symp.* **1991,** 48-9, 253-295.
137. Coates, G. W.; Waymouth, R. M., *Science* **1995,** 267, (5195), 217-219.
138. Zambelli, A.; Locatelli, P.; Bajo, G.; Bovey, F. A., *Macromolecules* **1975,** 8, (5), 687-689.
139. Leino, R.; Lin, S., Isotactic Polypropylene from C_2- and Pseudo-C_2-Symmetric Catalysts. In *Stereoselective Polymerization with Single-Site Catalysts*, Baugh, L. S.; Canich, J. A. M., Eds. Boca-Raton, 2008; pp 3-36.
140. Holden, G., Thermoplastic Elastomers. In *Polymeric Materials Enyclopedia*, Salmone, J. C., Ed. CRC Press: Boca Raton, 1996; Vol. 11, pp 8343-8358.

141. Cobzaru, C.; Hild, S.; Boger, A.; Troll, C.; Rieger, B., *Coord. Chem. Rev.* **2006,** 250, (1-2), 189-211.
142. Hild, S.; Cobzaru, C.; Troll, C.; Rieger, B., Elastomeric Homo-Polypropylene: Solid State Properties and Synthesis Via Control of Reaction Parameters. In *Stereoselective Polymerization with Single-Site Catalysts*, Baugh, L. S.; Canich, J. A. M., Eds. CRC Press: Boca Raton, 2008; pp 231-272.
143. Natta, G., *J. Polym. Sci.* **1959,** 34, (127), 531-549.
144. Mallin, D. T.; Rausch, M. D.; Lin, Y. G.; Dong, S. Z.; Chien, J. C. W., *J. Am. Chem. Soc.* **1990,** 112, (5), 2030-2031.
145. Llinas, G. H.; Dong, S. H.; Mallin, D. T.; Rausch, M. D.; Lin, Y. G.; Winter, H. H.; Chien, J. C. W., *Macromolecules* **1992,** 25, (4), 1242-1253.
146. Chien, J. C. W.; Llinas, G. H.; Rausch, M. D.; Lin, Y. G.; Winter, H. H.; Atwood, J. L.; Bott, S. G., *J. Polym. Sci., Part A: Polym. Chem.* **1992,** 30, (12), 2601-2617.
147. Gauthier, W. J.; Collins, S., *Macromolecules* **1995,** 28, (11), 3779-3786.
148. Ewen, J. A.; Elder, M. J., In *Ziegler Catalysts*, Fink, G.; Mülhaupt, R.; Brintzinger, H.-H., Eds. Springer: Berlin, 1995; p 99.
149. Rieger, B.; Jany, G.; Fawzi, R.; Steimann, M., *Organometallics* **1994,** 13, (2), 647-653.
150. Bravakis, A. M.; Bailey, L. E.; Pigeon, M.; Collins, S., *Macromolecules* **1998,** 31, (4), 1000-1009.
151. Schilling, F. C.; Tonelli, A. E., *Macromolecules* **1980,** 13, (2), 270-275.
152. Guerra, G.; Cavallo, L.; Moscardi, G.; Vacatello, M.; Corradini, P., *Macromolecules* **1996,** 29, (14), 4834-4845.
153. Bruce, M. D.; Coates, G. W.; Hauptman, E.; Waymouth, R. M.; Ziller, J. W., *J. Am. Chem. Soc.* **1997,** 119, (46), 11174-11182.
154. Carlson, E. D.; Krejchi, M. T.; Shah, C. D.; Terakawa, T.; Waymouth, R. M.; Fuller, G. G., *Macromolecules* **1998,** 31, (16), 5343-5351.
155. Kravchenko, R.; Masood, A.; Waymouth, R. M.; Myers, C. L., *J. Am. Chem. Soc.* **1998,** 120, (9), 2039-2046.
156. Resconi, L.; Jones, R. L.; Rheingold, A. L.; Yap, G. P. A., *Organometallics* **1996,** 15, (3), 998-1005.
157. Xie, M. R.; Wu, Q.; Lin, S. G., *Macromol. Rapid Commun.* **1999,** 20, (3), 167-169.
158. De Rosa, C.; Auriemma, F.; Perretta, C., *Macromolecules* **2004,** 37, (18), 6843-6855.

159. Kukral, J.; Lehmus, P.; Feifel, T.; Troll, C.; Rieger, B., *Organometallics* **2000,** 19, (19), 3767-3775.

160. Kukral, J.; Lehmus, P.; Klinga, M.; Leskela, M.; Rieger, B., *Eur. J. Inorg. Chem.* **2002**, (6), 1349-1356.

161. Cheng, S. Z. D.; Janimak, J. J.; Zhang, A.; Cheng, H. N., *Macromolecules* **1990,** 23, (1), 298-303.

162. Janimak, J. J.; Cheng, S. Z. D.; Giusti, P. A.; Hsieh, E. T., *Macromolecules* **1991,** 24, (9), 2253-2260.

163. Lu, H. B.; Qiao, J. L.; Xu, Y. B.; Yang, Y. L., *J. Appl. Polym. Sci.* **2002,** 85, (2), 333-341.

164. Brückner, S.; Meille, S. V.; Petraccone, V.; Pirozzi, B., *Prog. Polym. Sci.* **1991,** 16, (2-3), 361-404.

165. Chen, H. B.; Karger-Kocsis, J.; Wu, J. S.; Varga, J., *Polymer* **2002,** 43, (24), 6505-6514.

166. Leugering, H. J., *Makromolekulare Chemie* **1967,** 109, 204-216.

167. Ferro, D. R.; Meille, S. V.; Brückner, S., *Macromolecules* **1998,** 31, (20), 6926-6934.

168. Leugering, H. J.; Kirsch, G., *Angew. Makromol. Chem.* **1973,** 33, 17-23.

169. Somani, R. H.; Hsiao, B. S.; Nogales, A.; Fruitwala, H.; Srinivas, S.; Tsou, A. H., *Macromolecules* **2001,** 34, (17), 5902-5909.

170. Zhong, C. F.; Mao, B. Q., *J. Appl. Polym. Sci.* **2009,** 114, (4), 2474-2480.

171. De Rosa, C.; Auriemma, F.; Di Capua, A.; Resconi, L.; Guidotti, S.; Camurati, I.; Nifant'ev, I. E.; Laishevtsev, I. P., *J. Am. Chem. Soc.* **2004,** 126, (51), 17040-17049.

172. Natta, G.; Corradini, P., *Nuovo Cimento, Suppl.* **1960,** 15, 40-47.

173. Bassett, D. C.; Olley, R. H., *Polymer* **1984,** 25, (7), 935-943.

174. Addink, E. J.; Beintema, J., *Polymer* **1961,** 2, (2), 185-193.

175. De Rosa, C.; Auriemma, F.; Paolillo, M.; Resconi, L.; Camurati, I., *Macromolecules* **2005,** 38, (22), 9143-9154.

176. Thomann, R.; Wang, C.; Kressler, J.; Mülhaupt, R., *Macromolecules* **1996,** 29, (26), 8425-8434.

177. Alamo, R. G.; Kim, M. H.; Galante, M. J.; Isasi, J. R.; Mandelkern, L., *Macromolecules* **1999,** 32, (12), 4050-4064.

178. Press, K.; Cohen, A.; Goldberg, I.; Venditto, V.; Mazzeo, M.; Kol, M., *Angew. Chem. Int. Ed.* **2011,** 50, (15), 3529-3532.

179. Cecchin, G.; Morini, G.; Pelliconi, A., *Macromolecular Symposia* **2001,** 173, 195-209.

180. Qiao, J. L.; Guo, M. F.; Wang, L. S.; Liu, D. B.; Zhang, X. F.; Yu, L. Q.; Song, W. B.; Liu, Y. Q., *Polymer Chemistry* **2011,** 2, (8), 1611-1623.

181. Hosaka, M.; Yano, T.; Sato, M.; Kimura, K. **2006**, WO2006129773.

182. Ikeuchi, H.; Yano, T.; Ikai, S.; Sato, H.; Yamashita, J., *J. Mol. Catal. A: Chem.* **2003,** 193, (1-2), 207-215.

183. Hueffer, S.; Roesch, J.; Seelert, S.; Langhauser, F.; Lilge, D.; Hingmann, R.; Schweier, G. **2006**, US7022795B1.

184. Spaleck, W.; Antberg, M.; Rohrmann, J.; Winter, A.; Bachmann, B.; Kiprof, P.; Behm, J.; Herrmann, W. A., *Angew. Chem. Int. Ed. Engl.* **1992,** 31, (10), 1347-1350.

185. Guevara, J. L.; Quijada, R.; Saavedra, P.; Palza, H.; Galland, G. B., *Bol. Soc. Chil. Quim.* **2002,** 47, (2), 81-90.

186. Voegele, J.; Troll, C.; Rieger, B., *Macromol. Chem. Phys.* **2002,** 203, (13), 1918-1925.

187. Sacchi, M. C.; Barsties, E.; Tritto, I.; Locatelli, P.; Brintzinger, H. H.; Stehling, U., *Macromolecules* **1997,** 30, (14), 3955-3957.

188. Hart, J. R.; Rappé, A. K., *J. Am. Chem. Soc.* **1993,** 115, (14), 6159-6164.

189. Spaleck, W.; Kuber, F.; Bachmann, B.; Fritze, C.; Winter, A., *J. Mol. Catal. A: Chem.* **1998,** 128, (1-3), 279-287.

190. Lee, I. M.; Gauthier, W. J.; Ball, J. M.; Iyengar, B.; Collins, S., *Organometallics* **1992,** 11, (6), 2115-2122.

191. Spaleck, W.; Kuber, F.; Winter, A.; Rohrmann, J.; Bachmann, B.; Antberg, M.; Dolle, V.; Paulus, E. F., *Organometallics* **1994,** 13, (3), 954-963.

192. Kashiwa, N.; Kojoh, S.-i.; Imuta, J.-i.; Tsutsui, T., Characterization of Pp Prepared with the Latest Metallocene and $Mgcl_2$-Supported $Ticl_4$ Catalyst Systems. In *Metalorganic Catalysts for Synthesis and Polymerization*, Kaminsky, W., Ed. Springer-Verlag: Berlin Heidelberg, 1999; pp 30-37.

193. Resconi, L.; Balboni, D.; Baruzzi, G.; Fiori, C.; Guidotti, S.; Mercandelli, P.; Sironi, A., *Organometallics* **2000,** 19, (4), 420-429.

194. Izmer, V. V.; Lebedev, A. Y.; Nikulin, M. V.; Ryabov, A. N.; Asachenko, A. F.; Lygin, A. V.; Sorokin, D. A.; Voskoboynikov, A. Z., *Organometallics* **2006,** 25, (5), 1217-1229.

195. Ryabov, A. N.; Izmer, V. V.; Tzarev, A. A.; Uborsky, D. V.; Asachenko, A. F.; Nikulin, M. V.; Canich, J. A. M.; Voskoboynikov, A. Z., *Organometallics* **2009,** 28, (13), 3614-3617.

196. Petroski, R. J.; Weisleder, D., *Synth. Commun.* **2001,** 31, (1), 89-95.

197. Wang, W.; Snieckus, V., *The Journal of Organic Chemistry* **1992,** 57, (2), 424-426.
198. Meyer, N.; Seebach, D., *Chem. Ber. Recl.* **1980,** 113, (4), 1304-1319.
199. Deng, H.; Winkelbach, H.; Taeji, K.; Kaminsky, W.; Soga, K., *Macromolecules* **1996,** 29, (20), 6371-6376.
200. Soga, K.; Uosumi, S.; To, U. **1997**, JP09302015A.
201. Schulte, J.; Schottek, J.; Okumura, Y. **2004**, WO2004052945A1.
202. Schulte, J.; Sell, T.; Thorn, M. G.; Winter, A.; Dimeska, A. **2009**, WO2009054831A1.
203. Toto, M.; Cavallo, L.; Corradini, P.; Moscardi, G.; Resconi, L.; Guerra, G., *Macromolecules* **1998,** 31, (11), 3431-3438.
204. Imuta, J.; Saito, J.; Ueda, T.; Kiso, Y.; Mizuno, A.; Kawasaki, M.; Hashimoto, M. **2002**, EP1209165.
205. Leino, R.; Lehmus, P.; Lehtonen, A., *Eur. J. Inorg. Chem.* **2004**, (16), 3201-3222.
206. Barsties, E.; Schaible, S.; Prosenc, M. H.; Rief, U.; Roll, W.; Weyand, O.; Dorer, B.; Brintzinger, H. H., *J. Organomet. Chem.* **1996,** 520, (1-2), 63-68.
207. Luttikhedde, H. J. G.; Leino, R. P.; Wilén, C. E.; Näsman, J. H.; Ahlgren, M. J.; Pakkanen, T. A., *Organometallics* **1996,** 15, (13), 3092-3094.
208. Piccolrovazzi, N.; Pino, P.; Consiglio, G.; Sironi, A.; Moret, M., *Organometallics* **1990,** 9, (12), 3098-3105.
209. Schaefer, T.; Schneider, W. G., *Can. J. Chem.* **1963,** 41, (4), 966-&.
210. Kowala, C.; Wunderlich, J. A., *Acta Crystallographica Section B-Structural Science* **1976,** 32, (MAR15), 820-823.
211. Bajgur, C. S.; Tikkanen, W. R.; Petersen, J. L., *Inorg. Chem.* **1985,** 24, (16), 2539-2546.
212. Alt, H. G.; Milius, W.; Palackal, S. J., *J. Organomet. Chem.* **1994,** 472, (1-2), 113-118.
213. Nedorezova, P. M.; Veksler, E. N.; Novikova, E. S.; Optov, V. A.; Baranov, A. O.; Aladyshev, A. M.; Tsvetkova, V. I.; Shklyaruk, B. F.; Krut'ko, D. P.; Churakov, A. V.; Kuz'mina, L. G.; Howard, J. A. K., *Russ. Chem. Bull.* **2005,** 54, (2), 400-413.
214. Götz, C.; Rau, A.; Luft, G., *J. Mol. Catal. A: Chem.* **2002,** 184, (1-2), 95-110.
215. Schläfer, H. L.; Kling, O., *Angew. Chem. Int. Ed. Engl.* **1956,** 68, (21), 667-670.
216. Po, R.; Cardi, N.; Abis, L., *Polymer* **1998,** 39, (4), 959-964.
217. Baldwin, S. M.; Bercaw, J. E.; Brintzinger, H. H., *J. Am. Chem. Soc.* **2008,** 130, (51), 17423-17433.
218. Baldwin, S. M.; Bercaw, J. E.; Henling, L. M.; Day, M. W.; Brintzinger, H. H., *J. Am. Chem. Soc.* **2011,** 133, (6), 1805-1813.

219. Bravaya, N. M.; Panin, A. N.; Faingol'd, E. E.; Babkina, O. N.; Razavi, A., *J. Polym. Sci., Part A: Polym. Chem.* **2010,** 48, (13), 2934-2941.

220. Panin, A. N.; Dzhabieva, Z. M.; Nedorezova, P. M.; Tsvetkova, V. I.; Saratovskikh, S. L.; Babkina, O. N.; Bravaya, N. M., *J. Polym. Sci., Part A: Polym. Chem.* **2001,** 39, (11), 1915-1930.

221. Li, H. Y.; Neckers, D. C., *Can. J. Chem.* **2003,** 81, (6), 758-763.

222. Busico, V.; Brita, D.; Caporaso, L.; Cipullo, R.; Vacatello, M., *Macromolecules* **1997,** 30, (14), 3971-3977.

223. Beachley, O. T.; Victoriano, L., *Organometallics* **1988,** 7, (1), 63-67.

224. Stapleton, R. A.; Al-Humydi, A.; Chai, J. F.; Galan, B. R.; Collins, S., *Organometallics* **2006,** 25, (21), 5083-5092.

225. Stapleton, R. A.; Galan, B. R.; Collins, S.; Simons, R. S.; Garrison, J. C.; Youngs, W. J., *J. Am. Chem. Soc.* **2003,** 125, (31), 9246-9247.

226. Williams, V. C.; Dai, C. Y.; Li, Z. M.; Collins, S.; Piers, W. E.; Clegg, W.; Elsegood, M. R. J.; Marder, T. B., *Angew. Chem. Int. Ed. Engl.* **1999,** 38, (24), 3695-3698.

227. Busico, V.; Cipullo, R.; Cutillo, F.; Friederichs, N.; Ronca, S.; Wang, B., *J. Am. Chem. Soc.* **2003,** 125, (41), 12402-12403.

228. Song, F. Q.; Lancaster, S. J.; Cannon, R. D.; Schormann, M.; Humphrey, S. M.; Zuccaccia, C.; Macchioni, A.; Bochmann, M., *Organometallics* **2005,** 24, (6), 1315-1328.

229. Baker, J. W.; Eccles, A., *J. Chem. Soc.* **1927**, 2125.

230. Szöllosi, G.; Balázsik, K.; Bartók, M., *Applied Catalysis a-General* **2007,** 319, 193-201.

231. Liang, G. X.; Trauner, D., *J. Am. Chem. Soc.* **2004,** 126, (31), 9544-9545.

232. Al-Humydi, A.; Garrison, J. C.; Mohammed, M.; Youngs, W. J.; Collins, S., *Polyhedron* **2005,** 24, (11), 1234-1249.

233. Vatamanu, M.; Stojcevic, G.; Baird, M. C., *J. Am. Chem. Soc.* **2008,** 130, (2), 454-+.

234. Landis, C. R.; Christianson, M. D., *Proc. Nat. Acad. Sci. USA* **2006,** 103, (42), 15349-15354.

235. Khadir, A.; Gauthier, M., Highly Branched (Arborescent) Polymers as Meet Processing Additives. In *Antec'97 - Plastics Saving Planet Earth, Conference Proceedings, Vols 1 - 3*, 1997; pp 3732-3736.

236. Beigzadeh, D.; Soares, J. B. P.; Duever, T. A., *Macromolecular Symposia* **2001,** 173, 179-194.

237. Chum, P. S.; Kruper, W. J.; Guest, M. J., *Adv. Mater.* **2000,** 12, (23), 1759-1767.

238. Eckstein, A.; Suhm, J.; Friedrich, C.; Maier, R. D.; Sassmannshausen, J.; Bochmann, M.; Mülhaupt, R., *Macromolecules* **1998,** 31, (4), 1335-1340.

239. Liu, C. Y.; Yu, J.; He, J. S.; Liu, W.; Sun, C. Y.; Jing, Z. H., *Macromolecules* **2004,** 37, (24), 9279-9282.

240. Weng, W. Q.; Markel, E. J.; Dekmezian, A. H., *Macromol. Rapid Commun.* **2000,** 21, (16), 1103-1107.

241. Weng, W. Q.; Markel, E. J.; Dekmezian, A. H., *Macromol. Rapid Commun.* **2001,** 22, (18), 1488-1492.

242. Cherian, A. E.; Lobkovsky, E. B.; Coates, G. W., *Macromolecules* **2005,** 38, (15), 6259-6268.

243. Stadler, F. J.; Arikan-Conley, B.; Kaschta, J.; Kaminsky, W.; Munstedt, H., *Macromolecules* **2011,** 44, (12), 5053-5063.

244. Arikan, B.; Stadler, F. J.; Kaschta, J.; Münstedt, H.; Kaminsky, W., *Macromol. Rapid Commun.* **2007,** 28, (14), 1472-1478.

245. Karssenberg, F. G.; Wang, B.; Friederichs, N.; Mathot, V. B. F., *Macromol. Chem. Phys.* **2005,** 206, (16), 1675-1683.

246. Rieger, B. **1999**, DE19829828.

247. Sato, Y.; Ejima, T., *Nippon Kinzoku Gakkaishi* **1978,** 42, (9), 905-12.

248. Schmidt, W. **1956**, US2745802

249. Vijayanand, P. S.; Kato, S.; Satokawa, S.; Kojima, T., *Polym. Bull.* **2007,** 58, (5-6), 861-872.

250. Schwechtlik, K., *Organikum*. Wiley: Weinheim, 2001; Vol. 21, p 239-240.

251. Saljoughian, M.; Morimoto, H.; Williams, P. G., *J. Chem. Soc., Perkin Trans. 1* **1990**, (6), 1803-1808.

252. Lin, X.; Telepeni, I.; Blake, A. J.; Dailly, A.; Brown, C. M.; Simmons, J. M.; Zoppi, M.; Walker, G. S.; Thomas, K. M.; Mays, T. J.; Hubberstey, P.; Champness, N. R.; Schröder, M., *J. Am. Chem. Soc.* **2009,** 131, (6), 2159-2171.

253. Burkhardt, T. J.; Stehling, U. M.; Hart, J. R.; Haygood, W. T.; Li, R. T.; Vizzini, J. C.; Kuchta, M. C. **2002**, WO2002002576A1.

254. Mantina, M.; Chamberlin, A. C.; Valero, R.; Cramer, C. J.; Truhlar, D. G., *J. Phys. Chem. A* **2009,** 113, (19), 5806-5812.

255. Herrmann, W. A.; Rohrmann, J.; Herdtweck, E.; Spaleck, W.; Winter, A., *Angew. Chem. Int. Ed. Engl.* **1989,** 28, (11), 1511-1512.

256. Röll, W.; Brintzinger, H. H.; Rieger, B.; Zolk, R., *Angew. Chem., Int. Ed. Engl.* **1990,** 29, (3), 279-280.

257. Yamada, K.; Hikosaka, M.; Toda, A.; Yamazaki, S.; Tagashira, K., *Macromolecules* **2003,** 36, (13), 4790-4801.

258. Yamada, K.; Hikosaka, M.; Toda, A.; Yamazaki, S.; Tagashira, K., *Macromolecules* **2003,** 36, (13), 4802-4812.

259. Correa, A.; Talarico, G.; Cavallo, L., *J. Organomet. Chem.* **2007,** 692, (21), 4519-4527.

260. Burchat, A. F.; Chong, J. M.; Nielsen, N., *J. Organomet. Chem.* **1997,** 542, (2), 281-283.

261. Coulson, D. R.; Satek, L. C.; Grim, S. O., *Inorg. Synth.* **1972,** 13, 121-124.

262. Giardello, M. A.; Eisen, M. S.; Stern, C. L.; Marks, T. J., *Journal of the American Chemical Society* **1995,** 117, (49), 12114-12129.

263. Chien, J. C. W.; Tsai, W. M.; Rausch, M. D., *Journal of the American Chemical Society* **1991,** 113, (22), 8570-8571.

264. Coto, B.; Escola, J. M.; Suarez, I.; Caballero, M. J., *Polym. Test.* **2007,** 26, (5), 568-575.

265. Busico, V.; Cipullo, R., *Prog. Polym. Sci.* **2001,** 26, (3), 443-533.

266. Busico, V.; Cipullo, R.; Monaco, G.; Vacatello, M.; Segre, A. L., *Macromolecules* **1997,** 30, (20), 6251-6263.

267. Busico, V.; Carbonniere, P.; Cipullo, R.; Pellecchia, R.; Severn, J. R.; Talarico, G., *Macromol. Rapid Commun.* **2007,** 28, (10), 1128-1134.

268. Zhou, Z.; Kümmerle, R.; Qiu, X. H.; Redwine, D.; Cong, R. J.; Taha, A.; Baugh, D.; Winniford, B., *Journal of Magnetic Resonance* **2007,** 187, (2), 225-233.

269. Apex Suite of Crystallographic Software. Apex 2 Version 2008.4. Bruker Axs Inc., Madison, Wisconsin, USA (2008).

270. Saint, Version 7.56a and Sadabs Version 2008/1. Bruker Axs Inc., Madison, Wisconsin, USA (2008). .

271. L. J. Farrugia, "Wingx (Version 1.70.01 January 2005) ", J. Appl. Cryst. 1999, 32, 837-838.

272. Altomare, A.; Burla, M. C.; Camalli, M.; Cascarano, G. L.; Giacovazzo, C.; Guagliardi, A.; Moliterni, A. G. G.; Polidori, G.; Spagna, R., *J. Appl. Crystallogr.* **1999,** 32, 115-119.

273. Sheldrick, G. M. "Shelxl-97", University of Göttingen, Göttingen, Germany, (1998).

274. International Tables for Crystallography, Vol. C, Tables 6.1.1.4 (Pp. 500-502), 4.2.6.8 (Pp. 219-222), and 4.2.4.2 (Pp. 193-199), Wilson, A. J. C., Ed., Kluwer Academic Publishers, Dordrecht, the Netherlands, 1992